成都理工大学
优秀教学系部申报表

系部名称　　应用化学

系部负责人　　胡晓荣

所在学院　　材料与化学化工学院

成都理工大学教务处制

二〇一七年

填 表 说 明

1. 本表用钢笔填写，也可直接打印，不要以剪贴代填。字迹要求清楚、工整。
2. 本表所填内容必须真实、可靠，如发现虚假信息，将取消所在学院参评资格。
3. 本表涉及的项目、奖励、教材等所有数据，统计时间为 2015 年 9 月 1 日-2017 年 8 月 31 日。
4. 如表格篇幅不够，可另附纸。
5. 学院意见务必加盖公章，否则推荐无效。

一、系部基本情况简介

应用化学专业始建于1959年，由原成都地质学院二系开办的“岩石矿物分析”专业发展而来。依据1985年和1998年国家《普通高等学校本科专业目录》的规定相继更名为“工业分析”和“应用化学”。本专业自2009年作为校级特色专业建设，2015年起开始在本科第一批次录取学生。

应用化学专业依托成都理工大学地质学科优势和西部丰富的矿产资源、尤其是攀西战略矿产资源开发与综合利用的优势，紧密结合社会经济发展对专业人才的需求，历经长期的办学积累，发展形成了以岩石矿物分析及环境污染物痕量超痕量分析为特色的专业。本专业为国家地质矿产资源勘查与利用、环境监测与保护、食品药品安全监督等领域培养了大批具有系统基础理论知识和实践能力的应用研究型人才。本专业毕业生受到社会的广泛需求，每年实际就业率均在98%以上。毕业生遍布全国地质矿产、冶金、食品药品、质量技术监督等行业，其中一大批成长为业务领导和分析测试专家，本专业人才培养已在这些行业中产生较大影响。近年来由于第三方检测机构的蓬勃兴起，分析检测人才供不应求，本专业大批毕业生进入检测公司从事专业技术工作。

应用化学专业在校学生341名，应用化学系专职教师10名，其中教授5名，副教授2名，讲师3名；他们中9名拥有博士学位，1名拥有硕士学位；其中3名有海外博士后工作经历，2 名有出国访学经历。在长期的教学科研实践中，应用化学系形成了**“严谨、敬业、客观、奉献”**的优良作风，形成了新老教师更替**“传、帮、带”**的优良传统。

近年来，随着社会对分析化学人才素质、知识和能力要求的变化以及分析化学学科自身的发展，应用化学本科专业处于不断的发展和变化之中。在遵循**“保留传统、强化特色、开拓创新、与时俱进”**的专业发展思路下，今年的人才培养方案修订形成了新的人才培养目标和毕业要求，并以此为指导制定了本专业新的课程体系。近年来，专业建设主要在以下几个方面开展工作。

1. 加强课程建设

为实现人才培养目标，课程建设是核心内容。近两年来我系持续建设课程教学梯队，实行课程负责人制度并积极开展课程建设。课程组成员构成见附件1。“复杂物质分析”相继建设成为省级精品课程、省级精品资源共享课程；“环境分析化学”双语课程在省级精品资源共享课程建设的基础上，今年获批省级精品在线开放课程建设立项。“分析化学”在校级精品课程建设基础建设为精品资源共享课程。“仪器分析”立项建设校级精品资源共享课程。几门课程网站截图见附件2。2017年《岩矿分析》、《分析质量保证与实验室认证》、《仪器分析实验》三部教材立项

编写出版，其中《岩矿分析》已与科学出版社签订出版合同。

2. 加强教学管理和教研活动

为规范教学各环节的管理、保证教学质量，在学校学院两级教学管理的基础上应用化学系制定并执行系列系级管理文件:《应用化学系课程负责人职责》、《应用化学系生产实习指导教师职责》、《应用化学专业学生在科研单位或生产单位完成本科毕业设计和论文工作要求》、《应用化学专业本科毕业论文学术规范》、《应用化学专业生产实习质量控制系统评分标准》（附件 3）。规范课程实验报告和实践报告格式。定期开展教研活动，实行新教师助课、新老教师一对一的“传、帮、带”制度，实行教研室主任听课制度；这些文件和措施保证了教学环节的规范和质量，切实帮助青年教师的快速提高教学水平。

3. 加强生产实习基地的建设

为保证实践教学环节的培养质量，切实培养学生的动手能力，经过持续不断的努力，建立起 20 余个稳定的校外实习基地（附件 4）。2016、2017 年先后派出 79 名学生（占学生总人数的 45%）到基地进行为期 3 个月的生产实习。实习学生名单见附件 5。校内建设以分析化学实验室和岩石矿物分析实验室为主体的生产实习基地，开展多名教师分组指导的硅酸盐系统全分析为主要内容的生产实习。

4. 以科研促教学

为提高学生的创新能力，我系教师积极开展科学研究，近两年来承担了 20 项科研项目。其中国家自然科学基金项目 6 项（面上项目 2 项，青年项目 4 项）；中国博士后科学基金项目 4 项；四川省科技厅项目 2 项；教育厅项目 2 项（详细列表见附件 6）。近两年教师发表科研论文 32 篇，其中 SCI 源刊论文 17 篇，中文核心期刊论文 13 篇（详细列表见附件 7）。我系本科学生通过大学生创新创业项目和本科毕业论文参与到教师科研项目中来，其成果两年来在各类刊物上发表论文近 20 篇，其中本科生以第一作者发表 7 篇（其中 3 篇 SCI，3 篇中文核心），以第二作者发表（教师第一）1 篇（SCI，详见附件 15）。

为适应新形势下专业发展要求，迎接 2018 年审核性评估以及为将来的专业认证做准备，本专业需要在以下几个方面作好工作。一是继续加强师资队伍建设，增加师生比。接收优秀博士（后），引进高层次人才，形成一支年龄、学缘、职称结构更加合理的教学队伍；二是持续进行课程建设，提高现有精品课程的建设质量，建设新的精品课程，加强专业教材建设；三是加强教学研究、改进教学方法，让以“培养学生能力、以学生学习为中心”的理念成为教学基本思想，切实提高专业人才培养质量；四是持续加强科学研究，更好地以科研促进教学和学生创新能力的培养；五是加强教学管理、加强对学生专业思想和学习自觉性教育，保证教学活动高质量进行。

二、系部成员情况

1. 负责人情况

姓　名	胡晓荣	年　龄	52	参加工作时间	1986.7
职　称	教授	最终学历（学位）	研究生/博士	授予单位	四川大学

2. 系部成员情况

姓　名	年　龄	职　称	最终学历（学位）	主讲课程
李崇瑛	56	教授	研究生/硕士	仪器分析 专业导论
郎春燕	52	教授	研究生/博士	复杂物质分析 环境分析化学 专业英语
朱霞萍	49	教授	研究生/博士	分析化学 仪器分析
胡晓荣	52	教授	研究生/博士	分析化学 分析质量保证
张信凤	34	教授	研究生/博士（后）	仪器分析 食品分析
孙永华	42	副教授	研究生/博士	分析化学 药物分析
黄荣富	35	副教授	研究生/博士（后）	仪器分析 环境分析化学
钱 蕾	30	讲师	研究生/博士	分析化学 文献检索 产品质量检验
唐雨榕	30	讲师	研究生/博士（后）	分析化学 生物分析化学
贾 佳	33	讲师	研究生/博士（后）	分析化学 仪器分析

3. 师资队伍建设

（1）队伍组成及结构

应用化学系重视师资队伍建设，积极主动引进优秀人才。2017 年接收清华大学优秀博士后 1 名，进一步充实和优化师资队伍。目前我系共有专职教师 10 名，其中：教授 5 人，副教授 2 人，讲师 3 人；博士学位 9 名，硕士学位 1 人；4 名具有博士后工作经历，其中 3 名为海外博士；2 名有出国学习访问经历；最

高学历的学缘结构：5 人毕业于四川大学，3 人毕业于成都理工大学，1 人毕业于陕西师范大学，1 人毕业于中国科学院生态环境研究中心。教师队伍在年龄、学历和学缘上形成了合理的梯队，有利于本专业的持续发展。

此外，专业还聘请了 11 名地质矿产中心实验室和科研院所人员，2 名海外高校教授为我系客座教授或副教授（附件 8），加强补充学术交流和学生生产实习、本科毕业论文教学环节中的师资力量。

（2）政治素质与师德建设

我系定期开展的党支部民主生活会和教研活动，近两年深入开展“两学一做”教育实践活动。通过知识竞赛、专题讨论、党支部书记讲党课等多种方式深入学习党章党规、学系列讲话、做合格党员。系统深入的学习让本系党员对党的基本理论、基本路线、基本纲领、基本经验和前进方向有了更加深入的理解，更加坚定了为实现党的理想和目标共同奋斗的坚强决心。在建党 95 周年之际，应化系全体党员重温入党誓词，认真聆听习总书记的重要讲话，回顾历史，展望未来，坚信只要我们紧密团结在以习近平同志为核心的党中央周围，凝心聚力、奋发有为，就能把中国特色的社会主义事业推向新的胜利！全面建成小康社会！实现伟大的中国梦！实现我们每个人的事业梦。全体教师积极讨论学校和学院发展建设的各项决定和决议，积极参与到学院和学校发展建设的各项活动中。老教师引导年轻教师热爱教育事业、关心和爱护学生。让应用化学系的精神和优良传统传承发展。

（3）教学水平的促进

应用化学系定期认真开展互相听课和教学研讨，鼓励和支持教师外出学习和参加相关培训。近 2 年来，系主任共听课 20 余次，组织教学研讨会 20 余次（详见教研活动记录）；教师外出参加教学会议 8 人次，具体内容详见附件 9。新进年轻教师经过助课阶段再到主讲阶段，新老教师更替“传、帮、带”制度一直顺利开展。对今年新来的贾佳博士，系上指定朱霞萍老师为其教学指导教师，通过互相听课快速提高贾佳的教学水平。要求每位年青教师都要参加学院每年组织的讲课比赛。2015.07-2016.09 唐雨榕博士到德国亚琛工业大学完成博士后研究，进一步提高了科学研究能力。系上承担的质量工程和教改项目支持教师参加全国教学工作会议，增加与其他高校同行的教学交流，吸收最新的教学思想，学习新的教学模式，提高教学水平和人才培养质量。

4. 学生管理

(1)学风建设措施

学风建设的整体目标是学生明确学习目的、端正学习风气从而提升学习效率、提高学习成绩。针对这一目标，专业辅导员对学生制定了系列考查标准，例如年级学习量化评价表（包括平均成绩、学生干部平均成绩、补考率、重修率等内容），年级学习成果评价表（包括成级分布、评奖评优、课外活动参与、学生党员等内容）。通过任课教师考勤抓课堂氛围、学霸榜样引领寝室氛围、学生考勤管理自习氛围；专业教师参与小班班会总结引导学生开学、期中、期末三个阶段的学习特点和自我管理要求；分类引导学习成绩较好、成绩一般和后进学生；建设完善优秀学长队伍、班干部和入党积极分子队伍、辅导员和专业教师队伍。

通过专题教育促进学风。系主任、专业教师定期与辅导员沟通，了解学生学习状况，定期召开班级和部分学生座谈会，引导学生树立正确的学习思想，加强对专业的了解，改进学习方法；加强任课教师对学生课堂学习的督察，要求任课教师配合班干部检查、确认课堂出勤率；自 2014 年起，应用化学系为每个自然教学班按排专业指导教师。从 2015 级新生开始，学院为新生安排专业教师班导师。

注重新生帮助与学风建设。以学院朋辈互助交流中心为依托，选拔优秀学长和新生结对，以“朋辈互助、助人自助”为理念，有针对性的对新生进行学习、生活、交往等方面的指导，帮助新生解决大一阶段出现的困惑和问题，促进新生积极适应、主动发展。对新生班级进行集中晚自习制度，要求新生在晚间没有集中上课的时间进行集体自习。采用多种方式，对新生的大学学习生涯做规划并记录，采取“以班带个人、以个人促班级”的方式督促新生制定自我学习规划，并定期检查落实情况。

通过改进教学促进学风。应用化学系及课程组定期举行教学研讨会，就教学思想、教学方法、课程具体内容理解和讲解方法、教案设计、PPT 制作等内容进行讨论和交流。近两年来，以培养学生能力、以学生学习为中心的教学思想得到不断的强化，启发式和讨论式教学模式得到逐步的贯彻，对学生学习成绩的评价更多地加入了能力评价。在实践教学环节中，学生在教师引导下开展方案设计—讨论—实践—再讨论—完成报告的 5 步教学模式，充分调动学生学习的主动性和积极性，培养学生知识应用能力和解决复杂问题的能力。在作好课堂教学和实践教学的同时，积极进行精品课程建设。充分应用现代网络技术的优势，促进教学效果的提升。发挥我系精品课程资源作用，引导学生课前、课后利用课程网站进行学习。

通过学生参与教师科研促进学风建设。为了培养学生创新创业能力，让部分

优秀学生参与到教师科研实践中来，2017 年起，应化系在大二年级学生中选拔成绩优秀学生组建创新实验班，分组跟随专业教师开展科研实验。鼓励学生申报国家创新创业项目。首届创新实验班 11 个组 29 名成员名单见附件 10。通过科研实践提高学生学习兴趣、增进对专业的了解、加深对知识的理解、提高知识应用能力、培养创业创新能力。

严格教学过程管理。应用化学系按照学校、学院、专业三级教学管理模式，要求教师严格按照课表安排行课，严禁迟到早退，完备课程教学大纲、教案、讲稿等教学要件。生产实习、专业课程综合设计、创新实验设计、毕业实习和毕业论文等实践教学环节严格按照文件规定的指导教师职责和内容安排进行。严格落实系主任和传、帮、带教师听课制度。严格要求教师完成学生考勤、作业批阅、实验报告和实习报告批阅等工作。以严格的教风促进良好的学风。

(2) 考风建设措施

开展考风专题教育。每学期由年级辅导员定期开展考前教育，召开“考风考纪”主题班会，组织学习“成都理工大学学生考试违纪及作弊行为的认定和处理实施细则”，强调诚信、公平公正行为规则是每个大学生应有的道德基础，严肃考风考纪，端正考试态度，从思想上端正预防、杜绝违规行为的出现。要求学生诚实做人、遵纪守法、认真备考、诚实考试。同时，专业课教师从课程学习的特点引导学生认真复习积极备考。

严格规范考试的监督检查。要求教师严格落实教务处有关考试的规定。由课程组教师共同命题和制定评分标准、共同阅卷，按照教学大纲要求按照统一标准给出学生课程成绩。严格遵守试卷印制保密制度、遵守成绩报送时间。学院考风巡视组严格检查监考教师到岗情况、考场纪律、教师监考职责履行情况。以严格考试管理促进学生考风。

积极参加监考工作。我系教师积极参加学校和学院安排的监考工作，在监考工作中严肃认真地履行监考职责和遵守相关监考制度。

(3) 在教风和学风建设方面取得的成效

我系教师均把教学工作的重要性放在第一位，形成了认真履行教师职责的自觉性，对学生负责、耐心、热情，做到既教书又育人。专业学生学风整体良好，大部分学生认真努力，达到专业人才培养目标，毕业后受到用人单位的普遍好评。

三、教学运行情况

教学任务完成情况

应用化学系教师每学期严格按照教学计划安排课程，严格按照课表和教学大纲完成教学任务。

教学管理

在学校、学院、教学系三级管理体制下，应用化学系教师严格按照课表行课，按照教学大纲要求和教学必须要件开展专业培养方案中各教学环节工作。如因其它工作需要调整课程安排时，严格履行学校调课手续。两年来我系教师无一人因个人原因或健康问题调课，无教学事故，无迟到早退现象。

考试管理

严格要求试卷命题与教学内容的符合度，课程组教师共同命题；严格系主任对试题的审查制度；严格任课教师主考职责；严格按评分标准阅卷；严格完善考试文件；严格按时提交成绩。

四、教学效果

1、学生评教

我系教师除了承担应用化学系专业课程外，还承担化学、化学工程与工艺、制药工程、生物工程专业的分析化学和仪器分析课程教学。教师受到了广大学生的喜爱，教学受到了广大学生的认可，学生评分按照打分人数加权平均人均 90 分以上。

2、毕业率、受位率、考研率、就业率

应用化学专业学生 2015、2016 和 2017 届毕业率、授位率、过级率、考研率、就业率见下表。

应用化学专业毕业生情况统计表

评价指标 / 专业	人数	毕业率（%）	授位率（%）	英语四级通过率（%）	计算机二级过级率	考研率（%）	就业率（%）
2015 届	90	94.4	76.7	71.1	65.5	14.44	92.2
2016 届	94	96.8	86.2	74.47	/	19.15	91.39
2017 届	82	95.1	84.1	75.65	/	14.63	93.9

五、教学研究

应用化学系定期开展教研活动，坚持每两周的全系教师会议。教研活动探讨专业发展、理论课教学方法、实验课教学方法、实习管理和指导方法等；交流学习新的教学思想、理念和方法；要求教师参加教学会议和网上培训。积极参加国内外教学会议，2016-2017 年 8 人次参加全国教学工作会议。例如 2016 年在中国科技大学参加“两岸四地高校教学发展网络 2016 年会---目标导向的教育教学与教师发展”；在成都参加“全国高校教学改革与教师专业能力提升及师资队伍建设”等，具体参会情况见附件 9。

积极申报并开展各类教改项目和质量工程项目研究，近两年来我系教师承担了“复杂物质分析”省级精品资源共享课程建设，“环境分析化学”省级精品开放双语课程建设、“分析化学”和“仪器分析”校级精品资源共享课程的建设任务。通过课程建设，提高了课程组教师教学水平，拓展学生学习资源与渠道，加强专业课程教材建设（正在编写 3 部教材）。承担的“岩矿分析特色的应用化学专业人才培养模式的构建与实践”省级教改项目结题，“仪器分析课程内容和教学模式的改革与探索”校级教改项目。项目研究有效推动了专业人才培养模式的改革，形成以培养学生能力为核心的课程体系。以学生自主学习为中心的教学模式深入教师教学思想，启发式教学、讨论式教学、课堂学习结合网络学习等多种模式逐渐得以实现，从知识掌握到知识应用等方面全面评价学生的评价体系正在形成。两年来发表教改论文 2 篇，其中 1 篇为中文核心期刊（列表见附件 11）。2016 年，应用化学系课程建设获得学校优秀教学成果二等奖。（附件 13）

六、发展成效（选填项）

七、特色加分项（合计 21 分）

1. 本科生优秀毕业论文（附件 12）

编号	毕业论文（设计）题目	学生姓名	指导教师	获奖名称	时间
1	负载电化学发光分子的纳米金探针的性能研究	朱映雪	黄荣富	成都理工大学 百篇优秀学士学位论文	2017
2	纳米金粒径调控的表面增强电化学发光研究	向小芳	黄荣富	成都理工大学 百篇优秀学士学位论文	2016
3	基于川芎嗪-CuI 超分子化合物荧光猝灭的微量银分析方法研究	许 艳	胡晓荣	成都理工大学 百篇优秀学士学位论文	2016

2. 教师获奖情况：（含校级、省级、国家级奖励）（附件 13）

编号	项目名称	奖励名称	奖励级别	时间
1	教学成果奖	以岩矿分析为特色的应化专业系列精品资源共享课程的建设	校级 二等奖	2016.07
2	成都理工大学 2015~2016 先进教务工作者	先进教务工作者称号	校级	2017.01
3	教学成果奖 （第二完成人）	创新“传帮带”实践、加快青年教师成长	校级 二等奖	2016.07

3. 质量工程项目（附件 14）

编号	项目名称	类别	项目级别	获批时间
1	“环境分析化学”（双语）精品在线开放课程	质量工程	省级	2017 2017-2020
2	“环境分析化学”省级（双语）精品资源共享课程（11100-17Z0502）	质量工程	省级	2015 2016-2018
3	《岩矿分析》教材出版	教材建设	校级	2017 2017-2019
4	《分析质量保证和计量认证》教材出版	教材建设	校级	2017 2017-2019
5	《仪器分析实验》教材出版	教材建设	校级	2017 2017-2019
6	《分析化学》精品资源共享课程建设	质量工程	校级	2016 2017-2018
7	《仪器分析》精品资源共享课程建设	质量工程	校级	2016 2017-2018

4. 本科生竞赛获奖（附件 15）

编号	项目名称	奖励名称	奖励级别	时间
1	化学实验技能竞赛（第一组，袁伟 **袁磊** 2013 级 **吴倩** 2014 级）	第二届“梅特勒-托利多”杯川渝地区大学生化学实验技能竞赛	省级二等奖	2015.12
2	全国大学生英语竞赛（第二组，杨新明 王玥 **游相清** 2013 级）	第二届“梅特勒-托利多”杯川渝地区大学生化学实验技能竞赛	省级二等奖	2015.12
3	全国大学生英语竞赛（第三组，刘天早 马志刚 **张会会** 2013 级）	第二届“梅特勒-托利多”杯川渝地区大学生化学实验技能竞赛	省级三等奖	2015.12
4	全国大学生英语竞赛（袁小寒 2016 级）	全国大学生英语竞赛	国家级二等奖	2017.05
5	全国大学生英语竞赛（陈延诗 2016 级）	全国大学生英语竞赛	国家级二等奖	2017.05
6	数学建模竞赛 营晟哲 2016 级	认证杯 数学建模网络挑战赛二阶段	国家级三等奖	2017.09
7	大学生艺术展演活动	“五粮液”杯四川省大学生艺术展演活动“理工人之歌”	省级三等奖	2017.08
8	四川省大学生跆拳道联谊赛	竞技女子组雏量级	省级第一名	2016.05
9	知识竞赛（蒋玉玲 2016 级 袁小寒 2016 级）	大学生环保知识竞赛	省级优秀奖	2017.04
10	演讲比赛	“青春中国”主题演讲比赛	校级三等奖	2017.05

5. 专业教师发表教改论文（附件 11）

编号	论文名称	作者姓名	发表期刊名称	发表时间	收录情况
1	分析特色应用化学专业多维实践教学体系的构建	朱霞萍 胡晓荣 孙永华 周莉	实验验技术与管理	2016, 33(9): 151-154	中文核心
2	分析化学课程教学的精髓———量、度、新	朱霞萍 胡晓荣 孙永华 周莉	大学教育	2016, 06: 104-105	

6. 本科生第一作者发表论文（附件 16）

编号	论文（著）题目	作者	期刊名称、卷次
1	Label-free electrochemiluminescence assay for aqueous Hg^{2+} through oligonucleotide mediated assembly of gold nanoparticles	Dong-Mei Wang（王冬梅2017届）, Qi-Qi Gai（盖琦琪2016届）, Rong-fu Huang*	Biosensors and Bioelectronics 2017, 98, 134–139
2	A electro-thermal atomic absorption spectrometry-based assay for disease-related DNA	Xuemei Xu（徐雪梅 2013 届） Xiaorong Hu*	Microchemical Journal 2016, 126, 302-306.
3	A Both-End Blocked Peroxidase-Mimicking DNAzyme for Low-Background Chemiluminescent Sensing of miRNA	Xianming Li（李显明 2013 届）, Xinfeng Zhang (张信凤)	ACS sensors, 2017, 2, 810-816
4	In Situ generation and consumption of H_2O_2 by bienzyme-quantum dots bioconjugates for Improved chemiluminescence resonance energy transfer	Shuxia Xu（许淑霞), Xianming Li（李显明 2013 届）, Xinfeng Zhang (张信凤)	Analytical Chemistry, 2016, 88, 6418−6424
5	Cu-Mg-Al 层状超分子材料的制备及去除碘的研究	郑劫（2013 届） 朱霞萍*	功能材料, 2016, 47(9), 9231-6
6	聚乙二醇－硫酸铵－双水相萃取分光光度法测定地质物料中的镓	郑劫（2013 届） 朱霞萍	分析试验室, 2016，35(6): 629-632
7	丹参植株对亚硒酸钠和硒酸钠的吸收和积累	粟敏（2013 届），雷济华，杨帆，刘睿，胡晓荣*	中国科技论文 2017, 12(6): 647-651

八、学院推荐意见

（公章）

院长：（签字）　　年　月　日

成都理工大学优秀教学系部申报

应用化学系

支撑材料

2017 年 10 月 27 日

支撑材料目录

附件 1：应用化学专业课程组

表 1 专业课程组构成

课程名称	任课教师	负责人
分析化学	胡晓荣，朱霞萍，孙永华，钱蕾，唐雨榕	胡晓荣
仪器分析	李崇瑛，朱霞萍，张信凤，黄荣富，贾佳	李崇瑛
复杂物质分析	郎春燕，陈文，钱蕾	郎春燕
环境分析化学	郎春燕，黄荣富	郎春燕
食品分析	张信凤，许淑霞，孙永华	张信凤
药物分析	孙永华，张信凤	孙永华
分析质量保证	胡晓荣，黄荣富	胡晓荣
分子探针与显色试剂	陈文，唐雨榕	陈 文

附件 2 专业精品课程网站截图

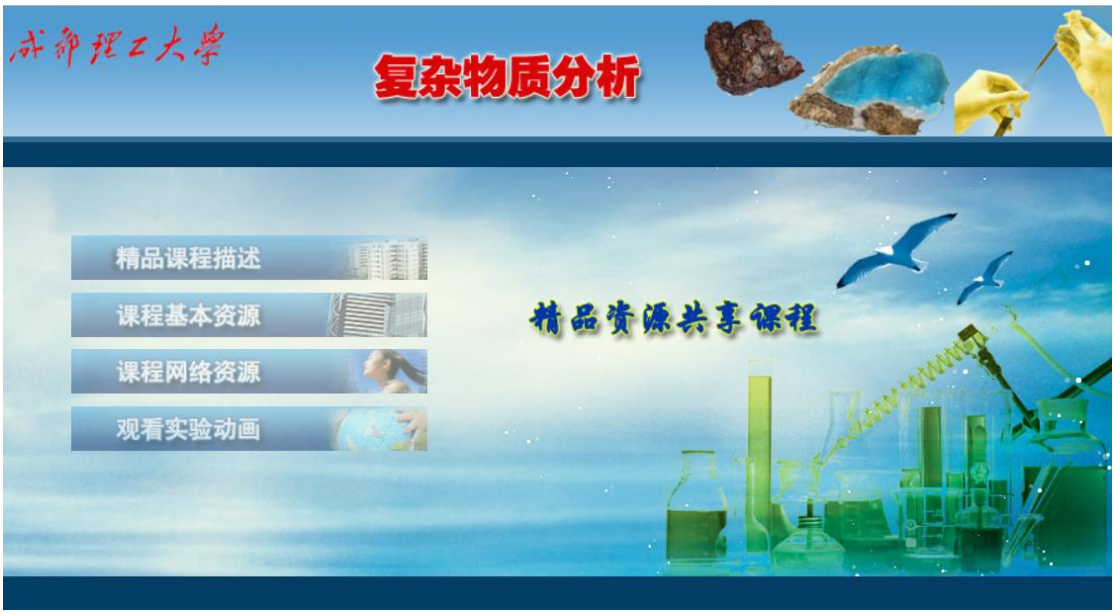


分析化学
精品课程网
网站首页
课程介绍
教学队伍
理论教学
实践教学
练习测试
在线问答
分析化学精品课程
成都理工大学精品课程欢迎您
教学大纲
教学计划
学习专栏
网络资源
本站公告
MORE
精品课程网站开通啦
课程简介
本课程的开设可追溯至1959年我校创办国内第一个“岩石矿物分析”本科专业时所设置的专业基础课程《分析化学》。作为当时该专业的主要专业...
.....
课程负责人
胡晓黑，四川西昌人，博士，副教授，硕士研究生导师。2000年毕业于四川大学化工学院，获得应用化学专业工学硕士学位；2003年毕业于四川大学化工学院，获得化学工艺专业工学博士学位。... .....
实验教学大纲
实验项目
实验视频
章节测试
校内链接
化学化工学院
成都理工大学
Chengdu University of Technology
成都理工大学图书馆
友情链接
精品课程网站
推荐网站
联系我们
电话：13730826334
地址：成都理工大学材化学院

附件 3 应用化学系级教学管理文件

应用化学专业课程负责人制度

课程建设是人才培养方案实施的核心内容，课程内容的确定、教学方法的改革、教师队伍的建设是课程建设的主要内容。本规定在成都理工大学教务处关于“本科课程设置和管理”文件的基础上就应用化学系课程负责人制及课程课程负责人职责作出规定。

一、课程教师组成

应用化学专业基础课程和专业课实行课程教师组，即一门课程由多名教师

二、论文内容

应用化学专业本科毕业设计（论文）内容必须符合专业培养要求，符合学校教务处对本科毕业设计（论文）的要求，具体内容参见《成都理工大学本科毕业设计（论文）指导意见》。论文内容可结合分析测试科研单位科研项目或生产单位分析实践中需解决的具体问题来确定。可在以下几方面但不仅限于以下几方面开展研究。

1．分析方法的建立。完成某分析方法对某物质分析过程的研究，可研究样品前处理方法（溶样、待测成分分离富集、干扰消除等）、测试条件优化改进、仪器联用技术等，内容要包括方法过程、分析数据质量评价指标（准确度、精密度、方法检出限等）和实际样品的分析测试数据。

2．元素形态分析方法建立。对环境样品、动物植物样品中某一元素化学形态或赋存形态分析方法的建立。

3．利用分析测试数据说明物质在环境、动物和植物中的分布、变迁或转移规律。

4．某一区域环境污染评价。

5．矿产资源综合利用方法研究。

三、时间安排

第七学期末确定论文题目，第八学期 3 月初到 5 月 20 日前后，学生可到校外单位完成论文实验内容，5 月 20 日前后返校进行论文的写作和修改。

四、其它

学生外出完成论文需签署《成都理工大学学生校外实习安全责任书》。学生往返外单位和学校的路费及实验费用，由外单位和应用化学系协商解决。

成都理工大学材料与化学化工学院

应用化学系

2011 年 11 月 30 日

应用化学系生产实习指导教师职责

应用化学系

2008 年 9 月制定　2013 年 6 月修订

生产实习是应用化学本科专业培养计划中重要的实践教学环节，在学生专业培养的基础课程和专业课程学习中起到承上启下的作用，该教学环节全面提升学生对《分析化学》、《仪器分析》等基础课程的知识应用能力和分析化学实验技术能力、系统掌握硅酸岩矿全分析的理论与实验方法、系统认识和熟悉冶金地质矿产部门中心实验室地质物料分析过程，奠定专业实践能力基础。为实现上述教学目标，采用校外基地实习 + 校内基地实习模式进行。为保证实习工作的顺利开展和教学质量，特制定以下指导教师职责。

校内实习：

1．学生分班进行实验，每班不超过 32 人，由两名指导教师和一名实验准备人员构成；

2．指导教师每天按时到达实验室，作息时间上午 8 点到 12 点，下午 2 点 30 分到 6 点 30 分。实习过程中，每个班必须保证有一个教师在现场；

3．指导教师负责学生考勤、检查学生的实验方案和过程记录，并作纪录；

4．指导教师实验前要组织学生讨论方案，实验过程中要指导学生规范操作，解决实验中的问题，实验后要组织引导学生总结实验，就实验原理、实验现象和实验结果进行讨论；

5．指导教师负责批改学生的实习报告、小论文、实习总结。根据评分标准评定学生实习成绩；

6．指导教师负责带领学生的外出参观；

7．指导教师负责学生实验室的安全责任；

8．指导教师要关心学生思想和学习状况，引导学生顺利完成实习工作。

校外实习：

1．指导教师要与实习单位领导和学生师傅进行经常性沟通，了解学生工作状态，了解并建议学生实习内容安排。

2．指导教师要定期到各实习单位看望指导学生，了解学生工作生活上的困难并协助实习单位解决；

3．指导教师本人应在实习单位学习岩石矿物等地质物料分析方法与质量管理，了解分析化学发展在生产一线的应用。

4．使用实习经费统一给外出学生购买短期人身意外保险。

5．指导教师负责批改学生工作日志与实习总结，在实习单位给定实习成绩的基础上，结合学生表现和工作日志与实习总结内容综合评定实习成绩。

应用化学专业学生在科研单位或生产单位
完成本科毕业设计和论文工作要求

本要求的制定是在成都理工大学本科毕业设计（论文）要求下，就应用化学系学生在校外科研单位或生产单位完成本科毕业设计（论文）的具体要求作出规定。

三、指导方式

由校外单位具有中级以上职称人员和校内专业教师共同指导学生。从题目拟定、论文内容确定、文献资料查阅、具体实验过程到论文写作与修改由校外单位和校内专业教师共同指导。学生在外单位实验期间，校内教师要通过电话、邮件等方式指导和关心学生。

四、论文内容

应用化学专业本科毕业设计（论文）内容必须符合专业培养要求，符合学校教务处对本科毕业设计（论文）的要求，具体内容参见《成都理工大学本科毕业设计（论文）指导意见》。论文内容可结合分析测试科研单位科研项目或生产单位分析实践中需解决的具体问题来确定。可在以下几方面但不仅限于以下几方面开展研究。

1．分析方法的建立。完成某分析方法对某物质分析过程的研究，可研究样品前处理方法（溶样、待测成分分离富集、干扰消除等）、测试条件优化改进、仪器联用技术等，内容要包括方法过程、分析数据质量评价指标（准确度、精密度、方法检出限等）和实际样品的分析测试数据。

2．元素形态分析方法建立。对环境样品、动物植物样品中某一元素化学形态或赋存形态分析方法的建立。

3．利用分析测试数据说明物质在环境、动物和植物中的分布、变迁或转移规律。

4．某一区域环境污染评价。

5．矿产资源综合利用方法研究。

三、时间安排

第七学期末确定论文题目，第八学期 3 月初到 5 月 10 日前后，学生可到校外单位完成论文实验内容，5 月 20 日前后返校进行论文的写作和修改。

四、其它

学生外出完成论文需签署《成都理工大学学生校外实习安全责任书》。学生往返外单位和学校的路费及实验费用，由外单位和应用化学系协商解决。

成都理工大学材料与化学化工学院

应用化学系

2011 年 11 月 30 日

成都理工大学

应用化学专业学士学位论文（设计）的

学术标准及基本规范

学分：14　　执笔人：胡晓荣　　审订人：

一、学士学位论文的目的

应用化学专业学士学位论文工作是应用化学专业学生在校学习期间最后的综合性实践教学环节，是对学生运用所学专业知识、专业技能进行某一科学问题研究或解决实际问题能力的系统训练与检验，要求学生综合运用化学专业及相关的数学、物理、计算机等领域的知识和技能在规定的时间内完成确定的研究性实验，并写出研究论文。通过这一过程培养学生综合运用所学知识和技能进行独立分析问题、解决问题的能力和初步进行科学研究的能力；培养创新意识和获取新知识能力；培养严谨、求实的治学态度和刻苦钻研、勇于探索的精神。在论文撰写过程中，深化专业理论知识，扩大相关知识面，学习专业论文书写方法，获得撰写专业论文的初步能力。

二、学士学位论文的选题

1、选题原则

（1）应用化学专业指导教师应根据专业培养要求按所需指导学生人数的 1.2 倍拟出论文题目提供给学生选择，题目工作量饱满，但应在学生实习时段内能够完成。

（2）学位论文（设计）原则上应一人一题，对于工作量较大、研究内容较多的综合性课题或产品研发项目，可以由多人共同完成，但每个人都应有独立完成的部分，且工作量和难度应符合毕业设计的基本要求。

（3）学位论文（设计）选题信息应包括指导教师的工程实践与科学研究经历及成果、学位论文（设计）题目来源、性质及具体的任务与时限要求、毕业实习实践或科学研究的地点场所等。指导教师的研究生助理应在选题上明确注明，原则上不能随意减少或变更。

(4) 对于到实习基地或签约单位进行毕业实习并完成学位论文实验工作的学生，学生需提出书面申请并经系主任同意，实习单位需指派两名具有中级职称的人员作为校外指导教师，学生根据实习内容提出选题要求并选择校内指导教师，由校外和校内指导教师共同确定论文题目和工作方案。

(5) 学位论文题目一经确定备案，原则上不能更改。学位论文的题目可以根据实际论文进展情况在毕业实习中期进行一次调整。在撰写论文时题目可根据完成实验的内容和结果

作出适当调整。

2、选题类型与主要研究内容

应用化学专业学位论文（设计）的类型原则上可分为三类，理论研究、应用研究和技术开发。

(1) 理论研究

主要包括认识物质的物理和化学性质，认识物质在时间或空间上的存在量、存在状态、迁移转化规律等现象，探索物质化学反应规律并根据物质物理和化学性质研究新的分析方法和方法建立的基本理论。

(2) 应用研究

应用研究为运用已有分析方法对矿产资源开发与利用、环境污染监测与治理、食品药品农副产品品质检验与安全监督、化工原料与产品质量监测；化工、医药、生物工程、材料等生产领域新产品开发过程中某些特定对象快速准确地进行定性定量分析的方法，对研究对象从样品处理到成分检测过程的方法改进和应用研究。运用化学和其它相关学科知识解决生产实践中的具体问题。

(3) 技术开发

主要包括把应用化学及相关领域研究所取得的一般科学知识应用于化工产品开发和生产工艺上的技术活动。应用化学技术开发的对象主要有：化工产品和新材料产品的开发、生产设备或分析仪器的开发、生产工艺的开发等。

如学位论文（设计）的内容符合应用化学专业培养规范，但是又难以明确归入上述三类的，可列入其它。

三、学士学位论文的要求

1、基本要求

（1）学士学位论文必须由学生本人独立完成，不得弄虚作假，不得抄袭他人成果。

（2） 学士学位论文篇幅一般应不少于 10000 字,论文要具有学术性和科学性，鼓励创新性，论文应观点正确、结构合理、层次分明、内容充实、论据充分、格式规范、文字流畅、结论解释合理。要有必要的相关资料、图表、参考文献、引文和注释等支撑论文。

（3）学士学位论文必须按学校统一格式要求排版。

2、内容要求

(1) 题目：应简洁、明确、字数不宜超过 25 个字。

(2) 摘要：要有高度的概括力，语言精练、明确。同时有中、英文对照，中文摘要约 300 汉字；英文摘要约 250 个实词。

(3) 关键词：从论文标题或正文中挑选 3～5 个最能表达主要内容的词作为关键词，同时有中、英文对照，分别附于中、英文摘要后。

(4) 目录：写出目录，标明页码。

(5) 正文：主要包括前言、论文正文、结论三个部分。前言是论文的开头部分，主要说明论文写作的目的、现实意义、对所研究问题的认识等，前言要写得简明扼要，篇幅不要太长。论文正文是论文的主体，应详细介绍研究方法、研究手段，对所得研究结果、实验结果进行分析和讨论，以揭示所蕴含的规律、机理等，尽量反映出自己的科研能力和学术水平。结论是论文的收尾部分，是围绕本论所得研究结果进行归纳总结。

(6) 致谢：根据自己的学位论文工作体会，对指导教师和协助完成论文的有关人员表示谢意。

(7) 参考文献：论文末尾要列出在论文中参考过的专著、论文及其它资料，所列参考文献应按论文参考或引证的先后顺序排列。参考文献格式参照学校统一格式要求。

(8) 附件：对于一些不宜放在正文中，但有参考价值的内容，可编入附件中。例如公式的推演、模拟计算编写的算法、语言程序等。

四、成绩评定标准

1、成绩评定标准

学士学位论文成绩由指导教师成绩、评阅人成绩和答辩成绩三部分汇总构成，其中指导教师成绩占 40%，评阅人成绩占 20%，答辩成绩占 40%，均以百分制计算。具体标准如下：

分值≥90 分：按期圆满完成学位论文（设计）任务书规定的任务；独立工作能力强，科学作风严谨；在学位论文（设计）报告中能熟练地运用所学理论和专业知识，立论正确，计算、分析和实验正确，结论合理；文字精炼流畅，逻辑性强；学位论文（设计）要有创新性，水平较高；组成图件齐全、准确、规范、美观；答辩时思路清晰，论点正确，回答问题有理论根据，基本概念清楚，对主要问题回答正确，深入。查重率应符合学校评优标准。

80≤分值＜90 分：按期圆满完成学位论文（设计）任务书规定的任务，有较强的独立工作能力；资料丰富，逻辑性较强，论述清楚；论据充分，方案正确，计算准确，对某些问题具有一定见解，能提出建设性意见；图表齐全、规范、格式符合要求；答辩时思路清晰，论点基本正确，能回答主要问题。

70≤分值＜80 分：按期完成学位论文（设计）任务书规定的任务，有一定独立工作能力；在毕业设计（论文）报告中运用所学理论和专业知识上基本正确，学位论文（设计）水平一般，文理通顺，但论述有个别错误（或表达不清楚），图表完备，基本正确，但质量一般或有小缺陷；答辩时对主要问题的回答基本正确，不能深入分析。

60≤分值＜70 分：在指导教师帮助下，能按期完成任务，独立工作能力一般，有一些小的疏忽和遗漏；在学位论文（设计）报告中能运用理论和专业知识中，无大的原则性错误：论点、论据基本成立，计算、分析、实验基本正确：论述不够恰当或表达不清楚；毕业设计（论文）达到基本要求；图表质量不高，有个别明显错误；答辩时主要问题能回答或经过启发后才能回答，回答问题较肤浅。

分值＜60 分：未按期完成指导书规定任务，或基本概念和基本技能未掌握；在学位论文（设计）报告中运用理论和专业知识中出现不应有的原则性错误；在方案论证、分析、实验等工作中，独立工作能力差，毕业论文未达到最低要求；学位论文（设计）文理不通，质量差；图表不齐全或有原则性错误；答辩时阐述不清学位论文（设计）的主要内容，基本概念模糊；对主要问题回答有错误，或不能回答。

2、成绩评定程序

(1) 学生应在规定时间内上交学位论文和任务书、开题报告、文献综述等所要求的全部资料；

(2) 指导教师应对学生的论文进行认真、全面的审查，对论文的工作能力和态度、论文完成情况和水平、学生的外语水平等进行公正评价，打分并写出评语；

(3) 按照学校教务部门和学院的有关文件中规定，评阅人对学士学位论文进行认真、仔细的评阅，打分并写出评语。

(4) 指导教师和评阅人给出的分数均在 60 分以上且均同意提交答辩的学士学位论文方可提交答辩小组，进行学位论文答辩。

(5) 答辩小组在学院答辩委员会指导下设立，一般设组长 1 名，组长应由具有副教授以上岗位技术职务的教师担任，答辩小组成员人数不少于 3 人，其工作职责有：审阅论文、指导教师评语、评阅人评审意见及了解毕业设计(论文)中期检查情况；参加答辩会议，听取学生对论文内容的宣读，并提出问题。答辩采取固定地点答辩会的形式，先由答辩小组组长宣布答辩小组成员名单、注意事项等，学生汇报学位论文工作内容，并回答答辩小组成员提出的问题。答辩小组集体给出答辩成绩。

(6) 答辩小组对有异议的指导教师和评阅人的论文评阅成绩，可提请学院答辩委员会复查，答辩委员会可以指派 2 位教师进行复查。

五、归档要求

毕业论文按下列顺序撰写编排并进行装订：

1、前面部分

（1）封面　（2）指导教师评语　（3）评审教师评审意见书　（4）答辩委员会决议书
（5）中文摘要（包括中文关键词）　（6）英文摘要（包括英文标题和关键词）　（7）目录

2、主体部分　（1）前言　（2）正文　（3）结论

3、结束部分　（1）致谢　（2）参考文献　（3）附件　（4）诚信承诺书

毕业论文工作相关资料按下列顺序单独装订成册

（1）学生毕业设计（论文）答辩记录表　（2）学生毕业设计（论文）任务书
（3）学生毕业设计（论文）开题报告　（4）学生毕业设计（论文）文献综述报告
（5）学生毕业设计（论文）外文译文（附原文）

应用化学专业生产实习质量控制系统评分标准

应用化学系　2008 年制定

1. 实习态度和考勤（对待生产实习的态度和是否遵守实习时间。）5%
2. 学习的主动性（实验中分析问题与解决问题的能力表现，应用理论知识的能力表现，主要通过讨论发言显示。）10%
3. 团队精神（包括实验室公共事务的处理、实验室整齐清洁的维持、同学之间的协作等。）5%
4. 原始记录（记录是否规范、真实、完整）5%
5. 结果报告（实验原理和方法的简明清楚的表现、结果报告、结果评价、问题讨论）5%
6. 小论文（选题结合实习内容中的某一具体问题，论述和分析要有实验依据和理论分析）5%
7. 在生产单位的表现 5%
8. 分析结果 60%

硅酸盐全分析 11 个指标

指标	烧失量	SiO_2	Fe_2O_3	Al_2O_3	CaO	MgO	TiO_2	P_2O_5	MnO_2	Na_2O	K_2O	总量
权重%	5	10	10	10	10	10	10	10	10	5	5	5

说明：按以上标准评出分数后，≥90 分评为优秀，80~89 分评为良好，70~79 分评为中等，60~69 分评为及格，＜60 分的为不及格。教师在评分时，对实习态度不认真或伪造数据的同学可实行一项否决。

附件 4 应用化学专业实习基地列表

表 15　应用化学专业校外实习、实训基地

序号	基地名称	建立时间	依托企业或单位	地址	每次可接纳学生数（人）
1	成都综合岩矿测试中心基地	2011	成都综合岩矿测试中心	成都市人民北路一段 25 号	10
2	四川西冶地质测试技术有限公司基地	2012	四川西冶地质测试技术有限公司	成都市郫县红光镇工业园光电工业	10
3	国土资源部成都矿产综合利用研究所基地	2011	国土资源部成都矿产综合利用研究所	成都市二环路南三段 5 号	4
4	成都科龙化工试剂厂基地	2011	成都科龙化工公司	成都市新都木兰开发区	60（参观）
5	成都市环境监测中心站基地	2000	成都市环境监测中心站	四川省成都市锦江区海桐街 69 号	4
6	成都市危险废物处置中心基地	2000	成都市危险废物处置中心有限公司	四川省成都市青羊区青江东路 368 号 1 幢 2 单元 3 楼	60（参观）
7	国土资源部成都地质矿产研究所基地	2000	国土资源部成都地质矿产研究所	四川省成都市一环路北三段 2 号	4
8	四川省地勘局成都岩土水质检测中心基地	2000	四川省地勘局成都岩土水质检测中心	成都 西青路 90 号附 3 号	4
9	中国冶金地质总局昆明地质勘查院分析实验室基地	2013	中国冶金地质总局昆明地质勘查院	云南省昆明市盘龙区龙泉路 702	2
10	广东省物料实验检测中心基地	2011	广东省物料实验检测中心	广东 广州 东风东路 7 5 1 号	4
11	贵州省地质矿产中心实验室基地	2014	贵州省地质矿产中心	贵阳市中华北路 242 号省府 5 号楼	2

12	川西北地质大队中心实验室基地	2014	川西北地质大队	四川省绵阳市剑门路西段 88 号	2
13	四川省冶金地质岩矿测试中心基地	2013	四川省冶金地质岩矿测试中心	四川省眉山市彭山区青龙镇(天府新区青龙工业园区)	5
14	山东鲁南地质工程勘察院中心实验室基地	2015	山东鲁南地质工程勘察院中心实验室	山东 济宁市 兖州建设路 104 号	2
15	德阳地质工程勘察院地矿检测中心基地	2013	德阳地质工程勘察院	四川省德阳市旌阳区天山南路二段 79 号	4
16	四川省地矿局华阳检测中心基地	2013	四川省地矿局华阳检测中心	成都市双流县华阳通济桥下街 198 号	4
17	攀西地质大队中心实验室基地	2013	攀西地质大队	四川西昌市北山	2
18	海南省地质测试研究中心基地	2013	海南省地质测试研究中心基地	海南省海口市龙华区金地路 1-3 号	4
19	四川省中晟环保科技有限公司基地	2016	四川省中晟环保科技有限公司	四川省眉山市东坡区	4
20	朴赛斯环境监测有限公司基地	2015	朴赛斯环境监测有限公司	成都市龙潭工业园	2
21	四川威尔检测技术股份有限公司	2016	四川威尔检测技术股份有限公司	成都高新区创业路 2 号 5 楼	8
22	中国测试技术研究院化学研究所	2015	中国测试技术研究院化学研究所	四川省成都市玉双路 10 号	5
23	农业部渔业环境及水产品检验测试中心	2015	农业部渔业环境及水产品检验测试中心	成都市金牛区一环路西三段 13	2

附件 5 应用化学专业学生校外实习名单

2016 年应用化学专业校外生产实习学生名单

编号	学号	姓名	性别	实习单位
1	201302030125	游相清	女	成都岩矿综合测试中心
2	201302030321	朱映雪	女	
3	3201302040333	陈小凤	女	
4	201302030220	曹心怡	女	
5	201302030124	张晓娟	女	
6	201302030219	张会会	女	
7	201302030211	杨飞翔	男	
8	201302030202	张家赫	男	海南省地质矿产局岩矿测试中心
9	201302030117	周文龙	男	
10	201302030115	唐坤	男	
11	201302030110	张彪	男	
12	201302030216	张潇一	男	四川冶金地质岩矿测试中心
13	201302030217	辜杰峰	男	
14	201302030205	余亨	男	四川中晟环保科技有限公司
15	201302030203	何映均	男	
16	201302030204	明浩	男	
17	201202030106	陈儒祥	男	
18	201302030116	肖飞龙	男	山西省地质矿产局岩矿测试中心
19	201302030327	李美菊	女	
20	201302030129	贺立红	女	
21	201302030313	王朝辉	男	中国测试技术研究院
22	201302030314	鲍召胜	男	
23	201302030318	唐子亮	男	
24	201302030319	赵悦	女	
25	201302030226	徐赟倩	女	
26	201302030209	廖梦龙	男	成都欣捷高新技术开发有限公司
27	201302030309	邱威	男	
28	201102030219	冷 曦	男	贵州省心实验室
29				四川威尔检测技术股份有限公司

30	201302030322	杨年驰	女	
31	201302030222	吴冬梅	女	
32	201302030221	崔婷	女	
33	201302030230	孙皓皓	女	
34	201302030121	杨次尔友珍	女	
35	201302030210	李根	男	
36	201302030207	尹继强	男	
37		郑均	男	四川省水产局检测中心
38	201302030103	黄永红	女	
39	201302030223	候芳	女	四川西冶地质测试技术有限公司
40		张玉洁	女	
41		徐小翠	女	
42	201302030310	赵寒静	男	四川省分析技术测试服务中心
43	201302030120	何宝成	男	
44	201302030104	李祥	男	
45		刘嘉	女	
46		邓兰蕊	女	

2017 年用化学专业校外生产实习学生名单

编号	学号	姓名	性别	实习单位
1	201402030104	何发	男	中晟环保公司
2	201402030107	柳成恩	男	
3	201402030217	方东	男	
4	201402030303	辜威龙	男	
5	201402030302	刘天浩	男	
6	201402030106	李晓锋	男	重庆地质矿产测试中心
7	201402030116	宋德福	男	
8	201402030113	刘鑫	男	
9	201402030222	胡雨佳	女	成都市食品药品检验研究院
10	201402030224	蒋蕊	女	
11	201402030125	廖薇		威尔检测技术中心
12	201402030226	周兆倩		
13	201402030315	赵凌	男	
14	201402030314	李洋锋	男	
15	201402030306	吴波	男	
16	201402030114	石化轩	男	
17	201402030225	潘白凤	女	
18	201402030316	蒲文权	男	成都岩矿综合测试中心
19	201402030208	李进刚	男	
20	201402030202	罗开桥	男	
21	201402030229	李秋霞	女	
22	201402030326	向敏	女	
23	201402030130	张维	女	四川省德阳地质工程勘察院德阳地矿检测中心
24	201402030121	唐建梅	女	
25	201402030101	李杰	男	
26	201402030103	甘小兵	男	

27	201402030323	冯蕾		成都新捷科技公司
28	201402030126	杨兰菊	女	
29	201402030123	唐子涵	女	中测标物
30	201402030313	王子谦	男	中国化学工程建设有限公司第七分公司
31	201402030317	赵洋	男	香港紫荆花制漆（中国）有限公司
32	201402030102	朱权虎	男	核工业 280 研究所

附件 6 应用化学专业教师承担的科研项目统计表

2016-2017 应用化学专业教师承担的科研项目统计表

序号	项目编号	项目名称	负责人	项目来源	级别	批准时间	起止时间	参加人员	经费(万元)	是否结题
1	21706018	$NiCo_2O_4$的表界面构筑及其甲醇光电协同催化氧化性能研究	钱蕾	国家自然基金青年项目	国家	2017	2018-2020		20	在研
2	80303-SHT081	沱江沉积物-水界面氮磷赋存形态及其分布规律研究	郎春燕	横向委托	横向	2017	2017-2018		2	否
3	2017CY-G-11	氧杂蒽酰肼化学发光法测定高纯钛产品中痕量铬和钒	孙永华	攀枝花市	横向	2017	2017-2019		2 万	否
4		火驱过程物理变化规律研究	孙永华	新疆油田公司工程技术研究院	横向	2017	2017-2018		5 万	否
5	21605010	构建氮化碳材料的新型三维光学传感器及其分析应用	唐雨榕	国家自然基金青年项目	国家	2016	2017-2019		20	在研
6	2016T90840	地表水重金属离子的光催化可视化阵列传感技术	张信凤	中国博士后科学基金特别资助项目	国家	2016	2017-2018		15	在研
7	SHL080	地下卤水制备特殊功能盐的工艺研究	朱霞萍	横向委托	横向	2016	2017-20189		7	在研
8	80303-SZR025	基于$NiCo_2O_4$的甲醇燃料电池阳极非贵金属催化剂的原位设计合成	钱蕾	四川省教育厅自然科学一般项目	厅级	2016	2016-2017		1	在研
9	41573014	碳酸盐岩中碳酸盐矿物的稀土元素分析方法研究	李崇瑛	国家自然基金面上项目	国家	2015	2016-2018		88.4	否
10	2015T80071	基于稀土纳米材料标记的多组分肿瘤标志	刘睿	中国博士后科学基金第	国家级	2015	2017-2017		15	否

		物免疫分析研究		八批特别资助项目						
11	21505008	基于稳定同位素标记的 DNA 测序方法初步探索	刘睿	国家自然科学基金青年项目	国家级	2015	2016-2018		25	否
12		中青年科研骨干教师	钱蕾	成都理工大学	校级	2015	2015-2017		6	否
13	2015M570773	基于核酸光催化体系的地表水污染物现场分析方法	张信凤	中国博士后科学基金	国家级	2015	2015-2017		8	否
14	2014M550704	基于元素标记和无机质谱检测的核酸测序方法研究	刘睿	中国博士后科学基金第 55 批面上项目	国家级	2014	2014-2016		5	否
15	2015GZ0243	超分子化合物技术综合治理化学实验室废水中多种污染物的应用研究	朱霞萍	四川省科技厅科技支撑	省级	2014	2014-2016		40	否
16	.	电镀废水制备铜基超分子材料及去除废水中放射性碘的研究	朱霞萍	四川省教育厅	厅级	2014	2014-2016		6	否
17	21407013	表面增强电化学发光免疫法检测食品中的环境雌激素类物质	黄荣富	国家自然科学基金青年项目	国家级	2014	2015-2017		24	否
18		中青年科研骨干教师	黄荣富	成都理工大学	校级	2014	2014-2016		6	否
19	2014JY0161	富硒中江丹参培育模式和抗氧化活性研究	胡晓荣	四川省科技厅应用基础	省级	2014	2014-2017		10	否
20	21475013	多功能核算光催化可视化传感平台	张信凤	国家自然科学基金	国家级	2014	2015-2017		82	否

附件 7 应用化学系教师科研成果列表

2016-2017 年应化系教师发表的科研论文

序号	论文名称	作者姓名	发表期刊名称	发表时间	收录情况
1	Tuning the aggregation/disaggregation behaviours of ZnSe quantum dots for high-sensitivity fluorescent rutin sensors	Yurong Tang （唐雨榕）	Analytical Methods	2017, 9, 5274-5280	SCI
2	Label-free electrochemiluminescence assay for aqueous Hg^{2+} through oligonucleotide mediated assembly of gold nanoparticles	**Dong-Mei Wang（王冬梅，201302030326）, Qi-Qi Gai（盖琦琪）,** Rong-Fu Huang*（黄荣富）, Xingwang Zheng	Biosensors and Bioelectronics	2017, 98, 134–139	SCI
3	Surface and interface engineering of CoNi layered double hydroxides for efficient methanol oxidation reaction	Shuli Luo, **Lei Qian*（钱蕾）**, **Menglong Liao**（廖梦龙 201302030209）, Xiaorong Hu, Dan Xiao	RSC Advances	2017, 7, 45294-303	SCI
4	Preparation of a Mg/Al/Fe layered supramolecular compound and application for removal of Cr(VI) from laboratory wastewater。	Xuejin Wang, Xiaping Zhu* （朱霞萍）and Xingrui Meng（孟兴锐，201202020205）	RSC Advances	2017, 7, 34984-34993	SCI
5	A Both-End Blocked Peroxidase-Mimicking DNAzyme for Low-Background Chemiluminescent Sensing of miRNA	Xinfeng Zhang (张信凤)	ACS sensors	2017, 2, 810-816.	SCI
6	Bienzyme-based visual and spectrophotometric aptamer assay for quantitation of nanomolar levels of mercury (II)	Xinfeng Zhang (张信凤)	Microchimica Acta	2017, 184: 541-546.	SCI

7	Synergy of adsorption and photosensitization of graphene oxide for improved removal of organic pollutants	Xinfeng Zhang (张信凤)	RSC advance	2017, 7, 16204-16209	SCI
8	One-step electrodeposition of S-doped cobalt-nckel layered double hydroxides on conductive substrates and their electrocatalytic activity in alkaline media	**Lei Qian*（钱蕾）**, Wen Chen, **Miaomiao Liu**（刘苗苗 201102030225）, **Qiannan Jia**（贾茜男 201102030126）, Dan Xiao	ChemElectroChem	2016, 3(6), 950-958	SCI
9	In Situ generation and consumption of H_2O_2 by bienzyme-quantum dots bioconjugates for Improved chemiluminescence resonance energy transfer	Xinfeng Zhang*（张信凤）	Analytical Chemistry	2016, 88, 6418−6424.	SCI
10	Photocatalytic electrosensor for label-free and ultrasensitive detection of BRCA1 gene	Shuxia Xu*（许淑霞） Xinfeng Zhang*（张信凤）	Biosensors and Bioelectronics	2016, 85, 957-963.	SCI
11	Amplified electrochemical detection of nucleic acid hybridization via selective preconcentration of unmodified gold nanoparticles	Huang Rongfu*（黄荣富）	Analytica Chimica Acta	2016, 934, 59-65	SCI
12	Removal of chromium from laboratory wastewater using preparation–adsorption technology with a Mg/Al/Cr layered compound	Xiaping Zhu（朱霞萍）	RSC Advances.	2016, 6, 85595-85602	SCI
13	A salt-assisted graphene oxide aggregation method for the determination of dimethylamine and trimethylamine by ion chromatography with conductivity detection	Shuxia Xu*（许淑霞） Xinfeng Zhang*（张信凤）	Anaytical Methods	2016, 8, 1828–1835.	SCI
14	A electro-thermal atomic absorption spectrometry-based assay for disease-related DNA	Xu, X , Xiaorong Hu*(胡晓荣) Rui Liu*（刘睿）	Microchemical Journal	2016, 126, 302-306.	SCI
15	A sensitive atomic absorption spectrometric	Chongying Li*（李崇瑛）	Microchemical	2016, 126,	SCI

	metalloimmunoassay with copper nanoparticles labeling	Rui Liu*（刘睿）	Journal	1-6.	
16	THERMODYNAMIC STUDIES ON THE ADSORPTION OF Cu^{2+} , Ni^{2+} AND Cd^{2+} ON TO AMINE-MODIFIED BENTONITE	Xiaping Zhu（朱霞萍）, Lumei Lan, Niannian Xiang, Wenhua Liu, Qiuxiang Zhao， Haiping Li	Bull. Chem. Soc. Ethiop.	2016, 30(3), 357-367.	SCI
17	COMPOSITE BENTONITE MODIFICATED BY 3-AMINOPROPYLTRIETHOXYSILANE AND SODIUM SILICATE AND ITS EFFECTIVENESS TO CADMIUM REMOVAL	Hao, XJ; Zhu, XP（朱霞萍*）, Zhou, L; Wu, L	FRESENIUS ENVIRONMENTAL BULLETIN	2016,25(10) : 4327-4333	SCI
18	镁铝层状超分子化合物去除废水中的六价铬	王雪瑾 朱霞萍* 蓝路梅	应 用 化 学	2017, 34(1): 98-104	中文核心
19	Cu-Mg-Al 层状超分子材料的制备及去除碘的研究	郑劫（2013 届） 朱霞萍*	功能材料	2016, 47(9), 9231-6	EI 中文核心
20	聚乙二醇－硫酸铵－双水相萃取分光光度法测定地质物料中的镓	郑劫（2013 届） 朱霞萍	分析试验室	2016，35（6），629-632	中文核心
22	原子荧光法测定青城野菜不同器官中的硒和碲	张秀雯，郎春燕*，曹建平，王小云，罗兰萍	广州化工	2016,44(14) :136-138	
21	混合原料优化配置制乙烯的研究进展	李佳，郎春燕*，周如金	现代化工	2016,36(2): 22-25	中文核心
23	不同生化工艺处理炼油废水的 GC/MS 分析及评价	方超，郎春燕*，李德豪，柳莎，曹建平，王小云	现代化工	2016,36(1): 183-186.	中文核心
24	PCBs 分析测定的样品前处理研究进展	张秀雯，郎春燕*，曹建平	山东化工	2016,45(19)	

				:33-35.	
25	醇类化合物热值改进剂的定量结构-性质关系研究	牛丽芳, 郎春燕*, 周如金	分子科学学报	2017, 33(1): 69-76	中文核心
26	环境中 PCBs 和 PBBs 的测定研究进展	张秀雯, 郎春燕*, 周如今, 曹建平	应用化工	2017,46(4) : 755-759	中文核心
27	SPME-GC 联用测定沉积物中 PCBs 的影响因素	张秀雯, 郎春燕*, 曹建平	当代化工	2017, 46 (2): 207-210	
28	丹参植株对亚硒酸钠和硒酸钠的吸收和积累	**粟敏**（2013 届），雷济华，杨帆，刘睿，胡晓荣*	中国科技论文,	2017, 12(6): 647-651	中文核心
29	中江丹参植株中镉、铅、铜的初级和次级形态分析	周莉, 董维兵, 邱倩, 胡晓荣*	中国测试	2017, 43(7): 66-71	中文核心
30	中江丹参植株中 Cd、Pb、Cu 的溶剂提取及离子交换去除研究.	周莉, 董维兵, 邱倩, 胡晓荣*	中国测试	2017, 43(8): 60-65	中文核心
31	密闭消解 HG-AFS 法测定丹参植株中的汞含量. 中国测试,	李瑶佳，**杨 超**（2015 届），胡晓荣*	中国测试	2016, 42(1): 45~48	中文核心
32	聚苯胺及磁性聚苯胺/Fe_3O_4 复合微球吸附铬(Ⅵ)的研究	文锐 孙永华* 李崇瑛	化学研究与应用	2016 , 28 (9) :1237-1242	中文核心

附件 8 应用化学系外聘教师列表

专业外聘客座教授和副教授

姓名	聘请职称	职位/职称	工作单位
漆 亮	教授	研究员	中国科学院地球化学研究所
杜 谷	教授	实验室主任/正高工	成都地质矿产研究所
李小英	教授	总工/正高工	成都岩矿综合测试中心
李 刚	教授	副总工/正高工	成都岩矿综合测试中心
刘 卫	教授	实验室主任/研究员	中国地质科学院矿产综合利用研究所
刘文华	副教授	总工/高工	广东省物料实验检测中心
朱志雄	副教授	总工/高工	贵州省地质矿产中心实验室
赵 平	副教授	总工/高工	贵州省地质矿产中心实验室
郭晋川	副教授	总工/高工	四川西冶地质测试技术有限公司
郑 松	副教授	实验室主任/高工	贵州省地质矿产中心实验室
杨 林	副教授	总工/高工	贵州省地质矿产中心实验室
Nelson Belzile	教授	教授	加拿大 Laurentian 大学
陈羽薇	教授	教授	加拿大 Laurentian 大学

附件 9 应用化学专业教师参加教学会议、进修详细情况

应用化学专业教师参加教学会议、进修详细情况

姓名	进修项目名称	进修地点、时间	进修内容	进修天数
胡晓荣	第一届全国分析化学教学研讨会	武汉 华中科技大学，2017.07	教学方式	3
胡晓荣	工科专业认证培训	成都，2017.07	专业认证	2
黄荣富	工科专业认证培训	成都，2017.07	专业认证	2
郎春燕	两岸四地高校教学发展网络 2016 年年会 - 目标导向的教育教学与教师发展	合肥 2016 年	教学方式	3
朱霞萍	两岸四地高校教学发展网络 2016 年年会 - 目标导向的教育教学与教师发展	合肥 2016 年	教学方式	3
孙永华	两岸四地高校教学发展网络 2016 年年会 - 目标导向的教育教学与教师发展	合肥 2016 年	教学方式	3
黄荣富	全国高校教学改革与教师专业能力提升及师资队伍建设	成都 2016 年	教学改革和教学技能	3
郎春燕	全国职业院校技能大赛拟设赛项监督人员培训会	北京 2016 年	技能大赛监督人员培训	3
唐雨榕	博士后	德国亚琛工业大学 2015.08-2016.07	氮化碳光催化性能研究	365

附件 10 首届创新实验班构成名单

首届创新实验班学生及指导教师名单

组 序	姓 名	学 号	负责人	导师
1	苟超 王香 郭琪	201502030110 201502030126 201502030125	苟超	郎春燕
2	张少冰 王琳华 唐尉	201502030124 201502030223 201502030109	唐尉	张信凤
3	雷凤洁 吴越	201502030129 201502030127	雷凤洁	钱蕾
4	张贵 孙雪娟 邱凤	201502030206 201502030226 201502030230	孙雪娟	胡晓荣
5	万兵 青树雄 林泳茵	201502030204 201502030205 201502030222	青树雄	李崇瑛
6	廖童 向漆	201502030114 201502030108	廖童	孙永华
7	郑智文 李云舟	201502030313 201502030312	郑智文	朱霞萍
8	刘丽枝 廖文强	201502030329 201502030309	廖文强	唐雨榕

	蔡佳莉	201502030323		
9	龙美名 粟玲	201502030327 201502030328	龙美名	黄荣富
10	张利娜 巫红霖	201502030330 201502030326	巫红霖	黄荣富
11	胡敏 杜新梅	201502030103 201502030122	胡敏	张信凤

附件 11 专业教师发表教研论文统计

专业教师发表教改论文统计表

论文名称	第一作者或通讯作者工号	作者姓名	发表期刊名称	发表时间	收录情况
分析特色应用化学专业多维实践教学体系的构建	10201401402	朱霞萍	实验验技术与管理	2016,33(9):151-154	中文核心
分析化学课程教学的精髓———量、度、新	10201401402	朱霞萍	大学教育	2016,06:104-105	

ISSN 1002-4956
CN11-2034/T

实 验 技 术 与 管 理
Experimental Technology and Management

第 33 卷 第 9 期 2016 年 9 月
Vol. 33 No. 9 Sep. 2016

DOI:10.16791/j.cnki.sjg.2016.09.039

分析特色应用化学专业多维实践教学体系的构建

朱霞萍，胡晓荣，孙永华，周 莉

（成都理工大学 材料与化学化工学院，四川 成都 610059）

摘 要：成都理工大学应用化学专业依托学校地质学科优势和西部矿产资源优势，形成了鲜明的分析特色，特别是针对岩石矿物等无机复杂物质系统分析的特色，阐述了成都理工大学分析特色的应用化学专业立体多维实践教学模式。该模式从实践内容和模式、实践过程、实践考核方式多方面进行构建，是培养学生具有超强动手能力、创新能力以及解决实际问题能力的保障。

关键词：分析特色；应用化学；多维化实践教学

中图分类号：G642.0 **文献标识码**：B **文章编号**：1002-4956(2016)9-0151-04

Construction of multi-dimensional practical teaching system with characteristics of analysis for Applied Chemistry specialty

Zhu Xiaping, Hu Xiaorong, Sun Yonghua, Zhou Li

(College of Materials and Chemistry & Chemical Engineering, Chengdu University of Technology, Chengdu 610059, China)

Abstract: The Applied Chemistry specialty of Chengdu University of Technology relies on the advantages of geological disciplinary in our university and mineral resources in western China, and has formed the distinctive analytical charateristics, especially analysis for rocks and minerals with complex matrix. The stereoscopic and multi-dimensional practical teaching system of applied chemistry with characteristics of analysis has been described. The system includes practical content and mode, the practical process, and the practical assessment. It can cultivate the ability of practical manipulative ability, innovative ability and the ability of solving realistic problems of students.

Key words: characteristic of analysis; applied chemistry; multi-dimensional practical teaching

第 13 届全国大学化学教学研讨会于 2015 年 10 月 30 日—11 月 1 日在湖北武汉举行，强调“以开放思维深化教学改革，进一步提高大学化学教学质量，推进大学化学教育的可持续发展”[1]。陕西师范大学房喻教授认为当今化学课程体系存在的重大问题之一，是不同学校化学专业课程结构雷同、内容相似，缺乏特色[2]。成都理工大学应用化学专业始建于 1959 年原成都地质学院二系开办的岩石矿物分析专业，随着学科的发展和社会的需要相继更名为工业分析和现在的“应用化学”。现阶段，“应用化学”专业人才培养核心内容和目标是以岩石矿物分析为专业特色，以化学和化工基础理论学习、岩石矿物分析专业技能训练及综合素质培养为核心内容，为国家地质矿产资源勘查和利用、环境监测与保护、食品药品安全监督等领域培养具有系统基础理论知识和实践能力的应用研究型人才[3]。办学 50 多年来，该专业依托成都理工大学地质学科优势和西部矿产资源优势，形成了鲜明的分析特色，特别是针对岩石矿物等无机复杂物质系统分析的特色。该专业本科毕业生实际就业率历年都在 95%以上，从事分析测试工作的学生比例基本都在 80%以上。本专业毕业的学生遍及全国的地质矿产和冶金地质部门的中心实验室、质检部门、食品药品检测部门、各种化工企业及下属单位，其中一大批毕业生成长为业务领导和分析测试专家或技术骨干。应用化学专业的学生在分析方面超强的动手能力得益于我校办学 60 年的经验积累。实践教学在创新型人才培养中占有重要的地位，是培养学生实践能力、创新能力和综合

收稿日期：2016-03-17 修改日期：2016-05-04

基金项目：四川省高等教育人才培养质量和教学改革重点项目（13JGZ13）

作者简介：朱霞萍（1968—），女，江西萍乡，博士，教授，主要从事分析化学教学和科研工作.

E-mail：zhuxiaping@cdut.edu.cn

素质的重要教学手段[4-6]。为培养学生的动手能力、创新能力以及解决实际问题的能力，我们狠抓实践教学，构建了一套立体多维化的实践教学体系，主要包括实践内容和模式、实践过程以及实践成绩考核的多维化。

1 实践内容和模式的多维化

实践内容和模式的设定首要考虑巩固理论知识。为了提高学生的兴趣，使实验内容与时俱进，解决实际问题具有重要的意义[7]。在此基础上，实践内容呈现从验证性实验到综合性实验，然后到设计性、创新性实验的维度变化，分析试样中待测组分的含量从常量到微量，再到痕量的维度变化；实践模式从基础课程实验到专业课程实验，再到生产实习，最后是毕业设计的维度变化。具体安排见表 1。

表 1 应用化学专业实验安排情况表(部分)

实验类型	实验名称	分析类型	实践模式
验证性	分析天平称量练习	—	基础课
	酸碱滴定练习	—	基础课
	EDTA 浓度的标定	常量	基础课
	胆矾中铜含量的测定(间接碘量法)	常量	基础课
	邻二氮菲吸光光度法测定水体中铁	微量	基础课
	原子吸收测定自来水中钾	微量	基础课
	……		
综合性	工业碱中总碱度和各分量连续测定(双指示剂法)	常量	基础课
	铁矿石中全铁含量的测定(样品消解，氧化还原滴定)	微量	基础课
	自来水总硬度和钙镁分量的连续测定(络合滴定法)	常量	基础课
	土壤中铅、汞、镉的测定(样品消解，原子荧光测定)	痕量	专业课
	聚羧酸减水剂的合成，表征(有机合成，元素定量分析，红外光谱、气相色谱-质谱结构分析)	—	专业课
	……		
设计性	Bi^{3+} 和 Fe^{3+} 混合溶液中各组分的分别测定	常量	生产实习
	HCOOH 和 CH_3COOH 混合溶液中各组分的分别测定	常量	生产实习
	自然水体水质全分析(色度、浊度、酸碱度、化学需氧量、油污、Cr、Cd、Pd、Ca、Mg)	常量-微量-痕量	生产实习
	水泥、岩石矿物全分析(K、Na、Ca、Mg、Fe(Ⅱ，Ⅲ)、Al、Ti、Mn、Si、S、P、烧失量)	常量-微量-痕量	生产实习
	……		
设计性	成都东郊稻田土-水界面上痕量铅、铬、镉的季节性分布研究	痕量	毕业实习
	巯基改性膨润土的制备及对水体中镉的吸附去除研究	—	毕业实习
	离子交换纤维分离富集-原子吸收测定钒钛磁铁矿中镓	痕量	毕业实习
	光催化可视化检测痕量 Hg^{2+} 的研究	痕量	毕业实习
	基于紫外光诱导化学蒸气发生原子荧光法的硒形态分析方法	痕量	毕业实习
	……		

在基础课里主要安排一些经典的、简单的、验证性的实验，分析试样大小以常量分析和微量分析为主。基础课程实验阶段主要任务是端正学生的实验态度，规范正确的实验操作，培养良好的实验习惯。

进入到专业课实验，增加综合性实验的比重，增加微量分析和痕量分析实验的比重。综合性实验主要强化学生综合实验能力的培养，因此对理论知识的要求较基础性实验要高。在这个阶段，我校最大的特色是针对应用化学专业的专业课(岩石矿物分析，环境分析，有机分析，食品药品分析，有机试剂在分析中的应用，产品质量检验，化学计量学)，专门设置了应用化学专业实验课程，一方面避免不同专业课实验内容的重复，另一方面又根据专业课的特点设定具有一定系统性和综合性的实验。例如实验“聚羧酸减水剂的合成、表征”，第 1 次实验安排 6 学时进行烯丙基聚氧乙烯醚聚羧酸减水剂的合成，第 2 次实验安排 4 学时进行合成产品的分离纯化和 C、H、N、S 元素分析，第 3 次实验安排 4 学时进行合成产品的结构分析(红外光谱和质谱)。在这 14 学时的实验中，学生学习有机合成及分离纯化的玻璃仪器的使用、有机合成操作以及元素分析仪、红外光谱仪、气相色谱-质谱仪的工作原理和使用，学习有机化合物的波谱解析，了解一个化学产品如何从原材料制备到监控产品质量、分析产品结构的过程。该实验涉及到有机化学、分析化学的基础理论知识，涵盖了有机化学、分析化学、仪器分析、有机分析、产品质量检验等课程的专业知识。

进一步的实践模式是生产实习，安排的时间是连续 6 周，一部分学生直接进入到与我校签订产学研协议的实际生产单位实习，一部分学生在校内实习。生产实习的内容更具有综合性和设计性，例如“岩石矿物样品全分析”，分析的内容包括 K、Na、Ca、Mg、Fe(Ⅱ，Ⅲ)、Al、Ti、Mn、Si、S、P、烧失量等 13 个项目。该实验的特色是样品基体复杂、实验项目多、每个实验项目

可供选择的方法也多。这是个综合性和设计性的实验项目，学生在设计实验方案时，需要综合各门课程的专业知识，选择合适的样品前处理方式，根据样品基体情况、共存组分的干扰情况，确定各个组分的测定方法。在实验过程中，必须严格遵守各步骤的规范操作，大胆细致。在结果处理阶段，要综合考虑实验中的误差及误差传递的问题。生产实习无疑可以很好地锻炼和考验学生的规范操作，提高学生发现问题、分析问题、解决问题的能力。

毕业前最后一个阶段的实践是毕业实习，安排的时间是 16 周，一般有 10％学生进入到自己联系的生产单位去学习，大部分学生的实习是在校内进行。这个阶段的实践内容除了具有综合性、设计性外，还具有明显的创新性。创新性实验既能保证本科生基本技能的培养，也能扩展到研究层面，进行科学研究的训练和创新实践能力的培养[8]。例如“成都东郊稻田土—水界面上痕量铅、铬、镉的季节性分布研究”：首先，学生需要围绕题目查找资料、了解成都东郊水稻土基本情况、稻田土—水界面基本情况，及铅、铬、镉的测定方法等研究背景，涉及的知识很广泛，学生要学会去伪存真，有选择地吸收接纳；其次，自主设计实验方案，在教师指导下，综合整个本科阶段学习的知识，提出解决实际问题的方案；最后按照设计的实验方案进行实验，在实验中修正方案，得出最终的结论。这个过程对学生来说既是整个大学阶段的一个考核，也是一次全面的能力提升过程，除了前面的实践提到的巩固知识、规范操作、分析问题等外，也进行了规范性科技论文写作能力的锻炼。

2 实践过程的多维化

第一种实践方式是学生按照教材要求独立完成实验内容，基础课和专业课实验基本属于这个范畴。过程包括学生实验前预习、课堂演示、学生独立完成实验、实验结果讨论以及实验报告的撰写。很多学生在思想深处认为实验是理论课的附属，刚开始抱着应付、混学分的学习态度。要纠正学生的这种态度，首先要从预习抓起。实验学时很有限，为了达到最佳的实验效果，实验课的课前预习就不能成一种形式，而是要充分熟悉实验原理、实验操作。对于课程实验，在理论课堂上就布置实验预习内容，实验前检查预习报告。课堂演示是实验，特别是普通化学实验不能缺少的，实验媒体是任何其他媒体所取代不了的，实验是最直接、最生动的媒体，化学教师不能舍本逐末，放弃课堂演示实验。所以每次实验前，授课教师必须细心地演示实验操作要点，有时候也叫学生上台演示，由台下学生指出正确与否，如果不正确，错在哪里，如何纠正。这样可使学生在课堂上集中精力。实验在教师指导下，尽量以独立操作为主。实验过程实行研究生辅助指导的方式，使实验指导师生比大于 1∶10，这样每个学生的操作都在教师的指导和监督之下。实验完成后要进行实验结果处理和讨论。对于基础课和专业课，要求实验报告撰写也在课堂中完成，经教师批改后该课程才算结束。这样操作对教师而言可能要稍微延长一些工作时间，但实际意义却很大。教师可以当面指出学生实验中存在的问题，及时指导学生改正错误，同时也促进了师生之间的交流互动。

第二种是通过学校课程网站、电话、邮件、聊天平台（QQ，微信）进行的翻转课堂实践模式[9-10]。成都理工大学校园网站上有实践课程简介、课程内容、实验操作视频等，也有部分虚拟实验，可为学生动态演示仪器的内部结构及操作步骤，学生通过人工交互虚拟操作模拟实验过程，熟悉正确的操作方法以及注意事项。学生在学习过程中遇到问题，通过上述方式与教师交流。比如，我们现在每上一门课会针对这门课程建立一个 QQ 群[11-12]。在开始视频教学之前，教师将课程视频、辅导资料和思考题上传到群共享，学生根据个人学习进程下载合适的资料进行学习。教师通过群视频和群签到了解学生是否进入了视频课堂，检查学生的学习情况。最重要的是让学生主动参与，由学生带动课程进程。交流模式有教师发言、学生自由发言等。

第三种实践方式是自主设计并完成实验，教师只是“提出问题，布置任务”。在生产实习中，针对实验内容，指导教师提供样品的种类、样品中的待测物质及待测物质的大致含量。学生自主查资料设计实验方案，学校提供方案所需要的药品，由学生自主配制所需药品，按照实验方案实施并完成实验。例如“Bi^{3+} 和 Fe^{3+} 混合溶液中各组分的分别测定”，教师给出的信息是测定混合溶液中 Bi^{3+} 和 Fe^{3+}，浓度大致为 0.1mol/L，硝酸介质，介质酸度为 pH 0.5。学生选择的实验方法有很多种，可以络合滴定测定总量，三价铁还原后测定分量；也可以先测定总量，光度法测定铁分量。可以选择直接滴定，也可以返滴定。例如“自然水体水质全分析”，教师提供自然水样，给出测定项目包括色度、浊度、酸碱度、化学需氧量、油污、Cr、Cd、Pd、Ca、Mg，并给出各项目大致含量范围。学生根据所学基本知识设计样品消解方式，设计各个项目的测定方法。一般这种综合性、系统性极强的项目很少能一遍做好，在学生完成第一遍实验后，教师小范围组织学生讨论实验过程中出现的问题以及实验结果的准确度、精密度，总结实践经验，在讨论的基础上进行第 2 遍、第 3 遍的实验。在毕业实习阶段，会开展涉及面更广、难度更大、独立性更强、与毕业后从事化学工作关系更

加紧密的研究型实验。研究型实验注重的是学生解决方案的能力以及对实验结果的整理能力。指导教师以1∶1.2的比例,根据自己的科研项目和实践中存在的问题拟定实习题目。学生首先根据自己的兴趣自主选题,然后根据所选研究内容查阅文献,了解国内外相关仪器、分析方法及研究内容的发展动态,在综合分析后,设计实验方案、进行开题报告,再根据确定的实验方案开展实验工作、实验总结、撰写毕业论文,最后进行毕业论文答辩,完成教师交代的任务。这种"以问题为核心、以任务为驱动"的实践教学模式能极大地锻炼学生独立思考问题及解决实际问题的能力。

3 实践成绩评定的多维化

对于实验课程,教师要有一套公平、合理、公开透明的评价体系,量化考核,使学生对自己或他人的实验成绩的高低有清晰的了解,促使学生重视实验课,认真地做好每一次实验。

实验考核的项目有预习报告、实验操作、实验原始记录、实验结果、实验讨论、实验报告。每次实验前教师和助课研究生要检查预习情况;实验中要在实验室巡视检查实验操作情况,及时纠正不正确的操作方式;实验结束后考核实验结果的准确度、精密度,检查针对实验过程和结果的讨论及实验报告。特别要强调两个方面的工作:一是原始实验数据的记录,实验数据必须真实、记录及修改要规范。对于任何一门课程实验,原始记录必须装订成册,在课程结束的最后一次实验要检查每一次实验的原始记录是否完整。二是实验报告必须以生产单位的检验报告为标准,为彰显实验数据的权威性,实验报告不能涂改。学生有完整的实验记录本,可以在实验记录本上完成实验数据的整理,实验报告只是把数据添上,出错的概率可以降到最小。对原始记录和实验报告的要求有利于培养学生诚实的科学态度、良好的实验习惯和严谨的工作态度。

4 结语

对于化学类学生,实践对于培养学生化学意识、动手能力,培养发现问题、观察问题、思考问题、解决问题的能力具有重要的意义。实践必须亲力亲为,没有任何其他学习方式可以取代。我校针对应用化学专业建立的立体多维化的实践模式,从实践内容和模式、实践过程以及实践考核方式多方面进行构建,多年来严格遵照模式中各项规定要求任课教师和学生。该模式是我校成功培养分析能力超强的应用化学学生的最大保障。

参考文献(References)

[1] 第13届全国大学化学教学研讨会组委会. 第13届全国大学化学教学研讨会纪要[J]. 大学化学,2015,30(6):1.

[2] 房喻. 化学学科发展与化学教育:挑战与机遇[J]. 中国大学教学,2009(9):13-15.

[3] 成都理工大学. 应用化学专业培养方案[Z]. 2014.

[4] 王丽梅. 基于创新性应用型人才培养的实验教学方法研究[J]. 实验技术与管理,2014,31(1):19-21.

[5] 郭栋才,詹拥共,旷亚非,等. 基于创新型人才培养的实践教学新体系的探索与实践[J]. 实验技术与管理,2013,30(11):141-143.

[6] 任伟宁. 地方高校实践教学队伍的建设[J]. 教育与职业,2012,29(5):53-55.

[7] 徐光宪. 对分析化学教学的两点初浅看法[J]. 大学化学,2008,23(2):1-10.

[8] 周锦兰,王宏,聂进. 多层次大学生创新实验平台的构建与实践[J]. 实验技术与管理,2011,28(4):16-19.

[9] Jerry Overmyer. Vodcasting and the Flipped Classroom[EB/OL]. <http://mast.unco.edu/programs/flipped/.

[10] Jonathan Bergmann, Aaron Sams. Flip your Classroom: Reach Every Student in Every Class Every Day [M]. Washington D C: International Society for Technology in Education, 2012.

[11] 钟志荣. 基于QQ群的网络学习共同体构建及其应用[J]. 中国电化教育,2011(8):92-95.

[12] 蔡佳璐. 黄荧倩. 叶伟东. 等. 基于QQ群的翻转课堂教学模式探索:以大学有机化学教学为例[J]. 大学化学,2015,30(6):7-12.

(上接第150页)

[5] 魏麒,方国娟,涂黎晖,等. MOOC平台和课堂相结合的教学模式探索:以非重点本科院校公共数学课为例[J]. 中国教育信息化,2014(13):13-15.

[6] 李曼丽,张羽,叶赋桂. 解码MOOC:大规模在线开放课程的教育学考察[M]. 北京:清华大学出版社,2013:136-151.

[7] 郎振红. 翻转课堂在Web程序开发实验教学中的应用研究[J]. 实验技术与管理,2016,33(2):151-154.

[8] 陈琳,陈耀华,张虹,等. 教育信息化走向智慧教育论[J]. 现代教育技术,2015,25(12):12-17.

[9] 祝智庭,刘名卓. 后MOOC时期的在线学习新样式[J]. 开放教育研究,2014(3):36-42.

[10] 胡小勇,李丽娟,郑晓丹. 在线环境下学习者协作解决问题的策略研究[J]. 中国电化教育,2015(1):44-49.

[11] 康叶钦. 在线教育的"后MOOC时代":SPOC解析[J]. 清华大学教育研究,2014(1):85-93.

[12] 苏小红,赵玲玲,叶麟. 基于MOOC+SPOC的混合式教学的探索与实践[J]. 中国大学教学,2015(7):60-65.

分析化学课程教学的精髓——量、度、新

朱霞萍 胡晓荣 孙永华 周 莉

（成都理工大学材料与化学化工学院，成都 610059）

[摘 要] 随着时代的发展，现代分析化学已经走出定性、定量分析的局限，进入一个新的阶段。“量”、“度”、“新”是分析化学课程教学的精髓，在教授学生分析化学基本原理、基本知识、基本技术的过程中，要好好把握“量”、“度”、“新”的输入。

[关键词] 分析化学；量；度；新

[中图分类号] G642.0 [文献标识码] A [文章编号] 2095-3437（2016）05-0104-02

我国化学前辈徐寿先生评价分析化学是“考质求数之学，乃格物之大端，而为化学之极致也”。考质求数即为定性、定量分析。随着时代的发展，现代分析化学已经走出定性、定量分析的局限，进入一个新的阶段。分析化学[1]是研究物质的组成和结构，确定物质在不同状态和演变过程中化学成分、含量、时空分布和相互作用的量测科学，旨在发展各种分析策略、原理和方法，研制各类器件、装置、仪器及相关软件，以获得物质组成和性质的时空变化规律。按照这个定义，分析化学是一门集研究分析方法、分析仪器、分析策略为一体的学科；同时，分析化学也是一门信息科学，分析化学工作者已不仅是单纯的分析数据提供者，而是有关化学信息的提供者、综合者和分析者，是解决实际问题的参与者。徐光宪先生[2]在全国分析化学学科人才培养与教学建设发展战略研讨会指出，21 世纪化学的核心任务已经演变为广义分子的合成化学和广义的分析化学，分析化学的应用领域已涉及生命科学、材料科学、信息科学、环境科学、资源和能源科学、医药和食品的检测、工业制造品的质量监控、毒品的分析监控、法医的鉴定等与人类生活息息相关的几乎所有方面。也正因为如此，分析化学是许多专业包括化学、化工、生物、医药、地质、能源、环境、材料、食品等的必修课程。为了把分析化学教学工作做好，很多同行进行了关于分析化学理论[3-7]、考试[8-9]、实践[10-12]等方面教学方法的探讨，提出了很多宝贵的建议。本人从事分析化学教学多年，教授过不同专业包括化学、应用化学、化学工程、制药工程、生物工程、环境监测、地球化学、核化工与核燃料的分析化学课程，针对不同的专业有不同的侧重点，但对不同的专业也有共性，即分析化学中关于“量、度、新”的阐述。

首先，在分析化学教学中注重“量”的概念的输入。定量分析是分析化学的基本任务。“量”的概念有三个方面的含义，首先就是准确定量。初级分析中使用量杯、烧杯、托盘天平；到了分析化学阶段就使用移液管、容量瓶、滴定管、分析天平，在滴定分析时注重 1 滴、半滴、1/4 滴溶液加入的变化；现在，分析化学进入分析科学阶段，取样量甚至是以微升、纳升计量。而待测组分的含量也从常量组分到微量组分，再到痕量、超痕量组分的分析，现阶段已经涉及单细胞、单分子、单原子分析。不管在哪个阶段，哪个层次，分析化学都讲究分析结果的准确定量。“量”的概念中第二方面含义是粗略估计物质的容量、质量，比如，对于 1 毫升、1 升、1 克、10 克……的容量和质量有大致的估算，对样品中组分含量、性质，以及含量和性质对分析测试信号的影响有粗略的估量。一个巧妇，能不经意地把一盘菜炒得口味合适，这是一种意识，而不是依赖看得见的某个具体数据；而分析化学中对物质的容量、质量、性质以及参数对分析信号的影响的粗略估量也需要经过长期、认真的实验体验才能培养出来。“量”的概念中第三方面含义就是精确表达分析结果，即注意实验结果的表达方式、误差的合理表达、有效数字的正确使用。实验结果的表达要符合实际情况。另外，真值是未知的，类似数学极限的概念。任何一个分析结果都存在或多或少的误差，正确地表达分析结果的误差很重要。结果表达中，有效数字位数的选择不同，误差的大小就不同，有效数字的取舍应根据给出的实验条件确定。在教学过程中注意把关于“量”的三个方面的含义准确地传授给学生，使其通过学习和实验，准确的了悟和把握分析化学中“量”的概念。

其次，在教学中注意培养学生对分析化学中的“度”的掌握。“度”即为衡量，在分析化学中意为分析。浅层次的“度”是指对物质进行测定，包括物质的定性、定量、结构分析；更深一层的含义是对测定结果的分析。也就是说，分析不仅仅是被动地提供物质的定性、定量、结构数

[收稿时间] 2015-10-22
[基金项目] 四川省高等教育人才培养质量和教学改革重点项目（13JGZ13）。
[作者简介] 朱霞萍（1968-），女，江西萍乡人，教授，博士，主要从事分析化学教学和科研工作。

据，分析工作者更要主动地提出问题、综合问题、分析问题，最终进一步解决问题。在给学生授课的时候，要让学生对分析化学“度”的更深层的意义即对分析结果的分析有深刻的认识。例如，针对某地区大米中镉超标的问题进行研究，不是简单地提供大米中镉的含量，而是为了解决问题，要针对整个课题做系统性研究。1.有代表性样品的采集：不仅采集稻米，还要采集与稻米息息相关的土壤、稻田水、空气等样品。2.测量所有样品中镉的含量及其他理化性质：不但要测定稻米、土壤、稻田水、空气中镉的总量，还要系统地测定不同深度土壤，空气中不同颗粒物的镉含量，测定稻田水、土壤、空气颗粒物中不同形态的镉含量。3.综合分析：讨论稻米中镉含量与土壤、稻田水、空气中总镉含量相关性如何，与土壤、空气颗粒物中不同形态镉的相关性如何，与土壤、稻田水其他理化性质的相关性如何，从而确定镉的来源，危害程度，迁移、转化状态，最后根据分析结果进一步提出降低稻米中镉含量的措施。这才是一个分析化学工作者针对这个课题该做的完整的工作。这样讲授分析化学中的“度”有利于学生充分认识到分析化学这门学科的任务、特点，拓展学生的思维尺度，提高学生综合分析问题、解决问题的能力。

最后，注重教学内容的出“新”。创新是任何一门学科的灵魂。在分析化学授课过程中，除了教授分析化学的基本原理和基本知识以外，还要注意补充本学科发展前沿的新理论、新方法和新技术。比如要做分析化学的信息化、智能化、微流控芯片化、在线化、实时化、原位化、仿生化、高灵敏化、高选择性化、高通量化、无损化等概念的介绍。在讲课中注意时效性例子的引入，比如，介绍 1999 年比利时布鲁塞尔发生的二恶英污染饲料事件，是分析化学家鉴定了二恶英的结构，从而拯救了比利时；介绍 2002 年诺贝尔化学奖的三位科学家都是因为率先建立了新的测定生物大分子的方法而获此殊荣；介绍 2009 年三位科学家因为各自独立的核糖体研究成果成为诺贝尔化学奖的获得者；还介绍生化武器、人类基因组工程的成就以及在医学研究、疾病诊断中的重要作用等。当然，这种“新”内容的引用要与所授课程的内容相联系才更容易被学生所接受，比如，在讲解分析结果表达方式时讲到物质中氮的测定结果可以以 NH_3，N_xO_y，N_2，N，蛋白质等方式表达，但是，2009 年发生的三鹿奶粉三聚氰胺事件就是由于分析奶粉中蛋白质含量时，以氮元素含量代替了蛋白质含量表示分析结果，被不法商家钻了空子引起的。所以，选择合适的分析方法，如何进行分析结果的表达一定要根据具体情况具体分析。俞汝勤院士[13]谈到现阶段国际国内分析化学改革的一些新动向时，就指出分析化学教育要作为解决实际问题的科学进行教授，要在教学中引入社会项目，引入时效性案例分析等。尹筱莉[14]在谈到化学老师有效利用教学资源时也强调要充分使教学内容新颖化、生活化。在讲授过程中引入与时俱进的实效性案例，一方面能极大提高学生学习分析化学的兴趣和积极性，另一方面能扩展学生视野，增强其社会责任感，提高学生综合素质。

总之，“量”、“度”、“新” 是分析化学课程教学的精髓，在教授学生掌握分析化学基本原理、基本知识、基本技术的过程中，要好好把握 “量”、“度”、“新”的输入。

[注 释]

[1] 庄乾坤，刘虎威，陈洪渊.分析化学学科前沿与展望 [M] .北京，科学出版社，2012：1-25.

[2] 徐光宪.对分析化学教学的两点初浅看法 [J] .大学化学，2008，23 (2)：1-10.

[3] 吴硕，刘志广，宿艳，等.分析化学“翻转课堂”的尝试与探讨 [J] .中国大学教学，2015 (1)：53-56.

[4] 樊铁波.分析化学课教学改革浅议 [J] .教育探索，2007 (5)：38-39.

[5] 黄丽英，杨宝华.浅谈高校化学教学中绿色化学理念的渗透 [J] .教育与职业，2012 (12)：131-132.

[6] 郭祥群. 浅谈课程教学核心知识与知识网络建构——以分析化学为例 [J] .中国大学教学，2009 (1)：32-35.

[7] 郭祥群.分析化学教学体系重构之思考 [J] .大学化学，2008 (5)：7-10.

[8] 吴性良.改革分析化学课程考核方法的实践 [J] .中山大学学报，2001 (1)：163-164.

[9] 萨木嘎，赵智宏.关于分析化学实验课程考试改革的设想 [J] .大学化学，1999 (3)：23-24.

[10] 姚思童，张进.分析化学实验教学改革与实践 [J] .大学化学，2010 (3)：23-27.

[11] 徐守芳，陆宏志.以科研促教学：新型分析方法在仪器分析教学中的体现 [J] .化学教育，2014 (2)：8-10.

[12] 王忠美.论高职学生分析化学实验能力的培养 [J] .中国成人教育，2008 (4)：156-157.

[13] 俞汝勤.漫谈分析化学教学改革与课程建设 [J] .大学化学，2008 (5)：1-6.

[14] 尹筱莉，孟凡丽.对化学教师有效利用教学资源的实践之评析 [J] .教育科学研究，2009 (1)：57-59.

[责任编辑 钟 岚]

附件 12 本科生优秀毕业论文证书

成都理工大學

百篇优秀学士学位论文（设计）证书

论文作者：朱映雪

指导教师：黄荣富

论文题目：双功能电化学发光纳米探针的性能研究

二〇一七年六月

成都理工大學

百篇优秀学士学位论文（设计）证书

论文作者：向小芳

指导教师：黄荣富

论文题目：纳米金粒径调控的表面增强电化学发光研究

二〇一六年六月

成都理工大學

百篇优秀学士学位论文（设计）证书

论文作者：许　艳

指导教师：胡晓荣

论文题目：基于川芎嗪-CuI超分子化合物荧光猝灭的微量银分析方法研究

二〇一六年六月

附件 13 教师获奖情况

成都理工大学2016年教学成果奖

获奖证书

获奖名称：以岩矿分析为特色的应化专业系列精品资源共享课程的建设

获 奖 者：郎春燕 胡晓荣 黄荣富 孙永华 朱霞萍

获奖等级：二等奖

二〇一六年七月二十五日

荣誉证书

李崇瑛 同志:

被评为成都理工大学 2015－2016 年

先进教务工作者

成都理工大学

二〇一七年一月十六日

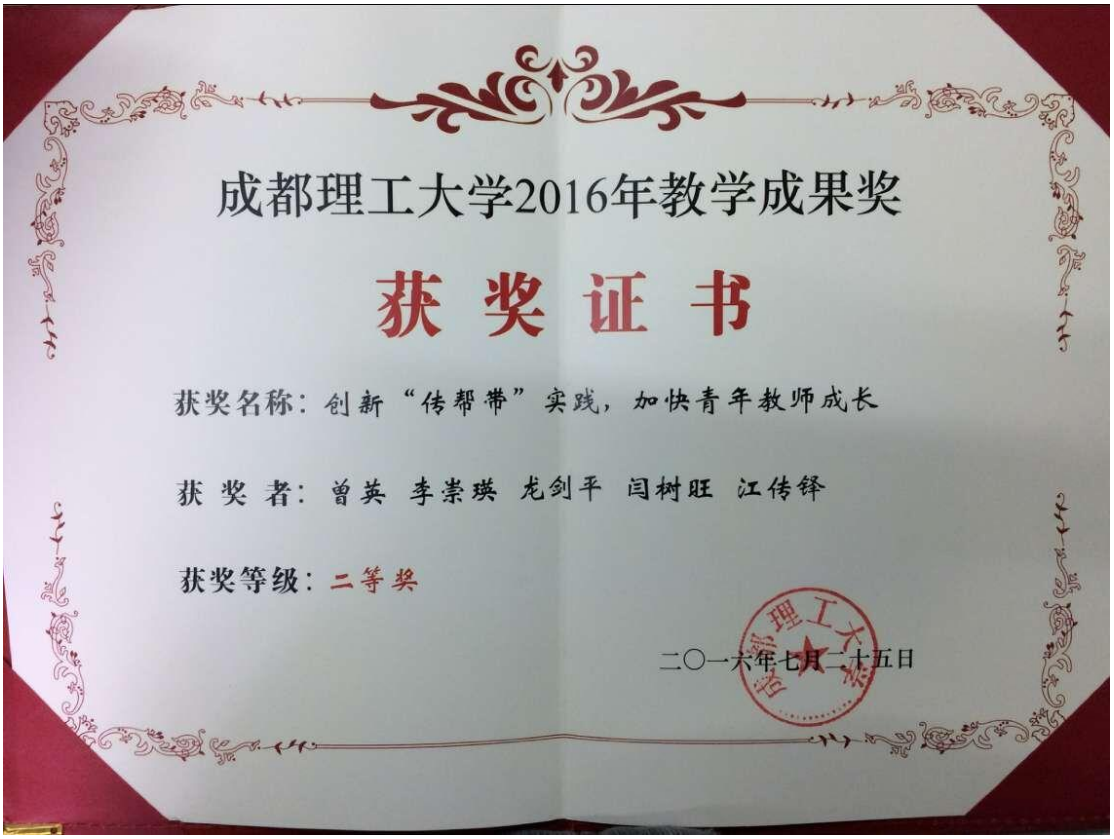

成都理工大学2016年教学成果奖

获奖证书

获奖名称：创新“传帮带”实践，加快青年教师成长

获 奖 者：曾英 李崇瑛 龙剑平 闫树旺 江传铎

获奖等级：二等奖

二〇一六年七月二十五日

来源：宣传部 教务处　作者：顾华宁　发布时间：2017-08-14 10:18:38　点击数量：1108

我校获批七门省级精品在线开放课程

日前，四川省教育厅下发了《关于公布第二批高等学校省级精品在线开放课程的通知》（川教函〔2017〕459 号），各高校共有260门课程被认定为省级精品在线开放课程。其中，我校七门课程名列其中。至此，我校已获批九门省级精品在线开放课程。

据了解，此次我校获批的七门省级精品在线开放课程分别是谭书敏教授负责的《形势与政策》，孙淑霞教授负责的《C/C++程序设计》，傅广海教授负责的《旅游学概论》，曾英教授负责的《化学工程原理》，郎春燕教授负责的《环境分析化学》，刘玉超副教授负责的《思想道德修养与法律基础》以及宋荣彩教授负责的《石油天然气地质学》。

在线开放课程是教育部和四川省在“十三五”期间重点建设的教学工程项目，是推动信息技术与教育教学深度融合，促进优质教育资源应用与共享，全面提升高校人才培养质量而采取的一项新举措。

新闻动态
政府信息
教育要闻
公示公告
视频新闻
市州区县动
高等学校动
基层学校动
教育纵深
教育信息化
教育厅文件
政策解读
人事任免
招考信息
办事服务
表格下载

[四川省教育网] >>公示公告 >>四川省教育厅关于对拟入选2015年度省级精品资源共享课进行公示的通知

四川省教育厅关于对拟入选2015年度省级精品资源共享课进行公示的通知

[四川教育网] [手机版本] [扫描] 发布时间：2015年12月2日 来源:

省内各高等学校：

根据《教育部关于国家精品开放课程建设的实施意见》（教高〔2011〕8号）和《四川省教育厅 四川省财政厅关于实施“高等教育质量工程”的意见》(川教〔2011〕149号)精神，我省启动了2015年度省级精品资源共享课建设工作。经学校申报，专家审核、评审，拟立项建设2015年度省级精品资源共享课187门，现将课程名单予以公示，公示期为2015年12月1日至2015年12月8日。公示期内，如对拟入选的2015年省级精品资源共享课有异议，请以书面形式向教育厅高等教育处反映。以单位名义反映问题的信件，须加盖本单位印章，并提供联系人及电话；以个人名义反映问题的信件，须签署本人真实姓名，并写明本人工作单位、通讯地址和联系电话。

高教处联系电话：028-86117120 。电子信箱：gaojiaochu508lx@163.com。地址：成都市青羊区陕西街26号，邮编：610041

附件：2015年度四川省省级精品资源共享课公示名单（排名不分先后）

附件

2015 年度四川省省级精品资源共享课公示名单

（排名不分先后）

序号	层次	学校	课程名称	课程负责人	学科门类	专业类
1	本科	成都东软学院	数据库原理与应用	余阳	工学	计算机科学与技术
2	本科	成都理工大学	环境分析化学	郎春燕	理学	化学类
3	本科	成都理工大学	单片微机原理及应用	周伟	工学	仪器类
4	本科	成都理工大学	大学计算机基础	孙淑霞	工学	计算机类
5	本科	成都理工大学	油层物理学	单钰铭	工学	矿业类
6	本科	成都师范学院	中学物理教学设计与实践	杨祖念	教育学	教育学类
7	本科	成都学院	出纳实务	胡世强	管理学	会计学
8	本科	成都学院	英语视听说	李萍	文学	外国语言文学
9	本科	成都医学院	医学遗传学	李亚	医学	基础医学
10	本科	成都中医药大学	药用植物学	严铸云	中药学	中药资源学
11	本科	成都中医药大学	内科护理学	高静	医学	护理学
12	本科	川北医学院	病理学	文彬	医学	基础医学
13	本科	电子科技大学	Physics I,II	吴昊	理学	物理学类
14	本科	电子科技大学	Calculus(微积分)	费铭岗	理学	数学类
15	本科	电子科技大学	电波传播	胡俊	工学	电子信息类
16	本科	电子科技大学	测量学	何彬彬	工学	测绘类
17	本科	电子科技大学	电力系统运行与控制	黄琦	工学	电气类
18	本科	电子科技大学	数字无线电系统基础	陈祝明	工学	电子信息类
19	本科	电子科技大学	信息系统开发与管理	汤志伟	管理学	管理科学与工程类
20	本科	电子科技大学	软件工程	吴磊	工学	计算机类
21	本科	电子科技大学	试验设计方法	何为	理学	化学类
22	本科	电子科技大学	职场英语	张文鹏	文学	外国语言文学类
23	本科	乐山师范学院	心理学	王立新	理学	心理学类
24	本科	乐山师范学院	大学信息技术基础	李林	工学	计算机类
25	本科	乐山师范学院	公共关系学	邓健	管理学	工商管理类
26	本科	乐山师范学院	物理化学实验	张元勤	理学	化学类

四川省教育厅

川教函〔2013〕895号

四川省教育厅关于公布

2013年四川省精品课资源共享课的通知

各高等学校:

按照《教育部关于国家精品开放课程建设的实施意见》（教高〔2011〕8号）和《教育部办公厅关于印发〈精品资源共享课建设工作实施办法〉的通知》（教高厅〔2012〕2号）要求，我厅组织开展了本年度省级精品资源共享课的申报、遴选工作。经各高校推荐、专家评审、网上公示、我厅审定，决定批准本年度精品资源共享课232门，其中包含2012年-2013年期间申报的国家级精品资源共享课97门，现予公布（名单见附件）。

一、所有批准立项的省级精品课程均应按照规定上网，取消登录用户名和密码，向所有高校师生免费开放。

二、各高校要高度重视精品资源共享课建设工作，要按照制定的建设计划逐步完善，及时了解、掌握课程教学内容的辐射效

果，收集、分析用户的反馈意见，统计课程网站的点击率，并接受我厅组织的年度检查和随机抽查。

三、各高校要重视“质量工程”的组织实施，进一步巩固教学工作的中心地位，严格按照承诺的经费额度投入并给予政策支持，推进优质资源的建设与共享，把精品资源共享课的建设、推广、应用、共享与教育创新结合起来，进一步推进教育教学改革，不断提高教学质量和办学水平。

四、未经著作权人许可，任何人不得将省级精品课程内容用作商业目的活动。

附件：2013年四川省省级精品资源共享课立项建设名单

四川省教育厅

2013年12月6日

附件

2013年四川省省级精品资源共享课立项建设名单

序号	单位	类型（本科、高职）	课程名称	所属专业类
1	四川大学	本科	现代生命科学基础	生物科学类
2	四川大学	本科	组织胚胎学	基础医学类
3	四川大学	本科	无机材料物理化学	材料类
4	四川大学	本科	内科学	临床医学与医学技术类
5	四川大学	本科	妇产科学	临床医学与医学技术类
6	四川大学	本科	外科护理学	临床医学与医学技术类
7	四川大学	本科	中国现代史	历史学类
8	四川大学	本科	遗传学	生物科学类
9	四川大学	本科	机械制造基础	机械类
10	四川大学	本科	药物化学	药学类
11	四川大学	本科	法医学	基础医学类
12	四川大学	本科	药用植物学	药学类
13	四川大学	本科	运筹学	管理科学与工程类
14	四川大学	本科	药理学	基础医学类
15	四川大学	本科	工程水文学	水利类
16	四川大学	本科	口腔材料学	口腔医学类
17	四川大学	本科	预防口腔医学	口腔医学类

序号	单位	类型（本科、高职）	课程名称	所属专业类
94	西南交通大学	本科	地下铁道	土木类
95	西南交通大学	本科	起重机金属结构	机械类
96	成都理工大学	本科	复杂物质分析	化工与制药类
97	成都理工大学	本科	现代工程制图	机械类
98	成都理工大学	本科	形势与政策	马克思主义理论类
99	成都理工大学	本科	电磁场与电磁波	电子信息类
100	成都理工大学	本科	石油与天然气地质学	地质类
101	成都理工大学	本科	工程地质分析原理	地质类
102	成都体育学院	本科	排球	教育学类
103	成都体育学院	本科	运动解剖学	教育学类
104	成都体育学院	本科	武术	教育学类
105	成都体育学院	本科	乒乓球	体育类
106	成都信息工程学院	本科	大学物理	物理学类
107	成都信息工程学院	本科	电路分析基础	电气类
108	成都信息工程学院	本科	地理信息系统原理	地理科学类
109	成都信息工程学院	本科	操作系统原理	计算机类
110	成都信息工程学院	本科	传感器与检测技术	仪器类
111	成都信息工程学院——银杏酒店管理学院	本科	酒店英语	旅游管理类
112	成都学院	本科	学前教育科学研究方法	教育学类

序号	单位	类型（本科、高职）	课程名称	所属专业类
227	四川航天职业技术学院	高职	平板电视原理与维修	电子信息类
228	四川航天职业技术学院	高职	资产评估与技能训练	财政金融类
229	四川化工职业技术学院	高职	大学生素质训练	公共基础课程类
230	四川化工职业技术学院	高职	流体输送与传热	化工技术类
231	宜宾职业技术学院	高职	PLC 控制系统组装与调试	自动化类
232	宜宾职业技术学院	高职	酿酒微生物	生物技术类

四川省教育厅办公室　　2013 年 12 月 12 日印发

成都理工大学教务处

教通字【2015】42 号（总第 247 号）

关于公布 2015 年校级精品资源共享课立项建设的通知

各学院：

根据《四川省教育厅办公室关于开展 2015 年高等学校省级精品资源共享课申报工作的通知(川教厅办函[2015]53 号)精神，学校组织了校级精品资源共享课的申报工作。经自愿申请，专家评审，决定将《原子及原子核物理》等 11 门课程作为校级精品资源共享课建设，具体名单详见附件。请各课程负责人按照精品资源共享课建设标准和课程建设目标任务做好建设工作，为申报省级及国家级精品资源共享课作好准备。

附件：校级精品资源共享课程名单

成都理工大学教务处

2015 年 12 月 30 日

附件：

2015 年校级精品资源共享课汇总表

序号	课程名称	负责人	所在学院
1	原子及原子核物理	郭江	地球物理学院
2	构造成矿学	钟康惠	地球科学学院
3	旅游规划与开发	李晓琴	旅游与城乡规划学院
4	传播学	吕辉	传播科学与艺术学院
5	语言艺术表现力	田力	传播科学与艺术学院
6	矿产资源勘查与开发	徐争启	地球科学学院
7	电磁学	何小燕	地球物理学院
8	地貌及第四纪地质学	孙书勤	环境与土木工程学院
9	电子系统设计	余小平	信息科学与技术学院
10	分析化学	胡晓荣	材料与化学化工学院
11	数据库程序设计	李思明	信息科学与技术学院

成都理工大学教务处

教通字【2016】29 号

关于2016年人才培养质量和教学改革项目立项的通知

各单位：

根据《关于组织申报2016年人才培养质量和教学改革项目的通知》（教通字〔2016〕5号）精神，经本人申请、学院推荐，学校组织专家评审，批准设立2016年人才培养质量和教学改革项目 62 项（见附件），现予以公布。

附件：

成都理工大学 2016 年人才培养质量和教学改革项目名单

教 务 处

2016 年 6 月 22 日

成都理工大学2016年人才培养质量和教学改革项目名单

序号	项目名称	项目类别	项目负责人	所在学院	项目编号
1	普通化学课程题库系统的构建	教学改革	李诚	材料与化学化工学院	201601
2	基于学生视角的沉积岩石学课程教学组织及考核方式的改革与实践	教学改革	林小兵	沉积院	201602
3	突出创新能力培养的古生物学实验教学改革与实践	教学改革	杨文光	沉积院	201603
4	“表演片段”课程中戏曲片段教学的探索与实践	教学改革	刘翼	传播科学与艺术学院	201604
5	科普信息化背景下广播电视学专业《科技新闻》课程群特色化建设的探索与实践	教学改革	沈丹	传播科学与艺术学院	201605
6	以创作促教学——“IP”影像时代下的戏剧影视文学专业实践课程建设研究	教学改革	赵晓	传播科学与艺术学院	201606
7	视觉传达设计专业毕业设计教学整合创新与实践研究	教学改革	吕南	传播科学与艺术学院	201607
8	勘技专业地质与地球物理综合实践能力培养---以马角坝实习为例	教学改革	张兵	地球物理学院	201608
9	核技术虚拟仿真实验教学平台建设与研究	教学改革	杨强	核技术与自动化工程学院	201609
10	地质与岩土工程虚拟仿真实验平台的构建与实践	教学改革	蔡国军	环境与土木工程学院	201610
11	基于微课的《材料力学》教学模式改革的探索与实践	教学改革	胡潇	环境与土木工程学院	201611
12	基于地学优势的固体废物资源化与处理处置课程教学的探索与实践	教学改革	韩智勇	环境与土木工程学院	201612
13	建筑结构实验课程一体化教学模式研究	教学改革	刘洋	环境与土木工程学院	201613
14	新形势下高校学生学籍异动原因及管理探析	教学改革	殷丽娟	教务处	201614
15	在校学生结构演化特征及预测分析	教学改革	李焓	教务处	201615
16	大学生创业现状、影响因素与创业教育体系构建研究	教学改革	程孝良	科技处	201616
17	《风景园林设计初步》课程空间设计能力培养模式研究	教学改革	赵印泉	旅游与城乡规划学院	201617
18	建筑学专业《建筑初步》课程与教学模式改革研究	教学改革	刘燕	旅游与城乡规划学院	201618
19	基于《城市地理信息系统》的学生空间分析能力培养模式研究	教学改革	倪忠云	旅游与城乡规划学院	201619

20	高校思想政治理论课“1+1”考核模式研究	教学改革	辜帆	马克思主义学院	201620
21	本科导师制育人模式创新研究	教学改革	吴仁明	马克思主义学院	201621
22	油矿生产实习优化及网络虚拟建构研究	教学改革	谢润成	能源学院	201622
23	石油地质及工程虚拟仿真平台建设及教学方法研究	教学改革	郑军	能源学院	201623
24	基于双创能力培养的经管类专业虚拟仿真综合实验教学平台构建与应用	教学改革	吴继	商学院	201624
25	“互联网+”背景下混合式学习中的大学生学习适应性研究	教学改革	何计蓉	商学院	201625
26	高校图书馆新技术体验服务研究及实践——以成都理工大学新图书馆为例	教学改革	王军	图书馆	201626
27	深化学科信息资源建设与服务，助力学校“双一流工程建设”	教学改革	曹 均	图书馆	201627
28	基于“项目运行”视角的社工专业人才培养模式研究	教学改革	李海梅	文法学院	201628
29	基于“第一原理”理论的创新型人才培养模式研究	教学改革	林凡强	信息科学与技术学院	201629
30	基于移动开发的半翻转式教学模式探讨	教学改革	刘恒	信息科学与技术学院	201630
31	基于计算机系列精品资源共享课程等资源实现重新学习课程在线学习与考试	教学改革	肖阳春	信息科学与技术学院	201631
32	“互联网＋”视角下的 VR 全景野外实践教学平台构建	教学改革	肖思和	宣传部	201632
33	《仪器分析》精品资源共享课程建设	课程建设	黄荣富	材料与化学化工学院	201633
34	《药物合成》精品资源共享课	课程建设	曾庆乐	材料与化学化工学院	201634
35	碎片化开放化学习在地质学实验教学中的探讨和实践	课程建设	徐冠立	地球科学学院	201635
36	矿产勘查地质学虚拟仿真实验教学的建设和研究	课程建设	张刚阳	地球科学学院	201636
37	《遥感数字图像处理》校级精品课程项目	课程建设	杨晓霞	地球科学学院	201637
38	构建基于“卓越计划”物理实验教学体系，强化学生实践创新能力	课程建设	赵秋瑭	地球物理学院	201638
39	基于移动平台的课程教学方法研究与实践	课程建设	张澎	地球物理学院	201639
40	《数值分析》精品资源共享课程建设与示范	课程建设	范安东	管理科学学院	201640
41	基于微课设计的《高等数学》精品资源共享课课程建设	课程建设	余海洋	管理科学学院	201641

成都理工大学教务处

教通字【2017】28 号

关于公布成都理工大学“十三五”本科规划教材立项的通知

各单位：

根据《关于申报成都理工大学“十三五”本科规划教材的通知》（教通字〔2017〕12 号）精神，经本人申请、学院推荐、学校组织专家评审，确定《普通地质学》等 35 本教材立项建设（见附件 1），现予以公布。根据学校经费安排及教材编写进度，2017 年资助《统计学》等 10 本教材（见附件 2），每本 2 万元，其余立项教材将根据下一年度经费预算进行资助。

附件：

1. 成都理工大学“十三五”本科规划教材立项名单
2. 成都理工大学“十三五”本科规划教材 2017 年资助名单

教 务 处

2017 年 10 月 11 日

附件 1：

成都理工大学“十三五”本科规划教材立项名单

序号	学院	教材名称	主编	职称
1	地球科学学院	普通地质学	陶晓风、吴德超	教授
2	商学院	统计学	刘后平	教授
3	核技术与自动化工程学院	单片微机原理及应用	周伟	副教授
4	法学院	社会问题概论	许传新	教授
5	管理科学学院	客户关系管理理论与应用（第 3 版）	李志刚	教授
6	旅游与城乡规划学院	城乡规划原理	何杰	教授
7	材料与化学化工学院	盐矿分析	郎春燕	教授
8	体育学院	大学体育.理论与基础	文烨	教授
9	材料与化学化工学院	分析质量保证与实验室认证	胡晓荣	教授
10	核技术与自动化工程学院	核测井原理及应用	周四春	教授
11	外国语学院	翻译技术教程	段成、张洁	教授
12	外国语学院	国学经典汉英对照选读教程	刘永志	教授
13	马克思主义学院	思想政治理论课实践教学指导（全套）	张春和	教授
14	管理科学学院	多元统计方法及其应用	魏友华	副教授
15	传播科学与艺术学院	戏剧表演本科教程	刘翼等	一级导演
16	材料与化学化工学院	普通化学	梁渠、李绛	教授
17	法学院	担保法	杨会	副教授
18	大学生创新创业中心	大学生创新创业基础	郭朝辉	教授
19	传播科学与艺术学院	科技新闻报道与写作	江昀等	教授
20	旅游与城乡规划学院	旅游学概论	傅广海	教授
21	核技术与自动化工程学院	可编程控制器原理及应用（简明教程）	王洪辉	副教授
22	材料与化学化工学院	仪器分析实验	黄荣富	副教授
23	商学院	证券投资分析	高辉	教授
24	能源学院	储层测井评价基础与应用	杨斌	教授

25	旅游与城乡规划学院	园林花卉栽培与应用学	周斯建	副教授
26	核技术与自动化工程学院	核环境工程基础	陆春海	教授
27	法学院	文科大学生科技创新教育	李奋生	教授
28	地球物理学院	勘查技术与工程专业英语（物探类）	吴朝容	副教授
29	商学院	国际市场营销	曾海	副教授
30	传播科学与艺术学院	互联网+文化创意类产业大学生创新创业教程	汤敏等	副教授
31	法学院	公共经济学	卢继宏	副教授
32	传播科学与艺术学院	声乐综合基础教程	张小燕等	教授
33	地球科学学院	高级岩矿鉴定与组构分析	倪志耀	教授
34	能源学院	石油工程地质学基础	傅恒	教授
35	法学院	公共管理（双语）	白秀银	副教授

附件 2：

成都理工大学“十三五”本科规划教材 2017 年资助名单

序号	学院	教材名称	主编	资助经费（万元）
1	商学院	统计学	刘后平	2
2	法学院	社会问题概论	许传新	2
3	材料与化学化工学院	盐矿分析	郎春燕	2
4	外国语学院	翻译技术教程	段成、张洁	2
5	马克思主义学院	思想政治理论课实践教学指导（全套）	张春和	2
6	旅游与城乡规划学院	旅游学概论	傅广海	2
7	核技术与自动化工程学院	可编程控制器原理及应用（简明教程）	王洪辉	2
8	商学院	证券投资分析	高辉	2
9	法学院	文科大学生科技创新教育	李奋生	2
10	商学院	国际市场营销	曾海	2

成都理工大学教务处文件

教通字【2013】48 号（总第 163 号）

关于 2013-2016 年高等教育人才培养质量和教学改革项目的立项通知

各单位：

根据《四川省教育厅关于 2013—2016 年高等教育人才培养质量和教学改革项目立项申报工作的通知》（川教函〔2013〕781 号）和学校《关于组织申报 2013—2016 年高等教育人才培养质量和教学改革项目的通知》（教通字〔2013〕39 号）的精神，经本人申请、学院推荐，学校组织专家评审，评选出 2013—2016 年校级高等教育人才培养质量和教学改革项目重点项目 20 项（附件 1）。经本人申请、学院评审，教务处复核，批准设立 2013—2016 年校级高等教育人才培养质量和教学改革项目一般项目 95 项（附件 2）。现予以公布。

附件：

1. 2013-2016 年校级高等教育人才培养质量和教学改革项目重点项目名单
2. 2013-2016 年校级高等教育人才培养质量和教学改革项目一般项目名单

教 务 处

2013 年 12 月 23 日

附件 1

2013-2016 年校级高等教育人才培养质量和教学改革项目重点项目名单

（按负责人姓氏笔画排序）

序号	项目名称	项目负责人	所在单位
1	英语专业学生自主学习能力培养模式创新	丁启红	外国语学院
2	公共体育课在理工类院校人才培养中新的探索与实践	文烨	体育学院
3	媒介融合时代传播艺术整合教学模式的创新与改革研究	刘迅	传播科学与艺术学院
4	以岩矿分析为特色的应用化学专业人才培养模式的构建与实践	朱霞萍	材料与化学化工学院
5	地质工程创新人才教育理念与实践	许强	环境与土木工程学院
6	石油地质综合实习虚拟网络教学结构体系研究	宋蓉彩	能源学院
7	思想政治理论课教学实效性的创新体系构建	张春和	政治学院
8	以文科本科生科研活动推动创新型人才培养的实践模式研究	李奋生	文法学院
9	高校智慧图书馆建设与创新型人才培养相结合的理念、路径与实践研究——以成都理工大学新图书馆建设为例	李勇	图书馆
10	以培养学生创新意识与创业能力为核心的大管理实践教学体系研究	李璞	管理学科学院
11	成都理工大学建筑学专业卓越人才培养模式构建与实践	杨尽	旅游与城乡规划学院
12	资源集成式实践教学互动平台体系研究	花海燕	商学院
13	机电类专业卓越工程人才培养模式改革与实践	陈光柱	核技术与自动化工程学院
14	“卓越计划”背景下资源勘查工程专业实践教学体系的建设与改革	陈翠华	地球科学学院
15	构建西部特色的土木工程专业探索与实践	赵其华	环境与土木工程学院
16	“三提一塑、通专结合”高素质人才培养路径研究与实践	倪师军	校长办公室、教务处
17	基于校内资源整合的财会专业实践教学模式研究	徐仕海	计划财务处、商学院
18	成都理工大学电子类基础课分级、进阶教学模式改革	郭勇	信息科学与技术学院
19	信息潮涌对大学生学习的影响与调控研究	曹俊兴	地球物理学院、教务处
20	高校基层党组织在人才培养中的保障机制研究	谭书敏	党委组织部

附件 2

2013-2016 年校级高等教育人才培养质量和教学改革项目一般项目名单

序号	项目名称	项目负责人	所在学院
1	探索数字化填图方法在马角坝实习中的应用与实现	赵德军	地球科学学院
2	以“虚拟校园”系统建设为载体的大学生创新实践平台建设	杨容浩	地球科学学院
3	半数字化地形测图实习方法研究与实践	余代俊	地球科学学院
4	基于“大地学”背景的《地图学》课程体系建设与改革	戴晓爱	地球科学学院
5	卓越工程师培养下生物工程综合实验教学体系的建设与改革	谢鸿观	材料与化学化工学院
6	“制药工程综合实验”实践教学体系的建设与改革	刘俊达	材料与化学化工学院
7	《仪器分析》课程内容和教学模式的改革与探索	李崇瑛	材料与化学化工学院
8	基于卓越计划的材料科学与工程专业实践教学体系建设	陈善华	材料与化学化工学院
9	理科综合化学实验课程体系建设	马晓艳	材料与化学化工学院
10	新层次大学化学教学质量保障体系建设	梁渠	材料与化学化工学院
11	基于工科力学互动式教学模式的研究和探索	罗艳	环境与土木工程学院
12	理论力学教辅教材建设研究与实践	任珊	环境与土木工程学院
13	市场主导下工程管理专业案例教学模式构建研究	敖仪斌	环境与土木工程学院
14	基于虚拟现实技术的实验教学模式研究及效果评价	王刚	环境与土木工程学院
15	适应当代水文地质学发展的教学方法探索	康小兵	环境与土木工程学院
16	基于卓越工程师计划培养的石油物探方向班的探索与实践	李琼	地球物理学院
17	基于教师科研平台的学生能力培养体系探索与实践	陆从德	地球物理学院
18	创新型人才培养过程中大学物理理论课程考核模式的探讨与研究	闫珉	地球物理学院
19	应用物理专业的实验创新教育体系探索	张传瑜	地球物理学院
20	大学物理课程研究型教学模式探讨和实践	程俭中	地球物理学院
21	核化工与核燃料工程专业建设	陆春海	核技术与自动化工程学院
22	机械工程专业实验教学体系的构建与创新	刘念聪	核技术与自动化工程学院
23	产品设计专业“可持续性设计”课程教学研究与实践	易姗姗	核技术与自动化工程学院

附件 15 学生获奖情况

荣誉证书

第二届“梅特勒-托利多”杯川渝地区大学生化学实验技能竞赛

团体二等奖

获奖学校：成都理工大学

获奖学生：袁伟、袁磊、吴倩

四川省化学化工学会

西南石油大学国家级化学化工实验教学示范中心

二〇一五年十二月五日

荣誉证书

第二届“梅特勒-托利多”杯川渝地区大学生化学实验技能竞赛

团体二等奖

获奖学校：成都理工大学

获奖学生：杨新明、王玥、游相清

四川省化学化工学会

西南石油大学国家级化学化工实验教学示范中心

二〇一五年十二月五日

荣誉证书

第二届“梅特勒-托利多”杯川渝地区大学生化学实验技能竞赛

团体三等奖

获奖学校：成都理工大学

获奖学生：刘天早、马志刚、张会会

四川省化学化工学会

西南石油大学国家级化学化工实验教学示范中心

二〇一五年十二月五日

杨素珍

2017年全国大学生英语竞赛（NECCS）

2017 National English Competition for College Students

获奖证书

CERTIFICATE OF AWARD

袁小雯 同学：

你在2017年全国大学生英语竞赛（NECCS）中，成绩优异，荣获 C 类二等奖。

特发此证，以示表彰。

You have obtained the ***Second Prize*** for Band_____ in 2017 National English Competition for College Students.

This certificate of commendation is hereby awarded to you as an encouragement.

高等学校大学外语教学指导委员会

二〇一七年五月十四日

Advisory Board for College Foreign Language Teaching

高等学校大学外语教学研究会

二〇一七年五月十四日

College English Teaching & Research Association of China

2017年全国大学生英语竞赛（NECCS）
2017 National English Competition for College Students

获奖证书
CERTIFICATE OF AWARD

陈江涛 同学：

你在2017年全国大学生英语竞赛（NECCS）中，成绩优异，荣获 C 类二等奖。

特发此证，以示表彰。

You have obtained the ***Second Prize*** for Band_____ in 2017 National English Competition for College Students.

This certificate of commendation is hereby awarded to you as an encouragement.

高等学校大学外语
教学指导委员会
二〇一七年五月十四日

Advisory Board for College Foreign Language Teaching

高等学校大学外语
教学研究会
二〇一七年五月十四日

College English Teaching & Research Association of China

证书编号：20170203041388
认证等级：高级认证

MATHMODEL

2017年第十届“认证杯”数学中国数学建模网络挑战赛

获 奖 证 书

学 生 营晟哲 罗仁威 胡孝林

成都理工大学 荣获

指导老师 无

第十届“认证杯”数学中国数学建模网络挑战赛

全国比赛第二阶段三等奖

内蒙古自治区数学学会

For and on behalf of
Globle Mathematical Modeling Certificate Authority
全球数学建模能力认证中心
Janma Beten
Authorized Signature(s)

比赛官网：http://www.tzmcm.cn/
证书查询网址：http://certificate.madio.net/

五粮液杯
2017
四川省第八届大学生艺术展演活动
THE EIGHTH COLLEGE STUDENTS' ART FESTIVAL OF SICHUAN PROVINCE

理想与信念
Ideals & beliefs

荣誉证书

冯晓蕾：

代表 **成都理工大学**

参加“五粮液杯”四川省第八届大学生艺术展演活动，

作品 **理工人之歌**

荣获

声乐 类 **普通** 组 **三等奖**

特发此证

以兹鼓励

THE EIGHTH COLLEGE STUDENTS' ART FESTIVAL OF SICHUAN PROVINCE

四川省教育厅

2017年8月26日

编号:20160015

跆拳道项目获奖证书

竞赛名称:2016年四川省大学生跆拳道联谊赛

竞赛项目:竞技女子组雏量级

姓名及单位:王　堃　成都理工大学

成　　绩:第一名

时间及地点:2016年5月7日 成都理工大学体育馆

四川跆协　世界武道联盟　高手会　四川跆拳道技术培训中心

四川省跆拳道协会官方网站
http://www.sctx.org.cn
请关注我
蜀道通

荣誉证书

成都理工大学　　蒋玉玲

身份证号码：51162119980520258x

积极响应环保部“加强生态环保，坚决打好'蓝天保卫战'”的号召，参加由我爱竞赛网、四川省生态文明促进会及全国百所高校组织联合主办的2017年大学生环保知识竞赛，成绩优秀，被评为优秀奖。

特发此证，以资鼓励！

我爱竞赛网 SAIJINGSAI.COM 比赛·公益·实践·机遇

四川省生态文明促进会

大学生环保知识竞赛组委会

二〇一七年四月

编号:HB209149525147

荣誉证书

成都理工大学　　袁小寒

身份证号码：511621199805080447

积极响应环保部“加强生态环保，坚决打好'蓝天保卫战'”的号召，参加由我爱竞赛网、四川省生态文明促进会及全国百所高校组织联合主办的2017年大学生环保知识竞赛，成绩优秀，被评为优秀奖。

特发此证，以资鼓励！

我爱竞赛网 比赛·公益·实践·机遇　四川省生态文明促进会

编号:HB399991368702

大学生环保知识竞赛组委会

二〇一七年四月


奖

荣誉证书

Certificate of honor

张腾收同学：

荣获成都理工大学思想政治理论课实践教学系列活动之

“青春中国”主题演讲比赛

三等奖

成都理工大学 党委宣传部

成都理工大学 教务处

成都理工大学 学生工作部(处)

共青团 成都理工大学委员会

成都理工大学 马克思主义学院

2017年5月3日

附件 15 本科生第一作者或第二作者（老师第一）发表论文

编号	论文（著）题目	作者	期刊名称、卷次
1	Label-free electrochemiluminescence assay for aqueous Hg^{2+} through oligonucleotide mediated assembly of gold nanoparticles	Dong-Mei Wang（王冬梅2017届）, Qi-Qi Gai（盖琦琪2016届）, Rong-fu Huang*	Biosensors and Bioelectronics 2017, 98, 134–139
2	A electro-thermal atomic absorption spectrometry-based assay for disease-related DNA	Xu, X.（徐雪梅 2013 届） Xiaorong Hu*	Microchemical Journal 2016, 126, 302-306.
3	A Both-End Blocked Peroxidase-Mimicking DNAzyme for Low-Background Chemiluminescent Sensing of miRNA	Xianming Li（李显明 2013 届）, Xinfeng Zhang (张信凤)	ACS sensors, 2017, 2, 810-816
4	In Situ generation and consumption of H_2O_2 by bienzyme-quantum dots bioconjugates for Improved chemiluminescence resonance energy transfer	Shuxia Xu（许淑霞), Xianming Li（李显明 2013 届）, Xinfeng Zhang (张信凤)	Analytical Chemistry, 2016, 88, 6418−6424
5	Cu-Mg-Al 层状超分子材料的制备及去除碘的研究	郑劫（2013 届） 朱霞萍*	功能材料, 2016, 47(9), 9231-6
6	聚乙二醇－硫酸铵－双水相萃取分光光度法测定地质物料中的镓	郑劫（2013 届） 朱霞萍	分析试验室, 2016，35(6): 629-632
7	丹参植株对亚硒酸钠和硒酸钠的吸收和积累	粟敏（2013 届），雷济华，杨帆，刘睿，胡晓荣*	中国科技论文 2017, 12(6): 647-651

Biosensors and Bioelectronics 98 (2017) 134–139

Contents lists available at ScienceDirect

Biosensors and Bioelectronics

journal homepage: www.elsevier.com/locate/bios

Label-free electrochemiluminescence assay for aqueous Hg^{2+} through oligonucleotide mediated assembly of gold nanoparticles

Dong-Mei Wang[a], Qi-Qi Gai[a], Rong-Fu Huang[a,*], Xingwang Zheng[b]

[a] College of Materials and Chemistry & Chemical Engineering, Chengdu University of Technology, Chengdu 610059, China
[b] Key Laboratory of Analytical Chemistry for Life Science of Shaanxi Province, School of Chemistry & Chemical Engineering, Shaanxi Normal University, Xi'an 710062, China

ARTICLE INFO

Keywords:
Label-free
Electrochemiluminescence
Hg^{2+}
Gold nanoparticles
Assembly

ABSTRACT

Development of ultrasensitive method for Hg^{2+} analysis is important for human health protection and environment monitoring. In this work, we present a highly sensitive and selective electrochemiluminescence (ECL) assay in a "turn-on" mode for the detection of Hg^{2+} through selective assembly of gold nanoparticles (AuNPs) on the surface of indium tin oxide (ITO) electrode. In the absence of Hg^{2+}, the nonthiolated ssDNA could protected AuNPs against its assembly on ITO surface, producing rather low ECL emission for $Ru(bpy)_3^{2+}$/TPA system. Conversely, binding of Hg^{2+} with the Hg^{2+}-specific oligonucleotide through thymine-Hg^{2+}-thymine coordination formed the double-stranded structure, which could not effectively adsorb to AuNPs in solution. The assembly of free-state AuNPs is achieved, which well preserves electronical conductivity. The presence of AuNPs can catalyze the electro-oxidation of TPA, producing significantly enhanced ECL signal. Through detecting the ECL signal mediated by assembly of AuNPs, the proposed method was able to ensure substantial signal amplification and a low background. It was demonstrated that the ECL intensity was correlated with the ssDNA-based recognition reaction, enabling quantitative analysis of Hg^{2+} over the range of 8 pM to 2 nM, with a detection limit of 2 pM. ECL intensity of the system were extremely specific for Hg^{2+} even in the presence of 1000-fold higher concentrations of other metal ions. Analytical results of Hg^{2+} spiked into water samples by the proposed ECL method were in good agreement with that obtained by atomic fluorescent spectrometry or mass spectrometry data.

1. Introduction

Mercury is a widespread heavy metallic contamination in the environment, which is coming from diverse anthropogenic and natural sources, such as coal and gold mining, fossil fuel combustion, chemical manufacturing, and so forth. Water-soluble mercuric ion (Hg^{2+}) is one of the most usual and stable form of mercury pollution. Hg^{2+} has lethal effects on human and ecosystem health. such as damaging the brain, heart, kidney and many other organs (Hoyle and Handy, 2005; Tchounwou et al., 2003). Moreover, Hg^{2+} can also be converted to more toxic methyl mercury and accumulates through food chain (Harris et al., 2003). Therefore, mercury species have been listed as a priority pollutant by many countries and international agencies (Leopold et al., 2010). Thus, the development of highly sensitive and selective method for environmental monitoring of mercury species is essential for risk assessment.

Until now, a numbers of traditional analytical methods for the detection of Hg^{2+} were proposed, including atomic absorption spectroscopy (AAS), atomic fluorescence spectrometry (AFS), inductively coupled plasma-mass spectrometry (ICP-MS). However, most of these approaches cannot be widely applied in routine monitoring of Hg^{2+} due to the tedious sample preparation, complicated or expensive instrumentation. To achieve this goal, the application of biosensor for detecting Hg^{2+} is a good choice, which combines the high selectivity provided by the biological recognition reactions and the high sensitivity of signal transduction techniques, including optical, electrochemical, piezoelectric, thermometric, etc (Huang and Guo, 2013). According to the reports, Hg^{2+} specifically interacts with the thymine-thymine (T-T) mismatch in DNA duplexes to form a T-Hg^{2+}-T complex, where the thymine residues bind to Hg^{2+} through the formation of N-Hg^{2+}-N bond (N3 of thymine) (Clever et al., 2007). It is found that the Hg^{2+} mediated T-Hg^{2+}-T pair is even more stable than the A-T pair (Miyake et al., 2006). This property has been widely employed to design DNA sensors for Hg^{2+} detection in aqueous solution (Gao et al., 2008; Jiang et al., 2009; Li et al., 2008; Miao et al., 2009; Zhang and Guo, 2012).

As a highly sensitive detection technique, electrochemilumines-

* Corresponding author.
E-mail address: huangrongfu13@cdut.cn (R.-F. Huang).

http://dx.doi.org/10.1016/j.bios.2017.06.054
Received 20 April 2017; Received in revised form 22 June 2017; Accepted 25 June 2017
Available online 28 June 2017
0956-5663/

cence (ECL) analysis has received considerable attention due to its simple instrument, versatility and robustness (Hu and Xu, 2010; Miao, 2008). As noted, ECL-based immunoassay have been successfully applied in the field of clinic diagnostics (Debad et al., 2004). The ECL biosensor for Hg^{2+} analysis using specific T-Hg^{2+}-T construction as recognition element has been widely reported, showing good analytical performance (Huang et al., 2015; Li et al., 2010; Ma et al., 2012; Tang et al., 2010; Yuan et al., 2011). For example, Ma et al. developed ECL sensor for Hg^{2+} analysis by introduction of the $Ru(bpy)_3^{2+}$ derivatives loaded on G4PAMAM dendrimer as ECL emitting species (Ma et al., 2012). The ECL labels can be attached to thymidine-riched oligonucleotide on electrode surface through the formation of T-Hg^{2+}-T complex, in which the detection of Hg^{2+} down to picomolar level was achieved. Additionally, the ECL sensor using dsDNA/emitters conjugates for signal transduction were also reported, such as $[Ru(bpy)_2dppz]^{2+}$ (dppz=dipyrido[3, 2-a: 2′, 3′-c] phenazine) or $Ru(phen)_3^{2+}$ (phen=phenanthroline) (Huang et al., 2015; Tang et al., 2010). Among these works, it is necessary to design the specific ECL emitting species to bind dsDNA-containing structure to achieve label-free analysis of Hg^{2+}. Additionally, the oligonucleotide as a recognition element should be immobilized on the surface of working electrode. The complicated operation procedures are time-consuming, which also affect the recognition ability for the Hg^{2+}-specific DNA probe. Therefore, it is desirable to develop a simple, label-free and immobilization-free method with high sensitivity and excellent selectivity for Hg^{2+} assay.

The interactions of citrate-capped gold nanoparticles (AuNPs) and nonthiolated DNA have been investigated for years (Li and Rothberg, 2004; Zhang et al., 2012a, 2012b). The formation of nonthiolated DNA functionalized AuNPs conjugates have enabled many new applications, including the development of novel biosensor (Wang et al., 2006), control of enzymatic reaction (Li et al., 2005) and synthesis of nanoparticle (Wang et al., 2010). It is found that the flexible single-stranded DNA (ssDNA) can partially uncoil its bases. The attractive van der Waals forces or specific chemical interactions between the bases and the AuNPs surface are sufficient to overcome an electrostatic barrier for adsorbing negatively charged DNA. Then, ssDNA was attached to the surface of AuNPs via DNA base adsorption, protecting AuNPs against salt-induced aggregation and increasing its stability in solution. However, it is not operative to the double-stranded DNA (dsDNA) due to its rigid double-helical structure, which does not permit the uncoiling needed to expose the bases. This will result in stronger repulsion and negligible bind of dsDNA to AuNPs surface. Based on the disparity in adsorption ability for ssDNA and dsDNA on AuNPs, a rapid identification assay for DNA sequence, ions and proteins has been extensively reported (Derbyshire et al., 2012; Tan et al., 2011; Wang et al., 2008). For instance, Yang's group developed an approach for visual and fluorescent sensing of Hg^{2+} in aqueous solution based on the Hg^{2+}-induced conformational change of a thymine (T)-rich ssDNA and the difference in electrostatic affinity between ssDNA and dsDNA with gold nanoparticles (Wang et al., 2008). Recently, Li et al. have proposed a simple approach for the detection of microRNA sequence based on the differential adsorption ability for nucleic acids onto AuNPs, in which the voltammetric signal was mediated by the selective preconcentration of AuNPs on a 1, 6-hexanedithiol blocked gold electrode (Li et al., 2016). Later, Cai et al. developed a label-free, immobilization-free and sensitive ECL strategy for Hg^{2+} assay in solution by taking advantage of differential adsorption ability on $Ru(bpy)_3^{2+}$ doped silica nanoparticle and the T-rich DNA probe recognition Hg^{2+} as the model (Cai et al., 2016). Inspired by these works, we present a novel “turn-on” ECL biosensor for Hg^{2+} analysis with high sensitivity and selectivity by exploiting the differences in the adsorption of ssDNA and Hg^{2+}-dependent dsDNA on AuNPs.

2. Experimental sections

2.1. Materials and Reagents

Indium-doped tin oxide film electrode (film thickness: 900 ± 100 Å, conductivity: 19 ± 2.1 Ω/□) was supplied by Weiguang Corp. (Shenzhen, China). Hydrogen tetrachloroaurate trihydrate ($HAuCl_4 \cdot 3H_2O$) and 3-mercaptopropyltriethoxysilane (MPTES), were purchased from J & K Scientific (Beijing, China). $Ru(bpy)_3Cl_2$ (bpy=2,2′-bipyrridine) and tripropylamine (TPA) were obtained from Aladdin (Shanghai, China). Hg^{2+} standard solution was purchased from national website for reference materials. The Hg^{2+} specific oligonucleotide (Sequences: 5′-TTCG TGTT GTGT TTCC AAA GGAT TCTC TACT CGTA-3′ (Huang et al., 2015)) was synthesized by Shanghai Sangon Biotechnology Co. Ltd. (Shanghai, China). According to Frens' method (Frens, 1973), a colloid solution of AuNPs with a diameter of 13 nm is prepared by the citrate reduction of $HAuCl_4$ method and the concentration of AuNPs in solution is calculated to be 4.4 nM. The other chemicals were from Kelong Reagent Corporation of Chengdu (Chengdu, China). All the reagents were of analytical-reagent grade without further purification and solutions were prepared using ultrapure water (18.3 MΩ cm). A concentration of 10 mM Tris-HCl solution (pH 7.4) was used to dissolve oligonucleotide.

2.2. Instruments

The ECL measurement was performed in 150 mM phosphate buffer solution (pH 7.4) containing 1 μM of $Ru(bpy)_3^{2+}$ and 50 mM of TPA on a CHI660E electrochemistry analyzer (Chenhua Co. Ltd., Shanghai) with a Pt counter electrode and an Ag/AgCl (3 M KCl) reference electrode. The collection of ECL light intensity was achieved by using an IFFL-D Flow-injection Luminescence Analyzer (Xi'an Remax Electronic Science Tech. Co. Ltd., Xi'an, China), in which the ECL cell was placed directly in front of the R456 photomultiplier (PMT). Scanning electron microscope (SEM) images were taken on a Hitachi model S4800 (Tokya, Japan).

2.3. Preparation of substrate electrode

ITO electrodes were pretreated as described before (Xu et al., 2001). In brief, ITO film electrode was cut into 2.5 cm × 0.5 cm size slices. To create hydroxyl group at its surface and eliminate organic contamination, the ITO slices were ultrasonically treated in a NaOH solution (5 M in methanol) for 30 min. After wash with water and dry in an oven at 100 °C, the cleaned ITO electrode reacted with 2% (V/V) MPTES in dry ethanol at room temperature overnight with gently shaking. After carefully washed with ethanol and water, the MPTES functionalized ITO electrode is denoted as ITO/MPTMS. The resulting electrode was characterized by cyclic voltammograms in the solution of 100 mM KCl with 1 mM potassium ferricyanide.

2.4. Procedure for Hg^{2+} detection

Hg^{2+} specific ssDNA was previously heated to 90 °C for 2 min and then allowed to cool to room temperature for 1 h before use. For Hg^{2+}detection, a 5 μL of Hg^{2+} solution (or blank buffer solution as control) was firstly mixed with 25 μL of Hg^{2+} specific oligonucleotide solution to incubate for 30 min at room temperature. Next, 70 μL of AuNPs solution was added in and allowed to react for 20 min. Subsequently, the assembly of AuNPs was achieved by casting a 10 μL of the above mixture solution to the surface of ITO/MPTES electrode on an area of about 0.25 cm × 0.25 cm, and reacting for 30 min. After careful wash with copious amount of water, the resulting electrode was measured in the mixture solution of $Ru(bpy)_3^{2+}$/TPA.

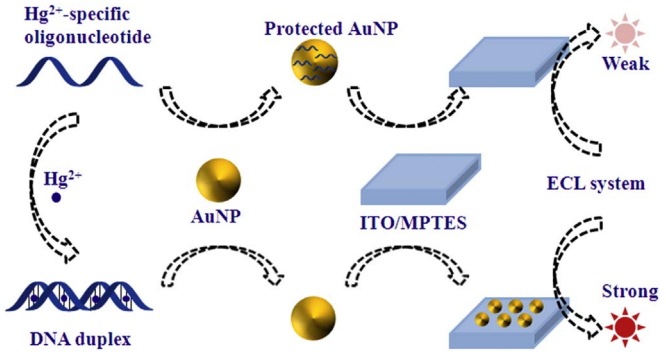

Scheme 1. Schematic diagram of the proposed method for electrochemiluminescence detection of Hg^{2+} by exploiting selective assembly of gold nanoparticles.

3. Results and discussion

In the proposed ECL strategy (Scheme 1), an ECL system sensitive to the attachment of AuNPs is selected, such as $Ru(bpy)_3^{2+}$ and its coreactant, TPA. According to the accepted ECL reaction mechanism (Miao and Choi, 2004), direct electro-oxidation of TPA plays a critical role in ECL signal generation, which is strongly dependent on the electrode materials, etc. For example, the oxidation activity of TPA on ITO electrode is extremely lower than that on metal (Au, Pt) and carbon (glass carbon) electrode, resulting in poor sensitivity for the detection of a trace amount of $Ru(bpy)_3^{2+}$. However, the preparation of metallic nanoparticles (e.g. AuNPs, PtNPs) modified ITO electrode can achieve high ECL activity, which catalyzes the electrochemical reaction of $Ru(bpy)_3^{2+}$/TPA. To more clearly observe deposition of AuNPs by ECL, an "ECL-inactive" ITO electrode was employed as substrate electrode, while the $Ru(bpy)_3^{2+}$/TPA system was selected as the signal reporters. In the absence of Hg^{2+}, the Hg^{2+}-specific oligonucleotide maintains a single-strand structure. Due to the formation of ssDNA protected AuNPs, ITO/MPTES electrode adsorbs very little AuNPs, resulting in low ECL response. However, in the presence of Hg^{2+}, a double helical DNA structure is formed through T-Hg^{2+}-T interactions, which facilitates the assembly of AuNPs on ITO surface. The presence of AuNPs can significantly enhance ECL signal for $Ru(bpy)_3^{2+}$/TPA system, leading to a Hg^{2+} concentration dependent enhancement of ECL response.

3.1. Interaction between AuNPs and Hg^{2+}-specific oligonucleotide probe

As shown in Fig. 1, the interactions of AuNPs with the Hg^{2+}-specific oligonucleotide probe with or without Hg^{2+} were studied by Uv–vis absorption spectra. We found a slight red-shift of 4 nm after oligonucleotide reacted with AuNPs (Curve a and b), indicating the formation of ssDNA protected AuNPs is well monodispersed (Photograph a' and b' In the absence of Hg^{2+}, the ssDNA protected AuNPs still kept a red color (Photograph c′) with a specific surface plasmon peak at 534 nm (Curve c) when 0.1 M NaCl was introduced. It could clearly be seen that there is no appreciable aggregation of these nanoparticles. This is because the adsorption of oligonucleotides can stabilize AuNPs against aggregation. If oligonucleotide previously reacted with Hg^{2+}, however, the mixture solution turned bluish violet immediately once adding in NaCl (Photograph d′). The adsorption peak at 520 nm decreased, red-shifted to 540 nm, and overlapped with the appearance of a new broad peak located at 634 nm (Curve d), indicating the aggregation of AuNPs. In our previous work, we found the a hairpin structure DNA was formed upon the binding of Hg^{2+} through thymine-Hg^{2+}-thymine coordination. Therefore, we infer that the formation of double helical structure in the presence of Hg^{2+} cannot effectively protected AuNPs against aggregation after addition of NaCl.

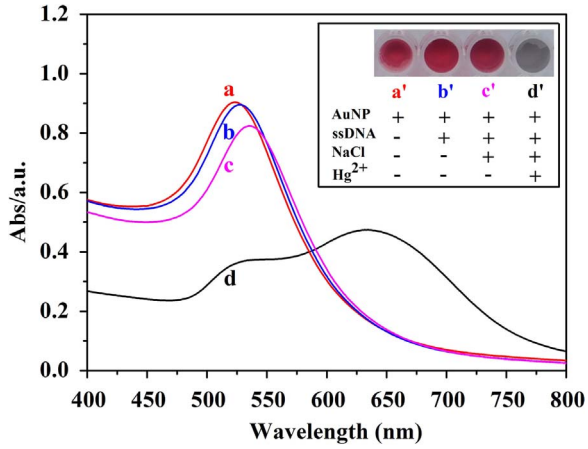

Fig. 1. Photographs and corresponding adsorption spectra of bare AuNPs or oligonucleotides protected AuNPs with or without Hg^{2+} against aggregation by adding salt.

3.2. SEM and electrochemical measurements of AuNPs on ITO electrode

To further confirm our design, a scanning electron microscope (SEM) was utilized to closely inspect the selective assembly of AuNPs. From Fig. S1, we observed the AuNPs in free state without both oligonucleotide and Hg^{2+} could be directly deposited on the surface of ITO electrode (A and B). The AuNPs with an average diameter of 13 nm were uniformly dispersed on the ITO surface and retained their original size and spherical shape. The results are similar to previous work (Huang et al., 2015). In the absence of Hg^{2+}, almost no AuNPs was found on ITO/MPTES surface after incubation with the oligonucleotide protected AuNPs (Fig. 2A). The appearance of small quantity of AuNPs on ITO/MPTES may be due to the unspecific adsorption or attachment of the AuNPs with uncovered surface at low concentration of oligonucleotide. In the presence of 1 nM Hg^{2+}, however, we found a monolayer of AuNPs were uniformly dispersed on the ITO surface and retained their original size and spherical shape (Fig. 2B). Adhesion of AuNPs to ITO is very strong and can withstand repeated rinse with water. Based on the particle number and diameter, the total surface area of gold is estimated to be about 0.061 cm^2 on 0.25 cm^2 ITO substrate. These phenomenon are well in accordance to our previous assumption, where the AuNPs in different states show varied adsorption ability.

Cyclic voltammograms (CVs) of the resulted bare ITO and AuNPs deposited ITO (ITO/AuNPs) electrodes obtained in 50 mM H_2SO_4 are shown in Fig. S2. No evident faradic current was observed at the bare ITO electrode. In contrast, the ITO/AuNPs electrode exhibited similar characteristic redox waves as a regular gold electrode, namely, an oxidation peak starting at ~1.12 V in the positive scan and a reduction peak at ~0.68 V in the reverse scan. The active surface area of the AuNPs of the ITO/AuNPs electrode was estimated based on the amount of charge consumed during the reduction of the gold surface oxide monolayer, and a reported value of 400 μC cm^{-2} was used for the calculation (Dai and Compton, 2006). From the reduction peak, the gold active surface area is 0.057 cm^2. This value is slightly smaller than the area estimated from the SEM image, suggesting that about 6.4% of the nanoparticles on ITO are electrochemically inactive. The partial loss of electrical activity for AuNPs can be explained by the formation of nonconductive organic film, resulting in a certain suppression of the charge transfer at the interface. Combining SEM images with voltammetric results, we testified that the formation of a double helical DNA structure through T-Hg^{2+}-T interactions facilitates ensured AuNPs in free state and allowed its assembly on ITO surface with well-preserved electronically conductive.

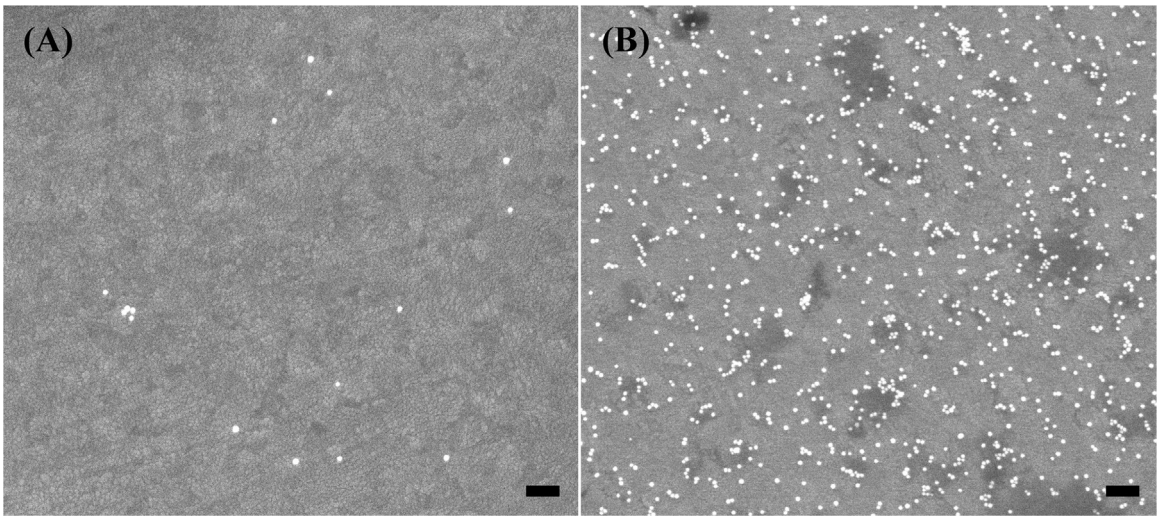

Fig. 2. SEM images of the ITO/MTPTES electrode after incubation in the mixture solution of AuNPs with oligonucleotides probe with (A) or without (B) 1 nM Hg^{2+}. Scale bar: 100 nm.

3.3. Hg^{2+}-dependent of AuNPs assembly on ITO electrode for ECL enhancement

Fig. 3 shows the ECL curve of proposed strategy to detect different concentration of Hg^{2+}. In the absence of Hg^{2+}, the resulted ITO electrode exhibited very low activity toward TPA oxidation. No faradic current was observed until the electrode potential reached ~1.05 V by the catalysis oxidation of TPA in the presence of $Ru(bpy)_3^{2+}$. The current increased gradually as further positive potential scan, while the direct electro-oxidation of TPA is beyond ca. 1.3 V (Inset, curve a). Correspondingly, the onset of luminescence occurs at ca. 1.1 V where $Ru(bpy)_3^{2+}$ gets oxidized. Light intensity keeps rising slowly with potential positive scan (Curve a). The voltammetric and electrochemiluminescent profiles of the resulted ITO electrode without Hg^{2+} are similar to that of a bare ITO electrode (Fig. S3a), indicating the absence of AuNPs, which is in accordance to previous SEM measurements and voltammetric response.

After adding in 1 nM Hg^{2+}, a broad irreversible anodic wave was primarily due to the direct oxidation of TPA, and the rather low concentration of $Ru(bpy)_3^{2+}$ on the CV is negligible. Apparently, electrochemical oxidation of TPA was facilitated significantly. In detail, the electro-oxidation current started to rise at about 0.65 V, which represented a negative shift of about 650 mV by comparison with that on the bare ITO electrode. The voltammetric current keeps rising with potential scan, and peaks at 1.1 V (Inset, curve d). Two ECL waves appeared at ca. 1.0 and 1.5 V (Curve d). The emission at higher potentials mainly followed the conventional ECL route where both $Ru(bpy)_3^{2+}$ and TPA were oxidized. Meanwhile, the electrode surface was oxidized too, leading to the formation of a surface oxide layer that suppressed TPA oxidation. For the first ECL peak, the low-oxidation-potential (LOP) signal around 1.0 V could be interpreted by a novel LOP ECL mechanism (Miao et al., 2002). The improved voltammetric and electrochemiluminescent behaviors can be attributed to the appearance of AuNPs with well-preserved electronically conductivity after Hg^{2+}-specific oligonucleotide probe interacted with Hg^{2+}. This was also confirmed by SEM (Fig. 2B) and electrochemical measurements (Fig. S2a). The ECL response is similar to that on an AuNPs modified ITO electrode, even incubation with a dsDNA solution (Fig. S3b and c). We also found that both voltammetric current and ECL intensity increased progressively with the addition of Hg^{2+}, resulting from a Hg^{2+} concentration dependent AuNPs deposition (Fig. 3, curve b→d). As noted, if a small amount of AuNPs are attached when adding in low concentration of Hg^{2+}, a significant enhancement in the ECL intensity as shown in Fig. 3 (curve a and b) can be observed, although no obvious change in the current is found (Fig. 3 inset, curve a and b). The results also reflected the higher ECL sensitivity than the voltammetric measurement.

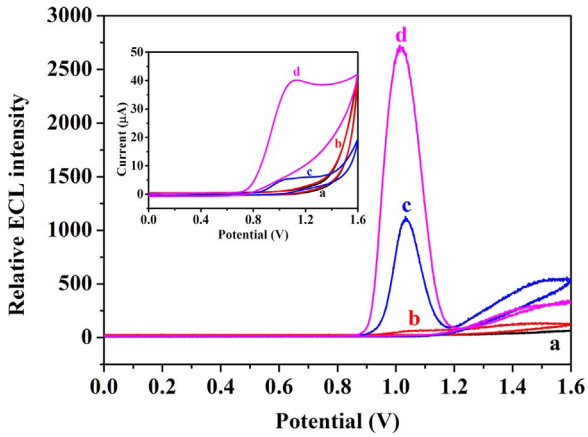

Fig. 3. ECL curves and voltammograms (inset) in 150 mM PB solution (pH 7.4) containing 1 μM $Ru(bpy)_3^{2+}$ and 0.05 M TPA at the ITO/MPTES electrode before (a) or after incubation with the mixture solution of AuNPs and oligonucleotide probe reacted with varying concentration of Hg^{2+} (0.1, 0.5 and 1 nM, curves b→d). Potential scan rate: 100 mV/s. Reference electrode: Ag/AgCl (3 M KCl).

3.4. Optimization of experimental conditions

3.4.1. Effects of molar ratio of oligonucleotide to AuNPs

As described in Scheme 1, we used the disparity in adsorption ability for single- and double-stranded oligonucleotide on citrate coated AuNPs suspended in solution to design a sensitive ECL assay for Hg^{2+}. The molar ratio of oligonucleotides to AuNPs would play an important role in current sensing strategy. To achieve higher sensitivity for quantifying Hg^{2+} inducing the conformational change of oligonucleotide, the Hg^{2+}-specific oligonucleotide was mixed with AuNPs solution at oligonucleotide/AuNPs molar ratio of 0.5, 1, 2, 3, 5, 10, 15 and 20 after addition to 100 pM Hg^{2+} solutions (Fig. S4). At low ratio, many of AuNPs are theoretically in free state, which can be attached on ITO surface and produce high ECL intensity as background. In addition to Hg^{2+} to liberate AuNPs to the free state, the increased attachment of AuNPs is limited, resulting in negligible ECL enhancement. When significantly increasing the ratio, the amount of oligonucleotide was much enough to protect against the immobilization of AuNPs. Under this condition, the small amount of Hg^{2+} cannot effectively change the AuNPs from protected state to free state, also leading to negligible ECL enhancement. As expected, we found both the

background and signal are high enough at low molar ratio, producing the low ratio of signal to background (S/B, closed to 1.0). The S/B ratio increased with the increasing molar ratio from 0.5 to 3 and reached a maximum at 3. Thereafter, it gradually decreased. At last, the ECL signal is as low as the background, while the S/B ratio is also calculated to be ca 1.0. Thus, the oligonucleotides/AuNPs ratio of 3 was selected for subsequent experiments, in which the concentrations of oligonucleotides and AuNPs are 5.4 nM and 1.8 nM, respectively.

3.4.2. Test conditions

According to the accepted ECL reaction mechanism for $Ru(bpy)_3^{2+}$/TPA, the relative contribution of the reaction routes to the formation of excited states and observed emission also depends on the relative concentrations of $Ru(bpy)_3^{2+}$ and TPA. To decrease the background and more clearly observe ECL enhancement, we employed lower concentrations of ECL reactants ($[Ru(bpy)_3^{2+}]$=1 μM and [TPA] =50 mM) in this experiment. At low concentration of $Ru(bpy)_3^{2+}$ and high concentration of TPA, the oxidation of TPA follows direct oxidation route, which is strongly dependent on the electrode materials. This would result in low background on ITO electrode and high signal amplification on AuNPs modified ITO electrode.

Next, the applied electrochemical parameters were investigated by compare multi-steps step with cyclic voltammeter (CV). It was found that the strongest ECL intensity was obtained when the multi-step mode was employed, while the formation of surface oxides significantly blocked the direct oxidation of TPA in CV mode. This mode was chosen in this work because of its higher sensitivity for the detection of Hg^{2+}. Meanwhile, the influence of the applied constant potential on the ECL intensity of the proposed strategy was investigated from +0.8 to +1.4 V, and the results are shown in Fig. S5. It can be seen that a much weak ECL signal on ITO substrate electrode can be detected below 1.0 V, which is attributed to the unspecific adsorption of AuNPs. The background increased gradually when low concentration of $Ru(bpy)_3^{2+}$ gets oxidized. Relatively, we found ECL signal on AuNPs assembled ITO electrode keeps rising when applied potential increased. However, the S/B ratio initially increases with increasing applied potential from +0.8 to +1.0 V, maximizes at about +1.0 V (S/B ca. 28), and decreased with further increase of the applied potential. This result can be attributed to the different ECL reaction mechanism for $Ru(bpy)_3^{2+}$/TPA system. In detail, ECL signal at the more negative potential related to the direct oxidation of TPA on the surface of AuNPs, while the electrocatalytic oxidation of TPA contributes more to the overall ECL intensity. To obtain high enough ECL intensity and S/B ratio, a constant potential of 1.0 V was eventually chosen in the following experiments (S/B ca. 28).

3.5. Analytical performance

To evaluate the sensitivity of the proposed assay, different concentration of Hg^{2+} from the stock solution were mixed with Hg^{2+} specific ssDNA probe solution and AuNPs solution to react for 30 min. The prepared mixture solution was then cast on ITO electrode for assembly process and next measured in the solution of $Ru(bpy)_3^{2+}$/TPA. We found that the ECL intensity initially increased upon increasing the Hg^{2+} concentration up to 10 nM, and then leveled off at higher Hg^{2+} concentrations. The plateau indicates saturation of Hg^{2+} binding sites to Hg^{2+} specific ssDNA probe. A linear relationship between the ECL intensity and the Hg^{2+} concentration over the range of 2 nM to 8 pM was shown in the insert of Fig. 4. The linear equation was I_{ECL} = 2.229C-8.181 (C: pM) with a linear correlation of r=0.9945. The relative standard deviation for 7 repetitive measurements of 200 pM was 7.2%. The detection limit ($3\sigma_{BL}$/S, where σ_{BL} is the standard deviation of the blank and S is the sensitivity) was calculated to be 2 pM, which met the requirement of U.S. Environmental Protection Agency (EPA) for Hg^{2+} in drinkable water. A satisfactory reproducibility of the proposed method is observed. To assess the selectivity of the proposed method, the ECL signal was measured in the presence of

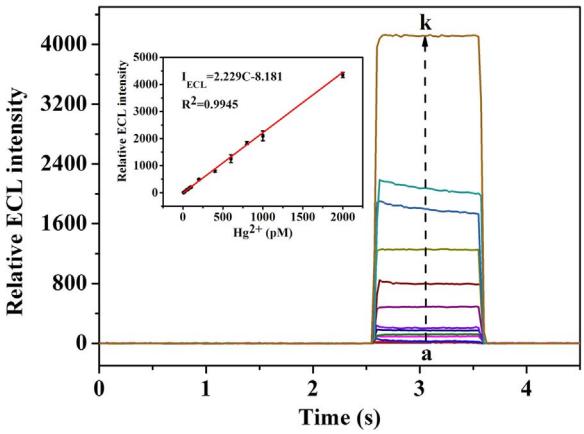

Fig. 4. ECL response of the proposed assay in the presence of Hg^{2+} (from a to m: 8, 10, 20, 40, 60, 80, 100, 200, 400, 600, 800, 1000, 2000 pM). Inset: linear relationship between ECL intensity and Hg^{2+} concentration. Applied potential: 1.0 V (vs. Ag/AgCl, 3 M KCl).

other metal ions (Ca^{2+}, Cd^{2+}, Co^{2+}, Cu^{2+}, Fe^{2+}, Mg^{2+}, Mn^{2+}, Pb^{2+}, Al^{3+}, Fe^{3+}). As shown in Fig. S6, even with 1000 times excess of another metal ion (200 nM versus 200 pM Hg^{2+}), the ECL response was substantially lower than that with Hg^{2+}. As we know, selective binding of Hg^{2+} to thymine-thymine (T-T) base pairs in DNA duplexes, which can reduce the influence of coexist metal ions (Ono and Togashi, 2004). Therefore, this excellent selectivity for the detection of Hg^{2+} can be attributed to highly specific interaction of T-Hg^{2+}-T, which led to the conformation change of Hg^{2+} specific oligonucleotides from linear chain to hairpin configuration.

3.6. Detection of Hg^{2+} in water samples

The application of the ECL assay was evaluated via the detection of Hg^{2+} in water samples collected from Yanhu Lake in campus, Chengdu University of Technology. The samples collected were filtered through 0.2 μm membrane to remove impurities, which were also measured by atomic fluorescence spectrometry (AFS) and ICP-MS methods. As shown in Table 1, the recoveries ranged from 88% to 107% for samples spiked with different amount of Hg^{2+}. The results were in good agreement with those obtained by AFS and ICP-MS, showing its potential practicality for environmental samples. The sensitivity of the proposed ECL assay is comparable to ICP-MS, which is much higher than AFS.

4. Conclusions

In summary, a novel ECL assay in “turn-on” mode was successfully applied to measure Hg^{2+} in environmental aqueous samples at picomolar level. This method depends on the differential adsorption of single-stranded and double-stranded oligonucleotide on AuNPs, where Hg^{2+} can induce its conformational change from linear chain to hairpin structure. Unlike commonly reported ECL system by direct deposition of AuNPs to catalyze ECL reaction, the most appealing characteristics of the proposed strategy is the target-dependent assembly of AuNPs for ECL enhancement. The change of electrode material is dependent on a bio-recognition reaction, leading to selectively turn on ECL emission. Without complicated chemical label procedures and immobilization of oligonucleotide probe, this strategy is much more convenient and low-cost, also showing high sensitivity and excellent selectivity. We believe this approach can be applied to other types of molecular probes by simply changing the sequences of the oligonucleotides to a specific target (e.g. detecting small molecules, and DNA hybridization, or probing of biomolecular interactions). These features establish the universality and simplicity of the platform and could,

Table 1
Detection of Hg^{2+} in aqueous samples by proposed method and comparison with AFS and ICP-MS.

Sample	Added (nM)	Detected by proposed method (nM)[a]	Recovery (%)	AFS (nM)[a]	ICP-MS (nM)[a]
Tap water	0	0.048 ± 0.011	N.A.[b]	N.A.	0.044 ± 0.013
	0.05	0.092 ± 0.021	88	N.A.	0.062 ± 0.017
	0.2	0.24 ± 0.015	96	N.A.	0.21 ± 0.041
Lake water	0	0.72 ± 0.06	N.A.	N.A.	0.68 ± 0.061
	2	2.77 ± 0.25	98	2.63 ± 0.32	2.73 ± 0.21
	4	4.98 ± 0.31	107	4.70 ± 0.13	4.79 ± 0.29

[a] Mean of three measurements with standard deviation.
[b] N.A.: Not available.

therefore, provide the groundwork for the design of design a new type of ECL sensor.

Acknowledgments

This work was supported by the National Natural Science Foundation of China (No. 21407013), and the Cultivating Program of Middle-aged Backbone Teachers in Chengdu University of Technology (KYGG201412).

Appendix A. Supplementary material

Supplementary data associated with this article can be found in the online version at doi:10.1016/j.bios.2017.06.054.

References

Cai, L., Guo, Z., Zheng, X., 2016. Microchim. Acta 183 (7), 2345–2351.
Clever, G.H., Kaul, C., Carell, T., 2007. Angew. Chem. Int. Ed. 46 (33), 6226–6236.
Dai, X., Compton, R.G., 2006. Anal. Sci. 22 (4), 567–570.
Debad, J.D., Glezer, E.N., Wohlstadter, J., Sigal, G.B., Leland, J.K., 2004. Clinical biological applications of ECL. In: Bard, A.J. (Ed.), Electrogenerated Chemiluminescence. Marcel Dekker Inc, New York, 359–396.
Derbyshire, N., White, S.J., Bunka, D.H., Song, L., Stead, S., Tarbin, J., Sharman, M., Zhou, D., Stockley, P.G., 2012. Anal. Chem. 84 (15), 6595–6602.
Frens, G., 1973. Nat. -Phys. Sci. 241 (105), 20–22.
Gao, X., Xing, G., Yang, Y., Shi, X., Liu, R., Chu, W., Jing, L., Zhao, F., Ye, C., Yuan, H., Fang, X., Wang, C., Zhao, Y., 2008. J. Am. Chem. Soc. 130 (29), 9190–9191.
Harris, H.H., Pickering, I.J., George, G.N., 2003. Science 301 (5637), 1203, (1203).
Hoyle, I., Handy, R.D., 2005. Aqua. Toxicol. 72 (1–2), 147–159.
Hu, L., Xu, G., 2010. Chem. Soc. Rev. 39 (8), 3275–3304.
Huang, R.-F., Liu, H.-X., Gai, Q.-Q., Liu, G.-J., Wei, Z., 2015. Biosens. Bioelectron. 71 (0), 194–199.
Huang, R., Guo, L.-H., 2013. Nanomaterial-based electrochemiluminescence biosensors. In: Li, J., Wu, N. (Eds.), Biosensors Based on Nanomaterials and Nanodevices. CRC Press, Boca Raton, 209–240.
Jiang, Z., Fan, Y., Chen, M., Liang, A., Liao, X., Wen, G., Shen, X., He, X., Pan, H., Jiang, H., 2009. Anal. Chem. 81 (13), 5439–5445.
Leopold, K., Foulkes, M., Worsfold, P., 2010. Anal. Chim. Acta 663 (2), 127–138.
Li, D., Wieckowska, A., Willner, I., 2008. Angew. Chem. Int. Ed. 47 (21), 3927–3931.
Li, H., Huang, J., Lv, J., An, H., Zhang, X., Zhang, Z., Fan, C., Hu, J., 2005. Angew. Chem. Int. Ed. 44 (32), 5100–5103.
Li, H., Rothberg, L., 2004. Proc. Natl. Acad. Sci. USA 101 (39), 14036–14039.
Li, Q., Zhou, X., Xing, D., 2010. Biosens. Bioelectron. 26 (2), 859–862.
Li, Y., Tian, R., Zheng, X., Huang, R., 2016. Anal. Chim. Acta 934, 59–65.
Ma, F., Zhang, Y., Qi, H., Gao, Q., Zhang, C., Miao, W., 2012. Biosens. Bioelectron. 32 (1), 37–42.
Miao, P., Liu, L., Li, Y., Li, G., 2009. Electrochem. Commun. 11 (10), 1904–1907.
Miao, W., 2008. Chem. Rev. 108 (7), 2506–2553.
Miao, W., Choi, J.-P., 2004. Coreactants. In: Bard, A.J. (Ed.), Electrogenerated Chemiluminescence. Marcel Dekker, New York, 213–271.
Miao, W., Choi, J., Bard, A., 2002. J. Am. Chem. Soc. 124 (48), 14478–14485.
Miyake, Y., Togashi, H., Tashiro, M., Yamaguchi, H., Oda, S., Kudo, M., Tanaka, Y., Kondo, Y., Sawa, R., Fujimoto, T., Machinami, T., Ono, A., 2006. J. Am. Chem. Soc. 128 (7), 2172–2173.
Ono, A., Togashi, H., 2004. Angew. Chem. Int. Ed. 43 (33), 4300–4302.
Tan, Y.N., Lee, K.H., Su, X., 2011. Anal. Chem. 83 (11), 4251–4257.
Tang, C.-X., Zhao, Y., He, X.-W., Yin, X.-B., 2010. Chem. Commun. 46 (47), 9022–9024.
Tchounwou, P.B., Ayensu, W.K., Ninashvili, N., Sutton, D., 2003. Environ. Toxicol. 18 (3), 149–175.
Wang, H., Wang, Y., Jin, J., Yang, R., 2008. Anal. Chem. 80 (23), 9021–9028.
Wang, L., Liu, X., Hu, X., Song, S., Fan, C., 2006. Chem. Commun. 36, 3780–3782.
Wang, Z., Zhang, J., Ekman, J.M., Kenis, P.J.A., Lu, Y., 2010. Nano Lett. 10 (5), 1886–1891.
Xu, J.Z., Zhu, J.J., Huang, Q., Chen, H.Y., 2001. Electrochem. Commun. 3 (11), 665–669.
Yuan, T., Liu, Z., Hu, L., Zhang, L., Xu, G., 2011. Chem. Commun. 47 (43), 11951–11953.
Zhang, B., Guo, L.-H., 2012. Biosens. Bioelectron. 37 (1), 112–115.
Zhang, X., Liu, B., Dave, N., Servos, M.R., Liu, J., 2012a. Langmuir 28 (49), 17053–17060.
Zhang, X., Servos, M.R., Liu, J., 2012b. Langmuir 28 (8), 3896–3902.

Microchemical Journal 126 (2016) 302–306

Contents lists available at ScienceDirect

Microchemical Journal

journal homepage: www.elsevier.com/locate/microc

A electro-thermal atomic absorption spectrometry-based assay for disease-related DNA

Xuemei Xu [a,b], Ying Gao [b], Shixi Zhang [c], Shuzhen Li [a], Ting Bai [a], Yue Zhang [a], Xiaorong Hu [a,*], Rui Liu [a,d,*]

[a] Collaborative Innovation Center for Comprehensive Utilization of Panxi Strategic Mineral Resources, College of Material Chemistry and Chemical Engineering, Chengdu University of Technology, Chengdu, Sichuan 610059, PR China
[b] College of Earth Sciences, Chengdu University of Technology, Chengdu, Sichuan 610059, PR China
[c] Beijing Key Laboratory for Microanalytical Methods and Instrumentation, Department of Chemistry, Tsinghua University, Beijing 100084, PR China
[d] College of Chemistry, Sichuan University, Chengdu 610064, PR China

ARTICLE INFO

Article history:
Received 2 December 2015
Received in revised form 15 December 2015
Accepted 18 December 2015
Available online 28 December 2015

Keywords:
Electro-thermal atomic absorption spectrometry (ETAAS)
DNA
Graphite furnace
Gold nanoparticles (Au NPs)
Element tagging
Inductively coupled plasma mass spectrometry (ICPMS)

ABSTRACT

Electro-thermal atomic absorption spectrometry (ETAAS) is a powerful element detector, thanks to its low cost, high sensitivity, multiple element detectability, and low sample consumption. In this work, a simple and sensitive DNA assay utilizing ETAAS detection was demonstrated with Au nanoparticles (NPs) tag. Ebola Virus (EV)-related DNA was detected by sandwich hybridization assay, using Au NPs-labeled reporter probes and magnetic microparticle (MMP)-labeled capture probes. The sandwich hybridization reaction conditions were optimized. After hybridization reaction, aqua regia was added to dissolve Au NPs and release Au ions, which were subsequently detected by ETAAS. A good linearity was obtained between the concentration of target DNA and the atomic absorbance signal intensity. The limit of detection (LOD) was 3 pM (LOD, 3σ), with the linear range of 10–200 pM (R = 0.9933). The relative standard deviation (RSD) for 20 pM target DNA was 1.07%. The target DNA results obtained by the proposed method correlated well with those obtained by inductively coupled plasma-based hybridization assay.

1. Introduction

Simple, sensitive, and quantitative determination of sequence-specific DNA is one of the central topics in biological science, forensic science, and clinical diagnosis [1]. The information of genetic mutations at molecular level provides an opportunity for diagnostics even before any symptom of a disease [2]. A large number of DNA detection systems based on the hybridization between a DNA target and its complementary probe have been described, such as colorimetric [3], fluorescent [4], chemiluminescent [5], and electrochemical [6] instruments. Among these, fluorescence-based techniques are most widely used. However, the inherent drawbacks such as sophisticated synthesis of fluorescent probes, photobleaching, and spectral overlap significantly limited their application in DNA quantification.

In recent years, element tagging-based biomolecules quantification has gained great attention by using atomic spectrometric detectors [7–14]. Metal atoms in element tags were directly detected, without the need of special characteristics such as fluorescent, chemiluminescent, electric, and electrochemical properties. This characteristic greatly alleviates the time- and labor-consuming work for the design and synthesis of element tags [15,16]. Recently, Zhu et al. [17] reported an Au nanoparticles (NPs)-based methodology for the detection of DNA by inductively coupled plasma atomic emission spectrometry (ICPAES), with a low detection limit of 350 pM. Zhang et al. [18] developed a multiplex nucleic acid assay by inductively coupled plasma mass spectrometry (ICPMS), without the need of complicated DNA chips. Fifteen clinical diseases (cancer, heredopathia, and virus) associated DNA targets were simultaneously detected with lanthanide element tags (i.e., Y, La, Ce, Pr, Nd, Sm, Eu, Gd, Tb, Dy, Ho, Er, Tm, Yb, and Lu). Furthermore, Au NPs, Ag NPs, and Pt NPs were utilized to acquire higher sensitivity for the determination of three DNA targets associated with clinical diseases (HIV, HAV, and HBV) [19]. Detection limit as low as 1 pM was realized for these DNA targets.

Electro-thermal atomic absorption spectrometry (ETAAS) is one of the most popular atomic spectrometric techniques with almost 60 element detection abilities [20,21]. The high atom density and long atom residence time in the graphite tube improve ETAAS detection limits by a factor of up to 1000 fold compared to flame AAS and ICPAES, down to the sub-ppb range. The maintenance and operation of ETAAS instrument are simple and cost-effective, especially compared with the sensitive but expensive ICPMS instrument. The low sample consumption of several microliter makes ETAAS an ideal match for biological and clinical samples of limited availability. Recently, our group successfully applied

* Corresponding authors.
E-mail addresses: huxiaorong@cdut.cn (X. Hu), liur.ray@gmail.com (R. Liu).

http://dx.doi.org/10.1016/j.microc.2015.12.026
0026-265X/

ETAAS to metalloimmunoassay of human IgG quantification at lower ng/mL level with Cu NPs tagging [22]. In this work, we developed an ETAAS-based DNA hybridization method for disease-related target detection. Ebola Virus (EV), which causes a severe and often fatal hemorrhagic fever of human and other mammals, was selected as a model for disease-related DNA target detection. The strategy of DNA sandwich hybridization is shown in Scheme 1. The report DNA was thiolated at the 3′-end for Au NPs conjugation, while the capture DNA was modified by biotin at the 5′-end for the immobilization on magnetic microparticles (MMPs). After the sandwich hybridization reaction between report DNA, target DNA, and capture DNA, aqua regia was added to dissolve Au NPs and release Au ions, which were then determined by ETAAS. The optimization of assay conditions, analytical performance, specificity of DNA hybridization, and method validation, were investigated and discussed in detail. To the best of our knowledge, this is the first report of ETAAS-based DNA hybridization assay.

2. Experimental section

2.1. Chemicals and materials

All reagents were of at least analytical reagent grade. Deionized water (DIW) was used throughout this study. Chloroauric acid ($HAuCl_4 \cdot 4H_2O$) was obtained from Aladdin (product No. G109455). Streptavidin coated MMPs (10 mg/mL, Dynabeads M-280) and a magnetic separator were purchased from Invitrogen Co. Bovine serum albumin (BSA) was purchased from Biodee Biotechnology Co. Ltd (Beijing, China). Nitric acid, hydrochloric acid, and trisodium citrate were obtained from Changzheng Chemical Reagent Co. Ltd. (Chengdu, China). All oligonucleotides were purchased from Sangon Inc. (Shanghai, China) and their sequences are listed in Table 1. All glassware was soaked with aqua regia for at least 12 h, rinsed with DIW, and then dried before use. The buffer solutions are as following: coupling buffer (0.01 M PBS, containing 0.15 M NaCl, pH 7.4), and washing buffer (0.01 M PBS containing 0.1% Tween 20, PBST, pH 7.4).

2.2. Instrument

An AAnalyst™ 800 atomic absorption spectrometer (PerkinElmer Inc., Shelton, CT, USA) was used in this work. The instrument is equipped with a graphite furnace atomizer, an AS 800 auto-sampler to facilitate precise sample introduction, and a radiation source of Au hollow cathode lamp (HCL). The signal measurements were performed using the peak area (integrated absorbance) mode.

2.3. Procedure

2.3.1. Synthesis of colloidal gold nanoparticles

The colloidal gold nanoparticles were synthesized by using the citrate reduction of $HAuCl_4$ in water according to reference [23]. Briefly, 120 mL 0.01% $HAuCl_4 \cdot 4H_2O$ was heated to boiling for five minutes. 1 mL of 1% (m/v) trisodium citrate was added to the solution. After 30 min, the colloidal suspension was cooled to room temperature and stored at 4 °C.

Table 1
The sequences of oligonucleotides used in this work.

Name	Sequence (5′–3′)
Target DNA	GGAGTAAATGTTGGAGAACAGTATCAACAA
Report DNA	TCCAACATTTACTCCAAAAAAAAAA-$(CH_2)_6$-SH
Capture DNA	biotin-AAAAAAAAAATTGTTGATACTGTTC
Single base pair-mismatched DNA	GGAGTAAATGTTGAAGAACAGTATCAACAA
Mismatched DNA	AATGGCATTTGTTGGGGTAACCAACTATTT

2.3.2. Preparation of DNA-modified Au NPs

The thiolated report DNA was immobilized on Au NPs using a modification procedure of literatures [24,25]. Briefly, 37 μL of thiolated report DNA (100 μM) was incubated with 2 mL Au NPs solution at room temperature for least 24 h. By slowly adding 2 M NaCl into the bottom of glassware for three times in 24 h, the concentration of NaCl was increased to 0.3 M during the salt aging progress. The mixtures were centrifuged to remove unreacted DNA strands. The Au NPs were washed with PBS (pH 7.4), and then redispersed in 2 mL PBS.

2.3.3. Preparation of DNA-modified magnetic microparticles

Biotinylated DNA was immobilized on MMPs according to the procedure provided by Invitrogen Co. In brief, 240 μL of streptavidin-coated magnetic microparticles (10 mg/mL) was rinsed three times with 240 μL of PBS and resuspended in 120 μL PBS. Subsequently, 108 μL of DIW and 12 μL of biotinylated capture DNA (100 μM) were added. After 2 h of gentle shaking at room temperature, the magnetic microparticles were separated and rinsed with washing buffer for three times. Finally, the beads were resuspended in 240 μL PBS and stored at 4 °C before use.

2.3.4. Sandwich hybridization reaction and ETAAS measurement

The proposed principle of the sandwich hybridization reaction is shown in Scheme 1. Before the hybridization process, the report DNA-modified Au NPs and the capture DNA-conjugated magnetic microparticles were equilibrated with BSA for 1 h, respectively. After rinsed with washing buffer, 100 μL of report DNA-modified Au NPs and 30 μL of capture DNA-conjugated magnetic microparticles were mixed in a centrifuge tube. Then 100 μL of target DNA of known concentrations were added, followed by gentle shaking at room temperature for one hour. The MMPs were separated from the solution and rinsed three times with PBST. Subsequently, the sandwich complexes were resuspended in 100 μL of H_2O. To release the Au NPs from the sandwich complexes, the suspension was heated to 95 °C for 20 min. After magnetic separation, 100 μL of diluted aqua regia was added to the supernatant to dissolve the Au NPs. Finally, the solution was measured by ETAAS with temperature program listed in Table 2.

3. Results and discussion

3.1. Optimization of assay conditions

The assay conditions, including the capture DNA concentration, the reaction time between biotin modified capture DNA and MMPs (T_{BM}), the reaction time of sandwich hybridization (T_R), the report DNA-Au

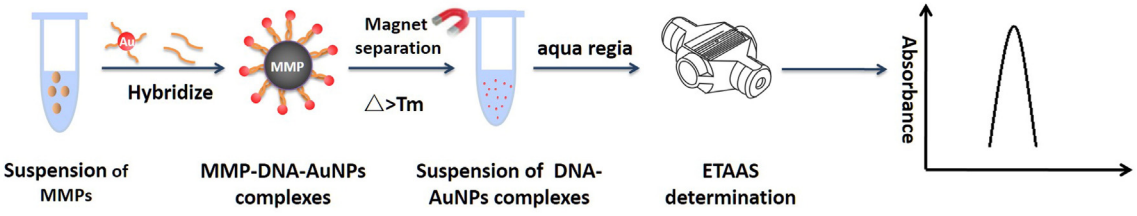

Scheme 1. Sandwich hybridization analysis based on Au NPs labeling and ETAAS determination.

Table 2
Temperature program of graphite furnace atomizer.

Steps	Temperature (°C)	Ramp time (s)	Hold time (s)	Ar gas flow (mL/min)
Drying	110	1	30	250
Drying	130	15	30	250
Pyrolysis	800	10	20	250
Atomization	2000	0	3	0
Clean	2450	1	3	250

NPs bioconjugate concentration, and the aqua regia concentration, were optimized in detail. In this study, capture DNA was firstly immobilized on magnetic microparticles. As shown in Fig. 1, the signal intensity significantly increased when the concentration of capture DNA was increased from 0.3 to 4.8 μmol/μL (1 μL MMPs react with 1 μmol capture DNA) and then leveled off. Thus 4.8 μmol/μL of capture DNA was used throughout this work.

Reaction times, including T_{BM} and T_R, are important influencing parameters. As shown in Fig. 2a, the signal intensity increased rapidly with the increase of T_{BM} ranging from 30 to 120 min and then leveled off after 120 min, indicating the completeness of the reaction between streptavidin and biotin. Thus 120 min of T_{BM} was chosen for the subsequent experiments. As shown in Fig. 2b, the signal intensity was stable in the range from 60 to 150 min. Thus T_R of 60 min was selected to save time in the subsequent studies.

In order to get the best signal to noise ratio, the concentration of report DNA-Au NPs bioconjugates was optimized. The signal intensity sharply increased with the increase of DNA-Au NPs bioconjugates concentration, while the noise intensity remained low and stable (Fig. 3). Hence, the dilution of report DNA-Au NPs bioconjugates is unnecessary and not performed in further investigations.

Aqua regia was used to disolve Au NPs to homogenous solution for ETAAS determination. However, high concentration of aqua regia can bring high background signal, as well as reduce the lifetime of graphite tubes. Fig. 4 shows that the blank signal intensity decreases after the dilution of aqua regia, while too much dilution caused the decrease of sample signal. Consequently, 1:6 dilution of aqua regia was selected to dissolve colloidal Au NPs considering both dissolve efficiency and blank signal control.

3.2. Assay performance

Under the optimized conditions, the quantitative relationship between the signal intensity and concentration of the target DNA

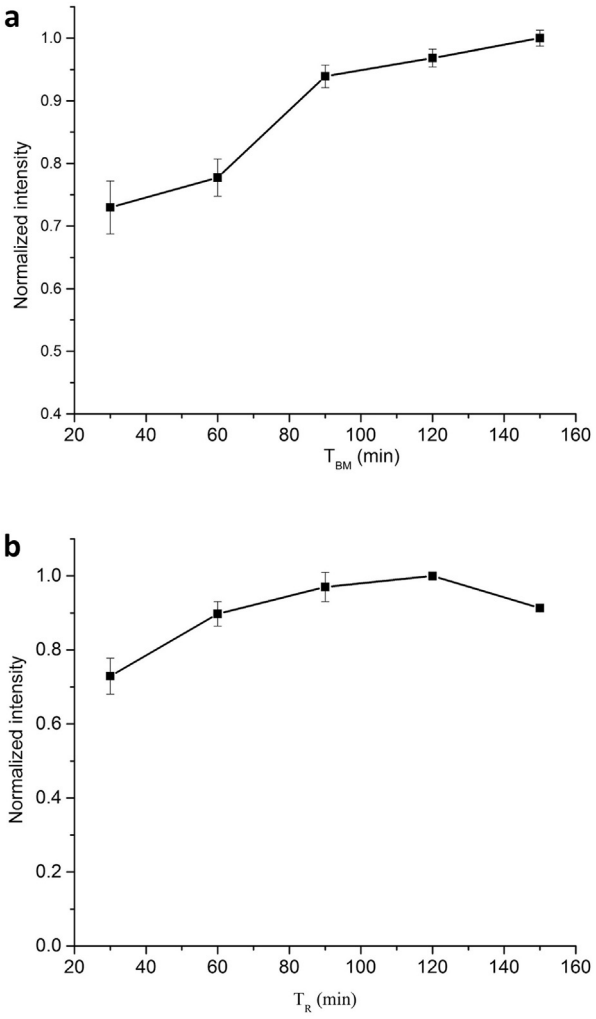

Fig. 2. Optimization of reaction times. (a) The reaction time between biotin modified capture DNA and MMPs (T_{BM}); and (b) the reaction time of sandwich hybridization (T_R). Experimental conditions: capture DNA concentration, 4.8 μmol/μL; dilution rate of report DNA-Au NPs bioconjugates, 1:0; target DNA concentration, 10 nM; dilution rate of aqua regia, 1:6.

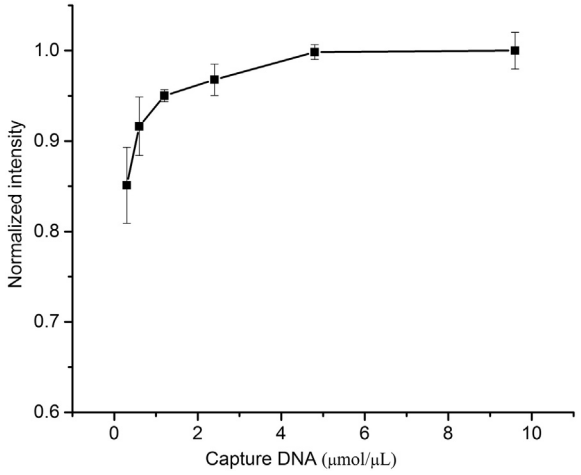

Fig. 1. Optimization of capture DNA concentration. Experimental conditions: T_{BM}, 2 h; T_R, 1 h; dilution rate of report DNA-Au NPs bioconjugates, 1:0; target DNA concentration, 10 nM; dilution rate of aqua regia, 1:6.

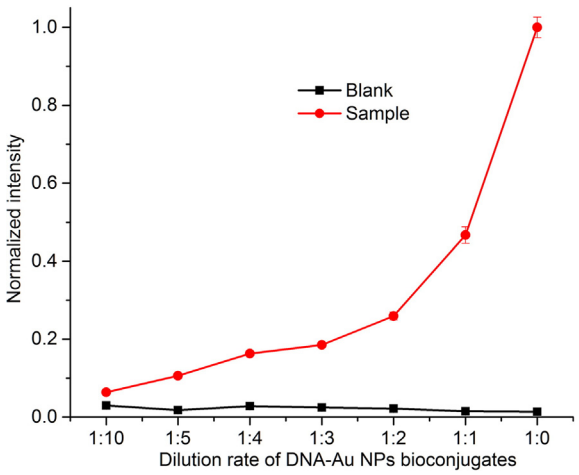

Fig. 3. Optimization of dilution rate of report DNA-Au NPs bioconjugates. Experimental conditions: capture DNA concentration, 4.8 μmol/μL; T_{BM}, 2 h; T_R, 1 h; target DNA concentration, 10 nM; dilution rate of aqua regia, 1:6.

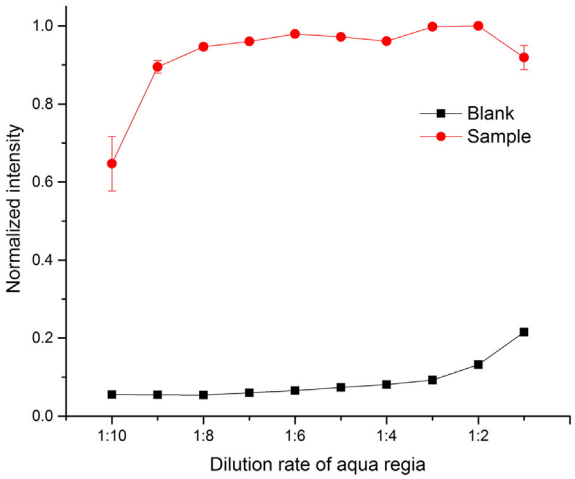

Fig. 4. Optimization of the dilution rate of aqua regia. 30 μL of Au NPs solution was dissolved by 100 μL different concentrations of aqua regia.

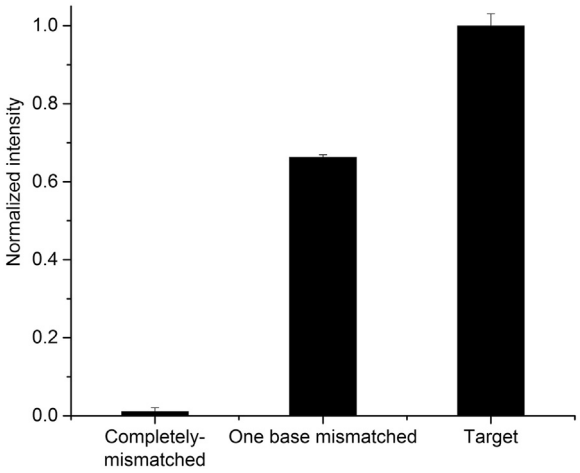

Fig. 5. Specificity of the proposed DNA hybridization assay. The concentration target DNA, mismatched DNA, and one base mismatched DNA were all 200 pM.

was investigated. A good linearity was obtained with the concentration of target DNA range from 10 to 200 pM, with the correlation coefficient of 0.9933 and the linear calibration curve of $y = 0.0018x + 0.0014$. The limit of detection (LOD, 3σ) was calculated to be 3 pM. The relative standard deviation (RSD) for 20 pM target DNA was 1.07%.

The LOD of the proposed method is compared with some literature values of direct DNA hybridization assay (Table 3). As shown in Table 3, the LOD of the proposed method is comparable to ICPMS hybridization assay, and better than those obtained by ICPAES, fluorescent, chemiluminescent, colorimetric, and electrochemical assay. It should be noted that either ICPMS or ICPAES is much more expensive than the ETAAS system.

To investigate the specificity of this assay system, a single-base mismatched DNA sequence and a completely mismatched DNA sequence were tested. As shown in Fig. 5, no obvious signal was obtained for completely mismatched target DNA, while the signal intensity of single base mismatched target DNA is much lower than fully matched target DNA.

3.3. Method validation

To verify the accuracy of this method, the correlation between the proposed ETAAS-based DNA assay and well-established ICPMS-based DNA assay was investigated. Different concentrations of target DNA were detected by ETAAS and ICPMS, respectively. As shown in Fig. 6, a good correlation was obtained ($R = 0.9924$) between these two methods, validating the accuracy of the proposed ETAAS DNA assay.

Table 3
Comparison of various DNA assay.

Detection methods	Labels	Limits of detection	References
Chemiluminescent	Graphene oxide	34 pM	[5]
Fluorescence	CdTe QDs	0.26–0.57 nM	[4]
Fluorescence	Pyrene-labeled hairpin DNA	10 pM	[26]
Colorimetry	Au NPs	50 pM	[3]
Colorimetry	Au NPs	8 nM	[27]
Electrochemistry	Anthraquinone	0.13 nM	[6]
ICPMS	Lanthanide elements	0.5–2 pM	[18]
ICPMS	Au NPs	1 pM	[19]
ICPAES	Au NPs	350 pM	[17]
ETAAS	Au NPs	3 pM	This work

4. Conclusions

A novel ETAAS-based method was developed for quantitative DNA assay. The disease-related DNA target can be detected at 3 pM with Au NPs labeling, which increases the sensitivity by several orders of magnitude over that of colorimetric methods, ICPAES methods, etc. The LOD is comparable with that obtained by the ultrasensitive ICPMS detection. It is worth noticing that the sensitivity could be further improved by combining with signal amplification methods such as polymerase chain reaction, rolling cycle amplification, silver enhancement, etc. ETAAS is able to detect NPs without any special optical or electrochemical properties, so a wide range of NPs such as TiO_2, CuO, Ag, Fe_3O_4, etc. could be easily adopted. As the ETAAS signal is almost unaffected by the sample matrix, the proposed method is potentially applicable for accurate determination of DNA in real clinical samples.

Acknowledgments

The authors gratefully thank the National Natural Science Foundation of China (Grant No. 21505008), the Specialized Research Fund for the Doctoral Program of Higher Education (Grant No. 20135122120001), the Education Department of Sichuan Province (Grant No. 15ZB0067), and National Training Programs of Innovation and Entrepreneurship for Undergraduates (Grant No. 201410616025) for funding this study.

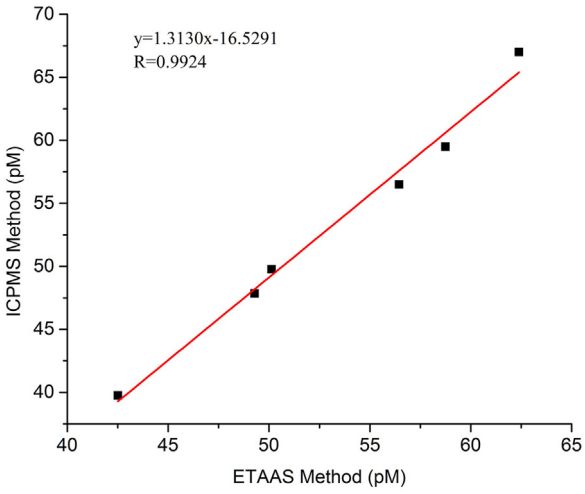

Fig. 6. Correlation of proposed ETAAS-based DNA hybridization assay and ICPMS-based DNA hybridization assay.

References

[1] J. Gratten, N.R. Wray, M.C. Keller, P.M. Visscher, Large-scale genomics unveils the genetic architecture of psychiatric disorders, Nat. Neurosci. 17 (2014) 782–790.
[2] T. Roemer, J. Davies, G. Giaever, C. Nislow, Bugs, drugs and chemical genomics, Nat. Chem. Biol. 8 (2012) 46–56.
[3] X. Mao, H. Xu, Q. Zeng, L. Zeng, G. Liu, Molecular beacon-functionalized gold nanoparticles as probes in dry-reagent strip biosensor for DNA analysis, Chem. Commun. (2009) 3065–3067.
[4] X. Ai, Q. Ma, X. Su, Multiplex DNA sensor for BRAF and BRCA detection, Anal. Biochem. 438 (2013) 22–28.
[5] M. Luo, X. Chen, G. Zhou, X. Xiang, L. Chen, X. Ji, Z. He, Chemiluminescence biosensors for DNA detection using graphene oxide and a horseradish peroxidase-mimicking DNAzyme, Chem. Commun. 48 (2012) 1126–1128.
[6] J. Kongpeth, S. Jampasa, P. Chaumpluk, O. Chailapakul, T. Vilaivan, Immobilization-free electrochemical DNA detection with anthraquinone-labeled pyrrolidinyl peptide nucleic acid probe, Talanta 146 (2016) 318–325.
[7] R. Liu, X. Liu, Y.R. Tang, L. Wu, X.D. Hou, Y. Lv, Highly sensitive immunoassay based on immunogold—silver amplification and inductively coupled plasma mass spectrometric detection, Anal. Chem. 83 (2011) 2330–2336.
[8] R. Liu, Y. Lv, X.D. Hou, Z. Mester, L. Yang, Protein quantitation using Ru-NHS ester tagging and isotope dilution high-pressure liquid chromatography–inductively coupled plasma mass spectrometry determination, Anal. Chem. 84 (2012) 2769–2775.
[9] R. Liu, X. Hou, Y. Lv, M. McCooeye, L. Yang, Z. Mester, Absolute quantification of peptides by isotope dilution liquid chromatography–inductively coupled plasma mass spectrometry and gas chromatography/mass spectrometry, Anal. Chem. 85 (2013) 4087–4093.
[10] S.D. Tanner, D.R. Bandura, O. Ornatsky, V.I. Baranov, M. Nitz, M.A. Winnik, Flow cytometer with mass spectrometer detection for massively multiplexed single-cell biomarker assay, Pure Appl. Chem. 80 (2008) 2627–2641.
[11] S.C. Bendall, E.F. Simonds, P. Qiu, E.A.D. Amir, P.O. Krutzik, R. Finck, R.V. Bruggner, R. Melamed, A. Trejo, O.I. Ornatsky, R.S. Balderas, S.K. Plevritis, K. Sachs, D. Pe'er, S.D. Tanner, G.P. Nolan, Single-cell mass cytometry of differential immune and drug responses across a human hematopoietic continuum, Science 332 (2011) 687–696.
[12] J. Hu, X. Hou, P. Wu, Ultrasensitive atomic fluorescence spectrometric detection of DNA with quantum dot-assemblies as signal amplification labels, J. Anal. At. Spectrom. (2015).
[13] C. Zhang, F.B. Wu, Y.Y. Zhang, X. Wang, X.R. Zhang, A novel combination of immunoreaction and ICP–MS as a hyphenated technique for the determination of thyroid-stimulating hormone (TSH) in human serum, J. Anal. At. Spectrom. 16 (2001) 1393–1396.
[14] R. Liu, Z. Xing, Y. Lv, S.C. Zhang, X.R. Zhang, Sensitive sandwich immunoassay based on single particle mode inductively coupled plasma mass spectrometry detection, Talanta 83 (2010) 48–54.
[15] R. Liu, P. Wu, L. Yang, X. Hou, Y. Lv, Inductively coupled plasma mass spectrometry-based immunoassay: a review, Mass Spectrom. Rev. 33 (2014) 373–393.
[16] Y. He, Y. Zhang, C. Wei, C. Li, Y. Gao, R. Liu, Illuminate proteins and peptides by elemental tag for HPLC–ICP–MS detection, Appl. Spectrosc. Rev. 49 (2014) 492–512.
[17] L.L. Wu, L.W. Qiu, C.S. Shi, J. Zhu, A nanoparticle-based solution DNA sandwich assay using ICP-AES for readout, Biomacromolecules 8 (2007) 2795–2800.
[18] G.J. Han, S.C. Zhang, Z. Xing, X.R. Zhang, Absolute and relative quantification of multiplex DNA assays based on an elemental labeling strategy, Angew. Chem. Int. Ed. 52 (2013) 1466–1471.
[19] S. Zhang, G. Han, Z. Xing, S. Zhang, X. Zhang, Multiplex DNA assay based on nanoparticle probes by single particle inductively coupled plasma mass spectrometry, Anal. Chem. 86 (2014) 3541–3547.
[20] W. Qiu, Y. Zhang, Y.M. Xu, Q.P. Su, R. Liu, C.H. Li, Sensitive and direct determination of lead in coffee drinks by graphite furnace atomic absorption spectrometry after in-furnace digestion, At. Spectrosc. 35 (2014) 260–264.
[21] P. Wu, H. Chen, G.L. Cheng, X.D. Hou, Exploring surface chemistry of nano-TiO(2) for automated speciation analysis of Cr(III) and Cr(VI) in drinking water using flow injection and ET-AAS detection, J. Anal. At. Spectrom. 24 (2009) 1098–1104.
[22] Y. Xu, Y. Gao, X. Zhao, X. Xu, W. Zhou, Y. Liu, C. Li, R. Liu, A sensitive atomic absorption spectrometric metalloimmunoassay with copper nanoparticles labeling, Microchem. J. 126 (2016) 1–6.
[23] R. Liu, Z. Xing, Y. Lv, S. Zhang, X. Zhang, Sensitive sandwich immunoassay based on single particle mode inductively coupled plasma mass spectrometry detection, Talanta 83 (2010) 48–54.
[24] S. Zhu, Y. Zhuo, H. Miao, D. Zhong, X. Yang, Detection of mercury(II) by DNA templated gold nanoclusters based on forming thymidine-Hg(2+)-thymidine duplexes, Lumin. J. Biol. Chem. Lumin. 30 (2015) 631–636.
[25] Q. Zhao, Aptamer-linked assay for thrombin using gold nanoparticle amplification and inductively coupled plasma-mass spectrometry detection, Anal. Chem. (2009) 7484–7489.
[26] H. Huang, X. Yang, K. Wang, Q. Wang, Q. Guo, J. Huang, J. Liu, X. Guo, W. Li, L. He, Amplified fluorescence detection of DNA based on catalyzed dynamic assembly and host-guest interaction between beta-cyclodextrin polymer and pyrene, Talanta 144 (2015) 529–534.
[27] J. Thavanathan, N.M. Huang, K.L. Thong, Colorimetric detection of DNA hybridization based on a dual platform of gold nanoparticles and graphene oxide, Biosens. Bioelectron. 55 (2014) 91–98.

analytical chemistry

Article

pubs.acs.org/ac

In Situ Generation and Consumption of H_2O_2 by Bienzyme–Quantum Dots Bioconjugates for Improved Chemiluminescence Resonance Energy Transfer

Shuxia Xu,[†] Xianming Li,[†] Chaobi Li,[†] Jialin Li,[†] Xinfeng Zhang,*[,†] Peng Wu,*[,‡] and Xiandeng Hou[‡]

[†]College of Materials and Chemistry & Chemical Engineering, Chengdu University of Technology, Chengdu 610059, China

[‡]Analytical & Testing Center, Sichuan University, 29 Wangjiang Road, Chengdu 610064, China

Supporting Information

ABSTRACT: Exploration of quantum dots (QDs) as energy acceptors revolutionizes the current chemiluminescence resonance energy transfer (CRET), since QDs possess large Stokes shifts and high luminescence efficiency. However, the strong and high concentration of oxidant (typically H_2O_2) needed for luminol chemiluminescence (CL) reaction could cause oxidative quenching to QDs, thereby decreasing the CRET performance. Here we proposed the use of bienzyme–QDs bioconjugate as the energy acceptor for improved CRET sensing. Two enzymes, one for H_2O_2 generation (oxidase) and another for H_2O_2 consumption (horseradish peroxidase, HRP), were bioconjugated onto the surface of QDs. The bienzyme allowed fast in situ cascaded H_2O_2 generation and consumption, thus alleviating fluorescence quenching of QDs. The nanosized QDs accommodate the two enzymes in a nanometric range, and the CL reaction was confined on the surface of QDs accordingly, thereby amplifying the CL reaction rate and improving CRET efficiency. As a result, CRET efficiency of 30–38% was obtained; the highest CRET efficiency by far was obtained using QDs as the energy acceptor. The proposed CRET system could be explored for ultrasensitive sensing of various oxidase substrates (here exemplified with cholesterol, glucose, and benzylamine), allowing for quantitative measurement of a spectrum of metabolites with high sensitivity and specificity. Limits of detection (LOD, 3σ) for cholesterol, glucose, and benzylamine were found to be 0.8, 3.4, and 10 nM, respectively. Furthermore, multiparametric blood analysis (glucose and cholesterol) is demonstrated.

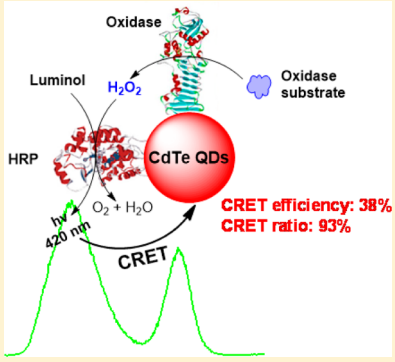

Chemiluminescence resonance energy transfer (CRET) is nonradiative energy transfer from a chemiluminescent donor to an energy acceptor, the mechanism of which is similar to that of fluorescence resonance energy transfer (FRET). Namely, the prerequisite for CRET is substantial overlap between the chemiluminescence (CL) of the donor and the absorption of the acceptor as well as their proximity.[1] Since no external light source is needed for excitation of CL, the nonspecific signals caused by external light excitation occasionally observed in fluorescence-based measurements can be minimized. Moreover, CRET also offers additional advantages of no direct excitation of the acceptor and minimized photobleaching of the fluorophores over FRET. These characteristics make CRET an attractive scheme in various bioassays.[2−14] However, conventional CRET often uses small-molecule fluorophores as energy acceptors. Their small Stokes shifts often result in poor spectral separation of the acceptor emission from the donor CL, thereby decreasing energy-transfer efficiency. Introduction of quantum dots (QDs) as energy acceptors to CRET largely alleviates these drawbacks due to their large Stokes shifts and high luminescence efficiency.[15−23] Besides, the narrow emission and broad absorption of QDs allows simultaneous arrangement of multiple-QD acceptors with the same CL donor, leading to CL multiplex.[24,25]

Due to their high CL efficiency in the blue region, luminol and its derivatives are by far the most used CL energy donors in CRET systems.[15−20,24,25] A strong and high concentration of oxidant is required for luminol CL, typically H_2O_2, and also other oxidants such as $K_3Fe(CN)_6$, $KMnO_4$, or NaBrO. The luminol–H_2O_2 CL reaction is one of the most sensitive CL reactions and widely used in CL bioassays. However, it has been reported that H_2O_2 could oxidize QDs and therefore quench the luminescence, and the quenching effect became more serious when increasing the exposure time in an oxidative environment.[26−28] Therefore, the application of the luminol–QD CRET systems in bioanalysis is greatly limited due to the use of H_2O_2 as oxidant for luminol CL. To inhabit the oxidation of QDs, an organo-modified hydrotalcite–quantum dot nanocomposite has been fabricated as a CRET probe, in which the hydrophobic dodecylbenzenesulfonate provided a protective microenvironment against the oxidation of QDs.[19]

Since H_2O_2 is indispensable for the luminol CL and CRET must occur in the proximity of luminol and QDs, an effective route to solve such a dilemma is fast generation and

Received: March 14, 2016
Accepted: May 25, 2016
Published: May 25, 2016

DOI: 10.1021/acs.analchem.6b01000
Anal. Chem. 2016, 88, 6418–6424

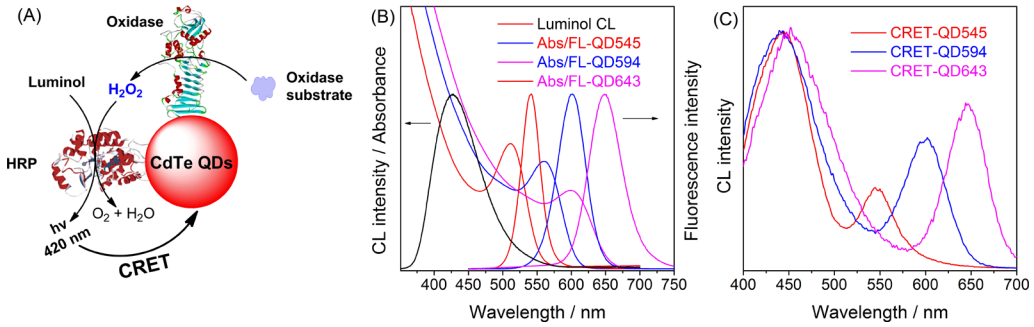

Figure 1. CRET from luminol to CdTe QDs: (A) schematic principle of CRET with bienzyme−QDs biconjugate, (B) luminol CL spectrum and absorption spectra of three CdTe QDs (QD545, 2.3 nm; QD594, 3.9 nm; QD643, 4.4 nm), and (C) CRET spectra obtained with GOx−HRP−QDs bioconjugate of three CdTe QDs. QD545 indicates CdTe QDs with maximum emission wavelength of 545 nm, similarly hereinafter.

consumption of H_2O_2. Limoges et al. pointed out that the reaction rates could be remarkably amplified when two enzymes were confined within a nanometric range.[29] Inspired by their research, we proposed here to use a bienzyme−QDs bioconjugate as energy acceptor moiety for CRET to alleviate the potential quenching of QDs by H_2O_2. The bienzyme system is appealing in bioanalysis since the substrate of the one enzymatic reaction can be produced in situ by another, thereby cascading the enzyme reactions.[30−32] Two enzymes, one for H_2O_2 generation (oxidase) and another for H_2O_2 consumption (horseradish peroxidase, HRP), were bioconjugated onto the surface of QDs assisted by 1-ethyl-3-(3-dimethylaminopropy)-carbodiimide (EDC) and *N*-hydroxysuccinimide (NHS).[26] The oxidant H_2O_2 was generated in situ and consumed immediately for the CL reaction, thus alleviating fluorescence quenching of QDs. The nanosized QDs accommodated the two enzymes in a nanometric range, and the CL reaction was confined on the surface of QDs accordingly, therefore amplifying the CL reaction rate and improving CRET efficiency.

EXPERIMENTAL SECTION

Materials. All reagents used in this work were of analytical grade. Tellurium powder (99.999%) was provided by Guoyao Reagent Co. (Chengdu, China), $CdCl_2$ (99.0%), *N*-Acetyl-cysteine (NAC), NaOH, glucose, and $NaBH_4$ were obtained from Kelong Reagent Co. (Chengdu, China). Luminol, cholesterol, cholesterol oxidase (COx), and benzylamine oxidase (BOx) were purchased from Aladdin (Shanghai, China). Glucose oxidase (GOx), plasma amine oxidase from bovine, benzylamine, and horseradish peroxidase (HRP) were provided by Sangon Biotech. H_2O_2 solutions were prepared fresh daily by dilution of a 30% (v/v) H_2O_2. A stock solution of 1.0×10^{-2} mol/L luminol was prepared by dissolving 1.77 g of luminol powder in 1000 mL of 0.1 mol/L NaOH solution. Ultrapure water (18 MΩ cm^{-1}) was used in all experiments.

Synthesis of CdTe QDs. *N*-Acetyl-cysteine (NAC)-capped CdTe QDs were synthesized according to a previous report with slight modification.[33] All glassware for preparation of CdTe QDs was thoroughly cleaned with freshly prepared 0.1 M HNO_3 and ultrapure water. First, NaHTe solution was prepared by the reaction between 50 mg of Te powder and 60 mg of $NaBH_4$ in 2 mL of ultrapure water at 60 °C for 10 min. Sequentially, the cadmium precursor solution was made by adding 0.57 g of NAC into 200 mL of 10 mmol L^{-1} $CdCl_2$ solution (adjusting the pH of mixing solution to 8.0 by NaOH) in N_2 atmosphere under vigorous stirring for 30 min. The molar ratio of Cd^{2+}/Te^{2-}/NAC was fixed at 4:1:7. Finally, a series of colloid CdTe QDs were obtained by mixing the freshly prepared NaHTe solution with cadmium precursor, and transferred to a Teflon lined stainless steel autoclave and heated to the growth temperature (150 °C). The prepared CdTe QDs were purified using an ultrafiltration membrane (Micoron YM-10-10 000 NMWL, Millipore, USA) and redispersed in ultrapure water. The as-prepared QDs were characterized by UV−vis spectrophotometry (Yuanxi Instrument Co., Ltd. China) and GE-100 gel electrophoresis (Puzhen, Shanghai). The separated QDs were illuminated with a 4-W 365 nm UV lamp (in a dark room) and the electropherogram was recorded by a camera.

Conjugating HRPand GOx/Cox/BOx with CdTe QDs. HRP and GOx/COx/BOx were conjugated to CdTe QDs using EDC/NHS-assisted coupling.[26] HRP and GOx/COx/BOx were dissolved in phosphate buffered saline solution (PBS, pH 7.4, 10 mM) to obtain solutions of 1800 and 900 U mL^{-1}, respectively, and were stored at 4 °C. For conjugation, CdTe (30 μM), EDC (2 mg), and NHS (1 mg) were mixed in phosphate buffered saline solution (PBS, pH 7.4, 10 mM, 1 mL) and the mixture was incubated at room temperature for 30 min to activate the QDs. Then, the HRP solution was added in the activated QDs to incubate at room temperature for 0.5 h. Finally, the GOx/COx/BOx solution was added in the above mixture to incubate for another 2.5 h. The conjugate was purified using an ultrafiltration membrane (Microcon YM-100-100000 NMWL, Millipore, USA). After ultrafiltration (10 000 rpm, 10 min), the purified products were redispersed in phosphate buffered saline solution (PBS, pH 7.4, 10 mM) and stored in a refrigerator at 4 °C.

Procedures for CRET Sensing and Imaging. To a 300 μL well, bioconjugate (40 μL) and luminol (110 μL, pH 9.10) were sequentially added. The CL reaction was triggered by adding the oxidase substrate, i.e., glucose/cholesterol/benzylamine standard solution (50 μL). The CRET spectra were obtained by an F-7000 fluorescence spectrophotometer (Hitachi, Japan). The CRET ratios were determined by dividing the area of the acceptor emission by the area of the donor emission. The CRET efficiency, *E*, was calculated by eq 1:

$$E = \frac{I(\mathrm{A})}{I(\mathrm{A}) + I(\mathrm{D})} \times 100\% \quad (1)$$

where $I(\mathrm{A})$ and $I(\mathrm{D})$ correspond to the integral areas of the acceptor and the donor emissions, respectively.

The CL signals were monitored by a CL analyzer (RLF-1A, Xi'an Remax Analysis Instruments Co., Xi'an, China). The data

DOI: 10.1021/acs.analchem.6b01000
Anal. Chem. 2016, 88, 6418−6424

integration time of the CL analyzer was set at 0.1 s per spectrum, and a working voltage of −700 V was used. CL signals produced from the well plates were recorded by a computer equipped with CL software, by which data were obtained and processed. The CRET imaging signals were recorded by a gel imaging system equipped with a CCD camera.

RESULTS AND DISCUSSION

Design and Validation of Bienzyme−CdTe QDs Bioconjugate for CRET. The principle of the proposed CRET with luminol as the CL energy donor and the bienzyme−QDs bioconjugate as energy acceptor moiety is illustrated in Figure 1A. To facilitate the cascade enzyme reactions, oxidase and peroxidase were used for H_2O_2 generation and consumption, respectively. H_2O_2 generated from the oxidase enzymatic reaction could oxidize luminol with HRP as a catalyst to emit blue light. Due to the broad absorption of CdTe QDs, substantial overlap between the CL emission of luminol (360−540 nm) and the absorption of the QDs exists (Figure 1B). The occurrence of the CL reaction on the surface of the QDs permits close proximity of the CL energy donor and acceptor, leading to CRET with high efficiency. Besides, the bienzyme−QDs bioconjugate confined both the oxidase enzymatic reaction and CL generation on the surface of the nanosized QDs, thereby accelerating the H_2O_2 consumption,[29] which is expected to largely alleviate potential quenching of the QDs by H_2O_2.

To facilitate CRET, HRP and oxidase were sequentially biconjugated with the carboxyl-terminated CdTe QDs through EDC/NHS-assisted coupling. Glucose oxidase (GOx) was taken as the model oxidase for generation of H_2O_2 upon catalyzing the oxidation of glucose. Three bioconjugates of CdTe QDs with different emission wavelengths (545 nm, QD545; 594 nm, QD594; and 643 nm, QD643; Figure 1B) were prepared. The corresponding HRP−CdTe QDs bioconjugates were also prepared as controls. The bioconjugated QDs were purified with an ultrafiltration membrane and characterized by UV−vis absorption spectrometry and gel electrophoresis. As shown in Figure 2A, the characteristic absorption bands of GOx (275 nm), HRP (410 nm), and CdTe QDs (620 nm) were all observed in the absorption profile of the bienzyme−CdTe QDs bioconjugate. The average loadings of HRP and GOx per QDs were evaluated as 4.0 and 1.6, respectively (see methods in the Supporting Information). Gel electrophoresis characterizations indicated that the electrophoretic mobility of QDs was almost unchanged when just mixing them with enzymes (HRP or HRP/GOx, Figure 2B). However, after bioconjugation with enzymes, the electrophoretic mobility of the QDs decreased obviously after being linked with enzyme (Figure 2C). Meanwhile, the quantum yield (QY) of the QDs before and after bioconjugation remained almost unchanged (Figure S1). Also, the bioconjugation process was monitored with capillary electrophoresis (Figure S2), with results agreeing well with those by gel electrophoresis. Also, the purity of the HRP/GOx-CdTe QDs bioconjugates could be verified to be more than 90%. These results validated successful bioconjugation of QDs with enzymes.

Successful CRET from luminol to CdTe QDs is evidenced in Figure 1C. Upon addition of glucose (200 μM), clear emissions of QD545, QD594, and QD643 were observed, which matched well with the fluorescence emission of these QDs. The spectra shifts of these CRET systems were 95, 144, and 193 nm for

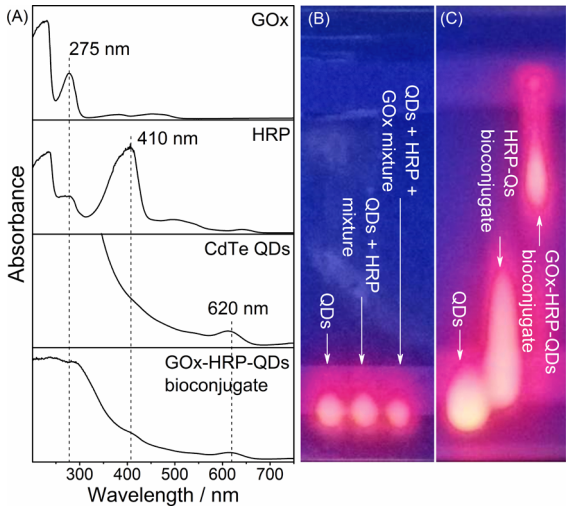

Figure 2. Characterization of bienzyme−CdTe QDs bioconjugate (QD643 as the model): (A) UV−vis absorption spectra of GOx, HRP, CdTe QDs, and GOx−HRP−CdTe QDs bioconjugate; (B) gel electropherograms of QDs, mixture of QDs and HRP, and mixture of QDs, GOx, and HRP; and (C) gel electropherograms of QDs, HRP−QDs bioconjugate, and GOx−HRP−CdTe QDs bioconjugate. Experimental conditions for gel electrophoresis: gel, 2% agarose; buffer, 20 mM phosphate solution (pH 7.0); voltage: 120 V; and separation time, 65 min.

QD545, QD594, and QD643, respectively, and this warrants distinct separation of excitation and emission and, thus, a much better signal-to-noise ratio in the CRET measurements.

To evaluate the necessity of bioconjugation of bienzymes with CdTe QDs, the CRET performance of the GOx−HRP−CdTe QDs bioconjugate (with glucose as substrate) was compared with those of HRP−CdTe QDs bioconjugate and a mixture of free HRP and CdTe QDs (both with H_2O_2 as substrate). As shown in Figure 3A, the CRET efficiency of the

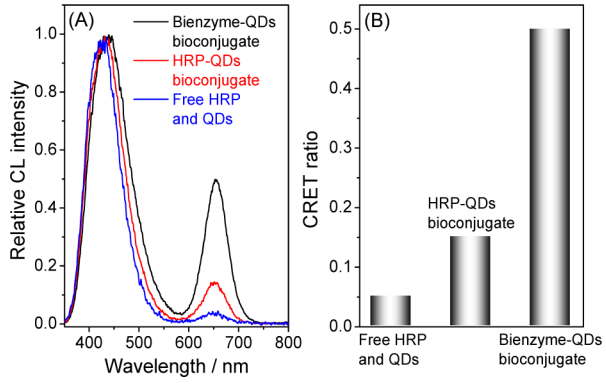

Figure 3. Comparison of CRET performances of GOx−HRP−CdTe QDs bioconjugate, HRP−CdTe QDs bioconjugate, and mixture of free HRP and CdTe QDs: (A) CRET spectra and (B) CRET ratio. Experimental conditions: luminol concentration, 0.5 mM; luminol pH, 9.10; and H_2O_2 concentration, 2 mM.

HRP conjugated QDs (bioconjugates of bienzyme−QDs and HRP−QDs) was considerably higher than those of free HRP and QDs. The CRET ratios of these three cases were 0.51, 0.15, and 0.05, respectively (Figure 3B; besides CRET efficiency, CRET ratios were also used here for better comparison with literature reports[15,17]). In the conjugated cases, the luminol CL

DOI: 10.1021/acs.analchem.6b01000
Anal. Chem. 2016, 88, 6418−6424

reaction occurred on the surface of QDs, leading to closer proximity of CL donor and acceptor and thus better CRET efficiency. In particular, the CRET ratio of the proposed bienzyme bioconjugate was more than 3-fold higher than that of single enzyme bioconjugate (HRP−QDs) or QDs with physically adsorbed bienzyme (Figure S3), demonstrating the superiority of bienzyme bioconjugates.

Lower Fluorescence Quenching Efficiency of H_2O_2 toward Bienzyme−CdTe QDs Bioconjugate. The oxidant used for the luminol CL reaction (H_2O_2) could quench the fluorescence of QDs,[26−28] resulting in decreased CRET efficiency. Hence, the fluorescence quenching of the bienzyme−CdTe QDs bioconjugate by CL reactant (0.5 mM luminol and 2 mM H_2O_2) was investigated, and HRP−QDs were taken as the control. As shown in Figure 4A,B,

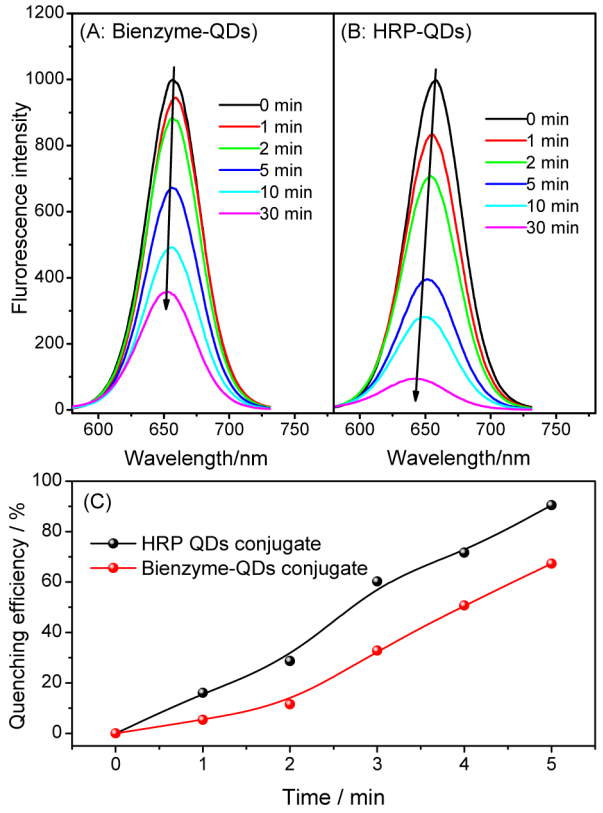

Figure 4. Fluorescence quenching of CdTe QDs (QD643) by CL reactants (0.5 mM luminol and 2 mM H_2O_2, λ_{ex} = 425 nm): (A) fluorescence emission spectra of bienzyme−QDs bioconjugate, (B) fluorescence emission spectra of HRP−QDs bioconjugate, and (c) time-dependent quenching efficiencies of the above two QDs. The concentrations of HRP−QDs and bienzyme−QDs were both 20 μM (based on the concentration of CdTe QDs).

fluorescence quenching of both QD-based bioconjugates was observed, but the bienzyme−CdTe QDs bioconjugate suffered less quenching effect (Figure 4C). Especially, the quenching efficiency of HRP−QDs was 3 times higher than that of bienzyme−CdTe QDs bioconjugate at an exposure time less than 1 min (Figure 4C). Control experiments indicated that luminol caused minimal fluorescence quenching to QDs. Therefore, the observed quenching could be majorly ascribed to H_2O_2-induced oxidation. Accompanied by quenching, blue shifting of the fluorescence spectra was also observed, which agreed well with a previous report.[34] Again, the bienzyme−CdTe QDs bioconjugate received less blue shift, i.e., less oxidation effect. It must be noted that in CRET with bienzyme−CdTe QDs bioconjugate, the exact amount of H_2O_2 generated via oxidase enzymatic reaction would be much less than that used for quenching investigations. Besides, the generated H_2O_2 would take part in the peroxidase enzymatic reaction (luminol CL reaction) quickly.

The fast in situ generation and consumption of H_2O_2 was also evidenced from the time-dependent CL profiles of the CRET system. As shown in Figure 5, at the same substrate

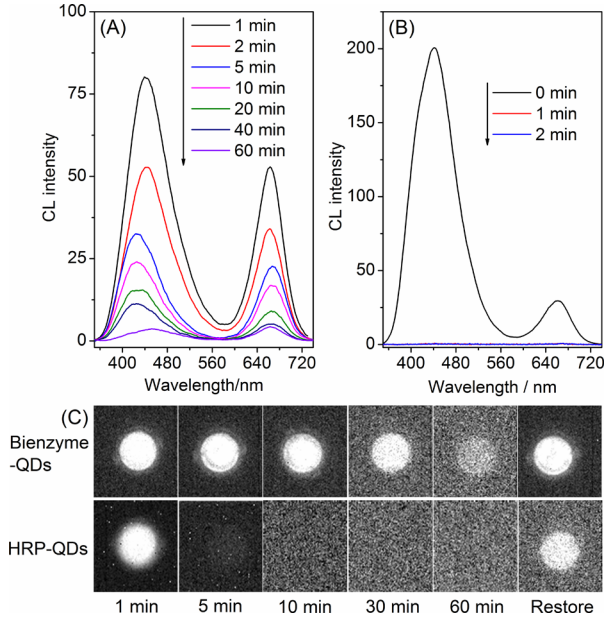

Figure 5. Time-dependent CRET investigations: (A) CRET profiles of bienzyme−CdTe QDs upon addition of 2 mM glucose, (B) CRET profiles of HRP−CdTe QDs upon addition of 2 mM H_2O_2, and (C) CL imaging brightness of the above two systems decayed with time. The CRET with bienzyme−CdTe QDs can be almost fully restored, but HRP−CdTe QDs cannot. Experimental conditions: luminol concentration, 0.5 mM; luminol pH, 9.18.

concentration (2 mM glucose or bienzyme−CdTe QDs and 2 mM H_2O_2 for HRP−QDs), the CRET signal of the bienzyme−CdTe QDs system lasted about 60 min, while that of HRP−CdTe QDs decayed in less 1 min. Even after 60 min, appreciable CRET signal was still observed for bienzyme−CdTe QDs (Figure 5A,C), revealing that efficient CRET still occurred. Such long-persistent CRET was not reported in other CRET systems.[15,17−19] This is attributed to the persistent CL reaction catalyzed by the bienzymes and the low fluorescence quenching efficiency of such a system. Particularly, the CRET with bienzyme−CdTe QDs can be restored to a large extent upon readdition of the same amount of substrate (glucose). But for the HRP−CdTe QDs, the restoration was only minimal (Figure 5C). Therefore, the above evidence proved that the bienzyme−QDs bioconjugate was more suitable than HRP−QDs as an acceptor for luminol-based CRET.

After careful optimization of the CRET parameters (Figure S4), the best CRET efficiency and ratios of 30−38% and 0.7−0.9 were obtained, respectively. As listed in Table 1, the CRET ratio and efficiency with the proposed bienzyme bioconjugates are much higher than those of previously reported QDs-based CRET systems. The superior CRET efficiency mainly benefited from the advantages of bienzyme bioconjugates, i.e., in situ

DOI: 10.1021/acs.analchem.6b01000
Anal. Chem. 2016, 88, 6418−6424

Table 1. Comparison of the CRET Performances of Bienzyme−QDs with Previously Reported Systems

CRET system	CRET efficiency (%)	CRET ratio (%)	ref
bieneyzmes−QDs (glucose)	30	72	this work
bieneyzmes−QDs (cholesterol)	38	93	this work
bieneyzmes−QDs (benzylamine)	37	85	this work
HRP−QDs	12	15	this work
HRP−QDs	–	32	15
DNAzyme−QDs	20	–	18
BrO^-−QDs	–	30	17
LDH−QDs[a]	24	–	19

[a]LDH−QDs is layered double hydroxide and quantum dot nanocomposite.

H_2O_2 generation, alleviated fluorescence quenching of QDs, and accelerated CL reaction on the nano-QDs surface.

CRET with Bienzyme−CdTe QDs for Biosensing. After successful demonstration of the improved CRET performance, the biosensing applications of bienzyme−CdTe QDs for oxidase substrates were explored. Here, three oxidases, namely glucose oxidase (GOx), cholesterol oxidase (COx), and benzylamine oxidase (BOx), were selected and conjugated onto QD643, QD594, and QD545 for CRET sensing of glucose, cholesterol, and benzylamine, respectively. As shown in Figure 6, successful CRET was obtained from all the three

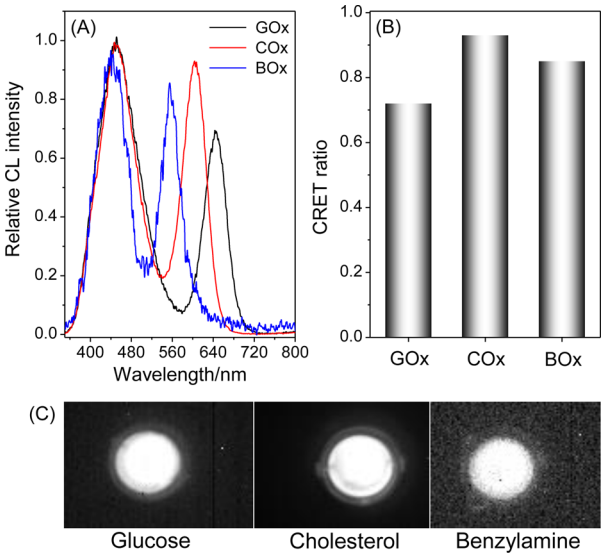

Figure 6. Analytical potential of CRET sensing with bienzyme−CdTe QDs: (A) CRET spectra obtained from GOx−HRP−CdTe QDs, COx−HRP−CdTe QDs, and BOx−HRP−CdTe QDs upon addition of 2 mM glucose, cholesterol, and benzylamine, respectively; (B) CRET ratios of the above three systems; and (C) CL imaging brightness of the above two systems. Experimental conditions: luminol concentration, 0.5 mM; and luminol pH, 9.18.

CRET systems with high CRET ratio and imaging brightness. Therefore, the proposed bienzyme−CdTe QDs bioconjugates were effective and universal for CRET sensing of a variety of oxidase substrates.

The analytical performance of the proposed CRET with bienzyme−CdTe QDs bioconjugates were demonstrated with glucose, cholesterol, and benzylamine as the oxidase substrates. As shown in Figure S5, increased CL intensity was observed upon increasing the concentration of oxidase substrate (exemplified with glucose). A linear relationship between the CRET intensity and the glucose concentration was found in the range of 10−1000 nM with a correlation coefficient $R > 0.990$, corresponding to a linear range over 2 orders of magnitude. The reproducibility for five replicated measurements of 500 nM glucose was 1.3% (relative standard deviation (RSD), Figure S6). The limit of detection (LOD, 3σ) was 3.4 nM, which is about 10−1000-fold more sensitive than the current QDs-based glucose sensor.[26,35−37] Such high sensitivity can be ascribed to the amplified reaction rate of bienzyme in the nanometric range and high CRET efficiency. Due to the high specificity of enzyme, the proposed assay possessed good selectivity for glucose detection (Table S1). The calibration graphs for cholesterol and benzylamine are given in Figure S7 and Figure S8, respectively. Besides, chemiluminescence imaging study was also performed for these three analytes. Figure S9 shows the representative CCD images obtained after addition of increasing amounts of glucose, cholesterol, and benzylamine. For all three analytes, increasing brightness of the CCD images were obtained, demonstrating the potential usefulness of this assay in screening analysis.

Blood glucose and cholesterol values are included in routine clinical settings. Particularly, hyperglycemia and hyperlipemia are threatening the public health nowadays. Therefore, quantitative measurement of glucose and cholesterol in blood or other biological samples is important for diagnosis and healthcare. The developed CRET with the bienzyme−CdTe QDs was tested for analysis of glucose and cholesterol in blood. Three human serum samples were collected from a local hospital and analyzed by the proposed CRET assay (Figure S10). Owing to the ultrahigh sensitivity and broad linear range of our method, the serum sample could be diluted different-fold depending on the amounts of serum obtained (Figure S11). Therefore, only a tiny amount of serum sample is required when assaying serum samples that are hard to obtain, for example, in newborn babies. As shown in Table 2, the measured blood glucose and free cholesterol values were in good agreement with the commercial assays, with spike recoveries ranging from 96 to 116%. These analytical results demonstrated the accuracy and potential usefulness of this assay in clinical screening. It should also be noted that large dilution could lead to a source of error in measurements; therefore great care should be taken for these operations.

To facilitate screening analysis of glucose and cholesterol in human serum, simultaneous imaging of the two analytes is desired. Since the CRET with bienzyme−CdTe QDs occurred immediately after introduction of the substrates or serum, the simultaneous imaging should be carried with the same QDs to eliminate the filter change for acquiring of images. In this manner, two aliquots of QD643 were bioconjugated with GOx/HRP and COx/HRP, respectively. A single optical filter (long-pass filter, 630 nm) was mounted in the front of the CCD imaging system. As shown in Figure 7, without serum, no CRET spectra or imaging brightness were obtained, while in the presence of serum (diluted 100-fold), both CRET spectra and imaging brightness were seen from the same serum sample, indicating that such a serum sample contained both glucose and cholesterol. Besides, the approximate glucose and cholesterol concentrations could also be evaluated from the brightness of the images. Therefore, fast screening of glucose and cholesterol

DOI: 10.1021/acs.analchem.6b01000
Anal. Chem. 2016, 88, 6418−6424

Table 2. Analytical Results for Glucose and Free Cholesterol in Human Serum Samples

sample no.	analyte	certified[a] (mM)	measured[b] (mM)	added (mM)	found[b] (mM)	recovery (%)
1	glucose	3.19	3.17 ± 0.34	3.00	2.99 ± 0.60	99.0
2		15.02	14.79 ± 1.21	12.00	12.36 ± 1.12	101
3		11.25	11.35 ± 1.08	12.00	12.93 ± 1.36	108
1	cholesterol	1.53	1.64 ± 0.34	2.00	1.92 ± 0.45	96.0
2		2.16	2.08 ± 0.50	2.00	2.32 ± 0.22	116
3		2.71	2.81 ± 0.64	3.00	3.39 ± 0.31	113

[a]Values determined by a local hospital. [b]Average ± 3SD (n = 3).

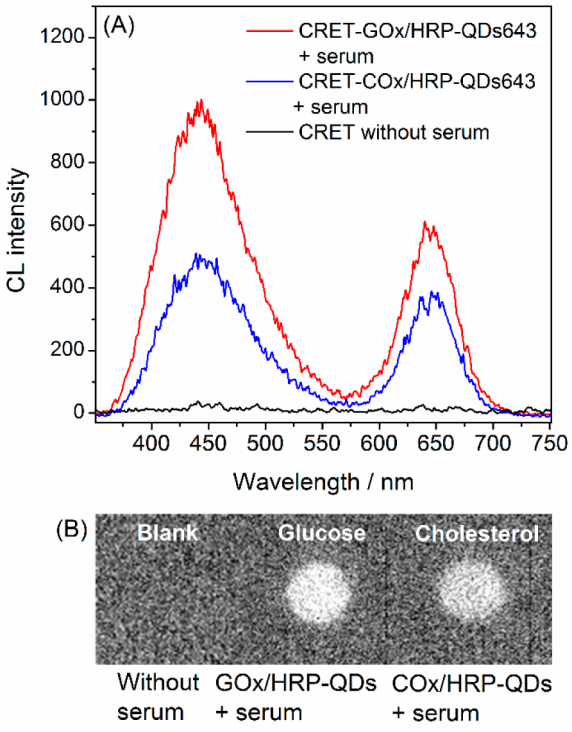

Figure 7. Screening analysis of glucose and cholesterol in serum: (A) CRET spectra and (B) CCD images. Experimental conditions: luminol concentration, 0.5 mM; luminol pH, 9.18.

in serum samples to diagnose hyperglycemia and hyperlipemia can be easily achieved.

CONCLUSION

In summary, we proposed here the use of bienzyme−QDs bioconjugates as the energy acceptor for CRET sensing. The nanosized QDs accommodated the two enzymes in a nanometric range and the CL reaction was confined on the surface of the QDs accordingly, therefore amplifying the CL reaction rate and improving the CRET efficiency. Besides, the oxidant H_2O_2 was generated in situ and consumed immediately for the CL reaction, thus alleviating fluorescence quenching of QDs. The CRET efficiency of bienzyme−QDs was found to be in the range 30−38%, which is the highest compared with HRP−QDs and previously reported CRET systems with QDs as an energy acceptor. One major limitation of this protocol is the basic pH needed for luminol CL, which may lower the activity of enzymes. The proposed CRET system could be explored for sensitive analysis of a series of oxidase substrates, for example, glucose, cholesterol, and benzylamine. We demonstrated the robustness of this assay for analysis of glucose and cholesterol in serum samples. This assay is promising for potential clinical diagnosis of hyperglycemia and hyperlipemia.

ASSOCIATED CONTENT

Supporting Information

The Supporting Information is available free of charge on the ACS Publications website at DOI: 10.1021/acs.analchem.6b01000.

Method for evaluation of average loading of enzyme per QD; electropherograms of free QDs, HRP−QDs, and bienzyme−CdTe QDs conjugates; optimization of different CRET parameters; CL calibration graph and selectivity evaluation; chemiluminescence imaging of the CRET system with bienzyme−CdTe QDs for analysis of increasing amounts of glucose, cholesterol, and benzylamine (PDF)

AUTHOR INFORMATION

Corresponding Authors

*E-mail: zhangxinfeng09@cdut.cn (X.Z.).
*E-mail: wupeng@scu.edu.cn (P.W.).

Notes

The authors declare no competing financial interest.

ACKNOWLEDGMENTS

The authors gratefully acknowledge financial support from the National Natural Science Foundation of China (Grants 21305009 and 21475090) and the Basic Research Program of Sichuan Province (Grant 2014JY0049).

REFERENCES

(1) Huang, X. Y.; Ren, J. C. *TrAC, Trends Anal. Chem.* **2012**, *40*, 77−89.
(2) Lee, J. S.; Joung, H. A.; Kim, M. G.; Park, C. B. *ACS Nano* **2012**, *6*, 2978−2983.
(3) Shuhendler, A. J.; Pu, K. Y.; Cui, L.; Uetrecht, J. P.; Rao, J. H. *Nat. Biotechnol.* **2014**, *32*, 373−U240.
(4) Zhang, N.; Francis, K. P.; Prakash, A.; Ansaldi, D. *Nat. Med.* **2013**, *19*, 500−505.
(5) Zhao, J. J.; Jin, X.; Vdovenko, M.; Zhang, L. L.; Sakharov, I. Y.; Zhao, S. L. *Chem. Commun.* **2015**, *51*, 11092−11095.
(6) Bi, S.; Chen, M.; Jia, X. Q.; Dong, Y. *Nanoscale* **2015**, *7*, 3745−3753.
(7) Baubet, V.; Le Mouellic, H.; Campbell, A. K.; Lucas-Meunier, E.; Fossier, P.; Brûlet, P. *Proc. Natl. Acad. Sci. U. S. A.* **2000**, *97*, 7260−7265.
(8) Du, J. X.; Wang, Y. D.; Zhang, W. M. *Chem. - Eur. J.* **2012**, *18*, 8540−8546.
(9) Huang, X. Y.; Ren, J. C. *Anal. Chim. Acta* **2011**, *686*, 115−120.
(10) Chen, H.; Li, H. F.; Lin, J. M. *Anal. Chem.* **2012**, *84*, 8871−8879.
(11) Wang, Z. H.; Teng, X.; Lu, C. *Anal. Chem.* **2015**, *87*, 3412−3418.

DOI: 10.1021/acs.analchem.6b01000
Anal. Chem. 2016, 88, 6418−6424

(12) Zhang, L. J.; He, N.; Lu, C. *Anal. Chem.* **2015**, *87*, 1351−1357.
(13) Mun, H.; Jo, E. J.; Li, T. H.; Joung, H. A.; Hong, D. G.; Shim, W. B.; Jung, C.; Kim, M. G. *Biosens. Bioelectron.* **2014**, *58*, 308−313.
(14) Bi, S.; Xiu, B.; Ye, J. Y.; Dong, Y. *ACS Appl. Mater. Interfaces* **2015**, *7*, 23310−23319.
(15) Huang, X. Y.; Li, L.; Qian, H. F.; Dong, C. Q.; Ren, J. C. *Angew. Chem., Int. Ed.* **2006**, *45*, 5140−5143.
(16) Wang, H. Q.; Li, Y. Q.; Wang, J. H.; Xu, Q.; Li, X. Q.; Zhao, Y. D. *Anal. Chim. Acta* **2008**, *610*, 68−73.
(17) Zhao, S. L.; Huang, Y.; Liu, R. J.; Shi, M.; Liu, Y. M. *Chem. - Eur. J.* **2010**, *16*, 6142−6145.
(18) Liu, X. Q.; Freeman, R.; Golub, E.; Willner, I. *ACS Nano* **2011**, *5*, 7648−7655.
(19) Dong, S. C.; Liu, F.; Lu, C. *Anal. Chem.* **2013**, *85*, 3363−3368.
(20) Zhao, S. L.; Huang, Y.; Shi, M.; Liu, R. J.; Liu, Y. M. *Anal. Chem.* **2010**, *82*, 2036−2041.
(21) Golub, E.; Niazov, A.; Freeman, R.; Zatsepin, M.; Willner, I. *J. Phys. Chem. C* **2012**, *116*, 13827−13834.
(22) Zhou, Z. M.; Yu, Y.; Zhao, Y. D. *Analyst* **2012**, *137*, 4262−4266.
(23) Al-Ogaidi, I.; Gou, H. L.; Aguilar, Z. P.; Guo, S. W.; Melconian, A. K.; Al-Kazaz, A. K. A.; Meng, F. K.; Wu, N. Q. *Chem. Commun.* **2014**, *50*, 1344−1346.
(24) Freeman, R.; Liu, X. Q.; Willner, I. *J. Am. Chem. Soc.* **2011**, *133*, 11597−11604.
(25) Hu, L. Z.; Liu, X. Q.; Cecconello, A.; Willner, I. *Nano Lett.* **2014**, *14*, 6030−6035.
(26) Wu, P.; He, Y.; Wang, H.-F.; Yan, X.-P. *Anal. Chem.* **2010**, *82*, 1427−1433.
(27) Gill, R.; Bahshi, L.; Freeman, R.; Willner, I. *Angew. Chem., Int. Ed.* **2008**, *47*, 1676−1679.
(28) Yuan, J. P.; Guo, W. W.; Wang, E. K. *Biosens. Bioelectron.* **2008**, *23*, 1567−1571.
(29) Limoges, B.; Marchal, D.; Mavre, F.; Saveant, J. M. *J. Am. Chem. Soc.* **2006**, *128*, 6014−6015.
(30) de Oliveira, R. F.; de Moraes, M. L.; Oliveira, O. N.; Ferreira, M. *J. Phys. Chem. C* **2011**, *115*, 19136−19140.
(31) Xu, S. X.; Qi, H. L.; Zhou, S. Y.; Zhang, X. F.; Zhang, C. X. *Microchim. Acta* **2014**, *181*, 535−541.
(32) Ali, M. A.; Srivastava, S.; Solanki, P. R.; Reddy, V.; Agrawal, V. V.; Kim, C.; John, R.; Malhotra, B. D. *Sci. Rep.* **2013**, *3*, 2661.
(33) Zhang, H.; Wang, L. P.; Xiong, H. M.; Hu, L. H.; Yang, B.; Li, W. *Adv. Mater.* **2003**, *15*, 1712−1715.
(34) Hay, K. X.; Waisundara, V. Y.; Zong, Y.; Han, M. Y.; Huang, D. J. *Small* **2007**, *3*, 290−293.
(35) Cao, L. H.; Ye, J.; Tong, L. L.; Tang, B. *Chem. - Eur. J.* **2008**, *14*, 9633−9640.
(36) Sağlam, Ö.; Kızılkaya, B.; Uysal, H.; Dilgin, Y. *Talanta* **2016**, *147*, 315−321.
(37) Li, Y.; Ma, Q.; Liu, Z.; Wang, X.; Su, X. *Anal. Chim. Acta* **2014**, *840*, 68−74.

DOI: 10.1021/acs.analchem.6b01000
Anal. Chem. 2016, 88, 6418−6424

ACS SENSORS

Article

pubs.acs.org/acssensors

A Both-End Blocked Peroxidase-Mimicking DNAzyme for Low-Background Chemiluminescent Sensing of miRNA

Xianming Li,[†] Houchun Zhang,[†] Yurong Tang,[†] Peng Wu,[‡] Shuxia Xu,*[,†] and Xinfeng Zhang*[,†]

[†]College of Materials and Chemistry & Chemical Engineering, Chengdu University of Technology, Chengdu 610059, China

[‡]Analytical & Testing Center, Sichuan University, Chengdu 610064, China

Supporting Information

ABSTRACT: G-quadruplex DNAzymes that exhibited peroxidase-like activity have been shown to be appealing reporters for amplified readout of biosensing events simply by their formation or dissociation in the presence of analytes. For low background signaling, the efficient preblock of DNAzymes is critically important. Herein, we report a both-end blocked DNAzyme beacon strategy for chemiluminescent biosensing. The catalytic activity of peroxidase-mimicking DNAzyme can be inactivated fully by fixing both ends of the DNAzyme sequence, and easily recovered via a strand displace reaction between the miRNA and the block DNA. The efficient block and recovery of DNAzymes provide the both-end blocked beacon the highest signal-to-background ratio (over 25) among the reported DNAzymes for amplification-free detection of miRNA. As a result, the beacon allowed detection of subpicomolar miRNA without any labeling and amplification procedures, which is about 40-fold more sensitive than the traditional hairpin fluorescence beacon. Also, it exhibited excellent discrimination ability that can distinguish single-base mismatch miRNA. The simplicity, high sensitivity, and selectivity provided by the beacon make it a promising alternative tool for nucleic acid detection.

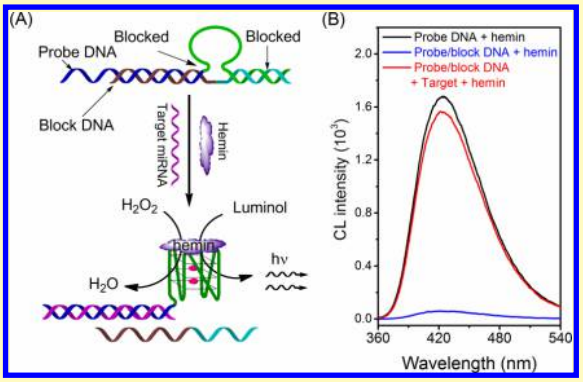

KEYWORDS: *DNAzyme, catalytic beacon, miRNA, chemiluminescence, biosensing*

DNAzymes, a kind of artificial enzyme, attract growing interest as new biocatalysts.[1,2] They have been extensively explored for various chemical reactions including RNA cleavage,[3] DNA ligation,[4] N-glycosylation,[5] and other reactions. G-quadruplex DNAzyme that exhibited peroxidase-like activity is a complex formed between hemin and a single-stranded guanine-rich aptamer.[6] Such G-quadruplex DNAzyme can catalyze the oxidation of luminol[7−9] or chromogenic substrates[10−12] by H_2O_2 to give sensitive chemiluminescence (CL) or visual signals, which is appealing as reporters for amplified readout of biosensing events.[13−15]

To explore the peroxidase activity of G-quadruplex DNAzyme for biosensing, it is desired that the probe DNA contains G-rich structure and the target analyte triggers the formation or dissociation of the G-quadruplex complex.[16,17] However, free G-rich structure has the tendency to form G-quadruplex complex in the absence of targets. Therefore, preblocking the G-rich structure is important to lower the background signal. For example, the frequently used turn-on sensing mode is commonly achieved by analyte-activating the preblocked DNAzyme.[17] A simple blocking strategy is to cage part of the DNAzyme sequence in a hairpin structure[9,10,18−21] or in the block DNA−DNAzyme complex (namely, single-end block of DNAzyme).[22] Target analyte can liberate the caged sequence through binding to recognition region to activate the G-quadruplex DNAzyme. Another popular DNAzyme inactivation approach is to split the DNAzyme sequence into two parts.[23−25] A block DNA is used to prevent the split sequences from self-assembly into the G-quadruplex.[26,27] In the presence of target analyte, the split DNAzyme can be reassembled for signaling.[23−27]

For signaling, blocking and target-induced activation efficiencies of DNAzyme are equally important. However, activation and block are usually contradictory, either in the caged or in split DNAzyme mode. Hence, part of DNAzyme sequence (free G-rich sequence) was always designed to be exposed outside for better folding into G-quadruplex during the recognition of analytes,[10,18−21,26,27] which probably leads to formation of intermolecular DNAzyme and, accordingly, background signals.[28] To improve the sensitivity, extra signal amplification procedures like target recycling amplification,[26] hybridization chain reaction,[29] and exonuclease-assisted signal amplification[19,30] were usually adopted. However, the problem of high background signals still existed.

Therefore, here we proposed a both-end blocked beacon strategy for the development of low-background G-quadruplex DNAzyme-based CL sensing of miRNA, a type of newly emerging biomarkers.[31,32] Since the G-rich DNAzyme sequence

Received: March 22, 2017
Accepted: June 1, 2017
Published: June 1, 2017

DOI: 10.1021/acssensors.7b00178
ACS Sens. 2017, 2, 810−816

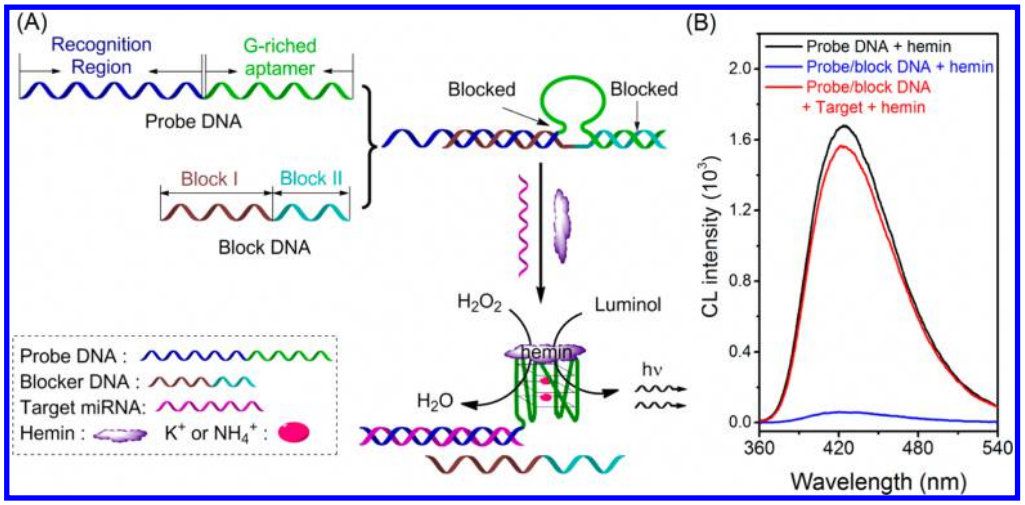

Figure 1. (A) Illustration of the fabrication of both-end blocked DNAzyme and its use for miRNA detection and (B) luminol CL spectra of different conditions. Experiment conditions: hemin, 12.5 nM; probe DNA, 25 nM; block DNA, 50 nM; target miRNA, 25 nM; luminol, 0.5 mM; H_2O_2, 5 mM.

is fixed at both ends, the potentiality for folding into G-quadruplex in the absence of target is largely restricted, leading to an extremely low background signal. More imporantly, the blocked DNAzyme in the beacon can be easily activated via a strand displacement reaction between miRNA and the block DNA, obtaining a strong CL signal. The high signal-to-background ratio as well the simplicity of the both-end blocked beacon will make it an appealing tool for sensing low-aboundance miRNA.

EXPERIMENTAL SECTION

Materials. Ultrapure water (18 MΩ cm^{-1}) was used in all experiments. Chloroform, ethanol anhydrous, EDTA, HCl, Tris, NaCl, KCl, and NH_4Cl were all analytical grade and purchased from Kelong Reagent Co. (Chengdu, China). Thioflavin T (ThT), diethypyrocarbonate (DEPC), dimethyl sulfoxide (DMSO), Triton X-100, *N*-[2-hydroxyethyl] piperazine-*N*′-2-ethanesulfonic acid sodium salt (HEPES, sodium salt), microRNA (miRNA) Miniprep Kit, and solid-phase RNase-Be-Gone were bought from Sangon Biotechnology Co (Shanghai, China). All nucleic acids were synthesized and purified by Sangon Biotechnology Co (Shanghai, China). The detailed sequences were listed in Table S1.

Fluorescent Validation of Blocking and Activating Processes. The experiment to demonstrate the progress of activating the both-end blocked G-quadruplex DNAzyme by miRNA was performed at 37 °C. FAM-labeled probe DNA (25 nM) and HBQ1-labeled block DNA (50 nM) were first incubated for 1 h in buffer (25 mM HEPES, 200 mM NaCl, 25 mM KCl, 150 mM NH_4Cl, 1% DMSO, pH 7.4) at 37 °C and another 2 h after adding different concentrations of target miRNA. Then the fluorescence signals were detected by fluorescence spectrophotometer (F-280, Tianjin Gangdong Sci. & Tech. Development Co., Ltd.) with excitation wavelength at 460 nm and emission wavelength from 480 to 600 nm.

The formation of G-quadruplexes was confirmed by fluorescence assay. Probe DNA (1 μM), block DNA (2 μM), and miRNA (1 μM) were first incubated as the above procedures. Thioflavin T (5 μM) was added in different conditions (only buffer, probe DNA, probe DNA +block DNA, probe DNA+block DNA+miRNA), and then incubated for another half an hour. Their fluorescence signals were detected by fluorescence spectrophotometer with excitation at 420 nm and emission wavelength from 450 to 550 nm.

Fabrication of Both-End Blocked DNAzyme Beacon. Probe DNA (500 pM) and block DNA (1000 pM) were incubated for 1 h in buffer (25 mM HEPES, 200 mM NaCl, 25 mM KCl, 150 mM NH_4Cl, 1% DMSO, 0.05% Triton X-100, pH 7.4) at room temperature to obtained the both-end blocked beacon.

Chemiluminescent Detection of miRNA Using Both-End Blocked DNAzyme Beacon. The standard miRNA solution or samples were incubated at 30 °C with the both-end blocked beacon solution (containing hemin) for 2 h before detection (Figure S1 shows that 2 h is enough for the displacement reaction between miRNA and block DNA). Subsequently, 100 μL of the resulted mixing solution was used to trigger the CL reaction between luminol (0.5 mM) and H_2O_2 (5 mM) at room temperature. The CL signals were recorded by a CL analyzer (300−650 nm, RLF-1A, Xi'an Remex Analysis Instruments Co., Xi'an, China). The blocking and activation efficiency values are calculated via eqs 1 and 2, respectively.

$$E_{(\text{block})} = \frac{I_{(\text{Probe})} - I_{(\text{beacon})}}{I_{(\text{Probe})}} \times 100\% \quad (1)$$

$$E_{(\text{activation})} = \frac{I_{(\text{miRNA})} - I_{(\text{beacon})}}{I_{(\text{Probe})} - I_{(\text{beacon})}} \times 100\% \quad (2)$$

where $E_{(\text{block})}$ is the blocking efficiency of DNAzyme; $I_{(\text{Probe})}$ is CL signal of free probe DNA; $I_{(\text{beacon})}$ is the CL signal of both-end blocked beacon; The $E_{(\text{activation})}$ is the activation efficeincy of both-end blocked beacon; $I_{(\text{miRNA})}$ is the CL signal of both-end blocked beacon after adding target miRNA.

Extract Total RNAs from miRNA-Spiked Serum and miRNA-Spiked HEPES Buffer. Total RNAs was extracted from 50 μL miRNA-spiked serum and miRNA-spiked HEPES buffer for detection. First, the samples were lysed by extraction solution and homogenized by pipet. After adding chloroform, the solution was separated by centrifugation. The supernatant was collected and then was filtered by Spin column TR after adding anhydrous ethanol (1.5 times more than the supernatant in volume). The RNAs on Spin column TR were purified by RPE solution twice and finally resolved in 50 μL RNase-free HEPES buffer. The resulting solution was subjected to analysis by the both-end blocked DNAzyme beacon as described above.

RESULTS AND DISCUSSION

Design and the Block/Activation Efficiency of Both-End Blocked DNAzyme. Figure 1A shows our design for both-end blocked G-quadruplex DNAzyme. A probe DNA was designed with target-recognition and DNAzyme sequence (G-rich hemin aptamer). A block DNA with two blocking sites was designed, in which the block I site was used to hybridize with the target-recognition region for blocking the 5′-end of the G-

DOI: 10.1021/acssensors.7b00178
ACS Sens. 2017, 2, 810−816

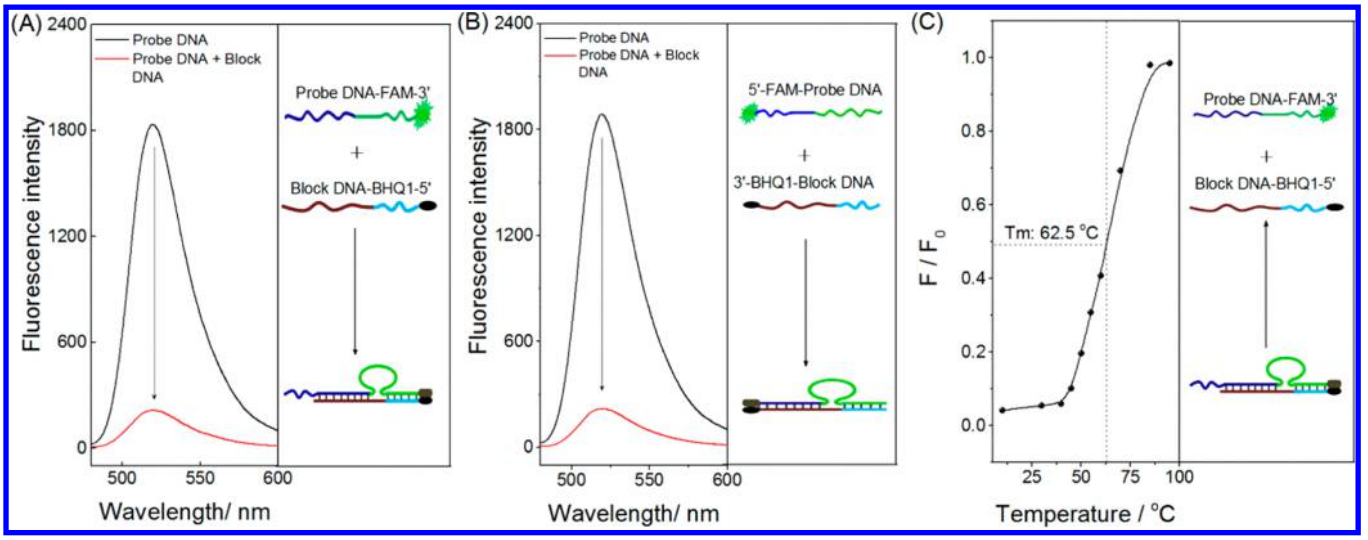

Figure 2. Validation of the both-end block of the probe DNA by the block DNA by fluorescence labeling: (A) block of the hemin aptamer at the 3′-end; (B) block of the recognition domain at the 5′-end; (C) thermal stability of the beacon (probe/block DNA complex). Experiment condition: probe DNA, 25 nM; and block DNA, 50 nM.

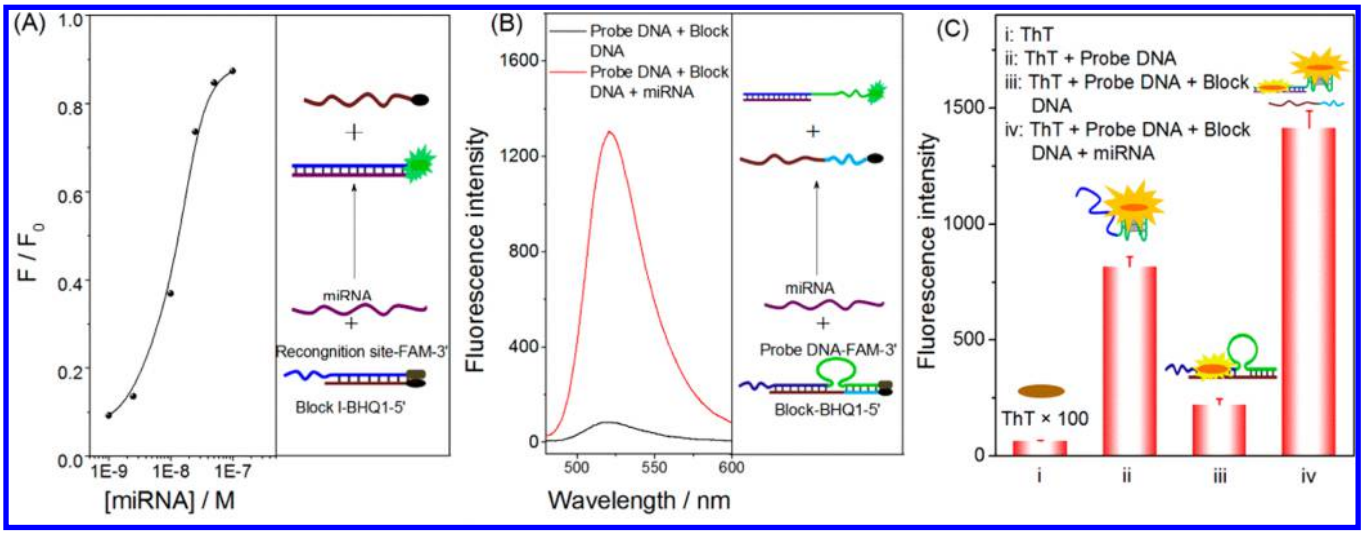

Figure 3. Fluorescent validation of the three activation processes: (A) strand displacement reaction between miRNA and block I; (B) automatic dissociation of block II after being displaced by miRNA; (C) formation of G-quadruplex through ThT fluorescence. Experimental conditions (A) and (B): probe DNA, 25 nM; block DNA, 50 nM; and (C) probe DNA, 1 μM; block DNA, 2 μM; and ThT, 5 μM.

rich hemin aptamer, while the block II site was explored for blocking of the 3′-end of the G-rich hemin aptamer. Therefore, a loop (beacon) containing the hemin aptamer with both ends blocked was formed. Such design is similar to the catalytic beacon by Li et al.[22] However, since the G-rich hemin aptamer was not fullly blocked, appreciable backgrounds of either colorimetric or chemiluminescent signals were obtained. While in the proposed mode, the potentiality for folding into G-quadruplex in the absence of target is largely restricted, namely, lower background signal. Since the number of bps of the target sequence (22 bps) is larger than that of the block I site (14 bps), the blocked DNAzyme sequence (loop structure) can be easily activated in the presence of the target miRNA, which catalyzes the oxidation of luminol by H_2O_2 to generate a strong CL signals.

Next, the performance of this assay in lowering the backgrond signal was preliminarily demonstrated. As shown in Figure 1B, without blocking, the probe DNA can fold into G-quadruplex DNAzyme to give the best catalytic activity. The formation of the blocked beacon structure in the presence of block DNA shows extremely low CL background signal, and the estimated blocking efficiency for DNAzyme is higher than 97% (eq 1). Upon target miRNA displacement of the block DNA, the DNAyme is activated with peroxidase-like activity of about 92.8% (eq 2). Such a DNA structure change could also be verified from the Soret band of hemin in the presence of probe DNA, probe DNA + block DNA, and probe DNA + block DNA + target miRNA (Figure S2). The ease of blocking and recovery of the DNAzyme in this design provides simplicity and high signal-to-background ratio for CL sensing.

Validation of the Both-End Blocks of the DNAzyme. To confirm the both-end block of the probe DNA by the block DNA, several controls were carried out. First, the 3′-end of probe DNA (hemin aptamer in the 3′-end) and 5′-end of block DNA were initially labeled with FAM and BHQ1 (a dark quencher), respectively. After incubation of the probe DNA with the block DNA, the fluorescence of FAM in the probe DNA was remarkably quenched by BHQ1 in block DNA

DOI: 10.1021/acssensors.7b00178
ACS Sens. 2017, 2, 810−816

(Figure 2A), indicating that the 3′-end of the hemin aptamer was fixed successfully. Second, the labeling place for FAM in the probe DNA was changed from the 3′-end to the 5′-end, and BHQ1 in block DNA from the 5′-end to the 3′-end. The fluorescence was also sharply quenched by BHQ1 in block DNA (Figure 2 B), confirming that the recognition region of the probe DNA was also successfully hybridized with the block DNA. The 5′-end of the hemin aptamer was conjugated to the recognition region and thus was also blocked successfully. Although the complex of the probe/block DNA has a loop in the middle of the double strand, the complex is quite thermally stable with a melting temperature as high as 62.5 °C (Figure 2C and Figure S3). Therefore, the both ends of the DNAzyme were blocked efficiently.

Activation Processes of DNAzyme in the Presence of miRNA. The activation of DNAzyme can be divided into three processes: first, the target miRNA displaces the block I of block DNA in 5′-end, leading to partial dissociation of the beacon. To verify this process, blocks I of the block DNA and recognition region were tagged with BHQ1 (5′-end) and FAM (3′-end), respectively. After incubation of the two oligonucleotides, a low fluorescence background was obtained. The presence of miRNA caused a sharp recovered fluorescent signal (Figure 3A), indicating that the displacement reaction between the block I of block DNA and miRNA could indeed occur.

Second, in the beacon structure (probe/block DNA complex), displacement of the block DNA by target should be verified. As shown in Figure 3B, this process was confirmed by the noticeably increased fluorescence signal of the probe DNA (tagged with FAM at 3′-end) in the presence of target, which replaced the whole block DNA (tagged with BHQ1 at the 5′-end) from the previous probe/block DNA complex (Figure S4). Therefore, the G-rich sequence in the probe DNA was liberated.

The third process is the formation of G-quadruplexes after dissociation of the block DNA from the beacon structure by the target miRNA. Here, we used thioflavin T (ThT) as a probe, since ThT has been confirmed as highly fluorecent responsive for G-quadruplexes as compared with duplex DNA.[33] Figure S5 further demostrates ThT is a good indicator for the formation of G-quadruplexes. As shown in Figure 3C, strong fluorescence was observed after adding of miRNA to the beacon, demonstrating the successful formation of G-quadruplexes.

Comparison with Other Catalytic Sensing Systems. To verify the both-end blocked DNAzyme for improving the signal-to-background ratio, several other control DNA structures, including fully blocked, single-end blocked, caged, and split DNAzymes, were also designed for CL sensing. Detailed information about the control DNA information was given in Supporting Information. As shown in Figure 4, the both-end blocked DNAzyme for miRNA-21 detection has much lower background signal than others except fully blocked DNAzyme. The caged DNAzymes in hairpin structure and single-end blocked DNAzyme were designed according to Willner et al.[18,22] Although here the stucture of single-end blocked DNAzyme is very much similar to the both-end blocked one, higher background signal was obtained. Probably, intermolecular DNAzyme was formed in such structure,[28] leading to high background. For example, we found that free G-rich fragments (with 6 and 9 G bases) led to at least 10-fold increase of the background as compared to that of free hemin (Figure S6). Such background should originate from intermolecular DNAzyme since these G-rich fragments could not form intramolecular G-quadruplexes. The fully blocked DNAzyme, although with extremely low background during sensing application, did not yield any CL signal for the target miRNA.

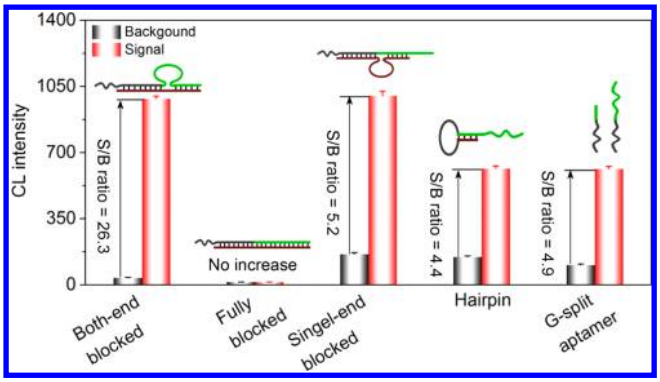

Figure 4. Signal-to-noise ratios of different DNAzyme for miRNA detection. Experimental conditions: hemin concentration, 12.5 nM; probe DNA concentration, 25 nM; block DNA concentration, 50 nM; miRNA concentration, 25 nM; hairpin beacon concentration, 25 nM; G-rich spit concentration, 25 nM; luminol concentration, 0.5 mM; and H_2O_2 concentration, 5 mM; amplification factor of CL analyzer, 2.

After investigation of the block length for block II, 8 bps was chosen as optimal since either 7 bps or 9 bps exhibited lower signal-to-background ratio (Figure S7). Therefore, the both-end blocked strategy gave the highest signal-to-background ratio (26.3) over other DNA structures. For the caged DNAzyme in the hairpin structure, it was found that the target miRNA yielded a low CL response probably because the small size of miRNA cannot effectively open the hairpin structure.[34] The split of hemin aptamer also caused a decline of the catalytic activity of the DNAzyme probably, because the short sequence of miRNA could not stabilize the assembled DNAzyme. In the both-end blocked DNAzyme, the ease of the strand displacement reaction makes the DNAzyme fully activated. Therefore, it displays the highest signal-to-background ratio for miRNA detection, over 5-fold higher than others.

Analytical Performance of the Sensor. Therefore, the both-end blocked DNAzyme was used for low background CL sensing of miRNA-21. The influences of NH_4^+ concentration, K^+ concentration, the concentration of hemin, the concentration of probe DNA, and the ratio of probe DNA to block DNA on the CL signals were investigated (Figures S8−S12). Under the optimum conditions, the CL intensity were linearly dependent on the amount of miRNA-21 in the range of 25 pM to 1 nM (Figure 5A). The correlation equation obtained is $Y = 0.765X - 2.94$ with a correlation coefficient of 0.9920. The reproducibility for five replicated measurements of 0.5 nM miRNA-21 was 2.6% (relative standard deviation, RSD), and the limit of detection based on 3σ is approximately 8 pM. This sensing system is about 40-fold more sensitive than the traditional hairpin fluorescence beacon, and is by far one of the most sensitive methods among the DNAzyme-based sensing systems that are free of amplification procedures (Table 1). Such high sensitivity should be ascribed to the high signal to backgound ratio of the present both-end blocked DNAzyme beacon. The sensitivity was even comparable to those assisted by an extra amplification procedure. By designing the recognition according to the target miRNAs/DNA sequences, the strategy can be readily used for detection of other miRNAs like miRNA let-7a (Figure S13) or DNA (Figure S14).

DOI: 10.1021/acssensors.7b00178
ACS Sens. 2017, 2, 810−816

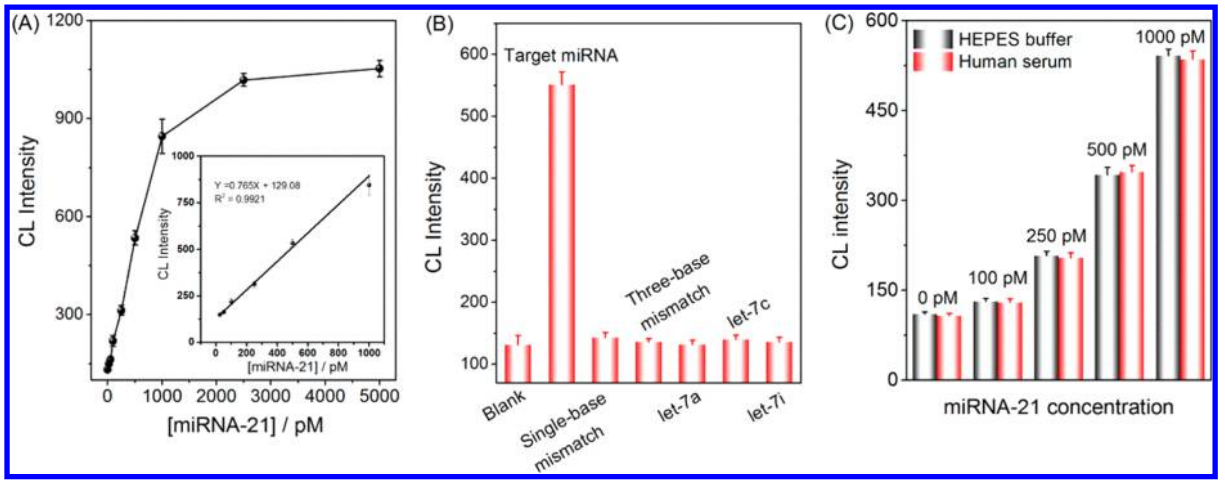

Figure 5. (A) CL response with the increasing concentrations of miRNA-21. (B) Specificity investigations of the catalytic beacon for detection of miRNA-21 (miRNA-21, 0.5 nM; other miRNAs, 50 nM). (C) CL response of different concentrations of miRNA in HEPES buffer and serum after extracion. Experimental conditions: probe DNA, 500 pM; block DNA, 1 nM; hemin, 2.5 nM; luminol, 0.5 mM; and H_2O_2, 5 mM; amplification factor of CL analyzer, 3.

Table 1. Comparison of Different Sensing Strategies for miRNA Detection

strategy[a]	target	detection method	label	amplification strategy	LOQ/LOD (pM)[b]	ref
Both-end blocked DNAzyme	miRNA	CL	-	-	25/8.6	this work
Caged DNAzyme	DNA	colorimetry	-	-	200000/NM	10
Split DNAzyme	DNA	colorimetry	-	-	10000/NM	24
Split DNAzyme	DNA	colorimetry	-	-	1000/NM	25
MGO/dsDNA/FAM	miRNA	CL	FAM	-	100/79	35
GQDs/dsDNA/Cy_3	miRNA	fluorescence	Cy_3	-	100/NM	36
AuNR/dsDNA/PDAMT	miRNA	fluorescence	AuNR	-	50/10	37
Traditional hairpin beacon	miRNA	fluorescence	FAM, BHQ1	-	1000/NM	38
GO/dsDNA/FAM	miRNA	fluorescence	FAM	-	1000/230	39
G4MB	miRNA	fluorescence	FAM, BHQ1	DSN	1/NM	40
YJS-SDA	miRNA	fluorescence	-	Nt.BbvCI, Phi29	10/3.2	41
GNP/dsDNA/MB	miRNA	colorimetry	GNP	DNA circuit	50/100	42
WS_2/dsDNA/FAM	miRNA	fluorescence	FAM	DSN	1/0.3	43
PDANP/dsDNA	miRNA	CL	-	DSN	100/80	44

[a]Abbreviations: MGO = magnetic graphene oxide; FAM = carboxyfluorescein; GQDs = grapheme quantum dots; GO = graphene oxide; G4MB = G-quadruplex molecular beacons; DSN = Duplex-specific nuclease; YJS-SDA = DNA Y-shaped junction structure-strand displacement amplification; Phi29 = Phi29 DNA polymerase; GNP = gold nanoparticle; MB = magnetic bead; WS_2 = WS_2 Nanosheet; AuNR = gold nanorods; PDAMT = Polydiacetylene microtubes; PDANP = Polydopamine nanospheres. [b]LOQ = limit of quantitation; LOD = limit of detection; NM = not mentioned.

The selective sensing of target is highly desirable during practical applications. As shown in Figure 5B, no obvious CL response could be detected upon addition of 50 nM of other miRNAs, i.e., single-base mismatched miRNA-21, three-base mismatched miRNA-21, miRNA-let 7a, miRNA-let 7c and miRNA-let 7i. However, the addition of only 0.5 nM miRNA-21 (100-fold lower than other miRNAs) produced a strong CL signal, confirming that the both-end blocked DNAzyme sensing system is a highly selective probe for miRNA-21.

To investigate the applicability of this sensing system, further experiments were carried out in human serum samples. Various concentrations of miRNA-21 ranging from 100 pM to 1000 pM were added in the human serums, and the same concentration of miRNA spiked in HEPES buffer was used as the control group. The miRNAs in the solutions were extracted by miRNA miniprep Kit and then subjected to analysis with the both-end blocked DNAzyme sensing system. The results shown in Figure 5C illustrate that the serum matrix did not yield a significant influence for miRNA detection in comparison with those signals in buffer. Hence, the sensing system is applicable in complicated sample analysis.

CONCLUSION

In summary, we have demonstrated a both-end blocked DNAzyme for low background CL sensing of miRNA. During sensing, the catalytic activity of DNAzyme can be fully blocked with a both-end blocked mode, and easily recovered via a strand displacement reaction between the target miRNA and the block DNA. The sensing system can be used for detection of subpicomolar miRNA without any labeling and amplification procedures. Also, it exhibited excellent discrimination ability that can distinguish single-base mismatch miRNA. Hence, the sensing system benefits the advantages of simplicity, low background, high sensitivity, and discrimination ability. By altering the recognition region, the system can be applied for detection of other miRNA as well as DNA (Figure S13 and S14); also, it is potentially useful in protein sensing by replacing the recognition probe with protein aptamer. In addition, by incorporating a target-initiated DNA nanomachine,[45,46] it might

DOI: 10.1021/acssensors.7b00178
ACS Sens. 2017, 2, 810−816

be a good alternative CL tool for sensing of trace biomolecules in the cell because the release of nucleotide from the DNA nanomachine can readily activate the both-end blocked DNAzyme. Therefore, we envision widespread biosensing applications of the both-end blocked DNAzyme.

■ ASSOCIATED CONTENT

Supporting Information

The Supporting Information is available free of charge on the ACS Publications website at DOI: 10.1021/acssensors.7b00178.

DNA or RNA sequences used; fluorescence assay; absorbance curves; fluorescence spectra; CL intensity; optimization of concentration and ratio (PDF)

■ AUTHOR INFORMATION

Corresponding Authors

*E-mail: xushux@cdut.edu.cn.
*E-mail: zhangxinfeng09@cdut.cn.

ORCID

Peng Wu: 0000-0002-9128-9027
Xinfeng Zhang: 0000-0002-0865-7061

Notes

The authors declare no competing financial interest.

■ ACKNOWLEDGMENTS

The authors gratefully acknowledge the financial support from the National Natural Science Foundation of China (No. 21475013 and 21305009).

■ REFERENCES

(1) Hollenstein, M. DNA Catalysis: The Chemical Repertoire of DNAzymes. *Molecules* **2015**, *20*, 20777−20804.
(2) Silverman, S. K. Catalytic DNA: Scope, Applications, and Biochemistry of Deoxyribozymes. *Trends Biochem. Sci.* **2016**, *41*, 595−609.
(3) Santoro, S. W.; Joyce, G. F.; Sakthivel, K.; Gramatikova, S.; Barbas, C. F. RNA cleavage by a DNA enzyme with extended chemical functionality. *J. Am. Chem. Soc.* **2000**, *122*, 2433−2439.
(4) Sreedhara, A.; Li, Y.; Breaker, R. R. Ligating DNA with DNA. *J. Am. Chem. Soc.* **2004**, *126*, 3454−3460.
(5) Sheppard, T. L.; Ordoukhanian, P.; Joyce, G. F. A DNA enzyme with N-glycosylase activity. *Proc. Natl. Acad. Sci. U. S. A.* **2000**, *97*, 7802−7807.
(6) Travascio, P.; Li, Y.; Sen, D. DNA-enhanced peroxidase activity of a DNA aptamer-hemin complex. *Chem. Biol.* **1998**, *5*, 505−517.
(7) Pavlov, V.; Xiao, Y.; Gill, R. G.; Dishon, A.; Kotler, M.; Willner, I. Amplified chemiluminescence surface detection of DNA and telomerase activity using catalytic nucleic acid labels. *Anal. Chem.* **2004**, *76*, 2152−2156.
(8) Zong, C.; Wu, J.; Liu, M. M.; Yang, L. L.; Yan, F.; Ju, H. X. Chemiluminescence Imaging for a Protein Assay via Proximity-Dependent DNAzyme Formation. *Anal. Chem.* **2014**, *86*, 9939−9944.
(9) Ma, F.; Yang, Y.; Zhang, C. Y. Ultrasensitive Detection of Transcription Factors Using Transcription-Mediated Isothermally Exponential Amplification-Induced Chemiluminescence. *Anal. Chem.* **2014**, *86*, 6006−6011.
(10) Xiao, Y.; Pavlov, V.; Niazov, T.; Dishon, A.; Kotler, M.; Willner, I. Catalytic beacons for the detection of DNA and telomerase activity. *J. Am. Chem. Soc.* **2004**, *126*, 7430−7431.
(11) Tang, L. H.; Liu, Y.; Ali, M. M.; Kang, D. K.; Zhao, W. A.; Li, J. H. Colorimetric and Ultrasensitive Bioassay Based on a Dual-Amplification System Using Aptamer and DNAzyme. *Anal. Chem.* **2012**, *84*, 4711−4717.
(12) Huang, Y.; Chen, J.; Zhao, S. L.; Shi, M.; Chen, Z. F.; Liang, H. Label-Free Colorimetric Aptasensor Based on Nicking Enzyme Assisted Signal Amplification and DNAzyme Amplification for Highly Sensitive Detection of Protein. *Anal. Chem.* **2013**, *85*, 4423−4430.
(13) Willner, I.; Shlyahovsky, B.; Zayats, M.; Willner, B. DNAzymes for sensing, nanobiotechnology and logic gate applications. *Chem. Soc. Rev.* **2008**, *37*, 1153−1165.
(14) Liu, J. W.; Cao, Z. H.; Lu, Y. Functional Nucleic Acid Sensors. *Chem. Rev.* **2009**, *109*, 1948−1998.
(15) Gong, L.; Zhao, Z. L.; Lv, Y. F.; Huan, S. Y.; Fu, T.; Zhang, X. B.; Shen, G. L.; Yu, R. Q. DNAzyme-based biosensors and nanodevices. *Chem. Commun.* **2015**, *51*, 979−995.
(16) Zhang, H.; Li, F.; Dever, B.; Li, X.; Le, X. C. DNA-mediated homogeneous binding assays for nucleic acids and proteins. *Chem. Rev.* **2013**, *113*, 2812−2841.
(17) Kosman, J.; Juskowiak, B. Peroxidase-mimicking DNAzymes for biosensing applications: A review. *Anal. Chim. Acta* **2011**, *707*, 7−17.
(18) Freeman, R.; Liu, X.; Willner, I. Chemiluminescent and Chemiluminescence Resonance Energy Transfer (CRET) Detection of DNA, Metal Ions, and Aptamer−Substrate Complexes Using Hemin/G-Quadruplexes and CdSe/ZnS Quantum Dots. *J. Am. Chem. Soc.* **2011**, *133*, 11597−11604.
(19) Bi, S.; Li, L.; Cui, Y. Exonuclease-assisted cascaded recycling amplification for label-free detection of DNA. *Chem. Commun.* **2012**, *48*, 1018−1020.
(20) Teller, C.; Shimron, S.; Willner, I. Aptamer-DNAzyme hairpins for amplified biosensing. *Anal. Chem.* **2009**, *81*, 9114−9119.
(21) Zhou, W.; Gong, X.; Xiang, Y.; Yuan, R.; Chai, Y. Target-Triggered Quadratic Amplification for Label-Free and Sensitive Visual Detection of Cytokines Based on Hairpin Aptamer DNAzyme Probes. *Anal. Chem.* **2014**, *86*, 953−958.
(22) Li, D.; Shlyahovsky, B.; Elbaz, J.; Willner, I. Amplified Analysis of Low-Molecular-Weight Substrates or Proteins by the Self-Assembly of DNAzyme-Aptamer Conjugates. *J. Am. Chem. Soc.* **2007**, *129*, 5804−5805.
(23) Xiao, Y.; Pavlov, V.; Gill, R. G.; Bourenko, T.; Willner, I. Lighting up biochemiluminescence by the surface self-assembly of DNA-hemin complexes. *ChemBioChem* **2004**, *5*, 374−379.
(24) Li, T.; Dong, S.; Wang, E. Enhanced catalytic DNAzyme for label-free colorimetric detection of DNA. *Chem. Commun.* **2007**, 4209−4211.
(25) Deng, M.; Zhang, D.; Zhou, Y.; Zhou, X. Highly Effective Colorimetric and Visual Detection of Nucleic Acids Using an Asymmetrically Split Peroxidase DNAzyme. *J. Am. Chem. Soc.* **2008**, *130*, 13095−13102.
(26) Fu, R.; Li, T.; Lee, S.; Park, H. DNAzyme molecular beacon probes for target-induced signal-amplifying colorimetric detection of nucleic acids. *Anal. Chem.* **2011**, *83*, 494−500.
(27) Fu, R.; Jeon, K.; Jung, C.; Park, H. G. An ultrasensitive peroxidase DNAzyme-associated aptasensor that utilizes a target-triggered enzymatic signal amplification strategy. *Chem. Commun.* **2011**, *47*, 9876−9878.
(28) Murat, P.; Singh, Y.; Defrancq, E. Methods for investigating G-quadruplex DNA/ligand interactions. *Chem. Soc. Rev.* **2011**, *40*, 5293−5307.
(29) Wu, H.; Liu, Y.; Wang, H.; Wu, J.; Zhu, F.; Zou, P. Label-free and enzyme-free colorimetric detection of microRNA by catalyzed hairpin assembly coupled with hybridization chain reaction. *Biosens. Bioelectron.* **2016**, *81*, 303−308.
(30) Gao, Y.; Li, B. G-quadruplex DNAzyme-based chemiluminescence biosensing strategy for ultrasensitive DNA detection: combination of exonuclease III-assisted signal amplification and carbon nanotubes-assisted background reducing. *Anal. Chem.* **2013**, *85*, 11494−11500.
(31) Li, X.; Chen, W.; Zeng, W.; Wan, C.; Duan, S.; Jiang, S. microRNA-137 promotes apoptosis in ovarian cancer cells via the regulation of XIAP. *Br. J. Cancer* **2017**, *116*, 66−76.

DOI: 10.1021/acssensors.7b00178
ACS Sens. 2017, 2, 810−816

(32) Sun, P.; Shen, Y.; Gong, J.; Zhou, L.; Sheng, J.; Duan, F. A New MicroRNA Expression Signature for Cervical Cancer. *Int. J. Gynecol. Cancer* **2017**, *27*, 339−343.
(33) Mohanty, J.; Barooah, N.; Dhamodharan, V.; Harikrishna, S.; Pradeepkumar, P. I.; Bhasikuttan, A. C. Thioflavin T as an efficient inducer and selective fluorescent sensor for the human telomeric G-quadruplex DNA. *J. Am. Chem. Soc.* **2013**, *135*, 367−376.
(34) Cissell, K. A.; Shrestha, S.; Deo, S. K. MicroRNA Detection: Challenges for the Analytical Chemist. *Anal. Chem.* **2007**, *79*, 4754−4761.
(35) Bi, S.; Chen, M.; Jia, X.; Dong, Y. A hot-spot-active magnetic graphene oxide substrate for microRNA detection based on cascaded chemiluminescence resonance energy transfer. *Nanoscale* **2015**, *7*, 3745−3753.
(36) Zhang, H.; Wang, Y.; Zhao, D. W.; Zeng, D.; Xia, J.; Aldalbahi, A.; Wang, C.; San, L.; Fan, C. H.; Zuo, X. L. Universal Fluorescence Biosensor Platform Based on Graphene Quantum Dots and Pyrene-Functionalized Molecular Beacons for Detection of MicroRNAs. *ACS Appl. Mater. Interfaces* **2015**, *7*, 16152−16156.
(37) Zhu, Y.; Qiu, D.; Yang, G.; Wang, M.; Zhang, Q.; Wang, P.; Ming, H.; Zhang, D.; Yu, Y.; Zou, G.; et al. Selective and sensitive detection of MiRNA-21 based on gold-nanorod functionalized polydiacetylene microtube waveguide. *Biosens. Bioelectron.* **2016**, *85*, 198−204.
(38) Baker, M. B.; Bao, G.; Searles, C. D. In vitro quantification of specific microRNA using molecular beacons. *Nucleic Acids Res.* **2012**, *40*, e13.
(39) Lee, J.; Park, G.; Min, D. A biosensor for the detection of single base mismatches in microRNA. *Chem. Commun.* **2015**, *51*, 14597−14600.
(40) Zhou, H.; Yang, C.; Chen, H.; Li, X.; Li, Y.; Fan, X. A simple G-quadruplex molecular beacon-based biosensor for highly selective detection of microRNA. *Biosens. Bioelectron.* **2017**, *87*, 552−557.
(41) Wang, R.; Wang, L.; Zhao, H.; Jiang, W. A split recognition mode combined with cascade signal amplification strategy for highly specific, sensitive detection of microRNA. *Biosens. Bioelectron.* **2016**, *86*, 834−839.
(42) Oishi, M.; Sugiyama, S. An Efficient Particle-Based DNA Circuit System: Catalytic Disassembly of DNA/PEG-Modified Gold Nanoparticle-Magnetic Bead Composites for Colorimetric Detection of miRNA. *Small* **2016**, *12*, 5153−5158.
(43) Xi, Q.; Zhou, D. M.; Kan, Y. Y.; Ge, J.; Wu, Z. K.; Yu, R. Q.; Jiang, J. H. Highly sensitive and selective strategy for microRNA detection based on WS_2 nanosheet mediated fluorescence quenching and duplex-specific nuclease signal amplification. *Anal. Chem.* **2014**, *86*, 1361−5.
(44) Wang, Q.; Yin, B.; Ye, B. A novel polydopamine-based chemiluminescence resonance energy transfer method for microRNA detection coupling duplex-specific nuclease-aided target recycling strategy. *Biosens. Bioelectron.* **2016**, *80*, 366−372.
(45) Yang, X.; Tang, Y.; Mason, S. D.; Chen, J.; Li, F. Enzyme-Powered Three-Dimensional DNA Nanomachine for DNA Walking, Payload Release, and Biosensing. *ACS Nano* **2016**, *10*, 2324−2330.
(46) Peng, H.; Li, X. F.; Zhang, H.; Le, X. C. A microRNA-initiated DNAzyme motor operating in living cells. *Nat. Commun.* **2017**, *8*, 14378.

DOI: 10.1021/acssensors.7b00178
ACS Sens. 2017, 2, 810−816

DETERMINATION OF IODINE SPECIES IN SEAWEED BY ALKALI FUSION-AMINO DERIVATIZATION-ION EXCHANGE PURIFICATION-ION CHROMATOGRAPHY

Xia Ping Zhu*, Jie Zheng, Xue Jin Wang, Jun Tan

College of Materials and Chemistry & Chemical Engineering, Mineral Resources Chemistry Key Laboratory of Sichuan Higher Education Institutions, Cheng du University of Technology, Chengdu, Sichuan, China

ABSTRACT

An alkali fusion-amino derivatization-ion exchange purification-ion chromatography (AAII) method had been established to detect different species of iodine in seaweed. The iodide (I^-) was determined directly after the sample was digested with a mixed solution of K_2CO_3-KCl and $KClO_3$-$ZnSO_4$. The iodate (IO_3^-) was determined after the digestion solution was purified by using a cation exchange column. The methyl iodide (CH_3I) was determined after the sample was extracted by ethanol and derivatized with tetraethylenepentamine (TEPA). The optimal derivatization conditions of CH_3I were that the molar ratio of methyl iodide to TEPA was 1:5, and the derivatization time and temperature were 120 min and 60 ℃, respectively. The linear range of I^- and IO_3^- was 0-50 mg/L, with the detection limit of 0.448 and 0.521 mg/L, respectively. The linear range of CH_3I was 0-112 mg/L, with the detection limit of 3.87 mg/L. The I^-, IO_3^- and CH_3I in kelp and porphyra were determined with recovery rates in the range of 77.19-94.61%.The AAII method had the advantages of simple instrument, conducive to popularization and simultaneous determination of I^-, IO_3^- and CH_3I.

KEYWORDS: Ion chromatography, iodide, iodate, methyl iodide, amino derivation, seaweed

1. INTRODUCTION

Iodine is a kind of multivalent and non-metal element. The valence of iodine ranges is -1 to +7 [1].The most frequent species of iodine in nature are I^-, I_2, IO_3^-, IO_4^- and organic iodide. The iodine is prone to be volatilized, oxidized, adsorbed and contaminated, and it is very easy to be damaged during the sample pre-treatment. So, iodine is one of the elements which are difficult to be determined [2].

Iodine is very important to human health owing to its biological activity. One adult needs 100 μg iodine per day. It will be toxic with an excessive intake of iodine, and the thyroid gland hypertrophy can be caused by lack of it [3].

Iodine is widely distributed in the air, soil, rock and water. The iodine concentration in sea-water is relatively stable at about 50-60 μg/L [4]. In general, the iodine concentration in organisms is higher than in an inorganic sample, and the iodine concentration in marine organisms is also higher than in terrestrial organisms. The seaweed contains more iodine than other marine organisms, and it is one of the best sources for humans to obtain iodine [5]. So, it is meaningful to study the analysis method of iodine in kelp and porphyra.

In recent years, there are many papers focusing on the determination of iodine. The methods can be classified into chemical and instrumental analysis methods. Chemical analysis method is usually applied to analyse constant iodine. Instrumental analysis methods include spectrophotography, electrochemical method, atomic absorption spectrometry, chromatography and mass spectrometry [2]. The vast majority of researches has just determined total iodine [6-10]. But, different species of iodine may exhibit dramatically different mobility, bio-availability and chemical behaviours in the ecological circle. The dominant iodine species in environmental and biological samples are iodide, iodate and organo-iodine. Furthermore, the "three" dominant iodine species may undergo transformation to one another in the ecological circle.

Some theoretical studies of the ultraviolet absorption spectra of I_2, I^-, IO_3^- and I_3^- in liquid media have been conducted for the simultaneous detection of different species of iodine, but there was not any determination of samples [11, 12]. The I^- and IO_3^- in brine and seafood have been determined simultaneously by ultraviolet absorption spectrometry [13]. The simultaneous kinetic spectrophotometric determinations of iodate and periodate in table salt, sea-tangle and water samples have been achieved by chemometric methods [14]. Chromatography can better determine different species of iodine simultaneously through linking different detectors, such as the

ion chromatographic linking conductance detector [15], ultraviolet detector [16], or ICP-MS detector [17-19]. The iodine species have been determined using high performance liquid chromatography (HPLC) and UV detection through conversion of IO_3^- and organo iodine into I^- [20]. An effective method for determining I^-, IO_3^- and organo-iodine in waters has been developed by derivatizing I^- and IO_3^- to organo-iodine and measuring organo iodine with HPLC-MS [21]. The capillary electrophoresis is also used for analysis of iodine species, especially when studying organo iodine analysis [22].

The determination of different species of iodine is not easy to conduct, especially that of organo-iodine, and correlative reports are few. This study has determined I^-, IO_3^- and CH_3I in seaweed by ion chromatography connected with conductivity detector through adding the pre-treatment process of alkali fusion, amino derivatization and ion exchange purification. Although the detection limit of I^-, IO_3^- and CH_3I is expected to be further reduced, the simultaneous determination of I^-, IO_3^- and CH_3I is very meaningful, and the pre-treatment procession of amino derivatization has provided a valuable reference for detection of CH_3I.

2. MATERIALS AND METHODS

2.1 Instruments and Reagents

All the experiments were performed with D1010 anion-exchange chromatography, equipped with a conductivity detector (Shanghai Hengke Instrument Co., Ltd. Shanghai, China). A Shodex IC SI 90 4E column was used to separate different species of iodine. A SHZ-82 Swing-type water-circulator bath oscillator (Jiangsu Jincheng Instrument Co., Ltd. Jiangsu, China) was used for derivatization experiments of CH_3I.

KI and KIO_3 stock solutions (2.000 g/L) were used for experiments: 0.2616 g KI and 0.2447 g KIO_3 were weighed, dissolved and set to the volume to 100 ml with water in a volumetric flask, respectively. CH_3I stock solution (22.40 g/L) was prepared as follows: 1 ml methyl iodide was dissolved with 10 ml of 10 % ethanol, and then, the volume was set to 100 ml in a volumetric flask with water. All the stock solutions were stored in the dark and diluted before use.

The CH_3I was purchased from Chengdu Aikeda Chemical Reagent Co., Ltd. Chengdu, China. The other experimental reagents included KI, KIO_3, NaOH, Na_2CO_3, $NaHCO_3$, $KClO_3$, $ZnSO_4$, KCl, K_2CO_3, and $H_2N(CH_2CH_2NH)_3CH_2CH_2NH_2$ (TEPA); they were purchased from Chengdu Kelong Reagent Co. Chengdu, China. All the chemicals were of analytical grade and used without further purification.

Kelp and porphyra were purchased in the market. The water was of high purity, and its resistance value was greater than 18.2 MΩ . cm

2.2 Experimental method

At first, the seaweed was washed with distilled water, dried at 80 ℃, crushed and sieved through a 40-mesh screen. Then, 2 g seaweed, 1.5 ml A solution (5% K_2CO_3 and 5% KCl) and 1.5 ml B solution (5% $KClO_3$ and 5% $ZnSO_4$) were mixed adequately, carbonized at 200-300 ℃, incinerated at 400-500 ℃, and extracted by hot water.

The I^- in the extract was determined directly by ion chromatography. The IO_3^- in the extract was determined by ion chromatography after ion exchange with a 732-type cat-ion exchange resin with a flow velocity of 10 ml/30 min.

The CH_3I in the seaweed was extracted by a 95% ethanol solution for 2 h in a bath oscillator. Then, the extract was derivatized with 0.1 ml/L TEPA at 60 ℃ for 2 h in a bath oscillator, prior to the determination with ion chromatography.

The eluent for ion chromatography consisted of 1.8 mmol/L $NaHCO_3$ and 2.4 mmol/L Na_2CO_3, the flow velocity was 1 ml/min, the conductivity range was 0-30 μs and suppression current was 50 mA (Fig. 1).

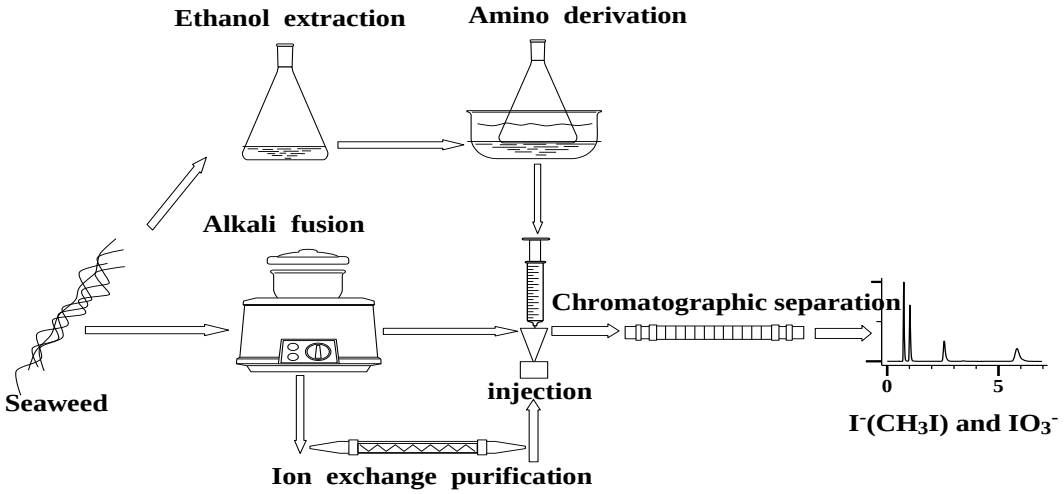

FIGURE 1 - Analytical process of iodine species in seaweed.

3. RESULTS AND DISCUSSION

3.1 Selection of sample digestion solution

Iodine is easy to be lost. It will volatilize in the form of HI in acidic medium; so, the sample shall be digested in alkaline or neutral medium. The NaOH, Na_2CO_3, and mixed solutions composed of A solution (5% K_2CO_3 and 5% KCl) and B solution (5% $KClO_3$ and 5% $ZnSO_4$) were selected to digest the seaweed [16]. The content of I^- determined by ion chromatography is listed in Table 1. The content of I^- after digestion by the Na_2CO_3 is the least, and the CO_2 produced by Na_2CO_3 will affect the process of ion exchange. The content of I^- after digestion by NaOH is higher than by Na_2CO_3, but a large amount of OH^- will interfere the determination of IO_3^-. The mixed solution composed of A solution (5% K_2CO_3 and 5% KCl) and B solution (5% $KClO_3$ and 5% $ZnSO_4$) is considered to be the optimum digestion solution.

3.2 Sample purification

The retention time of I^- is at 20 min, which is different from other impurity ions, and I^- is easily adsorbed by the ion exchange column; therefore, I^- is determined directly by ion chromatography after digestion. The retention time of other impurity ions, such as Cl^-, is similar to that of IO_3^- which is introduced by digestion solution. Therefore, the determination of IO_3^- shall be carried out after eliminating the interference from other impurity ions. The methods, such as adsorption, extraction, dialysis, combustion, alkali fusion, precipitation and ion exchange are often used to isolate and purify samples in ion chromatography [17]. The cat-ion exchange resin (styrene-type) was selected to remove most of impurity ions in this study. Ten g of cation exchange resin were activated by 5% HCl and packed into a column. Then, 10 ml digestion solution flew through the ion exchange column with a velocity of 10 ml/30 min. Then, the IO_3^- in the filtrate was determined by ion chromatography.

3.3 Derivatization of methyl iodide

3.3.1 Selection of derivatization reagent

The species of iodine in seaweed have organic and inorganic iodine. The main species of inorganic iodine is I^-, which occupies about 60-90% while the organic iodine only occupies 10-40% [18]. The C-I bond of CH_3I is easily broken. The CH_3I is also very easy to be oxidized. The oxidation experiments of CH_3I by H_2O_2 had been carried out. The results show that the H_2O_2 cannot quantitatively oxidize CH_3I, and residual H_2O_2 will affect the subsequent determination. The TEPA can break C-I bonds, and thus, the CH_3I can be determined through measurement of I^- derivatized from CH_3I. The chromatogram of CH_3I before and after derivatization is shown in Fig. 2. There is no signal of I^- before CH_3I derivatization, but the I^- peak at 21 min arises after CH_3I derivatization. So, the conditions of CH_3I derivatization have been further discussed.

3.3.2 Effect of derivatization conditions

The experimental results of molar ratio of CH_3I to TEPA, derivative time, derivative temperature are shown in Figs. 3-5. The signal of I^- increases when the molar ratio of CH_3I to TEPA varies from 1:1 to 1:6.5, but then, it decreases slightly. The derivatization is not entirely with scant amount of TEPA, and when TEPA is in overabundance, the peak area decreases. The peak area of I^- increases, then turns to stable with temperature increase, and

TABLE 1 - Determination results of different digestion solutions.

Result	NaOH	Na_2CO_3	Mixed digestion solution

	Kelp	Porphyra	Kelp	Porphyra	Kelp	Porphyra
I^-（μg/g）	289	151	238	34	441	349

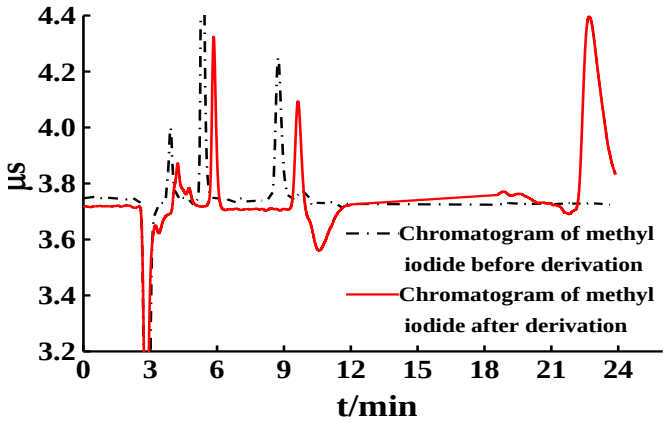

FIGURE 2 - Chromatogram of CH_3I before and after derivatization.

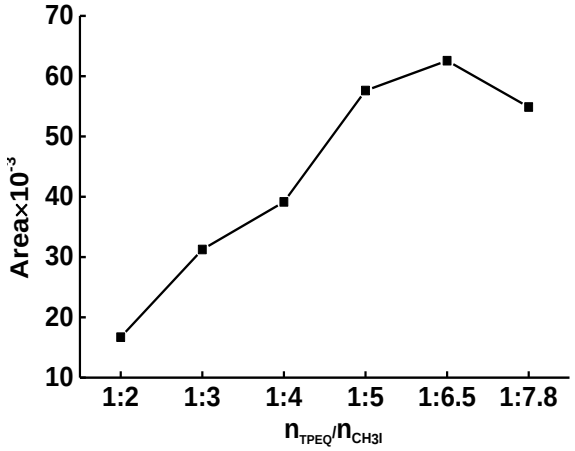

FIGURE 3 - Effect of molar ratio of CH_3I to TEPA.

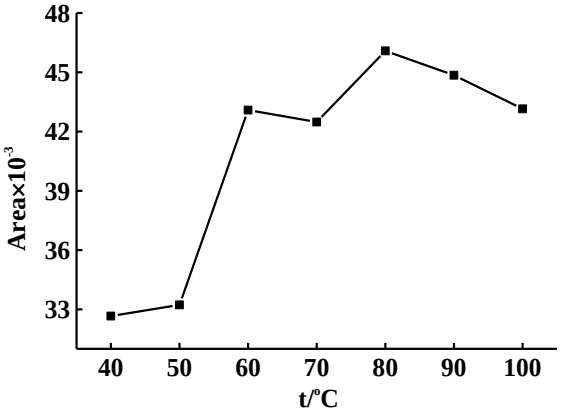

FIGURE 4 - Effect of derivatization temperature.

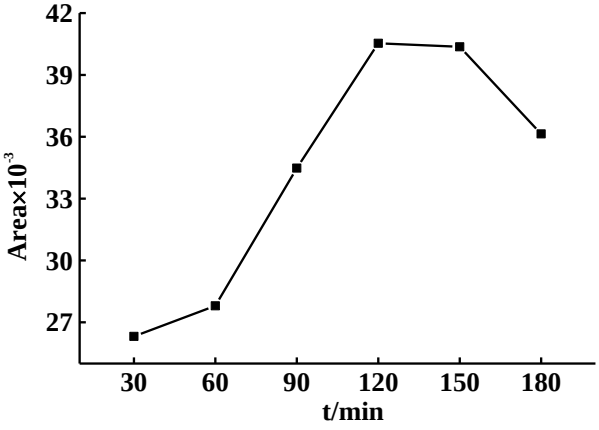

FIGURE 5 - Effect of derivatization time.

the best derivative temperature is at 60-100 ℃. The peak area of I^- increases within 120 min, and then decreases with derivatization time prolonging to 180 min, and the best derivatization time is 120-150 min. From derivatization effect and economic considerations, the optimal derivatization conditions of CH_3I are molar ratio of CH_3I to TEPA being 1:5, derivatization time and temperature of 120 min and 60 ℃, respectively.

3.4 Selection of ion chromatographic conditions

The ion chromatographic conditions are as follows: conductivity range of 0-30 μs, suppression current of 50 mA and eluent flow-rate of 1ml/min. The influence of eluent concentration on the retention time and peak shape of I^- and IO_3^- was discussed when the concentration of $NaHCO_3$ was 1.7 mmol/L, and the concentration of Na_2CO_3 varied from 1.8 to 3.0 mmol/L. The peak of I^- becomes wide and trail, and retention time is prolonged with a low concentration of Na_2CO_3. When the concentration of Na_2CO_3 is too high, the water peak and IO_3^- peak cannot be distinguished. The eluent consisting of 1.7

mmol/L $NaHCO_3$ and 2.4 mmol/L Na_2CO_3 are demonstrated to be the best conditions. The chromatograms of I^- and IO_3^- are shown in Fig. 6 under optimal conditions. The negative peak at 2.9 min is the water peak, and those at 4 and 21 min represent IO_3^- and I^-, respectively.

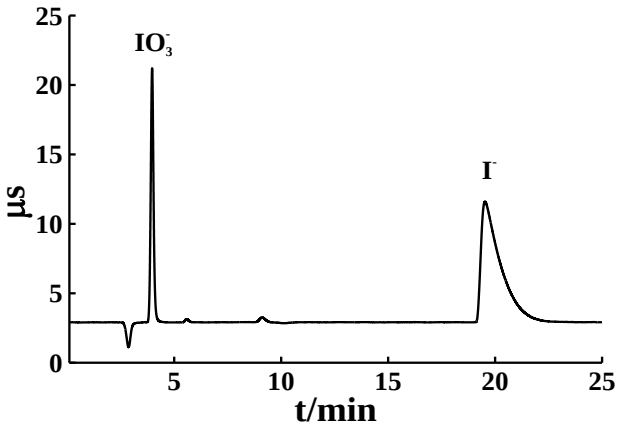

FIGURE 6 - Chromatogram of I^- and IO_3^-

3.5 Standard working curve, linear range and detection limit

The mixed standard solutions with different concentrations of I^-, IO_3^- and CH_3I were prepared. The concentrations of I^- and IO_3^- were obtained directly, and that of CH_3I was got through the difference of the peak area of I^- before and after derivatization of CH_3I under optimized conditions. The standard working curve, linear equation, linear range and detection limit of I^-, IO_3^- and CH_3I are shown in Figs. 7-8 and Table 2. The results show a favourable linear relationship (peak area vs. analyte concentration) in the range of 0-50 mg/L for I^-, IO_3^- and 0-112 mg/L for CH_3I. The detection limits of I^-, IO_3^- and CH_3I are 0.448, 0.521, and 3.87 mg/L, respectively. The linear range of this work is comparable to those of UV, IC-UV, IC-MS, CE-UV, HPLC-UV or HPLC-MS based methods (Table 3), and the sensitivity is not as good as those. However, in this work, the instrument is simple, beneficial to popularization, and the pre-treatment process of amino derivatization have provided a meaningful reference for the detection of CH_3I.

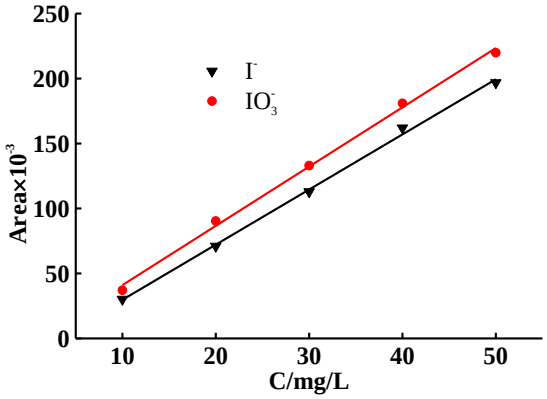

FIGURE 7 - Standard working curves of I^- and IO_3^-.

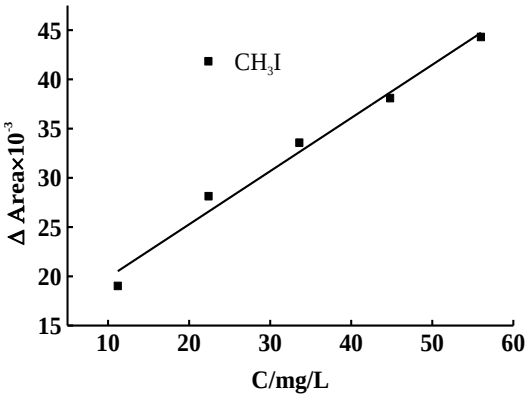

FIGURE 8 - Standard working curves of CH_3I.

TABLE 2 - Linear equation, linear range and detection limits of I^-, IO_3^- and CH_3I.

Speciation of iodine	Linear equation	R^2	Linear range (mg/L)	Detection limit (mg/L)
I^-	A = 4242.7c-12704	0.9980	0-50	0.4482
IO_3^-	A = 4868.5c-16372	0.9975	0-50	0.5214
CH_3I	ΔA = 605.12c+14471	0.9837	0-112	3.870

TABLE 3 - Comparison of determination methods of I^-, IO_3^- and CH_3I.

Method	Species	Linear range (mg/L)	LOD (mg/L)	Samples	Ref.
UV	I^- /IO_3^-	-	-	-	11[a]
UV	I^- /IO_3^- /I_3^- /I_2	-	-	-	12[a]
UV	I^- /IO_3^-	0-1.2/0-1.5	14.8/1.54(μg/L)	Seaweed, brine	13
UV	I^- /IO_3^-	0.1-1.2	0.027/0.015	table salt, seatangle water	14
IC-Con-UV	I^- /IO_3^-	0.08-16.4	3.2/2.8 (mg/kg)	seaweed	15

		/0.094-13.1			
IC-UV	I^- /IO_3^-	0.3-50/0.2-50	0.1044 /0.0697	Ironical liquids, underground water	16
IC-ICP-MS	I^- /IO_3^- /organic iodine	0.25-1000 (μg/L)	0.1(μg/L)	seaweed	17[b]
IC-ICP-MS	I^- /IO_3^-	0.1-10/0.2-20	0.1/0.2(μg/L)	mineral	18
IC-ICP-MS	I^- /IO_3^-	5-500(μg/L)	2.0/1.5(μg/L)	Seawater	19
HPLC-UV	I^-/IO_3^- /organic iodine	1-150(nM)	1(nM)	Fresh water seawater	20[c]
HPLC-MS	Organo iodine / I^-/IO_3^-	0-100 (μg/L)	3.7(μg/L)	tap water, seawater, urine, wastewater	21[d]
CE-UV	I-/IO_3^-/mono-iodo-thyrosine/di-iodo-thyrosine	0.2-100	0.052/0.040 /0.032/0.025	seaweed	22
IC-Con	I^- /IO_3^- /CH_3I	0-50/0-50 /0-112	0.448/0.521 /3.87	seaweed	AAII

[a] Theoretical research; [b] I^- and IO_3^- were determined directly by IC/MS, determination of the organic iodine was a differential method by determination of total iodine after high temperature cracking of the samples. [c] I^- was determined directly by HPLC-UV, the IO_3^- was reduced to I^- by $NaHSO_3$, organic iodine was transformed to I^- after decomposition by dehydrohalogenation and reduction by $NaHSO_3$. [d] The organo-iodine was measured directly by HPLC-MS, the I^- was derivatized to organic iodine, IO_3^- was reduced to I^-, and then, derivatized to organic iodine.

4. SAMPLE ANALYSIS

According to the experiment method introduced in section 2.2, the I^-, IO_3^- and CH_3I in kelp and porphyra had been determined. The recovery experiments had been done at the same time. The results are listed in Table 3. The I^- content is 300-500 μg/g, and the IO_3^- content is 100-200 μg/g in kelp and porphyra. The content of CH_3I in kelp and porphyra was below the detection limit. The recovery rates of I^-, IO_3^- and CH_3I in kelp and porphyra are in the range of 77.19-94.61%. The I^- was the main species in kelp and porphyra, accounting for more than 80% of total iodine.

TABLE 3 - Determination results of I^-, IO_3^- and CH_3I in seaweed samples.

Sample	Iodine species	Concentration (mg/L)	Adding (mg)	RSD (n=6) (%)	Recovery (%)	Content (μg/g)
Kelp	I^-	17.65	0.200	7.29	77.19	441.1
	IO_3^-	5.073	0.100	6.93	94.61	122.8
	CH_3I	-	0.224	-	86.56	-
Porphyra	I^-	13.98	0.200	4.34	82.74	349.4
	IO_3^-	6.858	0.100	8.14	91.19	171.5
	CH_3I	-	0.224	-	91.00	-

5. CONCLUSION

We have constructed an alkali fusion-amino derivatization-ion exchange purification-ion chromatography for the detection of different species of iodine in seaweed samples. Compared to the reported methods, this work provides the advantages of a simple instrument, is conducive to popularization, and allows the simultaneous determination of I^-, IO_3^- and CH_3I. Therefore, the proposed method will be a promising method for detection of I^-, IO_3^- and CH_3I in complicated environmental and food samples.

ACKNOWLEDGMENTS

The authors gratefully acknowledge the financial support from the Natural Science Foundation of the Education Department of Sichuan Province (15ZA0071).

The authors have declared no conflict of interest.

REFERENCES

[1] Liu, W., Yang, H., Li, B., Chen, D. and Zhang, H. (2007) Study on speciation stabilities of iodine in underground water by high performance liquid chromatography-inductively coupled plasma mass spectrometry. Chinese Journal of Analytical Chemistry, 35 (4), 571-574

[2] Shelor C. P. and Dasgupta P. K. (2011) Review of analytical methods for the quantification of iodine in complex matrices. Analytica Chimica Acta, (702),16-36

[3] Lin L., Chen G. and Chen Y. H. (2011) Determination of iodine and its species in plant samples using ion chromatog-

raphy inductively coupled plasma mass spectrometry. Journal of Chromatography, 29, 662-666 (in Chinese).

[4] Zeng. H.H. (2012) The organic iodine analysis after ganoderma lucidum richening inorganic iodine and the study of salt mixed with ganoderma lucidum powder containing organic iodine. Nanchang University, School of Life Science, Nanchang (in Chinese)

[5] Sun J.N., Wang D., Cheng H.Y., Liu J.H., Wang Y.C. and Xu Z.G. (2015) Use of ion-pairing reagent for improving iodine speciation analysis in seaweed by pressure-driven capillary electrophoresis and ultraviolet detection. Journal of Chromatography A, 1379,112-117

[6] Zhu Y. C., Cao L., Hao J., Qu Q., Xin S.G. and Zhang H.H. (2010) Electrochemical liquid-phase microextraction and determination of iodide in kelp based on a carbon paste electrode by cyclic voltammetry. Microchim Acta, 170,121-126

[7]. Zhang J.. Takata H., Tagami K., Aono T., Fujita K. and Uchida S. (2012) Rapid determination of total iodine in coastal seawater using SF-ICP-MS. Microchemical Journal, 100,42–47.

[8] Paramita D, Manju G. and Archana J. (2004) Single drop microextraction or solid phase microextraction-gas chromatography-mass spectrometry for the determination of iodine in pharma-ceuticals, iodized salt, milk powder and vegetables involving conversion into 4-iodo-N,N-dimethylaniline. Journal of Chromatography, 1023(1),33-39

[9] Mo S.M., Liang L.N., Cai Y.Q., Mou S.F. and Wen M.J.. (2006) Determination of trace level of iodide in different matrices by high performance anion exchange chromatography with pulsed amperometric detector. Journal of Instrumental Analysis, 25, 105-108 (in Chinese)

[10] Huang. Z, Ito. K. and Hirokawa. T. (2004) Further research on iodine speciation in sea water by capillary zone electrophoresis with isotachophoresis pre-concentration. Journal of Chromatography Analysis, 10(55), 229 - 234.

[11] Wei Y.J.，Liu C.G. and Mo L.P. (2005) Ultraviolet absorption spectra of iodine，iodide ion and triiodide ion. Spectroscopy and Spectral Analysis, 25(1), 86-88 (in Chinese)

[12] Kireev S. V., Symanovsky I. G. and Shnyrev S. L. (2009) Development of optical methods for simultaneous detection of I_2, I^-, IO_3^- and I_3^- in liquid media in real time. Laser Physics, 19(9),1939–1949.

[13] Tan J., Zhu X.P.，Liu M.M., Wei Z.C. and Sang S.H. (2015) Determination of iodine and iodate in brine and seafood simultaneously by ultraviolet absorption spectrometry. Spectroscopy and Spectral Analysis, 35(6),86-88 (in Chinese)

[14] Ni Y.N. and Wang Y. (2007) Application of chemometric methods to the simultaneous kinetic spectrophotometric determination of iodate and periodate based on consecutive reactions. Microchemical Journal 86, 216-226

[15] Zhong Z. X. and Li G. K. (2009) Determination of fluorine, bromine, iodine and sulphurin seafood by ion chromatography with conductivity-ultraviolet detector. Journal of Instrumental Analysis, 28, 572-575 (in Chinese)

[16] Li. M. Yu. H. and Zheng X.R. (2014) Simultaneous analysis of iodate, iodide, bromate and bromide by ion chromatography with ultraviolet detection. Chinese journal of chromatography, 32(3),299-303

[17] Lin L., Chen G. and Chen Y.H. (2011) Determination of iodine and its species in plant samples using ionchromatography-inductively coupled plasma mass spectrometry. Chinese journal of chromatography, 29(7),662-666

[18] Pantsar-Kallio M. and Manninen P. K.G. (1998) Speciation of halogenides and oxyhalogens by ion chromatography inductively coupled plasma mass spectrometry. Analytic Chemical Acta, 360, 161-166.

[19] Chen Z. L. Megharaj M. and Naidu R. (2007) Speciation of iodate and iodide in seawater by non-suppressed ion chromatography with inductively coupled plasma mass spectrometry. Talanta, 72,1842–1846

[20] Kathleen A. S. and Santschi P. H. (2003) Sensitive determination of iodine species, including organo-iodine, for freshwater and seawater samples using high performance liquid chromatography and spectrophotometric detection. Analytica Chimica Acta, 482,59–71

[21] Gong T.T. and Zhang X.R.. (2013) Determination of iodide, iodate and organo-iodine in waters with a new total organic iodine measurement approach. Water research,47,6660-6669

[22] Sun J.N., Wang D., Cheng H.Y., Liu J.H., Wang Y.C. and Xu Z.G.(2015) Use of ion-pairing reagent for improving iodine speciation analysis in seaweed by pressure-driven capillary electrophoresis and ultraviolet detection. Journal of chromatography A,1379,112-117

Received: January 20, 2015
Revised: March 23, 2015; July 29, 2015
Accepted: September 16, 2015

CORRESPONDING AUTHOR

Xia Ping Zhu
College of Materials and Chemistry & Chemical Engineering
Mineral Resources Chemistry Key Laboratory of Sichuan Higher Education Institutions
Cheng du University of Technology
Chengdu, Sichuan
P.R. CHINA

E-mail: zhuxiaping@cdut.edu.cn

AFS/ Vol 37/ No 4/ 2015 – pages 177 - 183

网络出版时间：2016-09-01 17:18:57
网络出版地址：http://www.cnki.net/kcms/detail/11.1759.TS.20160901.1718.062.html

ICP-AES 结合主成分分析和决策树模型的四种品牌白酒鉴别方法研究

郑劼[1] 吴文林[2*] 万渝平[2] 梁恒兴[2] 肖全伟[2] 朱霞萍[1]
（1. 成都理工大学 材料与化学化工学院，四川成都 610059；
2. 成都市食品药品检验研究院，四川成都 610100）

摘　要：采用电感耦合等离子体原子发射光谱（ICP-AES）测定了四种品牌 56 个白酒样品（五粮液，郎酒，全兴，五津醇）中的 16 种元素含量。通过对结果进行 z-score 标准化，消除各元素间量纲差异，再对其进行主成分分析。结果表明，第一主成分的方差贡献率为 40.3%，前十主成分的贡献率达 96.3%，基本保留了原变量的所有信息。选择前十主成分建立决策树分类预测模型，模型的交叉验证准确率高达 97.6%，再用模型预测未参与建模的 15 个白酒样品，准确率高达 100%。模型能够准确区分五粮液，郎酒，全兴，五津醇四种品牌白酒。

关键词：白酒，元素，ICP-AES，主成分分析，决策树模型

Study on discrimination of four Chinese brand spirits based on ICP-AES coupled the principal component and decision tree analysis

Zheng Jie[1] Wu-Wenlin[2*] Wan Yu-Ping[2] Liang Heng-Xing[2] Xiao Quan-Wei[2]
Zhu Xia-Ping[1]
(1 College of Materials and Chemistry & Chemical Engineering, Chengdu University of Technology, Chengdu, Sichuan, 610059, China.
2 Chengdu Institute for Food and Drug Control, Chengdu, Sichuan, 610100, China)

Abstract: The potential of ICP-AES for metal element profiling of Chinese spirit samples was examined. Sixteen elements in fifty six spirits samples representing four varieties of brands (Wuliangye, Lang Liquor, Quanxing, Wujinchun) were determined. The set of data was employed to construct a sample class prediction model based on z-score standardization followed by principal component analysis (PCA) and Decision Tree analysis (DT), which was employed to explore the structure of the data and construct classification and prediction model. The First principal component explained 40.3% of variance while the top ten components explained 96.3% of variance which was employed to construct the DT model. The validated DT model based on 5-fold cross-validation enabled correct classification of 97.6% of samples, and other 15 spirit samples could be predict correctly. The Wuliangye, Lang Liquor, Quanxing, Wujinchun can be classified intensively.

Key words: Spirit; Element; ICP-AES; PCA; Decision Tree
中图分类号：TS207.3　　**文献标识码**：A

作者简介：郑劼（1992—），男，硕士，研究方向：分析化学，E-mail：zhengj159@icloud.com。
基金项目：科技部国家重大科学仪器设备开发专项（2012YQ09016705）
*通讯作者：吴文林（1986-），男，硕士，工程师，研究方向：食品化学，E-mail：wuwenlin@163.com。

酒是一种广受全世界人民喜爱，具有极高商业价值的饮品[1]。白酒是我国具有 5000 多年历史的传统特色食品之一，其制作工艺独特，和白兰地（Brandy）、威士忌（Whisky）、金酒（Gin）、伏特加（Vodka）、朗姆酒（Rum）并称为世界六大著名蒸馏酒[2-3]。

据报道[4]，2015 年全年全国白酒折 65 度商品量达 1312.80 万千升。但在白酒产业蓬勃发展的同时，白酒的制假售假案件屡禁不止。由于行业门槛低，小规模酒厂数量众多，白酒生产流通环节监管不力等因素，导致消费者买到以假充真，以次充好的假冒伪劣白酒的案件时有发生，严重损害了消费者的健康和合法权益，对白酒行业的健康发展产生了巨大的影响。

随着人们对白酒的深入研究，白酒中的元素越来越受到人们的重视。一方面，白酒中元素含量的高低直接影响消费者的身体健康，另一方面，元素可以直接影响白酒的感官。对于不同的品牌白酒，由于其生产原料、蒸馏设备、储存器皿等不同，某些微量元素的含量也不尽相同。国内外研究者采用 ICP-OES[5]，ICP-MS[8]等测定酒中元素含量，并用 PCA[9]，PLS-DA[12]，SVM[15]等多元统计分析方法对采集的数据进行分析，挖掘数据内在联系，建立不同产地，不同品牌白酒的分类预测模型。Vivien F[16]用 ICP-MS 分析了加拿大两个主要产酒城市尼加拉瓜（Niagara）和奥肯那根（Okanagan）的酒的痕量金属指纹图谱。通过同时测定白酒中的 34 种痕量元素（Li，Be，Mg，Al，P，Cl，Ca，Ti，V，Mn，Fe，Co，Ni，Cu，Zn，As，Se，Br，Rb，Sr，Mo，Ag，Cd，Sb，I，Cs，Ba，La，Ce，Tl，Pb，Bi，Th，和 U）浓度，并用统计学工具建模。结果表明，两种产地的酒能够区分，且准确度高达 100%。Eugenio C[6]用 ICP-MS 研究了净化，过滤，储存等对白葡萄酒样品中的稀土元素（Rare Earth Elements，REEs）含量的影响。研究表明，净化、过滤等操作均会不同程度的影响稀土元素浓度但不会影响其它金属元素的含量，用木头或不锈钢储存会比用玻璃储存的浓度影响小。

现有研究多集中于白酒中香味物质的鉴别，通过白酒中微量元素浓度差异来区分各品牌白酒的研究较少。本实验采用 ICP-AES 测定了四种具有代表性的白酒（五粮液，郎酒，全兴，五津醇）中 16 种元素含量，再用 Matlab 软件分析其差异。对 z-score 标准化的数据进行主成分分析，并建立四种品牌白酒的决策树模型。建立的模型可正确预测四种品牌白酒，为白酒的鉴别提供科学有效的技术手段。

1 材料与方法

1.1 材料与仪器

白酒 S1~S11 为五粮液（WLY）；S12~22 为郎酒（LJ）；S23~38 为全兴（QX）；S39~56 为五津醇（WJC），其中五粮液的生产日期为 2012～2014 年，郎酒为 2009～2014 年，全兴为 2012～2014 年，五津醇 2013～2014 年。Al、As、Ca、Cd、Cr、Cu、Fe、K、Mg、Mn、Na、Ni、Pb、Se、Sr 和 Zn 标准储备液由国家有色金属及电子材料分析测试中心提供；硝酸（优级纯）由西陇化工股份有限公司提供；高氯酸（优级纯）由天津鑫源化工有限责任公司提供；实验用水为一级水。

电感耦合等离子体原子发射光谱仪，美国 Varian 公司 VISTA-PRO 型；Milli-Q 净化系统，美国 Millipore 公司；所有玻璃器皿均用 10%硝酸浸泡 24 h 以上。

1.2 样品前处理

准确称取 15 g（精确至 0.1 mg）白酒样品于 250 mL 锥形瓶中，置于电热板（250 ℃）蒸发浓缩至 1 mL，冷却后加入 10 mL 混合酸（硝酸:高氯酸，5:1），于电热板上消解至无色，继续加热至溶液剩约 1 mL；转移至 25 mL 容量瓶，定容。

1.3 仪器分析条件

功率：1.25 kW；等离子气流量：18.0 L/min；助燃气流速：2.25 L/min；喷雾压力：200 kPa；进样延迟：25 s；泵速：15 r/min；清洗时间：10 s。

1.4 数据处理与分析

1.4.1 原始数据标准化

对原始数据进行 z-score 标准化。将原数据减去该变量的平均数，然后除以该变量的标准差。以消除原始数据间的量纲影响，使数据更具可比性。

1.4.2 数据分析

采用 Matlab（R2015a）对不同品牌白酒元素浓度进行主成分分析并用经主成分分析降维的数据建立四种品牌白酒的决策树模型。

2 结果与讨论

2.1 白酒样品元素的测定

采用 ICP-AES 测定样品中 Al、As、Ca、Cd、Cr、Cu、Fe、K、Mg、Mn、Na、Ni、Pb、Se、Sr 和 Zn 等 16 种元素含量。测定结果如表 1 所示，箱型图如图 1 所示。结果表明，不同白酒样品中各元素含量差异较大，因此对数据进行标准化处理，消除量纲影响是很有必要的。

2.2 主成分分析

主成分分析法（Principal Component Analysis，PCA）是一种降低数据维度并且能够最大限度地保留了样本所固有的原始信息的有效方法。通过正交变换将一组可能存在相关性的变量转换为一组线性不相关的变量，使复杂的原始数据变成几个新变量，转换后的这组变量叫主成分。这是挖掘多变量间关联问题的有效方法[17]。

本研究以 56 个酒样中 16 种元素浓度构成 56×16 的矩阵，经 z-score 标准化后，利用 Matlab 软件进行主成分分析，其因子数目和特征值大小如图 2 所示。碎石图的拐点出现在第二和第三主成分之间。第一主成分的方差贡献率为 40.3%，前三主成分特征值累积占方差的 66.1%，解释了白酒样品间的大部分差异，后面的特征值贡献率越来越少。前十主成分方差贡献率为 96.3%，基本保留了原来变量的所有信息，故选择前十主成分进行品牌白酒的建模分析。

表 1 各品牌白酒元素浓度范围

Table 1 Concentration regions of elements measured in different brands of wine

单位：mg/L

元素	五粮液	郎酒	全兴	五津醇
Al	0.1144 ~ 0.5720	1.4096 ~ 4.1749	0.0289 ~ 1.1114	2.0053 ~ 11.6159
Ca	1.2691 ~ 3.6442	2.6933 ~ 8.4790	1.1835 ~ 5.7987	4.5977 ~ 24.2707
K	0.1944 ~ 0.6968	1.3317 ~ 2.8997	0.0518 ~ 1.1247	1.9942 ~ 6.3134
Mg	0.0000 ~ 0.9201	0.0537 ~ 0.9848	0.1826 ~ 1.2331	0.6745 ~ 6.8170
Na	1.7465 ~ 4.8823	1.9376 ~ 7.3351	46.8463 ~ 66.8684	4.6699 ~ 7.8194
Fe	0.0000 ~ 0.1723	0.1764 ~ 0.9105	0.0565 ~ 0.4924	0.5061 ~ 3.9270
As	0.0000 ~ 0.0131	0.0000 ~ 0.0088	0.0000 ~ 0.0306	0.0000 ~ 0.0280
Cd	0.0001 ~ 0.0012	0.0000 ~ 0.0025	0.0000 ~ 0.0021	0.0000 ~ 0.0039
Cr	0.0000 ~ 0.0363	0.0000 ~ 0.0405	0.0000 ~ 0.1097	0.0036 ~ 0.0563
Cu	0.0000 ~ 0.0032	0.0018 ~ 0.0344	0.0005 ~ 0.0365	0.0041 ~ 0.0128
Mn	0.0000 ~ 0.0279	0.0242 ~ 0.0518	0.0000 ~ 0.0537	0.0000 ~ 0.0933
Ni	0.0010 ~ 0.0060	0.0071 ~ 0.0231	0.0021 ~ 0.0079	0.0080 ~ 0.0320

Pb	0.0000 ~ 0.0023	0.0000 ~ 0.0136	0.0000 ~ 0.0281	0.0000 ~ 0.0487
Se	0.0000 ~ 0.0226	0.0000 ~ 0.0154	0.0000 ~ 0.0145	0.0000 ~ 0.0256
Sr	0.0000 ~ 0.0086	0.0000 ~ 0.0114	0.0034 ~ 0.0301	0.0328 ~ 0.0910
Zn	0.0000 ~ 0.0056	0.0183 ~ 0.1900	0.0066 ~ 0.1152	0.0192 ~ 0.0848

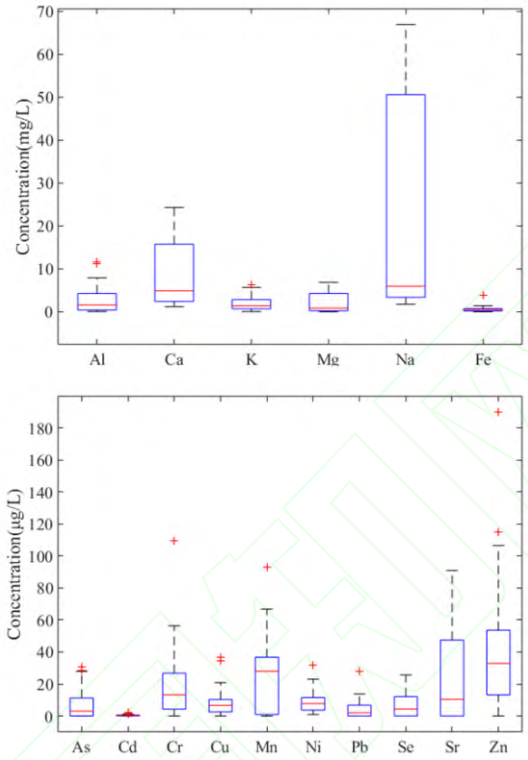

图 1　56 组白酒样品中的元素含量箱型图

Fig. 1.　Concentration box plot of elements in the 56 analyzed spirit samples

以主成分 PC 1 为 X 轴，分别以 PC 2，PC 3 为 Y 轴，建立每个白酒样品的得分图（图 3）。如图 3A 所示，五津醇白酒与郎酒、五粮液、全兴白酒相比差异明显，能与其它品牌白酒区分开，但其点相对离散，在主成分 1 上的得分范围较广。郎酒与五粮液可各自区分，但与全兴白酒部分分布存在交叉。

如图 3B 所示，四种品牌白酒能够有效区分，但其区分度不及图 3A。郎酒被五津醇、五粮液、全兴从三个方向包围，虽然在图中并没有交点，但是建立分类预测模型时极有可能误判。前三组分的方差贡献率为 66.1%，解释了四种品牌白酒样品的大部分差异，能将四种品牌白酒有效区分，但区分不明显，辨识度不高。由于白酒中各元素浓度受较多因素影响，同一品牌，不同品种、批次的样品的含量差异也较大。基于主成分分析的白酒区分方法体现了不同品牌白酒中 16 种元素种类和含量的个性和共性，反映了不同品牌白酒的典型性及相似性。

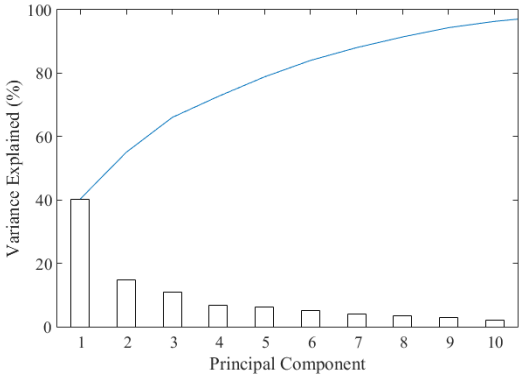

图 2　主成分碎石图

Fig. 2　Scree plot of PCA

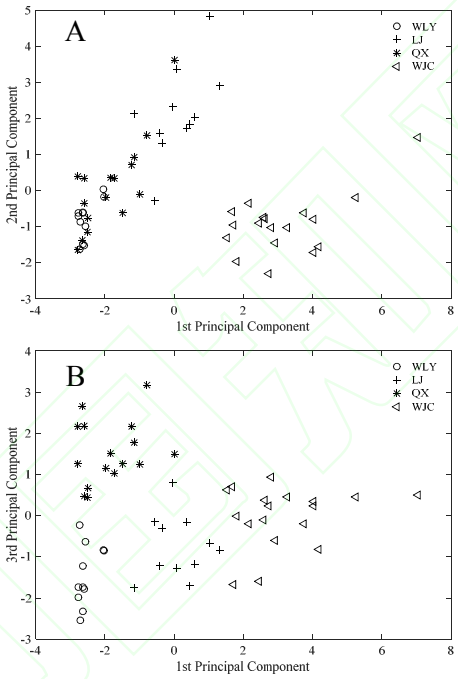

图 3　白酒样品主成分得分图

Fig. 3.　PCA score plot for spirit sample

2.3 分类预测模型建立

决策树（Decision Tree，DT）是一个树结构（可以是二叉树或非二叉树）。其每个非叶节点表示一个特征属性上的测试，每个分支代表这个特征属性在某个值域上的输出，而每个叶节点存放一个类别。使用决策树进行决策的过程就是从根节点开始，测试待分类项中相应的特征属性，并按照其值选择输出分支，直到到达叶子节点，将叶子节点存放的类别作为决策结果[17]。相比贝叶斯或偏最小二乘判别分析等算法，决策树的优势在于构造过程不需要任何领域知识或参数设置，因此在实际应用中，对于探测式的知识发现，决策树更加适用。

交叉验证[11]（cross-validation）是验证分类预测模型的最常用方法，它将样品分为两部分，一部分为训练集，另一部分为验证集，训练集和验证集均有不同类别的独立样品。模型的建立和验证过程会重复多次来保证每个样品都能作为训练或者测试的样本。通常采用的交叉验证方法分别为 Leave One Out 和 N-flod。N-fold 指所有样品被随机均分为 N 组，N-1 组作为训练集，1 组作为验证集。再以不同的组作为验证集，重复 N 次，直至每个样品都能作为一次训练集和一次验证集，输出其混淆矩阵。

本研究以经主成分分析降维后的数据为变量，将样品随机分为两组，训练集 41 个样品，验证集 15 个样品，以 5-flod 为交叉验证方法建立四种品牌白酒样品的决策树模型，验证结果如表 2。模型的总准确率达 97.6%。五粮液、五津醇、全兴的真阳率（Ture Positive Rates，TPR）为 100%，郎酒的假阴率（False Negative Rate，FNR）为 12.5%，有一个样品被误判，22 号郎酒样品被误判为全兴。22 号为郎酒原浆酒。8 组郎酒样品中 6 组为酱香型，1 组为浓酱兼香型，1 组为浓香型。由于酱香型和浓香型白酒的生产工艺不同，导致 22 号白酒样品的 16 种元素的浓度特征与其余郎酒样品有所差异，在该模型中被误判为正常现象。再用经交叉验证的模型预测 15 个未参与建模的白酒样品，预测准确率高达 100%。根据主成分分析结果（图 3），郎酒和五粮液，五粮液和五津醇，全兴和五津醇均无重叠区域，能直接区分，不存在误判的可能性，郎酒与其余三种品牌白酒的区分度较低，可能存在误判。在本模型中，两组郎酒样品分别被误判为全兴和五津醇。决策树模型结果与主成分分析结果相符。

表 2　决策树模型交叉验证及预测结果

Table 2　Overview of classification results obtained by DT model

	郎酒	全兴	五津醇	五粮液
交叉验证				
郎酒	7	1	1	0
全兴	0	12	0	0
五津醇	0	0	13	0
五粮液	0	0	0	8
准确率				97.6%
预测				
郎酒	3			
全兴		4		
五津醇			5	
五粮液				3
准确率				100%

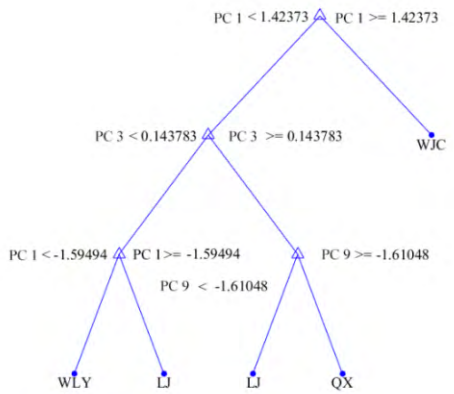

图 4　决策树模型图

Fig. 4　plot of Decision Tree

图 4 为所建立的决策树模型。五津醇首先通过 PC 1 与其它 3 个品牌白酒分开，然后通过 PC 3 将样品分为 2 组，一组为五粮液和郎酒，另一组为郎酒和全兴。最后再分别分开。结果表明，通过 ICP-AES 测定酒中的 16 种元素含量，经 z-score 标准化，主成分分析降维，可以有效区分四种品牌白酒。

3 结论

本文采用 ICP-AES 测定了四种品牌 56 个白酒样品中的 16 种元素含量。分析数据经 z-score 标准化后，进行主成分分析降维。前十主成分方差贡献率为 96.3%，基本保留了原来变量的所有信息。选择前十主成分建立决策树模型，交叉验证结果表明模型的总准确率达 97.6%，再用模型预测未参与建模的 15 个白酒样品，准确率高达 100%。模型能够有效区分五粮液、郎酒、全兴、五津醇四种品牌白酒，建立的模型可为品牌白酒鉴别提供参考。

参考文献

[1] Vaclavik L, Lacina O, Hajslova J, et al. The use of high performance liquid chromatography–quadrupole time-of-flight mass spectrometry coupled to advanced data mining and chemometric tools for discrimination and classification of red wines according to their variety[J]. Analytica Chimica Acta, 2011, 685(1): 45-51.

[2] 王传荣. 白酒的香型及其风味特征研究[J]. 酿酒科技, 2008(9): 49-52.

[3] 刘玉平, 黄明泉, 郑福平, 等. 中国白酒中挥发性成分研究进展[J]. 食品科学, 2010, 31(21): 437-441.

[4] 马勇. 中国白酒三十年发展报告(上)[J]. 酿酒科技, 2016(2): 17-22.

[5] Šelih V S, Šala M, Drgan V. Multi-element analysis of wines by ICP-MS and ICP-OES and their classification according to geographical origin in Slovenia[J]. Food Chemistry, 2014, 153(2014): 414-423.

[6] Rossano E C, Szilágyi Z, Malorni A, et al. Influence of Winemaking Practices on the Concentration of Rare Earth Elements in White Wines Studied by Inductively Coupled Plasma Mass Spectrometry[J]. Journal of Agricultural and Food Chemistry, 2007, 55(2): 311-317.

[7] Zhuang H, Ni Y, Kokot S. Combining HPLC–DAD and ICP-MS data for improved analysis of complex samples: Classification of the root samples from Cortex moutan[J]. Chemometrics and Intelligent Laboratory Systems, 2014, 135(2014): 183-191.

[8] Kruzlicova D, Fiket Ž, Kniewald G. Classification of Croatian wine varieties using multivariate analysis of data obtained by high resolution ICP-MS analysis[J]. Food Research International, 2013, 54(1): 621-626.

[9] Wang M, Avula B, Wang Y-H, et al. An integrated approach utilising chemometrics and GC/MS for classification of chamomile flowers, essential oils and commercial products[J]. Food Chemistry, 2014, 152(2014): 391-398.

[10] Bannur Z, Teh L K, Hennesy T, et al. The differential metabolite profiles of acute lymphoblastic leukaemic patients treated with 6-mercaptopurine using untargeted metabolomics approach[J]. Clinical Biochemistry, 2014, 47(6): 427-431.

[11] Zhu K, Nie S, Gong D, et al. Effect of polysaccharide from *Ganoderma atrum* on the serum metabolites of type 2 diabetic rats[J]. Food Hydrocolloids, 2016, 53: 31-36.
[12] Zheng J, Liang R, Wu C, et al. Discrimination of different kinds of Luzhou-flavor raw liquors based on their volatile features[J]. Food Research International, 2014, 56: 77-84.
[13] Worley B, Halouska S, Powers R. Utilities for quantifying separation in PCA/PLS-DA scores plots[J]. Analytical Biochemistry, 2013, 433(2): 102-104.
[14] Almeida M R, Fidelis C H V, Barata L E S, et al. Classification of Amazonian rosewood essential oil by Raman spectroscopy and PLS-DA with reliability estimation[J]. Talanta, 2013, 117: 305-311.
[15] 朱焯炜, 阙立志, 吴亚敏, 等. 三维荧光光谱结合 PARAFAC 和 GA 对中国白酒品牌的鉴别[J]. 中国激光, 2015, 42(06): 315-320.
[16] Taylor V F, Longerich H P, Greenough J D. Multielement Analysis of Canadian Wines by Inductively Coupled Plasma Mass Spectrometry (ICP-MS) and Multivariate Statistics[J]. Journal of Agricultural and Food Chemistry, 2003, 51(4): 856-860.
[17] Berrueta L A, Alonso-Salces R M, Héberger K. Supervised pattern recognition in food analysis[J]. Journal of Chromatography A, 2007, 1158(12): 196-214.

文章编号:1001－9731(2016)09－09231-06

Cu-Mg-Al 层状超分子材料的制备及去除碘的研究*

郑　劼[1],朱霞萍[1],李　品[1],白德奎[2],李　铭[3]
(1. 成都理工大学 材料与化学化工学院,矿产资源化学四川省高校重点实验室,成都 610059;
2. 四川省绵阳产品质量监督检验所,绵阳 621000; 3. 四川省产品质量监督检验检测院,成都 610100)

摘　要: 共沉淀法制备了 Cu-Mg-Al 层状超分子化合物,X 射线衍射图谱和热重分析表征了材料的结构,并研究了材料对溶液中碘离子的吸附去除性能。制备的材料为具有层状结构的 Cu-Mg-Al 的超分子化合物,具有结构"记忆效应",层间可以吸附碘,层板上的铜对碘也有特异化学作用,增强材料对碘的吸附能力。在优化制备和吸附条件下,Cu-Mg-Al 层状超分子化合物对碘离子的饱和吸附量为 279.15 mg/g,远高于普通层状氢氧化镁铝的 66.61 mg/g。材料可作为碘及放射性碘污染的吸附去除剂。

关键词: 层状金属氢氧化物;超分子; 铜;碘;去除
中图分类号: TB34　　**文献标识码:** A　　DOI:10.3969/j.issn.1001－9731.2016.09.045

0　引　言

碘是人体的必需微量元素之一,低碘和高碘对人体都有不良影响,人体摄入过多的碘引发"甲亢"。碘缺乏又使人体甲状腺肿大,甲状腺功能低下,精神功能受损,正常发育受到影响。碘的稳定同位素为^{127}I,碘还有 23 种放射性同位素。放射性碘是核电站的主要放射性产物之一[1],同时也广泛应用于治疗,生物实验和医学诊断等方面,随着我国核能与核技术深入开发及广泛应用,放射防护安全技术也不断进步,但核事故仍不可能绝对避免。现阶段,处理放射性碘的方法都是采用吸附剂吸附后封存起来,所以,提升吸附剂对放射性碘的吸附专属性和饱和吸附容量显得尤为重要。

层状双金属氢氧化物(layered double hydroxides,简称 LDHs)是由不同配比的二价和三价金属离子[2-6]、价态和组成不同的层间阴离子[7-14]构成的具有特殊结构[15]的多元素、多键型分子聚集体,是 1 种具有层状结构的超分子复合材料,化学通式为:

$$[M^{2+}_{1-x}M^{3+}_{x}(OH)_2]^{x+}A^{n-})_{x/n}\cdot mH_2O。$$

它是 1 种新兴的超分子材料,在催化[16-17]、离子交换和吸附[18,21-24]、合成材料助剂[19]、吸波、热传感器[20]等方面具有广阔的应用前景。

LDHs 作为吸附剂的应用越来越广,Joo-Yang Park 等[18]发现非晶的 Fe-Al LDHs 将砷酸盐吸附在表面,而纳米级的 Fe-Al LDHs 晶体在表面吸附砷酸根外,还允许部分砷酸根通过离子交换作用进入层间。Cu-Al LDHs 在高温下可实现对 CO_2 的吸附,吸附容量为 30.00 mg/g[21]。江秀芹[23]优化了 Mg-Al LDHs 对碘离子的吸附条件,但在 25 ℃时饱和吸附容量很小,仅为 25.61 mg/g。对 Mg-Al LDHs 进行改性成型有利于提高其对碘离子的吸附容量,实验吸附容量达到了 181.81 mg/g[24]。

现有层状金属化合物的研究多为双金属氢氧化物,其中对碘的吸附去除研究不多,已经报道的吸附容量也很低,层状多金属化合物的制备及对碘的吸附性能研究更是少见报道。铜的离子半径与镁铝离子大小相当,同时,Cu^{2+} 与 I^- 可发生特异性的氧化还原反应,生成的 CuI 也可吸附 I^-。本文制备的 Cu-Mg-Al 层状超分子化合物(Cu-Mg-Al LDHs)具有典型的 LDHs 的层状结构,对 I^- 具有优异的吸附性能,饱和吸附容量达到 279.15 mg/g,远高于 Mg-Al LDHs 对 I^- 的饱和吸附容量(66.61 mg/g),材料可应用于碘和放射性碘的吸附去除,对碘和放射性碘污染的防治具有实际应用价值。

1　实　验

1.1　Cu-Mg-Al LDHs 的制备

Cu-Mg-Al LDHs:在 150.00 mL 0.13 mol/L $Al(NO_3)_3\cdot 9H_2O$(以 Al^{3+} 计)和 0.40 mol/L $Mg(NO_3)_2\cdot 6H_2O$(以 Mg^{2+} 计)的混合溶液中,加入 5.00 mL 浓度为 0.40 mol/L 的 $CuSO_4\cdot 5H_2O$ 溶液,转入恒压滴液漏斗,缓慢滴入 300.00 mL 浓度为 0.25 mol/L Na_2CO_3 溶液中,剧烈搅动,用 1 mol/L 的 NaOH 调节 pH 值＝10,待金属混合溶液滴完之后继续搅动 0.5 h,60 ℃陈化 24 h。过滤,用蒸馏水洗涤滤饼,烘干,于马弗炉中 400 ℃焙烧 3 h,磨细待用。Mg-Al-LDHs 的制备:不掺铜,其余同 Cu-Mg-Al LDHs。

* 基金项目:四川省科技厅科技支撑资助项目(2015GZ0243);四川省教育厅重点资助项目(15ZA0071)
收到初稿日期:2015-07-21　收到修改稿日期:2016-03-24　通讯作者:朱霞萍,E-mail: zhuxiaping@cdut.edu.cn
作者简介:郑　劼　(1992－),男,成都人,硕士,师承朱霞萍教授,从事功能材料研究。

1.2 吸附实验

称取 0.1000 g 的材料放入干燥的 50 mL 锥形瓶中，再加入 25.00 mL 浓度为 200.00 mg/L 的 I^- 吸附液，35 ℃恒温振荡 1 h，转移至离心管中，3 000 r/min 离心 20 min。用紫外光度法测定上清液中 I^- 浓度，计算 I^- 的平衡吸附量 q_e(mg/g)

$$q_e = \frac{(c_0 - c_e)V}{m}$$

其中，c_0 为 I^- 初始浓度，mg/L，c_e 为 I^- 平衡浓度，mg/L，V 为 I^- 溶液体积，L，m 为材料的质量，g。

1.3 测定方法

紫外光谱法测定碘：取一定量的待测液于 50.00 mL容量瓶中，加水 10 mL，溴水 2 滴，摇匀，放置 5 min。加入甲酸 1.00 mL，摇至无色，加入磷酸 2.00 mL，摇匀，最后加入 1.00 mL 碘化钾溶液，用水稀释至刻度，摇匀，显色 30 min，以试剂空白为参比，用 1 cm 比色皿于 350 nm 处测定其吸光度。

2 结果与讨论

2.1 Cu-Mg-Al LDHs 材料的制备

2.1.1 掺铜量的影响

参照文献[6]，在 150.00 mL 0.13 mol/L $Al(NO_3)_3 \cdot 9H_2O$ 和 0.40 mol/L $Mg(NO_3)_2 \cdot 6H_2O$ 混合溶液中分别加入 0.40 mol/L 铜离子溶液 0.00，2.50，5.00，10.00，20.00，50.00 mL 配成金属混合液，按照 1 中所述实验方法进行材料制备和 I^- 的吸附实验，结果如图 1 所示。掺铜量过高或过低时，材料对 I^- 的吸附都不能达到理想的效果。当掺铜量过高时，铜可能大量取代了层板上的镁离子，由于铜的姜·泰勒效应，主客体间相互靠近使体系层间距减小，导致对 I^- 的吸附容量减小。而当掺入的铜量过少，材料对 I^- 的吸附作用提升不大。当掺铜量为 5.00～20.00 mL 时，得到的材料对 200.00 mg/mL I^- 的吸附率均在 90.00%以上。溶液中的 I^- 进入超分子材料的层间得以去除，另一方面，层板上的铜与碘发生特异性的氧化还原反应，生成的 CuI 进一步吸附 I^-，也提升了对 I^- 的吸附容量。确定掺入 0.40 mol/L 铜溶液 5.00～20.00 mL。

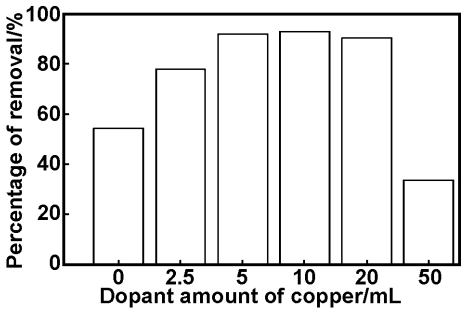

图 1 掺铜量对 Cu-Mg-Al LDHs 吸附性能的影响

Fig 1 Effect of dopant amount of copper on the adsorptive performance of Cu-Mg-Al LDHs

2.1.2 Mg-Al 比例的影响

分别制备 Mg∶Al 为 1∶1，2∶1，3∶1，1∶2，1∶3 的 Cu-Mg-Al LDHs，并对其进行 I^- 的吸附实验，结果如图 2 所示，当 Mg∶Al 比例为 3∶1 时，其吸附效果最好。Cu-Mg-Al LDHs 的层板可以看作是层板上的 Mg^{2+} 部分的被 Cu^{2+}，Al^{3+} 取代，形成 Mg^{2+}，Cu^{2+} 和 Al^{3+} 位于中心的复合氢氧化物八面体。所以，当 Mg^{2+} 的加入量增加时，形成了更多更稳定的 LDHs 层板结构，体系受 Cu^{2+} 的姜-泰勒效应的影响更小，因此具有更大的层间距，对 I^- 的吸附效果也更好。

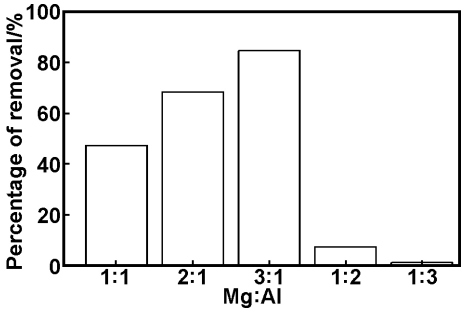

图 2 Mg∶Al 比例对 Cu-Mg-Al LDHs 吸附性能的影响

Fig 2 Effect of Mg∶Al on the adsorptive performance of Cu-Mg-Al LDHs

2.1.3 焙烧温度的影响

焙烧温度分别为 300，350，400，450，500 ℃，按照 1 所述实验方法进行材料的制备和 I^- 的吸附实验，结果如图 3 所示。

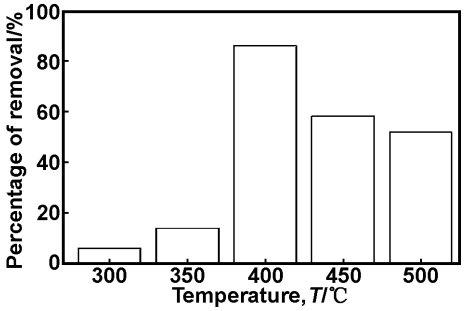

图 3 焙烧温度对 Cu-Mg-Al LDHs 吸附性能的影响

Fig 3 Effect of calcination temperature on the adsorptive performance of Cu-Mg-Al LDHs

当焙烧温度为 400 ℃时，Cu-Mg-Al LDHs 对 I^- 的吸附作用最强。对 Cu-Mg-Al LDHs 焙烧，主要是利用其“记忆效应”以消除 Cu-Mg-Al LDHs 的层间原有阴离子对 I^- 吸附的影响。因为 I^- 与 LDHs 的结合力与常见阴离子，如碳酸根，硝酸根等相比是最弱的，当层间有其它阴离子时，会影响 I^- 的吸附。焙烧使 Cu-Mg-Al LDHs 失去层状结构和层间阴离子，但是层板未被破坏，即未被烧结。当将焙烧后的产物中加入 I^- 溶液时，I^- 利用其“记忆效应”，仍能进入层板间。可能是一部分 I^- 先撑开层板边缘，恢复层状结构，然后，其余 I^- 相继进入层间。当焙烧温度过低，Cu-Mg-Al LDHs 只失去了部分层间阴离子，残余的层间阴离子

会影响 I^- 的吸附。而当焙烧温度过高,Cu-Mg-Al LDHs 在失去其层状结构和层间阴离子的同时,其层板也被破坏,被部分烧结或完全烧结,成为失去"记忆效应"的单纯的金属氧化物,对 I^- 的吸附率降低。因此选择 400 ℃焙烧 3 h。

2.2　材料表征

2.2.1　XRD 图谱

由图 4 可以看出,Cu-Mg-Al LDHs 具有典型 LDHs 层状结构的低角度特征衍射峰[4](在 2θ 值较低处有尖锐且强的衍射峰)。同时,材料的吸收峰符合 37-0630 图谱,具有 $Cu_6Al_2(OH)16CO_34H_2O$ 的特征峰,说明铜成功进入层状氢氧化镁铝的层间,制得含铜的层状金属氢氧化物。

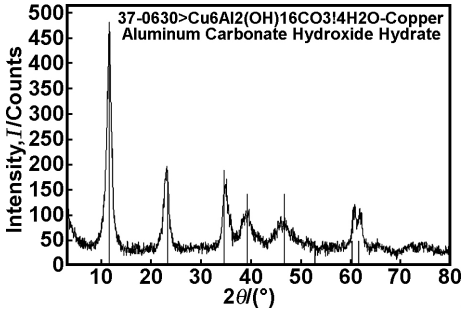

图 4　Cu-Mg-Al LDHs XRD 图谱

Fig 4 XRD diffraction patterns of Cu-Mg-Al LDHs

由图 5 可以看出,焙烧后 Cu-Mg-Al LDHs 失去了低角度的衍射峰,原有层状结构已被破坏。而吸附 I^- 后的焙烧 Cu-Mg-Al LDHs 又出现了 LDHs 层状结构的低角度特征衍射峰,说明吸附 I^- 后,恢复了原有层状结构,即焙烧后的材料仍具有"记忆效应"。

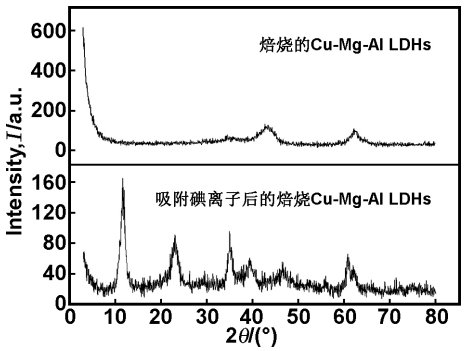

图 5　Cu-Mg-Al LDHs 的 XRD 图谱

Fig 5 XRD diffraction patterns of Cu-Mg-Al LDHs

2.2.2　DTA-TG-DTG 图谱

Cu-Mg-Al LDHs 的 DTA-TG-DTG 图谱显示共有 4 个吸收峰,第一吸收峰在 126.3 ℃,失重率6.96%,为表面吸附水的脱除,第二吸收峰为 157.3 ℃,失重率 3.66%,为层间吸附水的脱除,第三吸收峰为 200.3 ℃,失重率 5.63%,可能是层间阴离子的脱除,最后的吸收峰为 399.6 ℃,失重率 22.16%,为层板脱羟基。DTA 曲线在 410.5 ℃有一个强吸热峰,此时可能发生了层板结构的破坏,即层板失去"记忆效应",这也与前面焙烧温度的实验结果相一致。

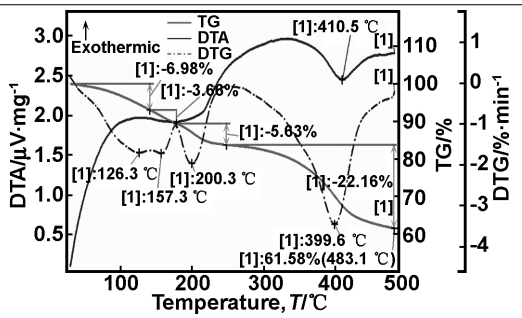

图 6　Cu-Mg-Al LDHs 的 DTA-TG-DTG 图谱

Fig 6 DTA-TG-DTG curves of Cu-Mg-Al LDHs

2.3　Cu-Mg-Al LDHs 对碘离子的吸附性能研究

2.3.1　吸附时间的影响

按照 1.2 所述实验方法,设计 Cu-Mg-Al LDHs 对 I^- 的吸附时间从 0～240 min 的吸附实验,结果如图 7 所示。I^- 的吸附率随着时间的增加而增加,I^- 与材料混合瞬间,吸附率已达 60%以上,说明材料对 I^- 的吸附非常快,60 min 后吸附率已达到 96.00%以上,并且随着时间的增加,吸附率保持平稳,本实验将吸附时间定为 60 min。

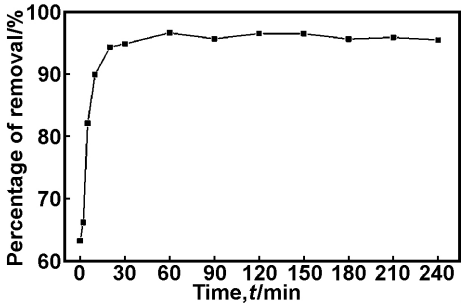

图 7　吸附时间的影响

Fig 7 Effect of adsorptive time

2.3.2　固液比的影响

吸附固液比分别为 1∶50;1∶100;1∶150;1∶200;1∶250;1∶350;1∶500,按照 1.2 所述实验方法进行 I^- 的吸附实验,结果如图 8 所示。当固液比大于 1∶250 时,I^- 的吸附率都在 90.00%以上,当固液比为 1∶350 时,吸附率也接近 90.00%,而当固液比为 1∶500 时,吸附率亦有 80.00%。吸附剂用量很少时也能获得较好的吸附效果,考虑经济,吸附效率等因素,确定固液比为 1∶250。

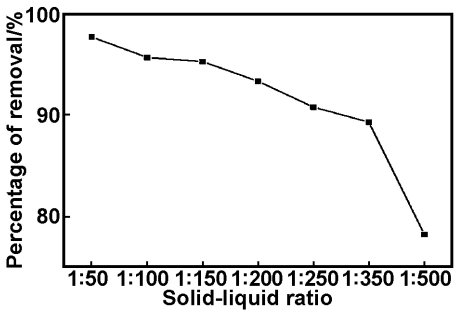

图 8　吸附固液比的影响

Fig 8 Effect of solid-liquid ratio

2.3.3 吸附温度的影响

分别在 25,35,45,55,65,75 ℃ 按照 1.2 所述实验方法进行 I^- 的吸附实验,结果如图 9 所示,吸附率随温度的升高先升高,当温度达到 35 ℃时,吸附率达到最高 90.00%,继续升高温度时,吸附率有所降低。温度较低,分子运动速度较慢,焙烧后的 Cu-Mg-Al LDHs 结构恢复较慢,I^- 较少的进入层间,吸附剂对 I^- 的吸附量减少。Cu-Mg-Al LDHs 对 I^- 的吸附为放热反应,当吸附温度高于 35 ℃其吸附率曲线有所降低。所以,确定吸附温度为 35 ℃。

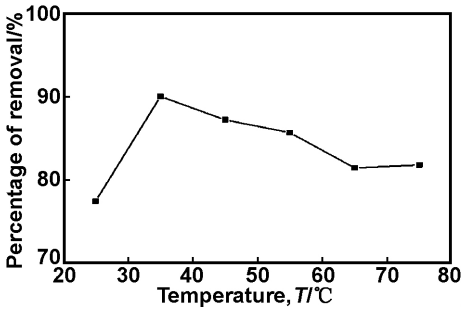

图 9 吸附温度的影响

Fig 9 Effect of adsorptive temperature

2.3.4 吸附初始 pH 值的影响

调节吸附 pH 值为 3,4,5,6,7,8,9,10,按照 1.2 所述实验方法进行 I^- 的吸附实验,结果如图 10 所示。

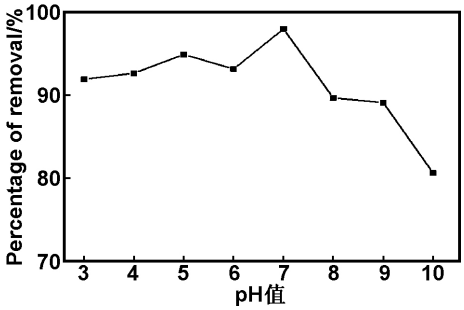

图 10 吸附液初始 pH 值的影响

Fig10 Effect of adsorptive pH

pH 值为 3～8 范围内吸附较为稳定,当 pH 值继续增加,吸附率开始降低。可能是由于 pH 值增大,氢氧根浓度过高,与 I^- 竞争吸附,导致其吸附率下降。所以,确定初始 pH 值为中性。

2.3.5 Cu-Mg-Al LDHs 对碘的饱和吸附容量

分别配制初始浓度为 50.00～3 000.00 mg/L 的 I^- 溶液,加入 0.1000 g Cu-Mg-Al LDHs 或 Mg-Al LDHs,按照 1.2 所述实验方法进行饱和吸附实验。

由图 11 可以看出,未掺铜的 Mg-Al LDHs 对 I^- 的吸附随着 I^- 的初始浓度增加而增加,但当 I^- 初始的浓度为 800.00 mg/L 时即达到吸附平衡,实验饱和吸附容量为 66.61 mg/g。而对 Cu-Mg-Al LDHs,随 I^- 的初始浓度增大,吸附量也随之增大,当 I^- 的初始浓度为 2 500.00 mg/L 时,达到吸附平衡,其饱和吸附容量为 279.15 mg/g,是未掺铜的 Mg-Al LDHs 饱和吸附容量的 4 倍。

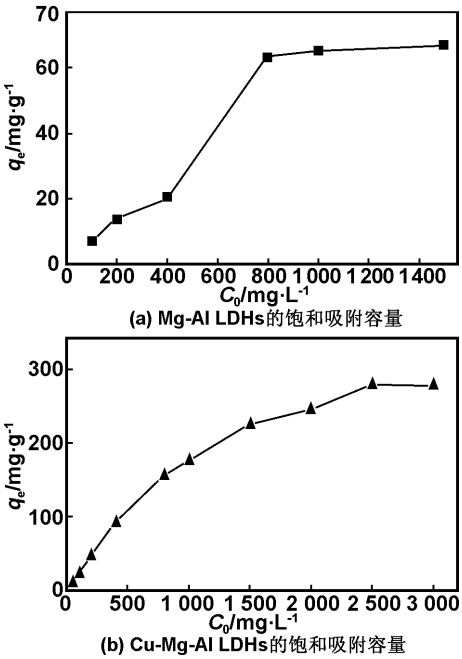

图 11 Cu-Mg-Al LDHs 和 Mg-Al LDHs 的饱和吸附容量

Fig 11 Adsorption capacity of Cu-Mg-Al LDHs and Mg-Al LDHs

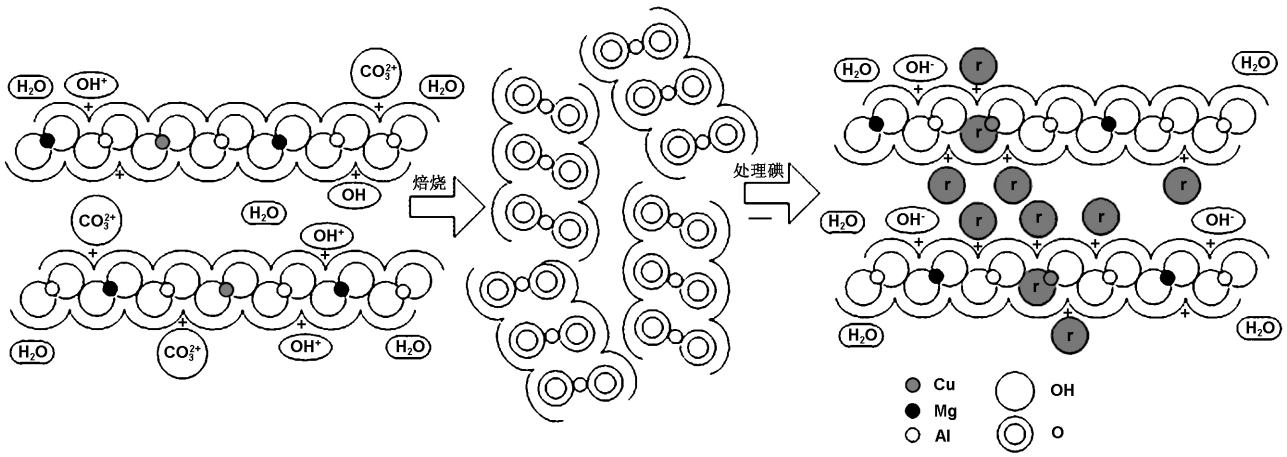

图 12 Cu-Mg-Al LDHs 结构和吸附碘的示意图

Fig 12 Diagram of structure and adsorption of Cu-Mg-Al LDHs

2.4 Cu-Mg-Al 层状超分子材料的结构及对 I^- 吸附机理探讨

结合 Cu-Mg-Al 层状超分子材料 XRD 和 TG-DTG-DTA 表征结果以及材料对 I^- 的吸附性能,推测制备的材料为层状结构,由铜镁铝的氢氧化物组成其层板,层间有水分子和阴离子以氢键等弱化学键结合;焙烧后弱化学键断键,失去层间阴离子和层状结构,但是层板未被破坏;材料加入到含 I^- 溶液后,I^- 可进入层间恢复其层状结构,还与层板上的铜离子发生特异氧化还原反应,大幅提升了材料对 I^- 的吸附性能。

3 结 论

制备了具有吸附性能的层状超分子复合材料 Cu-Mg-Al LDHs,由铜镁铝组成其层板,层间为碳酸根,羟基等阴离子和水分子。制备的材料焙烧后失去层间阴离子,使 I^- 可进入其层间,同时层板上的铜也可与 I^- 发生特异的化学反应,增强了材料对 I^- 的吸附去除能力,其对 I^- 的饱和吸附容量是未掺铜材料的 4 倍。

参考文献:

[1] González-García C M, González J F, Román S. Removal efficiency of radioactive methyl iodide on TEDA-impregnated activated carbons [J]. Fuel Processing Technology, 2011, 92(2): 247-252.

[2] Antonyraj C A, Gandhi M, Kannan S. Phenol hydroxylation over Cu-containing LDHs and their calcined forms: profound cobivalent metal influence[J]. Industrial & Engineering Chemistry Research, 2010, 49(13): 6020-6026.

[3] Britto S, Kamath P V. Structure of bayerite-based lithium-aluminum layered double hydroxides (LDHs): observation of monoclinic symmetry[J]. Inorganic Chemistry, 2009, 48(24): 11646-11654.

[4] Thomas G S, Radha A V, Kamath P V, et al. Thermally induced polytype transformations among the layered double hydroxides (LDHs) of Mg and Zn with Al[J]. The Journal of Physical Chemistry B, 2006, 110(25): 12365-12371.

[5] Wang C J, Wu Y A, Jacobs R M J, et al. Reverse micelle synthesis of Co-Al LDHs: control of particle size and magnetic properties[J]. Chemistry of Materials, 2011, 23(2): 171-180.

[6] Tongamp W, Zhang Q, Saito F. Preparation of meixnerite (Mg-Al-OH) type layered double hydroxide by a mechanochemical route [J]. Journal of Materials Science, 2007, 42(22): 9210-9215.

[7] Zhang S, Liu Q, Fan G, et al. Highly-dispersed Copper-based catalysts from Cu-Zn-Al layered double hydroxide precursor for gas-phase hydrogenation of dimethyl oxalate to ethylene glycol[J]. Catalysis Letters, 2012, 142(9): 1121-1127.

[8] Wei M, Guo J, Shi Z, et al. Preparation and characterization of l-cystine and l-cysteine intercalated layered double hydroxides [J]. Journal of Materials Science, 2007, 42(8): 2684-2689.

[9] Yadollahi M, Namazi H. Synthesis and characterization of carboxymethyl cellulose/layered double hydroxide nanocomposites [J]. Journal of Nanoparticle Research, 2013, 15(4): 1563-1572.

[10] Dinari M, Mallakpour S. Ultrasound-assisted one-pot preparation of organo-modified nano-sized layered double hydroxide and its nanocomposites with polyvinylpyrrolidone[J]. Journal of Polymer Research, 2014, 21(2): 350-358.

[11] Yang J, Chen F, Ye Y, et al. Preparation and characterization of polystyrene (PS)/layered double hydroxides (LDHs) composite by a heterocoagulation method [J]. Colloid and Polymer Science, 2010, 288(7): 761-767.

[12] Xu Z P, Braterman P S. Competitive intercalation of sulfonates into layered double hydroxides (LDHs): the key role of hydrophobic interactions[J]. The Journal of Physical Chemistry C, 2007, 111(10): 4021-4026.

[13] Thomas N. Synthesis of 3R1 and 1H polytypes of sulfate-intercalated layered double hydroxides (LDHs) by postintracrystalline oxidation and simultaneous intercalation-oxidation of thiosulfate[J]. Crystal Growth & Design, 2012, 12(3): 1378-1382.

[14] Radha A V, Kamath P V, Shivakumara C. Conservation of order, disorder, and "crystallinity" during anion-exchange reactions among layered double hydroxides (LDHs) of Zn with Al[J]. The Journal of Physical Chemistry B, 2007, 111(13): 3411-3418.

[15] Matei A, Birjega R, Vlad A, et al. Pulsed laser deposition of Mg-Al layered double hydroxide with Ag nanoparticles[J]. Applied Physics A, 2012, 110(4): 841-846.

[16] Baliarsingh N, Parida K M, Pradhan G C. Effects of Co, Ni, Cu, and Zn on photophysical and photocatalytic properties of carbonate intercalated MII/Cr LDHs for enhanced photodegradation of methyl orange[J]. Industrial & Engineering Chemistry Research, 2014, 53(10): 3834-3841.

[17] Jiang Z, Hao Z, Yu J, et al. Catalytic combustion of methane on novel catalysts derived from Cu-Mg/Al-hydrotalcites [J]. Catalysis Letters, 2005, 99(3-4): 157-163.

[18] Park J Y, Kim J H. Characterization of adsorbed arsenate on amorphous and nano crystalline MgFe-layered double hydroxides [J]. Journal of Nanoparticle Research, 2010, 13(2): 887-894.

[19] Wang G, Yang M, Li Z, et al. Synthesis and characterization of Zn-doped MgAl-layered double hydroxide nanoparticles as PVC heat stabilizer[J]. Journal of Nanoparticle Research, 2013, 15(9): 1582-1590.

[20] Yin H, Zhou Y, Liu T, et al. Amperometric nitrite biosensor based on a gold electrode modified with cytochrome c on Nafion and Cu-Mg-Al layered double hy-

droxides [J]. Microchimica Acta, 2010, 171(3-4): 385-392.

[21] Lwin Y, Abdullah F. High temperature adsorption of carbon dioxide on Cu-Al hydrotalcite-derived mixed oxides: kinetics and equilibria by thermogravimetry [J]. Journal of Thermal Analysis and Calorimetry, 2009, 97(3): 885-9.

[22] Lv L, Ph D. Adsorption and ion-exehange behavior of layered double hydroxides in the uptake of halide anions from aqueous solution[D]. Beijing: Beijing University of Chemical Technology, 2005.
吕 亮. 层状双金属(氢)氧化物对卤离子的吸附和离子交换性能研究 [D]. 北京:北京化工大学, 2005.

[23] Jiang X Q. Adsorption behavior of mg-al layered double-hydroxides to I^- [J]. J Salt and Chem Indu, 2006, 35(05): 1-2.
江秀芹. 层状氢氧化镁铝对碘离子的吸附性能 [J]. 盐业与化工, 2006,35(05): 1-2.

[24] Yu Y W, Ph D. Modification and granulation of Mg/A1 1ayered doubIe hydroxides and adsorption of ha1ide anions[D]. Qingdao: Ocean University of China, 2010.
于艳伟. 层状氢氧化镁铝的改性成型及其对卤素阴离子的吸附性能 [D]. 青岛:中国海洋大学, 2010.

Preparation and adsorptive behavior to iodine of Cu-Mg-Al layer supramolecular materials

ZHENG Jie[1], ZHU Xiaping[1], LI Ping[1], BAI Dekui[2], LI Ming[3]

(1. Institute of Material and Chemistry & Chemical Engineering, Mineral Resources Chemistry Key Laboratory of Sichuan Higher Education Institutions, Chengdu University of Technology, Chengdu 610059, China;
2. Mianyang Product Quality and Inspection Institute, Mianyang 621000, China;
3. Sichuan Insitute of Product Quality Supervision and Inspection, Chengdu 610100, China)

Abstract: The Cu-Mg-Al layer supramolecular materials(Cu-Mg-Al LDHs) was successfully prepared by coprecipitation method, characterized by XRD and DTA-TG-DTG, and used as the adsorption materials to iodine. The Cu-Mg-Al LDHs was layered hydroxides with memory effect. The iodine could intercalate the interlayer of Cu-Mg-Al LDHs and the Cu on the laminate could adsorb iodine specifically. The saturated adsorption capacity of Cu-Mg-Al LDHs to iodine was 279.15 mg/g, it was much higher than that of ordinary Mg/Al layered double hydroxide (66.61 mg/g). The materials might be used as the adsorption materials to radioactive iodine.

Key words: layerd metal hydroxides; supramolecular; copper; iodine; removal

(上接第 09230 页)

Synthesis and performance of waterborne polyurethane-polyacrylate containing sulfonated soft segment

XING Bo[1], WANG Tingping[1], LAI Xiaojuan[2]

(1. Department of Biological Engineering, Chaoyang Teachers College, Chaoyang 122000, China;
2. College of Chemistry & Chemical Engineering, Shananxi University of Science & Tecnology, Xi'an 710021, China)

Abstract: Waterborne polyurethane containing sulfonated soft segment (SWPU) was prepared with isophorone diisocyanate (IPDI) and sulfonated polyester-diol (SPOL) as main raw materials, then the sulfonated waterborne polyurethane-polyacrylate (SWPUA) composite emulsion was obtained by copolymerization with mixture monomers methylmethacrylate (MMA) and butylacrylate (BA). The synthesis process of SWPUA was simple and easy to control without any organic solvent and amine-free. The micellar conformation and diameter of the composite emulsion were characterized by transmission electron microscopic (TEM) and diameter analyzer. The crystallinity, thermal stability, mechanical properties and water resistance of films were investigated by X-ray diffraction analysis (XRD), thermogravimetric analysis (TGA) and tension test. The results showed that core-shell structure had formed between polyurethane and polyacrylate, degree of crystallinity of the films was 3.76%. After modified by polyacrylate, the thermal stability of SWPUA increased by 22 ℃. When the SPOL content was 40%, NCO/OH molar ratio (R) was 1.7, SWPUA with 50% solid content was obtained, the emulsion of SWPUA showed good appearance, and the average particle size and storage stability were 44 nm and 12 months.

Key words: high-solid-content; sulfonated; waterborne polyurethane; polyacrylate; amine-free

丹参植株对亚硒酸钠和硒酸钠的吸收和积累

粟 敏，雷济华，杨 帆，刘 睿，胡晓荣
（成都理工大学材料与化学化工学院，成都 610059）

摘 要：为了解丹参植株对不同价态无机硒的吸收积累情况，采用田间栽种叶面喷施亚硒酸钠和硒酸钠水溶液的方式，分别设置空白对照组和喷施 Se 质量浓度为 0.060、0.120、0.240 g/L 的剂量组，每 1 种处理重复 3 次，在丹参盛花期间隔 10 d 喷施 2 次。采用氢化物发生-原子荧光法测定丹参植株根、茎、叶和土壤中的硒含量。结果表明，丹参植株硒含量随喷施剂量的增加而增加，但增加量与喷施剂量增加不成正比；硒在丹参植株中的含量为茎最高，叶次之，根最低，部分硒经植株迁移交换到土壤，土壤中硒含量与喷施剂量成正相关；喷施硒酸钠的丹参根及对应土壤中硒含量高于喷施亚硒酸钠的丹参根和土壤，而茎和叶中的含量低于喷施亚硒酸钠的实验组。该现象表明硒酸钠比亚硒酸钠在丹参植株-土壤系统中有更好的迁移性。叶面喷施 2 种价态的无机硒均能有效增加丹参植株的硒含量，选择何种作为补硒试剂还需结合对植株硒的形态分析结果进行综合考虑。

关键词：中药化学；丹参；硒酸钠；亚硒酸钠；硒含量分布
中图分类号：R931.6 **文献标志码**：A **文章编号**：2095-2783(2017)06-0647-05

Uptake and accumulation of sodium selenite and selenate in Danshen (*Salvia miltiorrhiza*) plants

SU Min, LEI Jihua, YANG Fan, LIU Rui, HU Xiaorong

(*College of Materials and Chemistry & Chemical Engineering, Chengdu University of Technology, Chengdu* 610059, *China*)

Abstract: To understand the uptake and accumulation for different valence inorganic selenium in Danshen plants, Danshen was treated by spraying the leaves with sodium selenite and sodium selenate aqueous solution containing 0.060, 0.120, 0.240 g/L Se respectively. There were three Danshen plants treated at every concentration. When the plants were in full-bloom stage, spraying were performed twice with a 10-day interval. The Se contents in the three different tissues (stem, leaf and root) and the soil were determined by hydride generation atomic fluorescence spectrometry (HG-AFS). The results show that Se content in Danshen plants increases with the increase of selenium fertilizer concentration but there is no significant linearity. The Se content in stem of Danshen plant is the highest, followed by leavf and root. Partial selenium is moved and exchanged to soil by plant and the Se content of soil increases with the increase of dosage of Se fertilize. The content of Se in root of Danshen sprayed with selenate and its corresponding soil are higher compared with Danshen sprayed with selenite. In contrast to the root, Se content in stem and leaf of plants spraying with selenite is higher. It seems that selenate has a better mobility in Danshen than selenite. The Se content of Danshen plants can be effectively increased with spraying both kind of inorganic selenium aqueous solution. The selection of selenium reagent for Se supplement still depends on the results of speciation analysis of selenium.

Keywords: Chinese medicine chemistry; Danshen; selenite; selenate; distribution of selenium

丹参（*Salvia miltiorrhiza*）是 1 种唇形科鼠尾草植物，广泛用于心脑血管疾病、高血脂、急性缺血性中风的治疗。丹参的主要有效成分为脂溶性的二萜化合物和水溶性的酚酸类化合物[1]。脂溶性的丹参酮类为抗菌消炎的主要成分；水溶性的丹酚酸类（包括丹参素、原儿茶醛、迷迭香酸、丹酚酸 B 等）具有抗氧化、抗凝抗血栓、抗心肌缺血、调节血脂及增强机体免疫的作用[2]。

硒是 1 种人体必需微量元素，作为谷胱甘肽过氧化物酶（GSH-Px）的活性中心催化还原型的谷胱甘肽为氧化型，使有毒的过氧化物（ROOM）变成无毒的羟化物（ROM），分解过氧化氢和脂肪过氧化物，阻遏机体内的脂质过氧化链式反应，避免细胞损伤，从而提高机体的免疫力[3]。

硒的生理作用和丹参的药理作用基础都是抗氧化活性，但是二者又有着不同的机理，丹参活性成分直接参与清除过氧化物的反应，而硒是作为动物内生性抗氧化物酶的活性中心而发挥作用。如果丹参富含硒元素，其中硒化合物与丹参药效成分一起可能在人体内发挥抗氧化协同作用，增强人体器官内生性和外源性抗氧化能力，更好地消除氧化损伤。

植物是人体硒元素的重要来源，通过富硒栽培可有效地提高农作物中的硒含量，无机硒经过植物有机化后生物活性更高，更利于人体的吸收利用[4]。

收稿日期：2016-11-05
基金项目：四川省科技厅应用基础资助项目（2014JY0161）；高等学校博士学科点专项科研基金资助项目（20135122120001）
第一作者：粟敏（1990—），女，硕士研究生，主要研究方向为植物成份分离与分析
通信作者：胡晓荣，教授，主要研究方向为微量元素形态与毒理，huxiaorong@cdut.cn

富硒栽培可通过土壤补充和叶面喷施两种方式进行。土壤类型、氧化还原性质、pH值和微生物活性等因素的变化影响硒在土壤中的存在形态，从而影响植物对硒的可吸收利用率[5]，同时土壤补充还需要考虑硒积累可能带来的潜在的土壤污染。叶面喷施无机硒的水溶液，植物对硒的吸收受到干扰少且利用率高，因此是更好的选择。

四川省中江县是我国主要的丹参栽种基地，但中江县地处我国土壤缺硒地带，其种植的丹参中硒含量极低。由于不同的植物及补充不同价态的硒，硒被植物吸收、转化和积累的量不同[6-9]，本文采用叶面喷施不同浓度的亚硒酸钠和硒酸钠的田间实验，考察丹参植株各器官对不同浓度、不同价态硒的吸收、积累和分布情况，为丹参富硒栽培提供基础数据支持。

1 实验部分

1.1 仪器与试剂

AFS-3000型双道原子荧光光度计(北京海光仪器公司)；硒编码空心阴极灯(北京有色金属研究总院)；控温电热板(江苏省金坛市医疗仪器厂)；Se(Ⅳ)标准溶液(1.000 g/L，国家标准物质GBW(E)080215)；灌木枝叶(国家标准物质GSV-1、GSV-2)；硝酸、盐酸、高氯酸为优级纯，铁氰化钾、硼氢化钠为分析纯，水为实验室用二次去离子水。

1.2 仪器工作条件

灯电流80 mA；负高压340 V；原子化器高度8 mm；载气流量400 mL/min；屏蔽气流量900 mL/min；读数时间7 s；延迟时间1.5 s；测量方式为标准曲线法；读数方式为读取峰面积；载流5% HCl(质量:体积，下同)；还原剂2% KBH_4-0.05% NaOH溶液(质量:体积，下同)。

1.3 田间实验

在四川省中江县辑庆镇开展田间实验。设置空白对照组；Na_2SeO_3(剧毒，口服1 g即可致死，大鼠经口LD_{50}为7 mg/kg，使用时应做好防护)低、中、高剂量组；Na_2SeO_4低、中、高剂量组。每个剂量组重复3次，共21个小区，每个小区面积21 m^2。喷施Se质量浓度为0.060、0.120、0.240 g/L。在盛花期间隔10 d喷施2次。

采用随机采样法从21个实验小区随机采取10 kg丹参根及适量的茎、叶和耕作层土壤作为实验样品。分别用自来水和去离子水清洗丹参植株，40 ℃烘干、切片、粉碎、过80目筛，土壤过100目筛，密封装袋放置于阴凉处备用。样品编号分别为对照-1、对照-2、对照-3；Se(Ⅳ)低1-1、1-2、1-3；Se(Ⅳ)中2-1、2-2、2-3；Se(Ⅳ)高3-1、3-2、3-3；Se(Ⅵ)低1-1、1-2、1-3；Se(Ⅵ)中2-1、2-2、2-3；Se(Ⅵ)高3-1、3-2、3-3。

1.4 样品消解方法

根据文献[10]的方法：准确称取丹参粉末和土壤样品(0.500 0±0.000 5) g，置于50 mL烧杯中，每个样品平行称3份。加入混合酸($V(HNO_3)$：$V(HClO_4)$=4：1)10.0 mL，盖上表面皿，放置过夜，随带试剂空白。次日于温度控制为160～170 ℃的电热板上加热消解。加热过程中，补加5.0 mL混合酸，使样品充分消解。待有大量白烟产生后，移去表面皿，直至溶液剩余2.0 mL左右，取下冷却至室温。加入10.0 mL 6 mol/L的HCl，将电热板温度调节为110 ℃还原4价硒，加热至剩余溶液为2.0 mL左右取下冷却。加入1.0 mL 100 g/L的铁氰化钾溶液和1.0 mL浓HCl，转移至25 mL容量瓶中，用去离子水定容待测其硒含量。铁氰化钾作为掩蔽剂可以有效地消除常见金属离子对硒测定的干扰，并且不会影响硒的测定[10]。

1.5 标准曲线的绘制

准确移取硒标准储备液(10 mg/L)0、0.02、0.04、0.06、0.08、0.10 mL于10 mL比色管中，分别加入0.2 mL 100 g/L的铁氰化钾溶液，2.0 mL浓盐酸，用去离子水定容，配制成分别含硒0、20.0、40.0、60.0、80.0、100.0 μg/L的标准溶液，用5%的HCl作载流，2% KBH_4(0.05% NaOH介质)作还原剂，在仪器最佳条件下测定。曲线方程为$y=50.174x-14.382$，相关系数$R^2=0.999\ 14$，硒质量浓度在0～100.0 μg/L之间与荧光强度呈良好的线性关系。植物样品的测定按照工作曲线条件进行。

2 测试方法学评价

2.1 检出限

在仪器最佳工作条件下，以11个试剂空白荧光值标准偏差的3倍对应质量浓度作为分析方法定性检出限($D=3S/K$)，标准偏差的10倍对应质量浓度作为分析方法定量检出限($D=10S/K$)，(S为11个试剂空白荧光值标准偏差，K为标准曲线斜率)分别得到定性检出限0.702 μg/L和定量检出限2.34 μg/L。

2.2 精密度和准确度

对质量浓度为20.0 μg/L的硒标准溶液连续进样测定11次，由其荧光强度值计算相对标准偏差(relative standard deviation，RSD)为3.2%，说明仪器具有良好的精密度。同时分别平行称取6份标准物质的灌木枝叶GSV-1、GSV-2进行消解测定，计算结果的RSD为8.74%和9.32%，说明整个分析方法精密度满足痕量硒的测定要求。灌木枝叶测定结果(表1)与标准物质证书推荐值吻合。

表1 分析方法的精密度和准确度($\bar{x}\pm s$，$n=6$)

标准物质	测定值	推荐值	RSD/%
GSV-1	0.183±0.016	0.184±0.013	8.74
GSV-2	0.118±0.011	0.120±0.02	9.32

3　结果与讨论

3.1　土壤中的硒含量

喷施硒的实验小区耕作层土壤，丹参植株根、茎、叶中的硒含量如表 2 所示。实验数据显示空白对照组土壤硒含量在定性检出限附近，但低于定量检出限；空白对照组丹参植株硒含量低于定性检出限，不能给出可靠的硒含量数据，所以表 2 中未列出空白对照组土壤和植株各器官的硒含量。按照硒的分析方法检出限计算，空白对照组土壤硒含量低于国际公布的临界值 0.1 μg/g(Se)土壤，表明中江丹参种植地土壤缺硒，土壤中过低的硒含量导致丹参植株硒含量极低。

表 2　丹参根、茎、叶和土壤中总硒质量比($\bar{x}\pm s$，$n=3$)　　μg/g

样品名称	编号	根	平均值	茎	平均值	叶	平均值	土壤	平均值
	1-1	0.17±0.02		1.74±0.03		1.39±0.09		1.61±0.08	
Se(Ⅳ)低	1-2	0.14±0.01	0.16±0.02	1.87±0.11	1.86±0.11	1.30±0.02	1.32±0.06	1.75±0.13	1.85±0.30
	1-3	0.17±0.02		1.97±0.04		1.26±0.16		2.19±0.11	
	2-1	1.18±0.14		2.76±0.05		2.01±0.10		2.66±0.05	
Se(Ⅳ)中	2-2	1.09±0.02	1.04±0.17	2.37±0.05	2.56±0.19	2.23±0.11	2.15±0.12	2.27±0.05	2.46±0.53
	2-3	0.86±0.01		2.55±0.10		2.22±0.08		2.45±0.10	
	3-1	1.32±0.12		5.31±0.39		2.82±0.01		3.60±0.03	
Se(Ⅳ)高	3-2	1.57±0.11	1.43±0.13	5.80±0.26	5.39±0.38	3.14±0.13	2.89±0.23	3.59±0.11	3.64±0.07
	3-3	1.39±0.01		5.05±0.14		2.70±0.16		3.72±0.34	
	1-1	0.19±0.03		1.61±0.06		0.67±0.09		1.17±0.15	
Se(Ⅵ)低	1-2	0.22±0.03	0.18±0.05	1.20±0.01	1.41±0.20	0.75±0.03	0.70±0.04	1.31±0.05	1.24±0.07
	1-3	0.13±0.01		1.41±0.04		0.68±0.08		1.24±0.13	
	2-1	1.67±0.03		2.84±0.27		2.06±0.13		3.52±0.24	
Se(Ⅵ)中	2-2	1.19±0.04	1.44±0.24	2.12±0.33	2.32±0.45	2.21±0.12	2.15±0.08	3.80±0.23	3.69±0.15
	2-3	1.46±0.21		2.01±0.08		2.18±0.08		3.74±0.21	
	3-1	2.13±0.06		4.44±0.16		2.65±0.02		5.25±0.02	
Se(Ⅵ)高	3-2	2.18±0.12	2.16±0.03	4.38±0.23	4.00±0.70	2.64±0.08	2.63±0.03	5.84±0.25	5.37±0.42
	3-3	2.16±0.04		3.19±0.10		2.59±0.04		5.01±0.31	

实验数据表明，随着丹参叶面喷施硒剂量的增加，土壤硒含量增加，并且与喷施剂量呈正相关关系。喷施亚硒酸钠的土壤硒与剂量之间的相关系数为 0.97(如表 3 所示，$n=9$，$P<0.000\ 01$)；喷施硒酸钠的土壤硒与剂量之间的相关系数为 0.95(如表 3 所示，$n=9$，$P<0.000\ 1$)。丹参种植过程中使用地膜覆盖，采挖时先去掉了地膜，因此土壤硒主要来源于叶面吸收的硒经由茎到根再到土壤的迁移。如果是土壤施硒，植物根可吸收并向上输送至植物的各部分；相反，叶面吸收硒后亦可向下输送到根并且交换至土壤。但相比土壤施硒，叶面喷施避免了土壤对硒的固定，可提高补硒试剂的利用率，因此叶面喷施作为有效手段在很多富硒栽培中被采用[11-12]。

表 3　剂量组之间植株硒含量的倍数及植株硒含量与剂量之间的相关系数

剂量组		根	茎	叶	土
	中/低	6.50	1.38	1.63	1.33
Se(Ⅳ)	高/中	1.38	2.10	1.34	1.48
	相关系数	0.90	0.98	0.93	0.97
	中/低	8.00	1.65	3.07	2.97
Se(Ⅵ)	高/中	1.50	1.72	1.22	1.45
	相关系数	0.93	0.94	0.92	0.95

3.2　丹参植株硒含量与剂量之间的关系

喷施不同剂量亚硒酸钠和硒酸钠的丹参植株各部位硒含量均为高剂量组＞中剂量组＞低剂量组，丹参根、茎、叶中的硒含量与喷施剂量之间呈现显著的正相关关系，相关系数大于 0.90(如表 3 所示，$n=9$，$P<0.001$)。在喷施剂量的设置上，中剂量组硒含量是低剂量组的 2 倍、高剂量组硒含量是中剂量组的 2 倍，但植株硒含量的倍数变化并不如剂量倍数变化。表 3 给出了各剂量组之间丹参植株硒含量的倍数关系，可以看出，根中硒含量与剂量变化的关系很大，中剂量组 4 价和 6 价根中硒含量分别是低剂量组的 6.50 倍和 8.00 倍，而高剂量组根中硒含量只有中剂量组的 1.38 和 1.50 倍。茎和叶中硒含量随喷施剂量的变化在 0.92～3.07 倍之间，远远小于根中的变化。根中硒含量虽然低于地上部分，但是随剂量的增加倍数远超过喷施剂量的增加倍数。课题组前期就叶面喷施硒酸钠的丹参根中硒的形态进行过分析，结果显示，90%以上的硒与蛋白质和多糖结合转化为有机结合态[11]，表明丹参根有累积转化硒的能力。其它植物，例如油菜[12]、青花菜、胡萝卜、大蒜[13]喷施不同浓度的亚硒酸钠，也表现出植株吸收量与喷施剂量成正相关但不成比例的吸收积累特征。

3.3 丹参植株硒含量的分布

喷施4价和6价硒的低、中、高3个剂量组丹参植株不同部位的硒含量均为茎>叶>根。采用成对t检验，茎中硒含量高于叶中硒含量($P<0.03$，$n=6$)，叶中硒含量显著高于根中硒含量($P<0.002$，$n=6$)。茎中硒含量是叶中硒含量的1.08～1.86倍，叶中硒含量是根中硒含量的1.21～8.25倍。其他植物，如圣约翰草(贯叶连翘)[14]喷施硒酸钠后硒的植株分布为叶>花>茎；黄芪[15]叶面喷施亚硒酸钠后硒的植株分布为地上部分>地下部分；胡萝卜[16]叶面喷施或土壤根施4价硒和6价硒后，硒的植株分布为叶>根。以上几种植物富硒后的植株分布都表现出地上部分大于地下部分的相似性质，但地上部分分布有所不同。与之相反，生长在不同硒含量土壤中的水稻硒的植株分布为根系>茎叶>籽粒[17]；加入硒酸钠和亚硒酸钠营养液培养的苗期水稻和小麦[18]中硒的分布也表现为根系>地上部分。以上文献显示，不同植物不仅吸收硒的能力不同，而且硒的植株分布也不同。

胡萝卜[16]叶面喷施4价硒和6价硒的实验显示，当喷施剂量差10倍时，胡萝卜叶中硒含量差别是9.6～14.0倍，而根中硒含量的差别是3.7～4.4倍。这与本文实验结果不同。实验中胡萝卜生长周期为18周，最后1次喷施硒后1周收获。本文实验丹参生长期长达1 a，喷施硒6个月后才收获。对比这2个实验可以看出，随着时间的增加，硒从叶面到根的迁移量会增加。不同植物生长时间不同，硒的植物迁移积累是否与植物生长期有关是值得研究的问题。

3.4 丹参植株对不同价态硒的吸收和积累差异

由表2数据可以看出，喷施相同剂量的硒酸钠和亚硒酸钠的丹参植株硒含量不同。采用同剂量、同植株器官成对t检验法，丹参根中喷施6价硒的含量高于喷施4价硒的($P<0.10$，$n=3$)；茎的情况与根相反，喷施6价硒的含量低于喷施4价硒的含量($P<0.10$，$n=3$)；叶片与茎类似，但检验置信度低于茎($P<0.12$，$n=3$)。从检验结果和硒含量数据来看，喷施2种价态的硒在丹参植株不同器官中积累的量差别不大。由于硒酸根与硫酸根化学性质相似，植物可通过硫转移蛋白主动吸收和转运硒酸根[19]，因此，硒酸盐被植物根吸收后很容易转运至枝叶中去，并且在木质部汁液中主要以硒酸根的形式存在，而植物吸收亚硒酸根是非代谢依赖的被动吸收[20]，植物对亚硒酸盐的转运速率小于吸收速率，吸收的亚硒酸盐先转化为有效性高的硒酸盐及有机硒化合物，才能转运到植物地上部[19]，亚硒酸盐主要停留在根部并且转化为其他硒化合物的形式[20]。因此，一般植物土壤补充相同剂量的6价硒和4价硒时，6价硒被植物吸收利用率显著高于4价硒。相似的规律在叶面喷施富硒植物栽培中也能观察到，胡萝卜[16]喷施不同浓度的2种无机硒，叶和根吸收6价硒的量高于吸收4价硒的量。本文结果显示，叶面喷施硒酸钠的栽培土壤中硒含量高于喷施亚硒酸钠的土壤硒含量，表明叶面吸收6价硒后向植株根部转移并交换至土壤比4价硒的转移容易，或许因为这种转移的容易，使得喷施6价硒的丹参根硒含量只是略高于喷施4价的含量，叶片和茎中硒含量喷施6价的含量低于喷施4价的含量。

仅从含量的差异来看，叶面喷施亚硒酸钠和硒酸钠的丹参植株硒含量差异不大，富硒栽培的目的是通过植物的代谢将无机硒转化为有机硒。根据文献报道[20-21]，其他植物对2种无机硒的有机转化效率不同，因此丹参富硒栽培中2种无机硒化合物的选择依赖于进一步的硒的形态分析结果。

高浓度硒可导致植物不能正常生长，表现为植物根的生长缓慢、叶绿素含量减少，从而影响到其生物量[22]，本文喷施剂量没有对丹参的生长带来不良影响。

4 结 论

叶面喷施亚硒酸钠和硒酸钠均能有效提高丹参植株硒含量，硒在植株的不同部位积累的量不同，植株含量分布为茎>叶>根。植株对2种无机硒吸收和积累的量不同，但差别不大。硒酸钠在植株中，从叶面到根系再到土壤表现出更好的迁移性，喷施硒酸钠的丹参根中硒含量更高。选择补硒试剂一方面依赖于植物的吸收积累量，另一方面依赖于植物对不同价态无机硒的有机转化率。进一步的研究需要对丹参植株硒的存在形态及各形态含量分布进行分析对比，最终确定合适的补硒试剂。另外根据人体每日摄入硒的限量(小于400 μg/D，WHO，1996)，还应结合丹参每日用药量和丹参根中硒的可溶出率决定喷施剂量。

[参考文献] (References)

[1] HU P, LIANG Q L, LUO G A, et al. Multi-component HPLC fingerprinting of *Radix salviae mihiorrhizae* and its LC-MS identification [J]. Journal of Chromatography A, 2005, 53(6): 677-683.

[2] GUO Y X, ZHANG D J, WANG H, et al. Hydrolytic kinetics of lithospermic acid B extracted from roots of *Salvia miltiorrhiza* [J]. Journal of Pharmaceutical and Biomedical Analysis, 2007, 43: 435-439.

[3] ROTRUCK J T, POPE A L, GANTHER H E, et al. Selenium: biochemical role as a compound of glutathione peroxidase [J]. Science, 1973, 179: 588-590.

[4] THOMSON C D. Assessment of requirements for selenium andadequacy of selenium status: a review [J]. European Journal of Clinical Nutrition, 2004, 58: 391-402.

[5] HARTFIEL W, BAHNERS N. Selenium deficiency in

the Federal Republic of Germany [J]. Biological Trace Element Research, 1988, 15: 1-12.

[6] SLEJKOVEC M, GOESSLER W. Accumulation of selenium in natural plantsand selenium supplemented vegetable and selenium speciation by HPLC-ICP-MS [J]. Chemical Speciation and Bioavailability, 2005, 17: 63-73.

[7] POGGI V, ARCIONI A, FILIPPINI P, et al. Foliar application of seleniteand selenate to potato (*Solanum tuberosum*): effect of a ligand agent onselenium content of tubers [J]. Journal of Agricultural and Food Chemistry, 2000, 48: 4749-4751.

[8] HU Q, CHEN L, XU J, et al. Determination of selenium concentration in rice and the effect of foliar application of Se-enriched fertiliseror sodium selenite on the selenium content of rice [J]. Journal of the Science of Food and Agriculture, 2002, 82: 869-872.

[9] YANG F, CHEN L, HU Q, et al. Effect of the application of selenium onselenium content of soybean and its products [J]. Biological Trace Element Research, 2003, 93: 249-256.

[10] **徐珑珀，赵向阳，杨浩，等. 不同消解方法对** HG-AFS **测定植物样品硒含量的影响**[J]. **中国测试**, 2015, 41(3): 61-64.
XU Longpo, ZHAO Xiangyang, YANG Hao, et al. The influence of different digestion methods for the determination of selenium in plant samples by HG-AFS [J]. China Measurement & Test, 2015, 41(3): 61-64. (in Chinese)

[11] **胡晓荣，田丽，董维兵，等. 富硒栽培丹参中硒的赋存形态研究**[J]. **中药材**, 2014, 37(9): 1609-1611.
HU Xiaorong, TIAN Li, DONG Weibing, et al. Study on binding forms of selenium in selenium-enriched Salvia miltiorrhiza [J]. Journal of Chinese Medicinal Materials, 2014, 37(9): 1609-1611. (in Chinese)

[12] SEPPANEN M M, KONTTURI J, HERAS I L, et al. Agronomic biofortification of *Brassica*with selenium-enrichment of SeMet and its identification in *Brassica* seeds and meal [J]. Plant Soil, 2010, 337: 273-283.

[13] **王晋民，赵之重，段冰. 叶面施硒对不同蔬菜硒富集和产量的影响**[J]. **西北农林科技大学学报(自然科学版)**, 2007(7): 103-106.
WANG Jinmin, ZHAO Zhizhong, DUAN Bing. Effect of selenium applications on the selenium accumulation and yield on several kinds of vegetables [J]. Journal of Northwest A & F University (Natural Science Edition), 2007(7): 103-106. (in Chinese)

[14] MATEJA G, VEKOSLAVA S, SAMO K, et al. Selenium concentration in St. John's wort (*Hypericum perforatum* L.) herb after foliar spraying of young plants under different UV-B radiation levels [J]. Food Chemistry, 2009, 117: 204-206.

[15] **乔斌. 黄芪对硒的富集转运特性研究**[D]. **保定：河北农业大学**, 2013.
QIAO Bin. Study on characteristics of Se accumulation and translocation in astragalus membranaceus (Huangqi) [D]. Baoding: Agricultural University of Hebei Province, 2013. (in Chinese)

[16] KAPOLNA E, HILLESTROM P R, LAURSEN K H, et al. Effect of foliar application of selenium on its uptake and speciation in carrot [J]. Food Chemistry, 2009, 115: 1357-1363.

[17] **姜超强，沈嘉，祖朝龙. 水稻对天然富硒土壤硒的吸收及转运**[J]. **应用生态学报**, 2015, 26(3): 809-816.
JIANG Chaoqiang, SHEN Jia, ZU Chaolong. Selenium uptake and transport of rice under different Se-enriched natural soils [J]. Chinese Journal of Applied Ecology, 2015, 26(3): 809-816. (in Chinese)

[18] **陈思杨，江荣风，李花粉. 苗期小麦和水稻对硒酸盐亚硒酸盐的吸收及转运机制**[J]. **环境科学**, 2011, 32(1): 284-289.
CHEN Siyang, JIANG Rongfeng, LI Huafen. Uptake and translocation of selenate or selenite by wheat and rice seedlings [J]. Environmental Science, 2011, 32(1): 284-289. (in Chinese)

[19] ARVY M P. Selenate and selenite uptake and translocation in bean plants (*Phaseolus vulgaris*) [J]. Journal of Experimental Botany, 1993, 44: 1083-1087.

[20] LI H F, MCGRATH S P, ZHAO F J. Selenium uptake, translocation and speciation in wheat supplied with selenate or selenite [J]. New Phytologist, 2008, 178: 92-102.

[21] SÁNCHEZ-RODAS D, MELLANO F, MARTÍNEZ F, et al. Speciation analysis of Se-enriched strawberries (*Fragaria ananassa Duch*) cultivated on hydroponics by HPLC-TR-HG-AFS [J]. Microchemical Journal, 2016, 127: 120-124.

[22] de KOK L J, KUIPER P J C. Effect of short-term dark incubation with sulfate, chloride and selenate on the glutathione content of spinach leaf discs [J]. Physiologia Plantarum (Denmark), 1986, 68: 477-482.